SCUOLA DI DOTTORATO
UNIVERSITÀ DEGLI STUDI DI MILANO-BICOCCA

Department of

Medicine and Surgery

PhD program in Neuroscience, Cycle XXIX

Curriculum in Experimental Neuroscience

AIR POLLUTION IN NEURODEGENERATION: *IN-VITRO* AND *IN-VIVO* MODELS

Milani Chiara

Registration number 713298

Tutor: Prof. Paola Palestini

Co-tutor: Dr. Alessandra Bulbarelli

Coordinator: Prof. Guido Cavaletti

ACADEMIC YEAR 2015/2016

“Don't ask yourself what the world needs. Ask yourself what makes you come alive and then go do that. Because what the world needs is people who have come alive.”

Howard Thurman

INDEX

ABSTRACT

Particulate matter (PM) is a complex mixture of solid and liquid particles suspended in the air, and this suspension could be formed by a variety of particles of different size and composition depending on their origin (Marconi, 2003). Among the different fractions, ultrafine particles (UFPs) are thought to have the greatest health effects because of different characteristics: their small size, their high surface-to-volume ratio (high reactivity), their prolonged residence time in the lungs because of mitigated clearance efficiency, and their possible translocation rates across epithelial/endothelial barriers into the blood and lymphatic circulation (Schmid et al., 2009). UFPs derive primarily from combustion processes in urban settings (Cassee et al., 2013) and, in the Lombardy Region, solid biomass burning for residential heating and diesel combustion used for private and public transport represent their major sources (Longhin et al., 2016).

Exposure to PM has been identified as the cause of several health effects including increased hospital admissions, emergency room visits, respiratory symptoms, exacerbation of chronic respiratory and cardiovascular diseases, decreased lung function and premature mortality (Samoli et al., 2008; Halonen et al., 2009; Perez et al., 2012; Kim et al., 2015).

Interestingly, emerging evidences from different studies suggest that neurological diseases, such as AD, PD and stroke, may be strongly associated with ambient PM (Genc at al., 2012). It has been demonstrated that continuous exposure to significant levels of airborne PM may result in the direct translocation of pollutants to different extra pulmonary sites, including central nervous system (CNS), or trigger the release of soluble inflammatory mediators from primary entry organs or secondary deposition sites (Cunningham et al., 2009; Genc at al., 2012). Systemic inflammation could activate cerebral endothelial cells, alter BBB integrity, or trigger signalling cascades that lead to the activation of mitogen-activated protein kinase (MAPK) and Nuclear factor kappa-light-chain-enhancer of activated B cells (NFκB) pathways (Calderón-Garcidueñas et al., 2008; Genc at al., 2012). Notably, post-mortem examinations of adult humans resident in highly polluted urban areas exhibited significantly higher brain COX-2 expression and accumulation of $A\beta_{42}$ when compared to subjects living in cities with low pollution levels (Calderón-Garcidueñas et al., 2004; Genc et al., 2012).

Therefore, the aim of this project was to evaluate the detrimental effect of UFPs exposure, regarding oxidative stress and inflammation, on *in-vitro* and *in-vivo* models of CNS. Moreover, this work meant to investigate the possible physiopathological correlation between these two mechanisms and AD neurodegeneration.

First, we tested the effect of DEP administration on C6 glioma cells, which have properties of both astrocytes (Benda et al., 1968) and oligodendrocytes (Volpe et al., 1975). In fact, glial cells are now recognized as active players in the regulation of synaptic function, neural repair, and CNS immunity (Lee and MacLean, 2015), and astrocytes have been recently linked to neuroinflammatory and neurotoxic pathways induced by PM exposure (Li et al., 2016). We demonstrated that DEP treatment at sub-lethal concentrations induced

oxidative stress in glial cells, while inflammation was not involved. Moreover, we found that C6 glioma cells activate anti-oxidant pathways to contrast the oxidative status induced by DEP treatment and that the MEK-ERK1-2 pathway seems important in regulating these anti-oxidant strategies.

Afterwards, we selected HT22 nerve cell line as a neuronal *in-vitro* model to study the effect of direct DEP administration. We demonstrated that DEP treatment at sub-lethal concentrations induced oxidative stress and inflammation in neuronal cells, supporting the idea that neurons are more sensitive to DEP administration than glial cells. Moreover, we extended the analysis of DEP detrimental effects and we found lipid reshaping in HT22 cells. These mechanisms are supposed to be involved in AD neurodegeneration, and interestingly we observed the alteration of APP and BACE1 protein levels, despite future experiments will be necessary to clarify the role of direct DEP administration to neurons in AD onset.

Finally, we exposed male BALB/c mice to single and repeated Intratracheal instillation of BC and DEP by means of a MicroSprayer® Aerosolizer system. This analysis confirmed the inflammatory and oxidative potential of DEP exposure on mouse brain, which was accompanied by induction of PAHs metabolism and alteration of APP processing after sub-acute exposure. Moreover, BC mice showed activation of the above described mechanisms, although BC resulted generally less effective than DEP in inducing them. Whether this activation is due to the direct transport of UFPs or inflammatory mediators to the brain remains to be investigated.

In conclusion, these findings may contribute to the knowledge of the interplay between PM exposure, the chronic oxidative stress and inflammation generation and the development of neurodegenerative diseases.

CHAPTER 1: INTRODUCTION

AIR POLLUTION AND PARTICULATE MATTER

Particulate matter (PM) is a complex mixture of solid and liquid particles suspended in the air; this suspension, also named aerosol, could be formed by a variety of particles of different size and composition depending on their origin (Marconi, 2003). Traditionally, PM is classified in four major groups, which are dust, smoke, smog or soot, and mists (Marconi, 2003).

Among all, particles size is the most important parameter for the description of their behaviour and origin, whereas chemical composition, removal and residence time in the atmosphere are all characteristics related to particle's size (Marconi, 2003). However, concerning particle size, the term "particle diameter" alone is an over simplification, since the geometric shape of the particles is irregular and does not fully explain how they behave in their airborne state. Therefore, the most appropriate measure of particle size is aerodynamic diameter (d_{ae}, µm), defined as the diameter of a hypothetical sphere of density 1 g/cm^3 having the same terminal settling velocity in calm air as the particle in question, regardless of its geometric size, shape and true density (WHO, 1999). The aerodynamic diameter is strictly related to the ability of the particle to penetrate and deposit at different sites of the respiratory tract, as well as to particle transport in aerosol sampling and filtration devices (WHO, 1999).

Therefore, depending on aerodynamic diameter, particles in the atmosphere (total suspended particles, TSP) are typically divided into three fractions:

- **PM10** contains particles with d_{ae} < 10 µm. PM10 is defined as PM that passes through a size-selective inlet with a 50% efficiency cut-off at 10 µm aerodynamic diameter (Colbeck and Lazaridis, 2010).
- **PM2.5** consists of particles with d_{ae} < 2.5 µm. PM2.5 is defined as PM that passes through a size-selective inlet with a 50% efficiency cut-off at 2.5 µm aerodynamic diameter (Colbeck and Lazaridis, 2010).
- **PM0.1** is composed by particles with d_{ae} < 0.1 µm (Terzano et al., 2010).

Moreover, again according to the aerodynamic diameter, PM can be classified into:

- **Coarse fraction**, which consists of particles with d_{ae} between 2.5 and 10 µm (**Fig. 1**). Essentially, these particles are produced by mechanical processes (grinding, erosion, mechanical or wind resuspension). They contain elements found in soil and marine salts, such as Si, Al, Ca, Fe, Mn, Na, Sr and K. Because their relatively large dimension, these particles sediment in few hours or minutes and they are often found near emission sources as a function of their height (Marconi, 2003).
- **Fine fraction**, which consists of particles with d_{ae} between 0.1 and 2.5 µm (**Fig. 1**). Their formation takes place by coagulation of ultrafine particles (UFPs) and through gas-particle conversion processes, also known as heterogeneous nucleation, or for condensation of gas on pre-existing

particles. The major constituents of these particles in the industrialized areas are sulphates, nitrates and ammonium ion, which are essentially the products of gas particles conversion of sulphur dioxide (SO_2), nitrogen oxides (NO) and ammonia. Moreover, they contain elemental and organic carbon. Different metals in trace deriving from combustion processes represent additional components. This fraction can contain particles of biological origin, such as fungal spores, bacteria, yeast, pollen and viruses. In general, fine particles are too small to settle (by gravity) and too large to coagulate creating larger particles; for this reason they remains in the atmosphere for days and they can be transported over long distances (Marconi, 2003; Kim et al., 2015).

- **Ultrafine fraction**, corresponding roughly to PM0.1 (**Fig. 1**). These particles, also known as Aitken nuclei fraction, have a dimensional range between 0.01 and 0.1 μm and are generally constituted by the products of the homogeneous nucleation of supersaturated vapours (SO_2, NH_3, NO_x and combustion products) (Marconi, 2003; Cassee et al., 2013).

Among these fractions, exposure to PM2.5 and PM0.1 is thought to have the greatest health effects. For example, exposures to ambient PM2.5 have been linked to the development of respiratory infections, asthma onset and exacerbation of pre-existing asthmatic symptoms, and an increased risk of hospitalization in susceptible populations, such as young children and the elderly. Furthermore, exposure to PM0.1 has been correlated with decrements in lung development and function (Chan et al., 2013).

Air Quality Standards have been adopted by many countries around the world to protect public health and welfare against the adverse effects of air pollution. In fact, the World Health Organization (WHO) Environment and Health Information System (ENHIS) includes PM10 monitoring data from urban and suburban background locations and recommends daily PM10 concentrations not to exceed 50 $\mu g/m^3$ (Nemmar et al., 2013). Nevertheless, many countries have chosen to set more relaxed or more stringent Air Quality Standards with respect to the WHO Standards, that are generally created or revised according to national policy and scientific data that demonstrates a plausible association between health problems and exposure to pollutants (Nemmar et al., 2013). Almost 83% of the population living in cities where PM is monitored is exposed to PM10 levels exceeding the WHO air quality guideline levels. Although this proportion remains high, it is an improvement compared to previous years, with average PM10 levels slowly decreasing in most countries in the last decade (WHO, 2013). On the other hand, monitoring of PM10 and PM2.5 is very limited in countries of Eastern Europe, Caucasus and central Asia, with only a small number of monitoring stations in Belarus, Russian Federation and Uzbekistan (WHO, 2013).

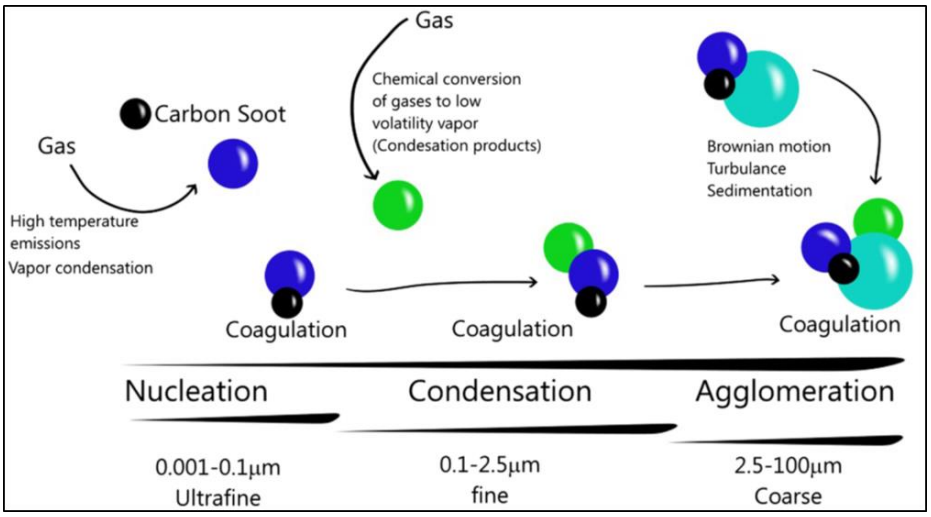

Figure 1: Atmospheric dynamics of particulate matter. The processes of particles formation is composed by three steps that can increase particles size or modify their composition. Nucleation is the first step in new particles generation; it depends on gases concentration, humidity and temperature in the atmosphere, and transition of the gaseous phase to liquid or solid phase by condensation or chemical reaction, forming the first nuclei or particles in the atmosphere. The second step is a condensation of hot gases, originating primary aerosols, an event similar to nucleation. The final step is coagulation, in which whole aerosols formed in previous steps could agglomerate by Brownian motion or turbulence and contact between particles. Consequently, particles grow in aerodynamic size forming secondary particles from primary particles (Falcon-Rodriguez et al., 2016).

ORIGIN OF PM

As mentioned above, the WHO established that PM chemical constituents are various and they include: nitrates, sulphates, elemental and organic carbon, organic compounds (e.g., polycyclic aromatic hydrocarbons), biological compounds (e.g., endotoxin, cell fragments) and metals (e.g., iron, copper, nickel, zinc and vanadium) (WHO, 2013).

Therefore, according to the different origin of the particles, it is possible to distinguish between primary and secondary origin aerosols. The primary aerosols include particles emitted directly into the atmosphere, while secondary particles are formed in the air through chemical reactions between gaseous pollutants; they are products of atmospheric transformation of NO (mainly emitted by traffic and some industrial processes) and SO_2 resulting from the combustion of sulfur-containing fuels, ammonia and non-methane volatile organic compounds. Secondary particles are mostly found in fine PM (Marconi, 2003; WHO, 2013; Kim et al., 2015).

Another system of classification of aerosols refers to natural or anthropogenic sources from which they derive:

- **Natural sources** are represented by sea spray, dust storms, volcanoes, biogenic materials, forest fires, living vegetation and products of natural gas-particle conversions (Marconi, 2003).

- **Anthropogenic sources** are extremely variable and comprise solid-fuel combustion (coal, lignite, heavy oil, and biomass), industrial and agricultural activities, erosion of the pavement by road traffic and abrasion of brakes and tires (Srimuruganandam and Nagendra, 2012).

Despite this classification, it is sometimes difficult to distinguish between natural and anthropogenic sources. For example, smoke from forest fires is often categorized as anthropogenic PM, while mineral dust entrained into the atmosphere from agriculturally eroded regions is considered as a natural source (Colbeck and Lazaridis, 2010). In Europe, anthropogenic sources of aerosols are dominant because of widespread urbanization and the large number of vehicle and combustion sources in both industrial and residential locations (Colbeck and Lazaridis, 2010).

The contributions from the different emission sources to ambient air concentrations depend not only on the amount of pollutant emitted, but also on the proximity to the source, emission conditions (such as height and temperature), and other factors, such as dispersion conditions and topography. Emission sectors with low emission heights, such as traffic and household emissions, generally make a larger contribution to surface concentrations than emissions from high stacks (WHO, 2015).

ULTRAFINE PARTICLES

Exposures to airborne UFPs have been experienced by humans throughout their evolutionary stages, but it is only with the advent of the Industrial Revolution that such exposures have increased dramatically. As discussed above, UFPs are particles with $d_{ae} < 0.1$ μm and they are ubiquitous in the ambient air, both indoor and outdoor, originating from many anthropogenic and natural sources (Oberdörster et al., 2004; Oberdörster et al., 2005). UFPs derive primarily from combustion processes in urban settings (Cassee et al., 2013). Emitted primary UFPs are transformed rapidly due to coagulation, adsorption and secondary particle formation, and they have greater spatial and temporal variability than the fine particle fraction (Cassee et al., 2013). The toxic potential of UFPs on human health is due to different characteristics: their small size, their high surface-to-volume ratio (high reactivity), their prolonged residence time in the lungs because of mitigated clearance efficiency, and their possible translocation rates across epithelial/endothelial barriers into the blood and lymphatic circulation (Schmid et al., 2009). UFPs (mainly soot) represents about 50% of the lung-deposited particle surface area and they might reach vulnerable (secondary) target organs (e.g. heart, liver and brain), therefore contributing significantly to the adverse health effects of ambient PM (Schmid et al., 2009).

In the Lombardy Region, solid biomass burning for residential heating and diesel combustion used for private and public transport are the major sources of fine particles emission, respectively accounting for 56% and 20% to PM2.5 concentration (**Fig 2**). However, these sources mainly produce particles of 15–30 nm in diameter, often aggregated, thus constituting the most relevant contribution to primary UFPs emissions (Zheng et al., 2007; Longhin et al., 2016).

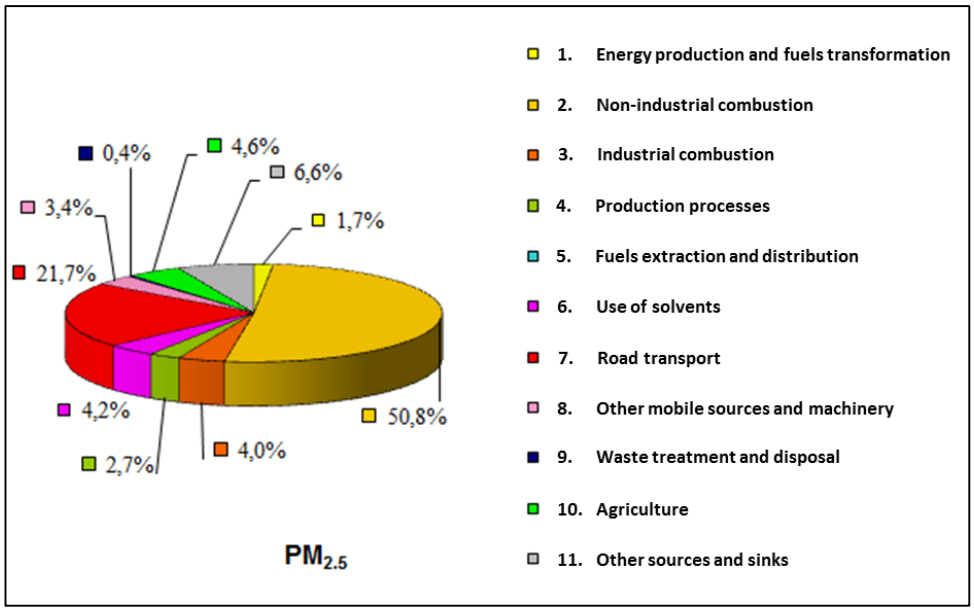

Figure 2: Summary graphs of Lombardy region PM2.5 emissions (Modified from ARPA INEMAR, 2012).

Biomass particles

During the last years the use of biomass burning for residential heating has increased in Northern Italy and elsewhere in Europe due to the lower price of solid biomass fuels when compared to the traditional fossil fuels, combined with the political actions aiming to reduce greenhouse gases (EU Directive, 2009/287/EC). This determined an increased contribution of biomass burning emissions to outdoor and indoor air pollution (Sigsgaard et al., 2015; Longhin et al., 2016). The relatively high PM emission from traditional domestic biomass burning is due to the general low combustion efficiency of appliances and boilers, compared to modern appliances with decreased emissions determined by improved combustion technologies (Sigsgaard et al., 2015; Longhin et al., 2016).

Wood consists primarily of two polymers, that are cellulose (50–70% by weight) and lignin (about 30% by weight) (Simoneit et al., 1998; Naeher et al., 2007); in addition, wood contains small amounts of organic compounds with low molecular weight (e.g., resins, waxes, sugars) and inorganic salts (Naeher et al., 2007). During combustion, pyrolysis occurs and the polymers break apart, producing a variety of smaller molecules. Biomass combustion is typically inefficient, and for this reason it generates a multitude of partially oxidized organic chemicals, many of which have been associated with adverse health impacts (Naeher et al., 2007).

Particles produced by biomass combustion are generally smaller than 1 µm, with a peak in the size distribution between 0.15 and 0.4 µm, and as other combustion mixtures, like diesel and tobacco smoke, it contains a large number of UFPs (Hays et al., 2002; Naeher et al., 2007). These particles are transported over hundreds of kilometres (Andreae et al., 1988). Haze layers with elevated concentrations of CO, carbon dioxide (CO_2), ozone (O_3), and nitric oxide (NO) have been observed. During transport, many of the gaseous species are converted to other gases or into particles. The “black carbon” from biomass emissions is now thought to contribute to regional and global climate change as well as adverse health effects in some parts of the world (Koch & Hansen, 2005; Naeher et al., 2007).

Approximately 5–20% of wood smoke particulate mass consists of elemental carbon, but the composition of the organic carbon fraction varies dramatically with the specific fuel and the combustion conditions (Naeher et al., 2007). In fact, a detailed analysis of organic wood smoke aerosol conducted by Rogge and collaborators in 1998 revealed almost 200 distinct organic compounds, many of them derivatives of wood polymers and resins (Rogge et al., 1998; Naeher et al., 2007). A number of toxic or carcinogenic compounds are present in biomass particles, including free radicals, polycyclic aromatic hydrocarbons (PAHs), and aldehydes (Naeher et al., 2007). Moreover, biomass particulate matter is enriched with several chemicals relative to pollutant mixtures from other sources of air pollution. Examples include potassium, methoxyphenols, levoglucosan, retene, and specific resin acids (e.g., abietic acid) (Rogge et al., 1998; Khalil and Rasmussen, 2003; Naeher et al., 2007).

Significant biomass exposures occur indoors and outdoors in all areas of developed countries, where wood is employed for residential heating and in fireplaces, especially in winter season. Wood smoke often comprises a significant fraction of ambient particle levels in such areas, on both a daily and an annual basis (Naeher et al., 2007). In developing countries, indoors exposures occur at concentrations that can be orders of magnitude greater than those observed in the developed world (Naeher et al., 2007). Wildland fires and agricultural burning can produce enormous quantities of smoke and can affect populated areas. Occupational exposures can be extremely high for wildland firefighters (Naeher et al., 2007).

Regarding toxicology, most available animal studies indicate that exposure to biomass particles results in significant impacts on the respiratory immune system and at high doses can produce long-term or permanent lesions in lung tissues. Not enough is currently known to reliably distinguish the toxicological effects of different types of biomass smoke (e.g., smoke from combustion of wood versus agricultural wastes) and more work in this area is needed to better understand the mechanisms by which adverse effects observed in exposed individuals might occur (Naeher et al., 2007).

Diesel particles

Road traffic generated PM has gained major interest over the last few decades due to its associated detrimental impacts on human health. PM from road vehicles can be generated from exhaust and non-exhaust emission types, like exhaust tailpipe and abrasion of vehicle parts including brakes, clutch and tyres, and re-suspension of dust (Alam et al., 2016). Diesel combustion used for private and public transport is the major source of fine particles road emission, and the increase in diesel engines has led to predictions that this fuel will be the number one transport fuel in the world by 2020 (Alam et al., 2016). In a “perfect” diesel engine, oxygen in the air would convert all the hydrogen in the fuel to water and the carbon into CO_2, while nitrogen in the air would remain unaffected. In reality, the combustion process is not “perfect”, and incomplete combustion results in the emission of CO, unburnt fuel and lubricating oil, and of their oxidation

and nitration products. These incomplete combustion products comprise thousands of chemical components present in the gas and particulate phases (IARC, 1988; Singh and Onkar, 2006) (**Table 1**).

Gas phase
Acrolein
Ammonia
Benzene
1,3-Butadiene
Formaldehyde
Formic acid
Heterocyclics and derivatives*
Hydrocarbons (C,-C'8) and derivatives*
Hydrogen cyanide
Hydrogen sulfide
Methane
Methanol
Nitric acid
Nitrous acid
Oxides of nitrogen
Polycyclic aromatic hydrocarbons and derivatives*
Sulfur dioxide
Toluene
Particulate phase
Heterocyclics and derivatives*
Hydrocarbons (C1rC3S) and derivatives*
Inorganic sulfates and nitrates
Metals (e.g., lead and platinum)
Polycyclic aromatic hydrocarbons and derivatives*

Table 1: Some compounds and classes of compounds in vehicle engine exhaust.
***Derivatives include acids, alcohols, aldehydes, anhydrides, esters, ketones, nitriles, quinones, sulfonates and halogenated and nitrated compounds, and multifunctional derivatives (modified from IARC, 1988).

Diesel exhaust is a complex mixture of solid, condensed (or liquid), and gaseous fractions (Steiner et al., 2016). The solid fraction is represented by diesel exhaust particles (DEP), which have a bio persistent core of about 10–30 nm in diameter composed of elemental carbon (Mazzarella et al., 2007; Liati and Eggenschwiler 2010). These primary particles can then agglomerate to form larger soot aggregates with mean diameters of 60–100 nm (Steiner et al., 2016). In addition, diesel UFPs contain metal and metal-oxides originating from lubrication, fuel additives and engine wear (Steiner et al., 2016). Some metals contained in oils are zinc and magnesium, whereas in fuels there are cerium, iron, manganese, platinum and copper (Mayer et al. 2010).
Importantly, the surface properties of DEP depend largely from toxic compounds adsorbed on particle surfaces (Steiner et al., 2016). In fact, about 18,000 high-molecular-weight organic compounds can be adsorbed on carbonic nucleus of DEP (Mazzarella et al., 2007). During the combustion process, the surfaces of the carbon particles become chemically activated, for example by the partial oxidation of PAHs in quinones, and participate in redox reactions, resulting in the formation of reactive oxygen species (ROS) such as hydrogen peroxide (Steiner et al., 2016). This process is worsened by the action of oxidizing gases and/or photochemical processes, which can also participate in activating particle surface (Steiner et al., 2016). Furthermore, the metals and metal-oxides take part in Fenton-type reactions by which the potency of the ROS is further increased (McWhinney et al. 2013; Antiñolo et al. 2015; Steiner et al., 2016).
The gaseous exhaust fraction consists of more than 99% by volume of non-toxic inorganic gases such as nitrogen, water and oxygen. The remaining part is composed by toxic inorganic gases, such as CO_2, CO, NO

and nitrogen dioxide (NO_2), and by a complex mixture of organic compounds (Steiner et al., 2016). Examples of these organic molecules are methanol, ethylene or formaldehyde, but mainly larger aliphatic compounds and more complex molecules such as benzene, naphthalene, pyrene, anthracene and their various functionalized derivatives, collectively referred to as PAHs, nitrated polyaromatic hydrocarbons (NPAHs) and heterocyclic aromatic compounds (HACs) (Heeb et al. 2010; Vieira de Souza and Corrêa 2015). Sources of these organic components are traces of fuel and lubrication oil that survived combustion, but also compounds that cannot be found in the fuel or oil and that are newly formed from partially combusted precursors (Rhead and Hardy 2003; Steiner et al., 2016). With increasing molecular weight, and depending on their functionalization and the exhaust temperature, organic compounds may not be present as gases but adsorbed onto soot, metal and metal-oxide particles or condense to form particles that together with water droplets comprise the liquid exhaust fraction (Steiner et al., 2016).

Interestingly, although diesel engines produce a minor quantity of CO than gasoline engines, they release 10 times the amount of NO, aldehydes and particles compared to unleaded gasoline engines, and over 100 fold more than catalysed unleaded gasoline engines (Mazzarella et al., 2007).

Acute exposure to diesel exhaust has been associated to irritation of nose and eyes, lung function and respiratory changes, headache, fatigue and nausea. Chronic exposures effects include cough, sputum production and lung function decrements. In addition to symptoms, exposure studies in healthy humans have documented a number of profound inflammatory changes in the airways, before detecting changes in pulmonary function (Sydbom et al., 2001). Notably, in 2012 IARC classified diesel engine exhaust as Group 1 (carcinogenic to humans) based on ‘‘sufficient evidence that exposure is associated with an increased risk for lung cancer’’ (IARC, 2013).

IMPACT OF PM ON HUMAN HEALTH

Exposure to PM has been identified as the cause of several health effects including increased hospital admissions, emergency room visits, respiratory symptoms, exacerbation of chronic respiratory and cardiovascular diseases, decreased lung function and premature mortality (Samoli et al., 2008; Halonen et al., 2009; Perez et al., 2012; Kim et al., 2015). Moreover, scientists have suggested that exposure to high particle levels may also lead to diverse symptoms, including low birth weight in infants, pre-term deliveries and possibly foetal and infant deaths (Kim et al., 2015). Mild problems associated with PM2.5 exposure include shortness of breath (dyspnoea), chest discomfort and pain, and coughing and wheezing (Kim et al., 2015). Recently, Pearson and colleagues found that PM2.5 may contribute to increased diabetes prevalence in the adult U.S. population and that the correlation between adult diabetes and particulate air pollution persists after adjustment for other risk factors like obesity and ethnicity (Pearson et al., 2010; Kim et al., 2015).

Although the impact of air pollution has been analysed mainly with respect to the observable physical damage to human health, another issue to be reckoned with is its economic cost. In fact, PM related illness

could ultimately lead to financial and non-financial welfare losses of patients and their families and of a significant portion of gross domestic product (Hou et al., 2012; Kim et al., 2015). For example, an epidemiological study conducted in China in 2004 calculated that the health effects of pollution caused by PM10 in 111 Chinese cities was approximately US$ 29 billion (Zhang et al., 2008).

To date, it is recognised that the effect of exposure to PM on human health is greatly influenced by local conditions such as weather, seasons, topography, sources of particles, concentrations of emission and microenvironments (Kim et al., 2015). In this context, in addition to the physical characteristics of individual persons, the size of particles in considered the main cause of health problems (Brown et al., 2013; Kim et al., 2015). Indeed, the smaller a particle is, the more deeply it will penetrate in the respiratory tract. In nasal-breathing, the cilia and the mucus act as a very effective filter for most particulates exceeding 10 µm in diameter, whereas particles with $d_{ae} \leq 10$ µm have the most impact on human health, because they can penetrate within the respiratory tract and reach the alveoli (Londahl et al., 2007; Kim et al., 2015).

Most sampling conventions have been defined in terms of particle penetration into respiratory regions. The size plays an important role in human airways because it will define the deposition site in the lung. The deposition of aerosol in the human lung occurs through a combination of inertial impaction, gravitational sedimentation and Brownian diffusion (Falcon-Rodriguez et al., 2016). Therefore, the European Committee for Standardization (CEN) adopted these specific definitions (Brown et al., 2013):

- **Inhalable fraction**, the mass fraction of total airborne particles that is inhaled through the nose and mouth.
- **Extrathoracic fraction**, the mass fraction of inhaled particles failing to penetrate beyond the larynx.
- **Thoracic fraction**, the mass fraction of inhaled particles penetrating beyond the larynx.
- **Respirable fraction**, the mass fraction of inhaled particles penetrating to the unciliated airways.

In the specific, particles between approximately 5 and 10 µm are most likely deposited in the tracheobronchial tree, while those between 1 and 5 µm are deposited in the respiratory bronchioles and the alveoli, where they can affect gas exchange (Londahl et al., 2007; Kim et al., 2015) (**Fig 3**). Eventually, these particles will escape into the bloodstream to cause significant health problems (Kim et al., 2015) (**Fig 3**). Particles smaller than 1 µm in general behave similar to gas molecules and will therefore penetrate down to the alveoli (deposition by diffusion forces), and can translocate further into the cell tissue and/or circulation system (Kim et al., 2015).

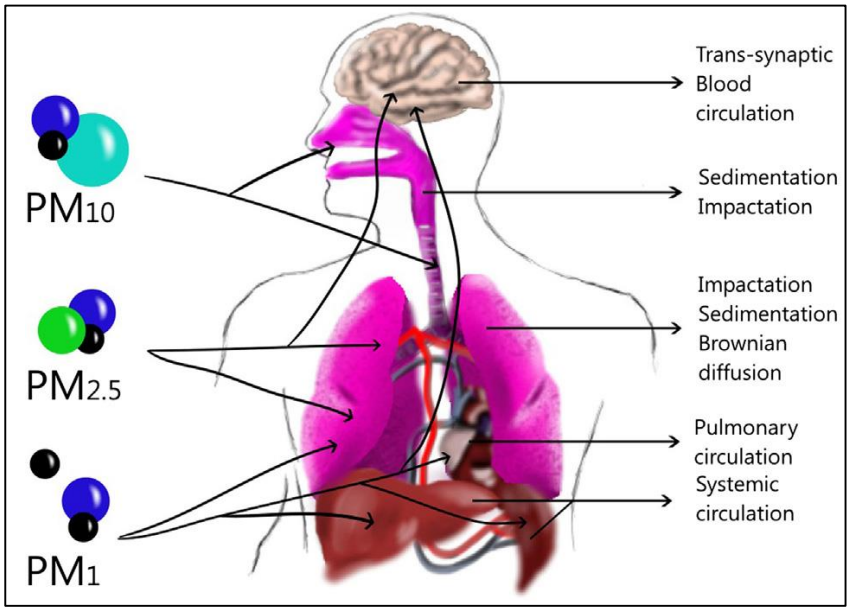

Figure 3: Size and Dynamic of particles in the lung and other tissues (Falcon-Rodriguez et al., 2016).

During the last 15 years, evidence has linked surface area, reactivity, and different components of the particles with their toxicity (Happo et al., 2010; Nemmar et al., 2013).

Among all components that are present in PM, biological components seem to play a central role in biological effects, as in lungs they are responsible for stimulating alveolar macrophages (AMs) and respiratory epithelial tissue to release pro-inflammatory cytokines and chemokines, and they may also have synergetic effects with other components of the PM (Nemmar et al., 2013). The biological components may be released by passive or active mechanisms from plants, soil, biofilms, solid or liquid sources to become suspended in the air. Because of their size, airborne biological particles or dust containing biological agents are important components of the coarse and fine PM. They represent about 1–4% of the total mass of PM10 for urban and rural areas and their general indication can be obtained by measuring the protein associated with PM (Nemmar et al., 2013). Endotoxin lipopolysaccharides (LPSs) represent an example of pro-inflammatory compounds from microbial origin present in PM. LPS is a component of the cell wall of Gram negative bacteria, and when it is resuspended in the air and inhaled, it stimulates AMs and respiratory epithelial tissue to release cytokines/chemokines, initiating an inflammatory cascade (Nemmar et al., 2013).

Recently, the International Agency for Research on Cancer (IARC) classified outdoor air pollution as a group I carcinogen (IARC, 2013). PAHs and metals contained in PM represent both strong mutagenic and carcinogenesis agents, and they have been associated to genetic damage, which may increase the frequency of human cancer (Gilli et al., 2007; De Oliveira Galvão et al., 2014; Falcon-Rodriguez et al., 2016). PAHs are a large group of organic compounds with two or more fused aromatic (benzene) rings and represent important component of PM. Exposure to diesel particles can induce DNA single-strand break, producing 8 hydroxyguanine, which cause DNA adducts by oxidation (Vineis and Husgafvel-Pursiainen, 2005). Moreover, the formation of DNA adducts is generated by CYP1A1 and GSTM1 PAHs metabolism (Vineis and Husgafvel-Pursiainen, 2005). Some reports have mentioned that in vivo exposure to PAHs increases the rate of

chromosome aberration, and micronuclei in lymphocytes (Falcon-Rodriguez et al., 2016). Furthermore, there is evidence that PAHs can generate deletion of an arm of the chromosomes, as well as K-ras and P53 mutations, the principal oncogene and tumor suppressor, respectively (Vineis and Husgafvel-Pursiainen, 2005; Falcon-Rodriguez et al., 2016).

In addition, metals contained in PM act as possible mediators of airway injury and inflammation through the Fenton reaction (Diociaiuti et al., 2001; González-Flecha, 2004; Kim et al., 2015), which refers to the reaction between hydrogen peroxide and ferrous salts to produce reactive species capable of oxidising a wide variety of organic substrates (Winterbourn, 1995). It has been demonstrated that iron, and other transition metals present in particles, increase the production of reactive oxygen species (ROS) *in-vivo*, which can result in cellular and tissue damage, and thus in initiation or exacerbation of inflammatory processes (Kadiiska et al., 1997; Kim et al., 2015). In addition, the content of these metals can be held responsible for the genotoxic effects attributed to PM.

EFFECTS OF PM ON RESPIRATORY SYSTEM

PM exerts its lung effects because it easily deposits on bifurcations or angle ramifications of the bronchial tree due to airflow and turbulence, increasing its interaction with the mucous membrane through an impact process (Falcon-Rodriguez et al., 2016). Once deposited in a particular region of the lung, PM can penetrate in or be absorbed onto the mucous layer, generating local damage (Zhang et al., 2001; Falcon-Rodriguez et al., 2016). However, despite numerous studies completed so far, the precise mechanism by which PM may influence health and lung function is unknown. Studies have suggested that PM could mediate adverse health effects via the generation of ROS, activation of cell signalling pathways and alterations of respiratory tract barrier function and antioxidant defences, all of which may lead to airway inflammation and changes in pulmonary function (Paulin and Hansel, 2016). Moreover, PM can increase cellular permeability and reduce the mucocilliary activity by ROS production and cytokine releases (Falcon-Rodriguez et al., 2016). Finally, cellular changes resulting from PM exposure may cause epigenetic modifications, leading to alterations in gene expression (Falcon-Rodriguez et al., 2016).

Since 1980, many reports have mentioned that exposure to PM increases cancer and death. It is well known that exposure to PM cause pulmonary diseases such as Chronic obstructive pulmonary disease (COPD), asthma, and fibrosis (Jones and Richeldi, 2014; Falcon-Rodriguez et al., 2016). Older adults and children or people with lung disease are subject to much stronger risk from particles than other people are (Paulin and Hansel, 2016). Exposure to PM was reported to affect lung development in children, including reversible and long-term deficits in lung function and chronically reduced lung growth rate (Brauer et al., 2012; Kim et al., 2015).

EXTRA PULMONARY EFFECTS OF PM

Nowadays, it has been established that PM can reach and act on different extra pulmonary organs and tissues, and there are four primary hypotheses that are under investigation to explain this phenomenon (Nemmar et al., 2013):

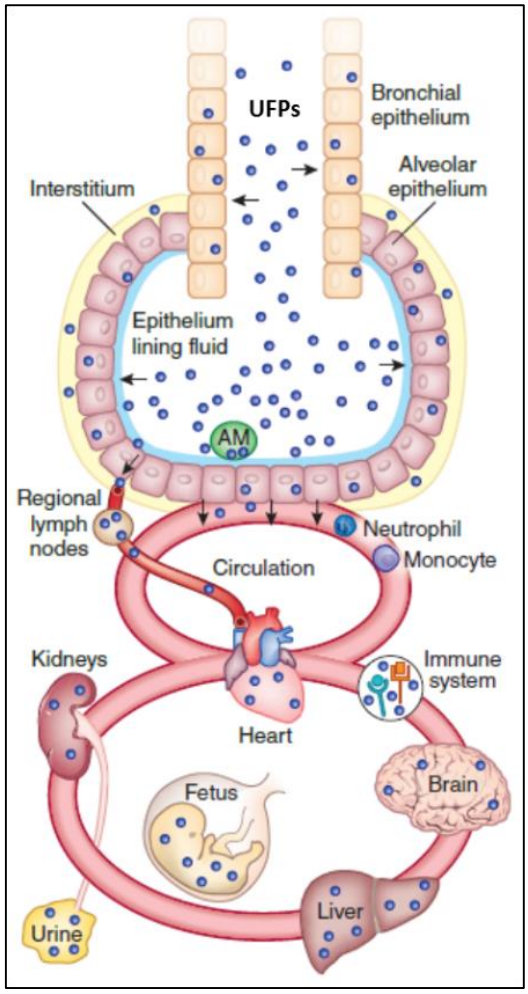

1. UFPs, owing to their small size, could avoid normal phagocytic defences in the respiratory system and gain access to the systemic circulation and therefore to different extra pulmonary sites (Nemmar et al., 2002; Wallenborn et al., 2007; Genc at al., 2012) (**Fig 4**). In humans, the literature on UFPs translocation is still conflicting and the amount of UFPs that translocate into blood and extra pulmonary organs differed between the various studies (Takenaka et al., 2001; Kreyling et al., 2002; Elder et al., 2006; Wallenborn et al., 2007). However, given the deep penetration of nanoparticulate matter into the alveoli and close apposition of the alveolar wall and capillary network, particle translocation seems plausible either as a naked particle or after ingestion by AMs (Geiser et al., 2005). Naked particles have been reported to be taken up by erythrocytes and can presumably be distributed to various organs (Nemmar et al., 2012).

Figure 4: Schematic representation of UFPs translocation from the lung epithelium to regional lymph nodes and blood circulation (Modified from Kreyling et al., 2010).

2. Inhaled particles may affect the cardiovascular system through inflammatory mediators produced in lungs as a consequence of chronic pollutant-induced epithelial and endothelial injury and released into the circulation. These mediators can be IL-6, TNFα or histamine, and oxidative stress products (Oberdörster et al., 2005; Genc at al., 2012).
3. Particles have the ability to affect the autonomic nervous system through mechanisms that may involve activation of pulmonary neural reflex arcs and direct effects of pollutants on cardiac ion channels. In this context, the exposure to particulate air pollution favours sympathetic nervous system activation and parasympathetic withdrawal, leading to changes in the pattern of breathing and heart rate (Seaton and Donaldson, 2005).

4. UFPs can reach the central nervous system (CNS) through the olfactory mucosa, which is a neuronal epithelium that is in direct contact with the environmental air (Elder et al., 2006; Wang et al., 2007; Genc et al., 2012). Olfactory receptor neurons are bipolar sensory neurons that mediate the sense of smell by carrying sensory information from the nose to the CNS. These neurons extend their dendrites into the mucous layer covering the olfactory epithelium where they directly interact with odorants inhaled with the air (Genc et al., 2012). Nasally inhaled pollutants that reach the olfactory mucosa could enter the cilia of olfactory receptor neurons by pinocytosis, simple diffusion, or receptor-mediated endocytosis. Once incorporated into sensory neurons, they could be transported by slow axonal transport along the axons to the olfactory bulb (Illum, 2004; Genc et al., 2012) (**Fig 5**). From there, pollutants could be transported further into the CNS along mitral cell axons that project from the olfactory bulb to multiple brain regions, including olfactory cortex, anterior olfactory nucleus, piriform cortex, amygdale, and hypothalamus (Genc et al., 2012).

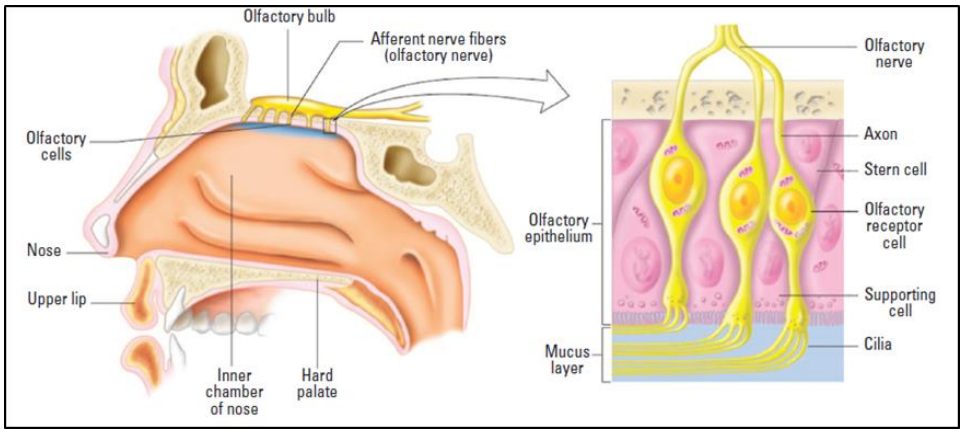

Figure 5: Close proximity of olfactory mucosa to olfactory bulb of the CNS (Oberdörster et al., 2005).

In the past 15 years, numerous studies have demonstrated that translocation of UFPs play a significant role in several cardiovascular diseases. PM has been related to an increased risk of hospital admission for myocardial infarction among the elderly and exacerbation of congestive heart failure (Wellenius et al., 2005; Dominici et al., 2006; Kim et al., 2015). Sun and collaborators in 2010 also suggested a possible association between changing PM levels and transient increases in plasma viscosity, acute-phase reactants, endothelial dysfunction, and altered autonomic control of the heart (Sun et al., 2010). Moreover, the effective role of PM in increased cardiac risk is also explained by initiation and progression of atherosclerosis, which is responsible for most cardiovascular diseases (Suwa et al., 2002; Kim et al., 2015). Finally, PM has been associated to Type 2 diabetes mellitus and obesity (Sun et al., 2010; Cui et al., 2016).

Liver represent another vulnerable target organ since its microvasculature allows ready access to hepatocytes. Direct effects of UFPs on hepatocytes include the induction of oxidative stress and DNA strand breaks. In addition, airborne pollutants contribute to the pathogenesis of steatohepatitis by alteration of lipid metabolism and induction of a pro-inflammatory milieu (Kim et al., 2014).

Recent findings supported the hypothesis that long-term PM2.5 exposure negatively affects renal function and increases renal function decline (Mehta et al., 2016), and it is associated to an increased risk for membranous nephropathy, especially at a high level of exposure (Xu et al., 2016). Moreover, Nemmar and collaborators demonstrated that prolonged pulmonary exposure to DEP worsen renal oxidative stress, inflammation and DNA damage in mice with adenine-induced chronic renal failure (Nemmar et al., 2016).

Effects of PM on the central nervous system

About a decade ago, the CNS has been proposed to be a target organ for the detrimental effects of airborne pollutants (Oberdörster and Utell, 2002). Certainly, emerging evidence from epidemiological, observational, clinical, and experimental studies suggests that different neurological diseases, such as Alzheimer's disease (AD), Parkinson's disease (PD), and stroke, may be strongly associated with ambient air pollution (Genc at al., 2012). As mentioned above, continuous exposure to significant levels of airborne UFPs, PM, and LPS may result in the direct translocation of these pollutants to different extra pulmonary sites, including CNS, or trigger the release of soluble inflammatory mediators from primary entry organs or secondary deposition sites (Genc at al., 2012) (**Fig 6**).

The first histopathological evidence for a link between air pollution and neuropathology came from studies conducted by Calderón-Garcidueñas and collaborators on animal populations that were naturally exposed to polluted urban environments in Mexico City (Block and Calderón-Garcidueñas, 2009). Using light and electron microscopy, they reported significant inflammatory and neurodegenerative changes in the olfactory mucosa, the olfactory bulb as well as in subcortical and cortical structures in otherwise healthy mongrel canines, whereas similar changes were not evident in control groups inhabiting less-polluted rural areas (Block and Calderón-Garcidueñas, 2009; Genc et al., 2012).

Nowadays, we know that mechanistically air pollution may affect the CNS through a variety of cellular, molecular, and inflammatory pathways that directly damage brain structures or lead to a predisposition to neurological diseases (Genc at al., 2012). UFPs that reach the circulation could directly affect vascular endothelium cells by creating local oxidative stress or causing pro-inflammatory effects that, together with inflammatory mediators produced in the respiratory tract, can lead to systemic inflammation (Cunningham et al., 2009; Genc at al., 2012). This process is attended by the production of pro-inflammatory cytokines that could activate cerebral endothelial cells, alter the blood-brain barrier (BBB) integrity, or trigger signalling cascades that lead to the activation of mitogen activated protein (MAP) kinase, and nuclear factor kappa B (NFκB) transcription factor-mediated pathways. Alteration of the BBB could then be followed by trafficking of mast cells and inflammatory cells expressing CD163, CD68, and HLA-DR to the damaged site (Calderón-Garcidueñas et al., 2008; Genc at al., 2012). In addition, circulating cytokines that are released by inflamed peripheral organs or endothelial cells could stimulate peripheral innate immune cells, activate peripheral neuronal afferents, or enter the brain by diffusion and active transport thus worsening the condition (Genc

at al., 2012). Moreover, airborne LPS may induce neuroinflammatory responses directly by activating the brain's innate immune system (Tracey, 2009; Genc at al., 2012).

Interestingly, post-mortem examinations of adult humans resident in highly polluted urban areas of Mexico City exhibited significantly higher cyclooxygenase enzyme 2 (COX-2) expression in olfactory bulb, hippocampus, and frontal cortex, and greater neuronal accumulation of $A\beta_{42}$ when compared to age-, gender-, and education-matched subjects from cities with low pollution levels (Calderón-Garcidueñas et al., 2004; Genc et al., 2012). Moreover, a recent post-mortem study on children and young adults who died suddenly has shown that lifelong exposure to air pollution is associated with neuroinflammation, altered innate immune responses, alteration of the BBB, endothelial activation, and accumulation of disease proteins (Aβ42 and α-synuclein) in the CNS (Calderón-Garcidueñas et al., 2008; Genc et al., 2012).

Finally, animal studies have shown region specific inflammation and alterations in gene expression after DEP exposure, suggesting a selective vulnerability of specific neuronal subpopulations similarly to the selective loss of specific neurons that is typical for certain neurodegenerative diseases (Van Berlo et al., 2010; Gerlofs-Nijland et al., 2010; Genc et al., 2012).

Even though the translocation rate of UFPs from their site of entry to secondary organs might be rather low, continuous or chronic exposure to air pollution may result in the accumulation of toxic molecules in the brain as a secondary target organ in significant amounts (Oberdörster et al., 2009; Genc et al., 2012). No data on brain UFPs elimination are available yet, but they could be transferred from the CSF to the blood circulation through arachnoid vili or via the nasal lymphatic system (Oberdörster et al., 2009; Genc et al., 2012).

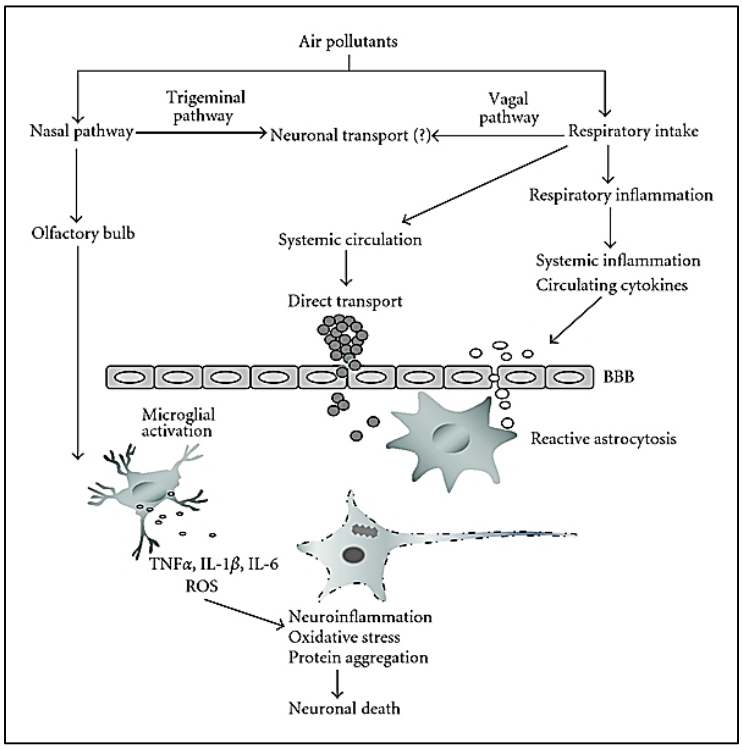

Figure 6: The multiple pathways by which UFPs can reach and affect the brain (Genc et al., 2012).

ALZHEIMER DISEASE

Alzheimer's disease (AD) is one of the most common neurodegenerative disease and it is characterized by deterioration in cognition and memory, progressive impairment in the ability to carry out activities of daily living, and a number of neuropsychiatric and behavioural symptoms (Jalbert et al., 2008; Anand et al., 2014; Kumar et al., 2015; Pająk et al., 2016). AD accounts for more than 80% of dementia cases worldwide in elderly people. Epidemiological data indicate that in USA over 5.5 million people are affected by AD and it is estimated that worldwide there are about 24 million of victims. The incidence of AD is proportional to the age of the population and it is expected that in 2040 the number of people affected by AD could double, since the average age of the population is increasing both in industrialized countries and in developing ones (Mayeux and Stern, 2012; Jalbert et al., 2008).

The neuropathological features of AD are:

5. Extracellular neuritic plaques. They consist of a central core of beta amyloid (Aβ) peptides clumped together with fibrils of Aβ, dystrophic neurites, reactive astrocytes, phagocytic cells, and other proteins and protein fragments derived from degenerating cells or liberated from neurons (Jalbert et al., 2008). The accumulation of Aβ observed in AD brains may be the result of faulty Aβ clearance, cleaving of the amyloid precursor protein (APP) by enzymes to yield free Aβ peptides, or overproduction of Aβ peptides caused by mutations in APP or presenilins genes or in the presence of the APOE ε4 genotype. Aβ fibrils aggregate and form neuritic plaques, triggering a locally induced, non-immune-mediated, chronic inflammatory response involving microglial cell activation and stimulation of a cerebral acute-phase reaction (Jalbert et al., 2008). Activated microglial cells release potentially neurotoxic pro-inflammatory cytokines (e.g., interleukin-6), ROS and nitrogen species (RNS), and proteolytic enzymes that may exacerbate neuronal damage (Jalbert et al., 2008).
6. Intracellular neurofibrillary tangles (NTFs). They consist of insoluble aggregates of tau protein that alter the structure and functionality of the cytoskeleton. While under normal conditions tau binds and stabilizes microtubules in axons, several studies indicate that, under pathological conditions, tau becomes hyperphosphorylated. This phenomenon causes the detachment of tau from microtubules, and promotes the formation of insoluble tau aggregates, thus leading to the occurrence of paired helical filaments and NFTs typical of AD brains. Consequently, microtubules are degraded and lost, causing loss of neuronal function (Di Paolo and Kim, 2011).
7. Congophilic angiopathy. It is also known as cerebral amyloid angiopathy (CAA) and consists of extracellular deposition of $A\beta_{42}$ and $A\beta_{40}$ in the cerebral blood vessels. These plaques can be visualised through Congo Red coloration (Claeysen et al., 2012; Sagare et al., 2012; Kumar et al., 2015).

Interestingly, the idea that Aβ and phosphorylated tau are pathologic molecules is slowly changing, and it appears that they represent a cellular adaptive strategy to oxidative stress. Apart from them, various deranged mechanisms such as chronic oxidative stress, mitochondrial dysfunction, hormone imbalance,

inflammation, mitotic dysfunction, calcium mishandling, and genetic components play a role in the AD onset and progression. Although the mechanisms are diverse, neuronal death represents a common denominator that results in AD (Anand et al., 2014).

APP: synthesis, maturation and processing

APP is a transmembrane glycoprotein, synthesized on three different templates (APP695, APP751, and APP770) which resulted from alternative splicing of its transcript (Kang et al., 1987). After its synthesis on polysomes, APP undergoes different post translational modification in endoplasmic reticulum (ER) and Golgi apparatus, like N-glycosylation, phosphorylation, and sulphonation (Pająk et al., 2016). Great deal of mature APP protein is stored in Golgi and trans-Golgi network (TGN), while approximately 10% of APP is transported by kinesins in TGN vesicles or in elongated tubular structures along microtubules in soma, dendrites, and axons (Kamal et al., 2001). APP glycoprotein inserted in plasma membrane can be processed or internalized via endocytosis. Endosomic APP and its processed fragments can return to plasma membrane, be proteolytically degraded in the lysosome or transported from early endosome to TGN (Pająk et al., 2016).

APP695 is the most prevalent isoform in neurons. In membrane, APP is recognised by a family of enzymes called secretase, which work in pairs and make proteolytic cleavage on specific amino acid sequences. If this cleavage is mediated in turn by α-secretase and γ-secretase the processing is defined non-amyloidogenic, while the combined action of β-secretase and γ-secretase give rise to amyloidogenic processing of APP with Aβ peptide production (Claeysen et al., 2012; Pająk et al., 2016) (**Fig 7**). Given that different isoforms of the protein involved in amyloidogenic processing of APP exist, several Aβ peptides ($A\beta_{37–43}$) can be generated, with $A\beta_{40}$ and $A\beta_{42}$ being predominant species (Claeysen et al., 2012; Pająk et al., 2016). $A\beta_{42}$ is not soluble and therefore tend to aggregate to form oligomers and, in the extracellular environment, fibrils and senile plaques (Claeysen et al., 2012; Pająk et al., 2016).

In brain physiological conditions, the balance between α-secretase and β-secretase activities favour the α-secretase. Thus, the Aβ amount produced results not harmful for the normal functioning of nerve networks (Claeysen et al., 2012). With aging, and for reasons yet to be defined, this balance become altered and increases the frequency of the amyloidogenic processing of APP, which leads to the inability of the system to metabolize $A\beta_{42}$ peptide and promotes the pathological formation of aggregates and senile plaques (Claeysen et al., 2012). Amyloidogenic processing of APP occurs preferentially in endosomes, both early and late, but can also take place at the level of the ER, in the TGN or on the cell membrane; in all these compartments it is, in fact, also expressed the γ-secretase (Sathya et al., 2012).

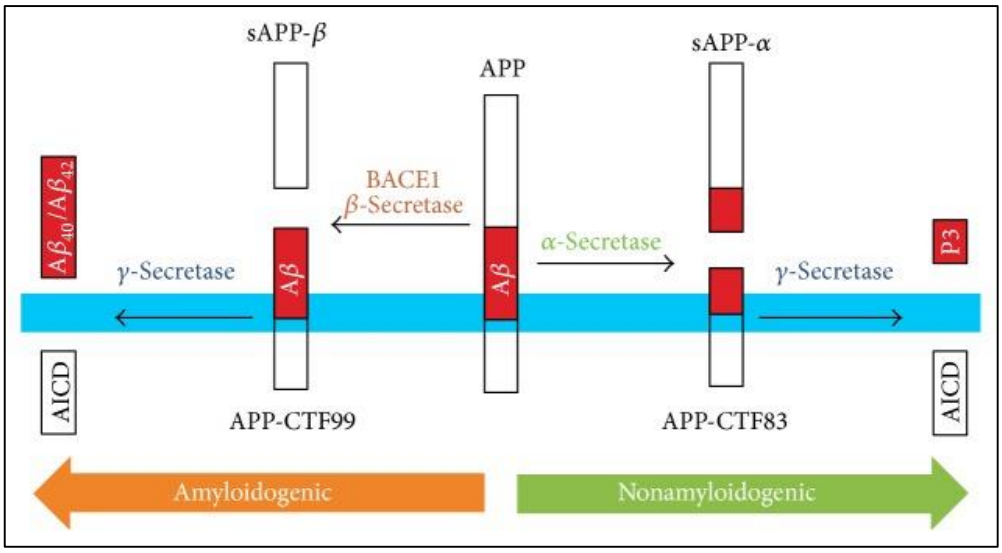

Figure 7: Diagram of APP processing pathway. Transmembrane APP can be processed by two pathways: the non-amyloidogenic α-secretase pathway and the amyloidogenic β-secretase pathway. In the non-amyloidogenic pathway, α-secretase cleaves in the middle of the Aβ region to release the soluble APP-fragment sAPP-α. The APP C-terminal fragment 83 (APP-CTF83, αCTF) is then cleaved by γ-secretase to release the APP intracellular domain (AICD) and P3 fragment. In the amyloidogenic pathway, β-secretase cleaves APP to produce the soluble fragment sAPP-β. APP-CTF99 (βCTF) is then cleaved by γ-secretase to produce $Aβ_{40}$, $Aβ_{42}$, and AICD (Pająk et al., 2016).

BACE1

BACE1 (β-site Amyloid precursor protein-Cleaving Enzyme) is the β-secretase responsible for amyloidogenic processing of APP and consequent Aβ production in the brain (Claeysen et al., 2012; Sathya et al., 2012; Pająk et al., 2016).

BACE1 is a transmembrane protein with N-terminal cytoplasmic tails that contains sorting signals, required for proper intracellular trafficking, and appears to be associated with lipid rafts in a cholesterol-dependent way (Sathya et al., 2012). The dimerization of BACE1 and its localization in lipid rafts require palmitoylation, a post-translational modification. In this portion of the membrane, BACE1 is further stabilized by interacting with proteins that possess the GPI anchor and become able to participate to APP processing (Vetrivel et al., 2009; Sathya et al., 2012).

BACE1 catalytic site contains two aspartate residues (Asp), which are essential for its enzymatic activity, and it is exposed to extracellular ambient or to the lumen of organelles where acid pH (around 5) is optimal for its activity (Sathya et al., 2012).

Furthermore, the C-terminal portion of BACE1 possesses a Leu-Leu domain that, by altering the topography of the membrane, allows the internalisation of the BACE1/APP complex and the formation of an endosome, where predominantly occurs the amyloidogenic cleavage of APP (Sathya et al., 2012). From the endosome,

BACE1 can return in plasma membrane directly or through the TGN, or can be directed to the lysosome where it is degraded (Zhou et al., 2004).

BACE1 activity is present in the majority of cells and tissues of the body, while maximal activity is found in neural tissue and neuronal cell lines (Claeysen et al., 2012; Sathya et al., 2012). Interestingly, astrocytes exhibit less BACE1 activity than neurons (Sathya et al., 2012). On the contrary, α-secretase cleavage of APP is highly active in non-neuronal cells (Claeysen et al., 2012).

BACE1 has been shown to have higher activity in the brains of AD patients compared to healthy subjects, in agreement with the great amount of $A\beta_{42}$ that has been found. On the contrary, the comparative analysis of BACE1 transcription and expression levels provided ambiguous results. In fact, some studies do not show significant changes in transcript levels in the AD brains, while others indicate an increased expression of the protein even if not comparable with the increase of activity previously described. Therefore, it is clear from many studies that increased BACE1 enzyme activity in AD is not reflected by equal increases in BACE1 protein levels (Stockley and O'Neill, 2008). Moreover, these observations suggest the existence of regulatory mechanisms not related to BACE1 expression, such as the subcellular localization, the membrane microdomains and post-translational modifications (Stockley and O'Neill, 2008).

Alzheimer disease and oxidative stress

Oxidative stress is a condition induced by an imbalance in the redox state, that can result from high production of free radicals or by a decrease in antioxidants defences usually present in cell, such as vitamin E, glutathione, catalase and superoxide dismutase. Thus, this condition is characterized by excessive levels of ROS that can result in tissue damage (Markesbery, 1999; Huang et al., 2016).

Brain is particularly vulnerable to free radical attacks. In fact, the brain membrane phospholipids are composed of polyunsaturated fatty acids, susceptible to peroxidation, and the brain itself requires a high consumption of oxygen for its metabolism (Halliwell, 1992; Huang et al., 2016). Consequently, oxidative stress on nervous tissue may seriously damage the brain via several interacting mechanisms, including an increase in intracellular free Ca^{2+}, release of excitatory amino acids, and neurotoxicity (Halliwell, 1992; Huang et al., 2016). Other important sources or modulators of oxidative stress include NO and peroxynitrite, which can be extremely reactive with proteins, lipids, nucleic acid and other molecules leading to detrimental effects for the brain (Lee et al., 2004; Huang et al., 2016).

An increase of the damage caused by oxidative stress to cellular components has been definitely associated to different neurodegenerative disease, including AD (Markesbery, 1999; Halliwell, 2001; Huang et al., 2016). The typical accumulation and precipitation of proteins that occur in these pathologies can be intensified by oxidative damage, and in turn they can increase brain oxidative stress by interfering with the function of the proteasome. It has been demonstrated that inhibition of the proteasome increases the oxidation levels of proteins and other biomolecules (Halliwell, 2001). The oxidative damage observed in AD brain is associated with the abnormal marked accumulation of Aβ and the deposition of neurofibrillary tangles (Christen, 2000).

In addition, protein oxidation by free radicals may be significant in AD as it can affect enzymes critical to neuron and glial functions. This is the case for glutamine synthetase and creatine kinase, two enzymes particularly sensitive to oxidative modification, that are markedly reduced in AD brains (Butterfield et al., 1997), reflecting the alteration of glutamate concentrations and enhancement of excitotoxicity, and decreased energy metabolism, respectively (Moreira et al., 2005; Huang et al., 2016). Furthermore, brain oxidation can affect DNA, producing strand breaks, sister chromatid exchange, DNA-protein crosslinking, and base modification (Cooke et al., 2003; Huang et al., 2016).

Alzheimer disease and inflammation

Inflammation is a response that aim to eliminate both the initial cause of cell injury as well as the necrotic cells and tissues resulting from the original insult. If tissue health is not restored, inflammation becomes a chronic condition that continuously erodes the surrounding tissues (Rubio-Perez and Morillas-Ruiz, 2012).

Chronic brain inflammation is a pathological hallmark of AD and clearly occurs in pathologically vulnerable regions of the brain because of microglia, astrocytes, and neurons inflammatory reaction that increased expression of acute phase proteins and pro-inflammatory molecules (Finch and Morgan, 2007). Example of such inflammatory mediators are pro-inflammatory cytokines, chemokines, prostaglandins, leukotrienes, thromboxanes, coagulation factors, ROS (and other radicals), NO, complement factors, proteases, protease inhibitors, pentraxins, and C-reactive protein (Rubio-Perez and Morillas-Ruiz, 2012).

The idea is that Aβ plaques, soluble Aβ species, neurofibrillary tangles and pro-inflammatory molecules constitute a stressful microenvironment that activates quiescent microglia (Thériault et al, 2015). Amoeboid activated microglial cells can adopt two main phenotypes that coexist in Alzheimer's disease brain: M1 classically activated microglia (AM1) and M2 alternatively activated microglia (AM2). The switch between these two extreme phenotypes is influenced by age and disease progression. The AM1 phenotype is involved in Aβ phagocytosis and pro-inflammatory actions, such as secretion of cytokines/chemokines within the brain parenchyma. The AM2 phenotype is also involved in Aβ phagocytosis, but in contrast they have anti-inflammatory actions, including damaged tissue repair and remodelling, and cytokine/chemokine production (Thériault et al, 2015). Moreover, circulating monocytes are mobilized by brain-derived inflammatory signals; they adhere to brain endothelium, infiltrate brain parenchyma and differentiate macrophages. Perivascular macrophages could contribute to parenchymal Aβ deposit elimination via an efficient Aβ species clearance at the BBB (Thériault et al, 2015). Inflammatory mediators secreted by microglial cells and astrocytes contribute to neuronal dystrophy. Furthermore, chronically activated glia can kill adjacent neurons by releasing highly toxic products, which in turn enhance APP production and its amyloidogenic processing (Rubio-Perez and Morillas-Ruiz, 2012). Moreover, these conditions also inhibit the formation of soluble APP fraction that has a neuronal protective effect (Rubio-Perez and Morillas-Ruiz, 2012). On the other hand, Aβ induces the activation of the complement cascade, the induction of inflammatory enzyme systems such as

the inducible nitric oxide synthase (iNOS) and COX-2, as well as the already mentioned expression of pro-inflammatory cytokines (Rubio-Perez and Morillas-Ruiz, 2012). Several lines of evidence suggest that all of these factors can contribute to neuronal dysfunction and cell death, either alone or in concert (Rubio-Perez and Morillas-Ruiz, 2012).

Alzheimer disease and particulate matter exposure

Almost all neurodegenerative disorders possess a relatively minor genetic element and a larger idiopathic component, in which is it possible to find low but pervasive levels of toxic materials present in the environment (Bondy, 2016). A significant range of chemicals has been proposed to contribute to the initiation or progression of AD. These include excess levels of several metals, like aluminium, copper, lead and mercury (Becaria et al., 2006; Maloney et al., 2012), which are contained in PM. Air pollution derived organic compounds that may be implicated in AD pathogenesis include bisphenol A, phthalates and PAHs such as dioxins and polychlorinated biphenyls. These lipophilic compounds can cross the blood brain barrier, are only slowly metabolized and eliminated and thus can gradually accumulate to reach neurotoxic levels (Bondy, 2016).

A deeply examined example is DEP, which activates and primes microglia leading to neuroinflammation and dopaminergic neurotoxicity (Levesque et al., 2011). Small nanoparticles derived from DEP reach the olfactory bulb by their nasal depositions. The combination of such effects with normal aging may lead to the early onset of different neurodegenerative diseases (Bondy, 2016).

Furthermore, ambient factors can also influence brain aging by way of the endocrine system. Glucocorticoids are adrenal hormones secreted in response to stress and have valuable anti-inflammatory properties, but their prolonged presence has a generally adverse effect. In fact, extended glucocorticoid or corticotrophin administration releasing hormones exacerbate AD-like cognitive and neuropathological changes in experimental animals (Joshi et al., 2012). Interestingly, the hippocampus is selectively vulnerable to such endocrine stress-related damage due to its high density of glucocorticoid receptors (Frodl and O'Keane, 2013). Recently, it has been shown that inhalation of particulate matter or ozone activates the hypothalamic-pituitary-adrenal axis in rats and increases plasma levels of the glucocorticoid corticosterone (Thomson et al., 2016).

Finally, epidemiological evidences showed a correlation between air pollution and neuroinflammation, oxidative stress and neuropathology in young urban residents. For example, 40% percent of children and young adults exposed to polluted urban air exhibit frontal tau hyperphosphorylation and 51% have amyloid-β diffuse plaques compared to 0% in low pollution controls. In similarly exposed adults, elevated levels of inflammatory and oxidative markers are correlated with greater cortical atrophy than the expected value for their age (Calderón-Garcidueñas et al., 2008; Calderón-Garcidueñas et al., 2012).

Thus, research and epidemiology data suggest a correlation between particulate matter exposure and AD onset and progression, although more experiments are required to confirm this association.

CHAPTER 2: AIM OF THE STUDY

About a decade ago, the CNS has been proposed to be a target organ for the detrimental effects of airborne pollutants (Oberdörster and Utell, 2002), and emerging evidences from different studies suggest that neurological diseases, such as AD, PD and stroke, may be strongly associated with ambient PM (Genc at al., 2012). It has been demonstrated that continuous exposure to significant levels of airborne PM may result in the direct translocation of pollutants to different extra pulmonary sites, including CNS, or trigger the release of soluble inflammatory mediators from primary entry organs or secondary deposition sites (Genc at al., 2012). UFPs that reach the circulation could directly affect vascular endothelial cells by creating local oxidative stress or causing pro-inflammatory effects that, together with inflammatory mediators produced in the respiratory tract, can lead to systemic inflammation (Cunningham et al., 2009; Genc at al., 2012). Moreover, systemic inflammation could in turn activate cerebral endothelial cells, alter BBB integrity, or trigger signalling cascades that lead to the activation of mitogen-activated protein kinase (MAPK) and Nuclear factor kappa-light-chain-enhancer of activated B cells (NFκB) pathways (Calderón-Garcidueñas et al., 2008; Genc at al., 2012). Interestingly, post-mortem examinations of adult humans resident in highly polluted urban areas of Mexico City exhibited significantly higher COX-2 expression in olfactory bulb, hippocampus, and frontal cortex, and greater neuronal accumulation of $A\beta_{42}$ when compared to subjects living in cities with low pollution levels (Calderón-Garcidueñas et al., 2004; Genc et al., 2012).

Therefore, the aim of this project was to evaluate the detrimental effect of UFPs exposure, regarding oxidative stress and inflammation, on *in-vitro* and *in-vivo* models of CNS. Moreover, this work meant to investigate the possible physiopathological correlation between these two mechanisms and AD neurodegeneration.

2.1 C6 GLIOMA CELLS

C6 glioma cells represent a rat cell line with properties of both astrocytes (Benda et al., 1968) and oligodendrocytes (Volpe et al., 1975) widely used in neurobiological research. Moreover, this cell line has been already used to test oxidant toxicity of various components (Han et al., 2012), because it results sensitive to oxidative stress (Goncharov et al., 2005).

C6 glioma cells have been treated with different doses of diesel particles (DEP: 25µg/ml, 50µg/ml and 100µg/ml) and have been screened for oxidative stress (Heme oxygenase 1, HO-1, and Cytochrome P450 1b1, Cyp1b1) and inflammatory (inducible nitric oxide synthase, iNOS) markers. One of the key regulator of the cellular response to oxidative stress is Nrf2 (nuclear factor E2-related factor 2), that controls both the inducible and constitutive gene expression mediated by ARE, cis-acting elements found in the promoter of genes encoding phase II antioxidant enzymes, such as HO-1 (Nguyen et al., 2009). Nrf2 has a short half-life; in normal conditions, in the cytoplasm Keap1 promotes constitutive ubiquitination of Nrf2 addressing it to the proteolytic degradation catalyzed by the 26 S proteasome (Stewart et al., 2003). Oxidants could interfere

with Nrf2/Keap1 interaction and subsequent degradation by proteasome, resulting in Nrf2 nuclear localization, dimerization with other transcription factors, and eventually target gene activation (Kwak et al., 2002). Moreover, it has been suggested that the phosphorylation of Nrf2 triggered by Extracellular signal–regulated kinases (ERK1-2) may facilitate Nrf2 release from Keap1 and translocation into the nucleus (Li et al., 2007). Notably, in biopsies of lung tissues from human volunteers exposed to DEP, activation of MAPKs has been detected (Pourazar et al., 2005). As ERK1-2 could be involved in Nrf2 activation (Li et al., 2007), and HO-1 is one of Nrf2 target genes (Nguyen et al., 2009), we can hypothesize that MAPKs transduction pathway and Nrf2-mediate oxidative stress response may be important in CNS exposed to pro-oxidant particles, such as DEP.

To test this hypothesis, we analysed ERK1-2 phosphorylation and Nrf2 expression with the selected dose of DEP 25µg/ml. The same markers have been examined after inhibition of MEK, the kinase upstream to ERK1-2. Finally, we evaluated the effect of MEK inhibition on antioxidant enzymes generation and consume by means of a total antioxidant capacity assay.

2.2 HT22 CELLS

The HT22 nerve cell line is a subclone of HT4 (Morimoto and Koshland, 1990), which was derived from the mouse hippocampus. They are immortalized neurons, employed as a successful *in-vitro* model to study oxidative stress related neurotoxicity (Li et al., 1997).

HT22 cells have been treated with different doses of DEP (10µg/ml and 50µg/ml) and have been screened for oxidative stress (HO-1, Heat shock protein 70, Hsp70, and Cyp1b1) and inflammatory (COX-2 and iNOS) markers. Oxidative stress can induce lipids peroxidation (Rizzo et al., 2014) and one of the major products of this process is malondialdehyde (MDA). Therefore, MDA was evaluated as a marker of lipid peroxidation after DEP treatment.

Assuming that *in-vivo* studies and epidemiological evidences from young urban residents showed a correlation between air pollution, neuroinflammation and oxidative stress -crucial mechanisms for AD onset and progression (Calderón-Garcidueñas et al., 2008; Calderón-Garcidueñas et al., 2012)-, we analysed some markers involved in amyloidogenic processing (P-APP thr668, APP and BACE1).

Finally, literature data suggest lipid reshaping after PM exposure. It has been demonstrated that mouse PM10 administration causes liver, heart and brain changes in total fatty acids composition (Rizzo et al., 2014). Thus, in collaboration with Prof. Angela Maria Rizzo (UniMi), the effect of DEP exposure on fatty acids (FA) and cholesterol (free cholesterol, CHOL, and esterified cholesterol, CE) was also investigated. This is important because the effect of PM on cell membrane and lipid profile represents a topic that has been so far poorly investigated, and because in the last years several molecular mechanisms connecting membrane lipids to the metabolism of AD related proteins have been identified, in particular Aβ generation and aggregation.

2.3 MALE BALB/c MICE BRAIN

Male BALB/c mice were selected as *in-vivo* model to study oxidative stress and inflammation induction in the brain after intratracheal administration of UFPs from two anthropogenic sources: BC (biomass combustion generated emissions) and DEP (diesel particles). This *in-vivo* model has already been used in our laboratory to study the systemic effects of different kinds of particulate matter (Mantecca et al., 2010; Farina et al., 2013; Rizzo et al., 2014).

Male BALB/c mice were intratracheally instilled with 50µg of BC or DEP/100µl 0.9% NaCl. 3h after single instillation or 24h after the last of repeated instillations, animals were sacrificed and the brain of sham and treated mice were dissected and divided in three parts: RoB, cerebellum and hippocampus. The purpose of this choice was to assess how different brain regions respond to different UFPs peripheral administration. Thus, RoB, cerebellum and hippocampus have been screened for oxidative stress (HO-1, Hsp70, and Cyp1b1) and inflammatory (iNOS) markers. Moreover, to better evaluate brain inflammation, sham and treated mice were submitted to fluorescence molecular tomography (FMT®) technique at different times of treatment and after intravenous injection of the MMPSenseTM 750 FAST probe.

Assuming the existence of a correlation between air pollution, neuroinflammation, oxidative stress and AD neurodegeneration (Calderón-Garcidueñas et al., 2008; Calderón-Garcidueñas et al., 2012), we analysed some markers involved in amyloidogenic processing (P-APP Thr668, APP and BACE1).

Finally, in collaboration with Prof. Guido Cavaletti (UNIMIB) we performed brain histopathological evaluations.

As a final goal of this part of the project, the evaluation of different markers allowed us to compare the effects generated by the two kind of UFPs (BC and DEP) on mouse brain after acute and sub-acute peripheral administration.

In conclusion, this project will allow to consider air pollution as environmental risk for late onset AD that might synergistically act with already known risk factors in the concept of “risk stratification”. According to that, these results might lead to development of prevention strategies against AD development, encouraging the society to different choice in the own lifestyle, such as healthy daily diet (antioxidant rich foods) and improvement in air quality (change in car fuel and heating typology).

CHAPTER 3: MATERIALS AND METHODS

MATERIALS

- 30% Acrylamide/Bis Solution (37.5:1): Bio-Rad (Milan);
- Antibody anti-Cyp1b1, anti-ERK1-2, anti-HO-1, anti-Hsp70, anti-iNOS: Santa Cruz Biotechnology (USA);
- Antibody anti-phospho T202 + Y204 ERK1-2, anti-BACE1: Abcam (UK);
- Antibody anti-Nrf2: R&D Systems.
- Antibody anti-COX-2, anti-phospho Thr668 APP: Cell Signaling Technology (USA);
- Antibody Anti-βactin: Sigma Chemical CO (Milan);
- Antibody anti-APP,: Invitrogen Corporation (Milan);
- β-mercaptoethanol: Sigma Aldrich (Milan);
- BALB/c mice: Envigo (Udine);
- BCA reagents (Bicinchoninic acid and $CuSO_4$): Sigma Aldrich (Milan);
- Bis-Acrilammide 30%: Bio-Rad (Milan);
- Bromophenol Blue: Sigma Aldrich (Milan);
- Cell culture solutions: EuroClone (Milan);
- DEP SRM1650b (Standard Reference Material): National Institute of Standards and Technology (USA);
- Glycerol: Sigma Aldrich (Milan);
- MMPSenseTM 750 FAST probe: Perkin Elmer (Milan);
- MycoZap™ (Lonza): EuroClone (Milan);
- Nitrocellulose membrane: GE Healthcare Life Sciences (Milan);
- N,N,N',N'-Tetramethylethylenediamine (TEMED): Sigma Aldrich (Milan);
- Pierce™ ECL Western Blotting Substrate: Thermo Fisher Scientific (Monza);
- Ponceau staining: Sigma Aldrich (Milan);
- Powdered reagents and solvents with the highest purity degree: Sigma Aldrich (Milan);
- Precision Plus Protein Standards (All Blue): Bio-Rad (Milan);
- PrestoBlue® assay: Thermo Fisher Scientific (Monza);
- Protease inhibitor cocktail tablets (Complete): Roche Diagnostics S.p.A. (Milan);
- TAC Colorimetric Assay Kit: BioVision (USA);
- Thiazolyl Blue Tetrazolium Bromide (MTT): Sigma Aldrich (Milan);
- Tween 20: Sigma Aldrich (Milan);
- U0126: Merck Millipore (USA).

EQUIPMENTS

- Branson 2510 Ultrasonic Cleaner;
- Electrophoresis apparatus and Power Supply: Bio-Rad (Milan);
- FMT 1500TM fluorescence tomography *in-vivo* imaging system: Perkin Elmer (USA);
- Hettich Mikro 20 Centrifuge;
- ImageQuant™ LAS 4000: GE Healthcare Life Sciences (Italy);
- Jouan centrifuge: Thermo Electron Corporation s.r.l. (Italy);
- Microplate reader 550: Bio-Rad (Milan);
- MicroSprayer® Aerosolizer system (MicroSprayer® Aerosolizer- Model IA-1C and FMJ-250 High Pressure Syringe): Penn Century (USA);
- Potter tissue grinder: *Privet Drive*;
- SpeedVac concentrator 5301, F45-48-11 rotor: Eppendorf;
- Stereoscopic microscope;
- Thermoblock: FALC, Italy;
- Vibracell Ultrasonic processor: Sonics & Materials Inc. (USA);
- Western blot apparatus: Hoefer Inc. (USA).

3.1 IN-VITRO MODELS

CELL COLTURES

C6 glioma cells

C6 glioma cells were purchased from the American Type Centre Collection (ATCC, Manassas, VA, USA).

Cells were grown in tissue culture flasks and maintained at 37°C, 5% CO_2 in Dulbecco's modified Eagle's medium (DMEM) containing 10% foetal bovine serum, 1% penicillin and streptomycin and 1% L-Glutamine. Once they had reached the confluence, C6 glioma cells were dissociated with trypsin and centrifuged at 160xg for 2 minutes. Following resuspension in complete medium, they were diluted 1:40 in order to reach the confluence in four days.

For experiments, cells were plated on 24 multiwell plates, 20,000 cells per well (about 10,000 cells/cm^2), and treated at 80% confluence.

HT22 cells

HT22 cells were a generous gift of Dr David Schubert (Salk Institute for Biological Studies, La Jolla, CA, USA).

Cells were grown in tissue culture flasks and were kept at no more than 50% confluence at 37°C, 5% CO_2 in DMEM containing 10% foetal bovine serum, 1% penicillin and streptomycin, 1% L-Glutamine and 0.2% MycoZap™. HT22 cells were dissociated with pancreatin and centrifuged at 120xg for 3 minutes. Following resuspension in complete medium, they were diluted 1:10 in order to reach 50% confluence in three days.

For experiments, cells were plated on poly-lysine pre-coated Petri dishes, 50,000 cells per well (6,250 cells/cm^2) and treated at 50% confluence.

CELL TREATMENTS

Treatment with DEP

Cells were treated with DEP SRM1650b, a diesel particulate with mean aerodynamic diameter of 0,18 µm. Diesel particles were suspended at different concentration (10µg/ml, 25µg/ml, 50µg/ml, 100µg/ml) (Levesque et al., 2011) in culture medium supplemented with 0.00005% Tween 20 to allow proper resuspension of particles. Based on *in-vivo* models of near road and occupational exposure (0.5mg/m^3 and 2mg/m^3), Levesque and colleagues calculated that an *in-vitro* concentration of about 5–50µg/ml of nanometer-sized particles falls within the current estimates of what may reach the brain. Immediately before treatment, DEP suspensions were sonicated for 5 min to obtain a proper particle dispersion.

C6 glioma and HT22 cells were treated with DEP for 3h and 24h; in parallel, control cells were treated with culture medium supplemented with 0.00005% Tween 20. For western blot analyses, at the end of the treatments cells were lysed with denaturing buffer (DB: 2% SDS, 50mM Tris HCl pH 6.8, 1X proteases inhibitors, 1X phosphatases

inhibitors). For total antioxidant capacity assay, at the end of the treatments cells were lysed with sonication in phosphate saline buffer (PBS) (see below). For lipid analyses, at the end of the treatments cells were removed by scraping in PBS plus proteases and phosphatases inhibitors and centrifuged at 4°C, 845xg for 10 minutes. Supernatants were separated and pellets were used by Prof Angela Rizzo and collaborators for malondialdehyde and fatty acids evaluation (see below).

Treatment with DEP and U0126

C6 glioma cells were treated with 25µg/ml DEP in presence of the selective non-competitive MEK inhibitor U0126 (Lind et al., 2006). Briefly, cells have been pre-treated with complete medium, serum free medium or serum free medium + U0126 (U0126 from a 100mM solution in DMSO, final concentration 10µM) for 30 min (Xie et al., 2004). Then, C6 glioma cells were treated for 5h with 25µg/ml DEP suspended in complete medium supplemented with 0.00005% Tween 20 (CM+DEP25), in serum free medium supplemented with 0.00005% Tween 20 (SFM+DEP25), or in serum free medium added with U0126 and 0.00005% Tween 20 (SFM+U+DEP25). In parallel, respective controls were treated with complete medium supplemented with 0.00005% Tween 20 (CM), serum free medium supplemented with 0.00005% Tween 20 (SFM) and serum free medium added with U0126 and 0.00005% Tween 20 (SFM+U).

For western blot analyses, at the end of the treatments (5h) cells were lysed with DB. For total antioxidant capacity assay, at the end of the treatments (5h) cells were lysed with sonication in PBS (see below).

VIABILITY ASSAYS

PrestoBlue® viability assay

After different treatments times (3h and 24h), C6 glioma cell viability was evaluated using the PrestoBlue® assay, a cell permeable resazurin-based solution that functions as a cell viability real-time indicator by using the reducing power of living cells. When added to cells, the PrestoBlue® reagent is modified by the reducing environment of the viable cells and turns red in colour, thus being detectable using absorbance measurements. At the end of C6 glioma cells treatment with DEP, the media were taken and conserved at -20°C and wells were washed with PBS. Each well was filled with a solution that contained PrestoBlue® and fresh DMEM (1:10 v:v) and maintained at 37°C for 1h. The solution in each well was transferred to a new 96-well plate, which were read using a multi-well spectrophotometer at 570 nm with a reference wavelength of 600 nm. Cell viability was expressed as a percentage, normalizing on the control with 0.00005% Tween 20.

MTT viability assay

After different treatments times (3h and 24h), HT22 cell viability was evaluated using MTT (3-[4,5-dimethylthiazol-2-yl]-2,5-diphenyl-2H-tetrazolium bromide) viability assay. MTT is a water soluble tetrazolium

salt yielding a yellowish solution when prepared in media or salt solutions lacking phenol red. Dissolved MTT is converted to an insoluble purple formazan by cleavage of the tetrazolium ring by mitochondrial succinate dehydrogenase. This water insoluble formazan can be solubilized using solvents and the dissolved material is measured spectrophotometrically yielding absorbance as a function of concentration of converted dye. Therefore, accumulation of formazan directly reflects the activity of mitochondria, an indirect measurement of cell viability.

At the end of HT22 cells treatment with DEP, MTT stock solution (5mg/mL) was added to each plate to a final concentration of 1.2mM, and cells were incubated for 1.5h at 37°C. After removing MTT solution, the reaction was stopped by adding EtOH. Resuspended cells were centrifuged 10 min at 800xg and the absorbance was measured with a spectrophotometer at a wavelength of 560nm and at reference wavelength of 690 nm.

TOTAL ANTIOXIDANT CAPACITY ASSAY

Total antioxidant capacity (TAC) was evaluated on C6 glioma cells according to manufacturer's instructions.

TAC assay employs Trolox to standardize antioxidants, with all other antioxidants being measured in Trolox equivalents. Measurement of the combined nonenzymatic antioxidant capacity of biological fluids and other samples provides an indication of the overall capability to counteract ROS, resist oxidative damage and combat oxidative stress-related diseases. TAC Assay Kit can measure either the combination of both small molecule antioxidants and proteins or small molecules alone in the presence of a specific Protein Mask. Cu^{2+} ion is converted to Cu^{+} by both small molecules and proteins. The Protein Mask prevents Cu^{2+} reduction by protein, enabling the analysis of only the small antioxidant molecules. The reduced Cu^{+} ion is chelated with a colorimetric probe giving a broad absorbance peak around 570 nm, proportional to the total antioxidant capacity.

After the treatments, C6 glioma cells were removed by scraping, pelleted and re-suspended in 200µL of cold PBS plus protease and phosphatase inhibitor. Cell membranes were disrupted by sonication on ice and cell lysates centrifuged at 4°C, 10,000xg for 20 min; supernatant was separated from cell debris and used for TAC analysis. All measurements were normalized to the total protein content evaluated by means of Bicinchoninic acid assay.

LIPID ANALYSES

Lipid analyses were performed on HT22 cells by Prof Angela Maria Rizzo and collaborators.

Cell lipid extraction

Each solvent used for extraction and analysis contains 0.045mM 3,5-Di-tert-4-butylhydroxytoluene (BHT) to avoid polyunsaturated fatty acids oxidation. Lipids were extracted with minor modifications of Folch method (Lowry et al., 1951). Briefly, cells were homogenized with chloroform/methanol 1:2, centrifuged to recover the

lipid extract and extracted again two times with chloroform/methanol 2:1, 1:1 (v/v). The organic phase was dried and resuspended in chloroform/methanol 2/1, for further analysis (see below).

MDA analysis

Lipid peroxidation products levels, as malonyldialdehyde (MDA), were measured in cells according to the method of Karatas and collaborators (Karatas et al., 2002). MDA was determined by HPLC (Jasco, Japan) equipped with a UV detector. A C18 column was used at ambient temperature. To prepare MDA standards, 10 µl of TEP (1,1,3,3 tetraethoxypropane) were accurately diluted to 10 ml with 0.1 M HCl in a screw-capped test tube and placed in a boiling water bath for 5 min and then rapidly cooled on ice, generating a hydrolyzed acetal. A working stock solution of MDA was prepared by pipetting 1 ml of the hydrolyzed acetal into a 100 ml calibrated flask and diluted with water.

The working stock solution was 40 µM MDA. The stock solution was further diluted and used to construct the calibration curve.

For samples preparation, 100 µg of cell proteins were added to 40 µl 0.1 M $HClO_4$. Samples were centrifuged at 4,500g for 5 min and supernatants were used for HPLC analysis. This procedure allows protein precipitation and release of MDA bound to the amino groups of proteins, and other amino compounds. The mobile phase was KH_2PO_4 (6.8g KH_2PO_4 in 100ml distilled water) /methanol/acetonitrile (72/18/11, v/v); the flow rate was 1ml/min. Chromatograms were monitored at 254 nm and injection volume was 20µl.

Gas chromatography fatty acid analysis

The fatty acid composition was determined by gas chromatography (GC) as methylesters (Corsetto et al., 2012). Lipids were derivatized with sodium methoxide in methanol 3.33% (w/v) to obtain fatty acid methyl esters (FAME). Prior to derivatization a known amount of internal standard (C17:0 triglyceride) was added to each sample to correct for yield and recovery of the reaction.

FAME were rapidly extracted with hexane, dried and resuspended in a known volume of chloroform/methanol prior to injection into a gas chromatograph (Agilent Technologies 6850 series II, CA) equipped with flame ionization detector.

The separation was achieved as follows: capillary column, AT Silar length 30m, film thickness 0.25µm; carrier gas, helium; injector temperature, 250°C; detector temperature, 275°C. The oven temperature was controlled at 50°C for 2 min and then increased at a rate of 10°C min^{-1} to 200°C, and maintained at this temperature for 20 min. A standard mixture containing all fatty acid methylesters (Sigma Aldrich, MO) was injected as calibration for quantitative analysis.

Cholesterol quantification by HPLC-ELSD system

Free and esterified cholesterol from cell lipid extracts were separated and accurately quantified by high performance liquid chromatography on a Lichrospher SI 60 5mm, 250x4 HPLC column, using ELSD detector according to Christie W.W. (Christie, 1985). The mobile phase consisted of solvent A: isooctane, tetrahydrofuran 99:1 vol/vol and solvent B: acetone, dichloromethane 2:1 vol/vol. The flow rate was 1.6 ml/min. ELSD detector was settled as follows: pressure 3.5 bar, temperature 50°C, gain 8. The injection volume was 20µl. Different concentrations of free and esterified cholesterol standards were injected prior to sample to construct a calibration curve.

3.2 IN-VIVO MODELS

BALB/c MICE

Male BALB/c mice (7-8 weeks) were housed in plastic cages under controlled conditions (temperature 19-21°C, humidity 40%-70%, lights on 7 a.m. to 7 p.m.), where food and water were administered *ad libitum*. Animal use and care procedures were approved by the Institutional Animal Care and Use Committee of the University of Milano-Bicocca and complied with guidelines set by Italian Ministry of Health (*DL 4 marzo 2014 n°26, ''Attuazione della direttiva 2010/63/UE sulla protezione degli animali utilizzati a fini scientifici''*). Invasive procedures have been performed under anaesthesia and all efforts were made to minimize suffering.

UFPs SAMPLING

UFPs sampling were performed by ENEA in collaboration with the Fuel Experimental Station as sub-contractor.

Biomass particles (BC)

Biomass burning generated emissions were sampled accordingly to the experimental system reported (**Fig 8**). The flue gas of a boiler, fuelled with pellet of certified origin and composition as required by the norms for the efficiency tests, were derived by using a sampling probe. The fumes were kept warm in the first tract of the sampling line to avoid condensation of water vapour and other condensable compounds. The hot flue gases were then derived into different sampling points, which allowed the measurement of the organic gaseous compounds (OGC) by using a cooling system and dedicated XAD-2 resin cartridges according to the US Environmental Protection Agency guidelines. The quantification of different PM fractions were performed by a Dekati impactor system according to the ISO23210 standard. Finally, the analysis of other gaseous pollutants (carbon monoxide (CO) and OGC) were useful for the overall characterization of the combustion process. The pressure during the sampling were monitored to maintain isokinetic conditions and avoid pressure drops along the sampling line.

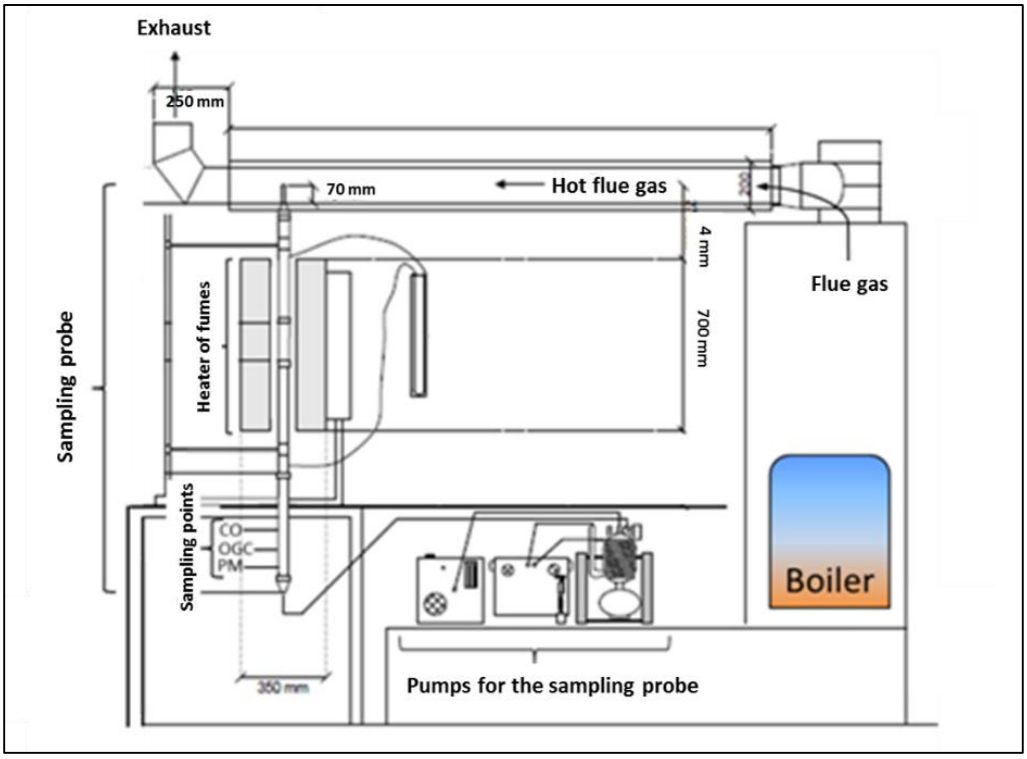

Figure 8: Schematic representation of BC sampling.

Diesel particles (DEP)

The EURO 4 diesel light duty vehicle emissions (CO, HC+NOx, NOx, total PM) were preliminarily characterized accordingly to specific norms (Directive 98/69/EC; E/ECE/324/Rev.1/Add.82/Rev.4; European Standard EN 590). The UFPs emitted were sampled by performing several "URBAN" Driving Cycles chassis dyno tests (**Fig 9**), developed within the European Project ARTEMIS (Report INRETS-LTE 0411, 2004) and representative of real average driving conditions typical of a European city urban context. To better simulate real urban driving conditions, cold start tests were performed. Simultaneously through a suitable probe, the Particle Number (PN) emission were carried out by an Electrical Low Pressure Impactor (ELPI Dekati) with mean aerodynamic diameter range to determinate the UFP emission distribution. A further part of diluted exhausts previously taken from the dilution tunnel were analysed by Microsoot Sensor AVL in order to evaluate the soot emission. All the URBAN test cycles were performed in the same conditions to guarantee the repeatability of the results obtained by measurements and analysis.

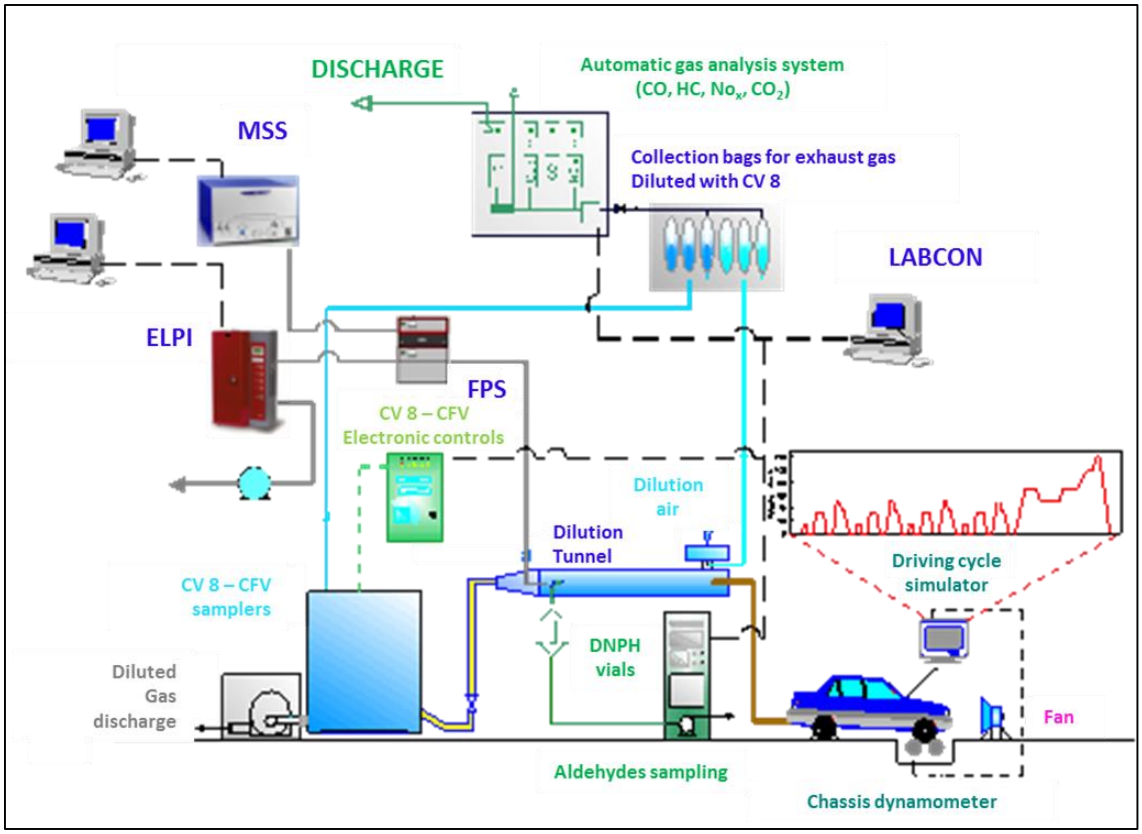

Figure 9: Schematic representation of DEP sampling.

UFPs CHEMICAL, MORPHOLOGICAL AND PHYSICAL CHARACTERIZATION

UFPs from biomass and diesel combustion were analysed by ENEA and the Fuel Experimental Station to determine the elements (by ICP-MS according to the UNI EN ISO 17294-2:2005 procedure) and the PAHs adsorbed onto the particles (by GC-MS following the UNI EN ISO 11338 methods).

The particles were detached from sampling filters by ENEA according to the techniques developed by Maurizio Gualtieri and collaborators (Gualtieri et al., 2012). Briefly, Teflon filters underwent to sequential sonication in a Soltec water-bath (SONICA, four cycles of 20 min each) in sterile water. By this procedure, particles were mechanically detached from filters together with the adsorbed compounds, and the extraction efficiency was above 65% (ratio between the mass of particles recovered and the mass of particles sampled), assuring the similarity among the extracted particles and the pristine ones. Particle suspensions, dried into a desiccator at room temperature, were weighed and stored at -20°C until use for biological tests. Just before use, particles were re-suspended in sterile water at a final concentration of 2µg/µl.

BC and DEP particles morphology was characterized by transmission electron microscopy (TEM) and scanning electron microscopy (SEM). Chemical characterization of UFPs was performed on a pool of randomly selected filters in order to obtain a mean characterization representative of the combustion processes. PAHs were

evaluated by GC/MS (HRGC-MS Agilent 5973 Agilent Technologies, CA) after Accelerated Solvent Extraction (ASE) using a mix hexane/acetone (ratio 4:1 v/v). Selected metals were analyzed after microwaves mineralization of the samples using a mixture HNO3/H2O2 (2:1 ratio v/v) and final dilution with ultrapure water. Metals were quantified by ICP-MS (Perkin Elmer SCIEX mod. ELAN 9000) (Longhin et al., 2016).

Both BC and DEP samples consisted of aggregates of round carbonaceous particles, in addition biomass samples shown the presence of ash particles (**Fig. 10**) that completely dissolved in aqueous media. PAHs and transition metals concentration was higher in DEP compared to BC, which conversely resulted to be enriched in elements typical of wood combustion, such as Mn, K and S (**Fig. 11**).

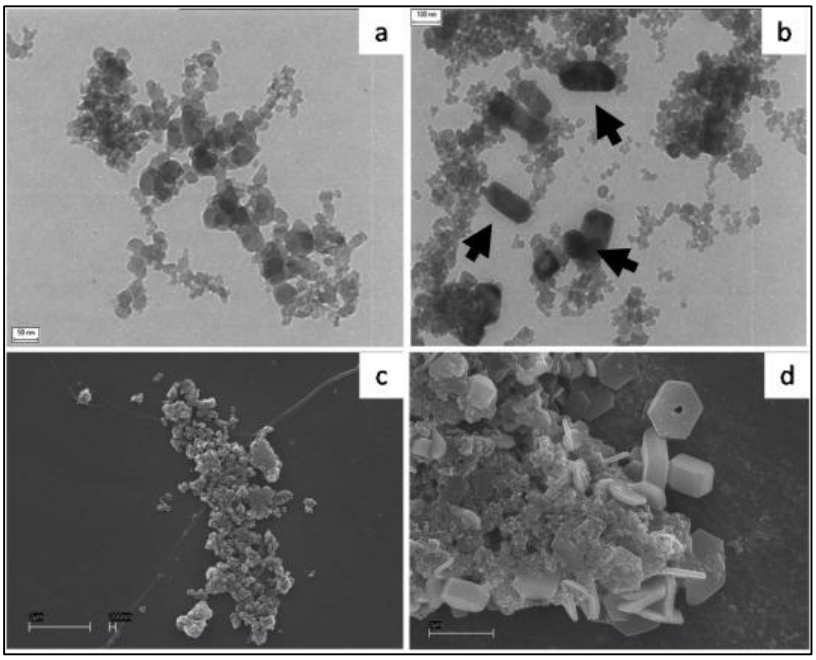

Figure 10: Physico-chemical characterization of particles. TEM and SEM images, and SEM-EDX analysis of diesel **(a, c)** and biomass **(b, d)** samples. Arrows indicate ash particles in biomass samples (Longhin et al., 2016).

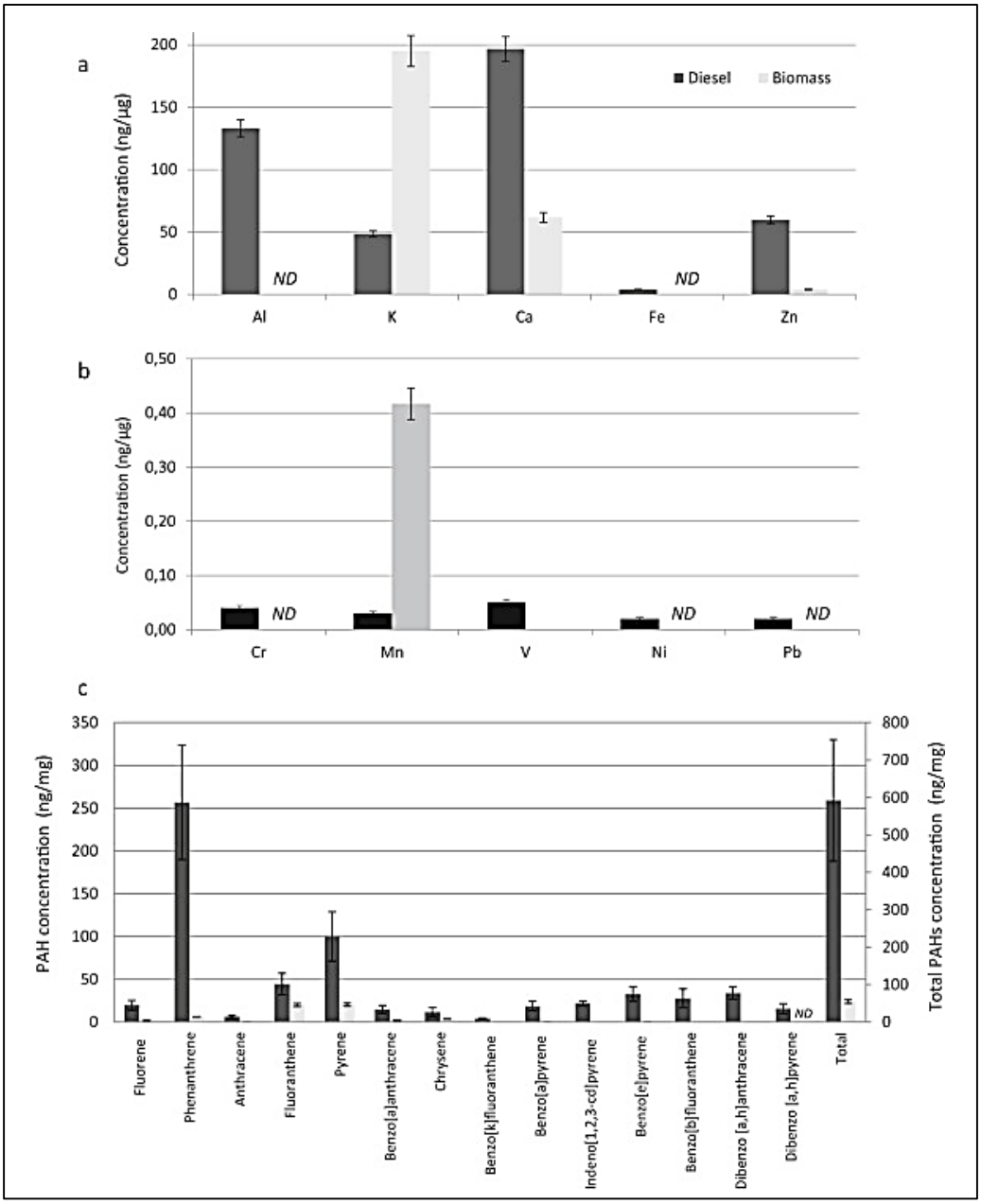

Figure 11: Chemical characterization of UFPs. Metals mean concentrations (±S.D.) are reported in ng/µg **(a, b)**, and PAHs in ng/mg **(c)** (Longhin et al., 2016).

INTRATRACHEAL UFPs INSTILLATION

Ultrafine particle suspensions were prepared as follows. Immediately prior to intratracheal instillation, UFPs from diesel (DEP) and biomass (BC) combustion were suspended in sterile isotonic saline solution (0.9% NaCl), in order to prepare a stock solution (50µg UFPs/100µl NaCl). Then, stock solution was sonicated for 15 minutes to obtain a uniform dispersion and to prevent particle aggregation.

Male BALB/c mice were briefly exposed to a mixture of 2.5% isoflurane (Flurane) anaesthetic gas and kept under anaesthesia for the whole instillation procedure (about 5 minutes). Each mouse was placed in a supine position, the mouth was opened, and the tongue was gently moved aside using a pince to better cannulate the trachea.

Intratracheal instillation with 100 µl of UFPs stock solution was achieved by means of a MicroSprayer® Aerosolizer system (**Fig 12**), that enables a uniform lung distribution of the UFPs solution. Control mice (sham), running parallel to UFPs-treated animals, were instilled with 100 µl of isotonic saline solution (Bivas-Benita et al., 2005; Mantecca et al., 2009; Mantecca et al., 2010; Farina et al., 2011).

Figure 12: MicroSprayer® Aerosolizer- Model IA-1C and FMJ-250 High Pressure Syringe, Penn Century, USA.

Two different exposures were performed:

- Acute exposure (mice were euthanized 3h following a single instillation) (Farina et al., 2013);
- Sub-acute exposure (the intratracheal instillation was performed on days 0, 3, and 6, for a total of three instillations; mice were euthanized 24h following the last instillation) (Happo et al., 2010; Saunders et al., 2010) (**Fig 13**).

Nine animals were treated for each experimental group.

Immediately following instillation, treated and sham mice were allowed to recover under visual control before placing them back in plastic cages under controlled environmental conditions.

FLUORESCENT MOLECULAR TOMOGRAPHY

Fluorescence molecular tomography (FMT®) is an imaging technique for improved localization and quantification in deep tissue. This requires the transillumination of animals (i.e. the passing of light through the animals). Experimental animals must be prepared for transillumination imaging by hair removal, must be properly injected with imaging agents for optimal delivery to imaging sites and minimization of artefacts, and scans must be set up and acquired under optimal conditions and settings.

Male BALB/c mice were injected intravenously with MMPSense™ 750 FAST probe immediately before the first instillation (day 0). At 6h and 24h after injection, anesthetised mice were depilated and placed into the imaging cassette inside the chamber of FMT 1500™ fluorescence tomography *in-vivo* imaging system. This procedure

was repeated at day 6 (**Fig 13**). Scanning was performed using the 670nm channel, and the fluorescence signal was filtered with 750nm filter emission.

The total amount (in picomoles) of fluorophore in a selected tridimensional region of interest (ROI) was calculated by the TrueQuant software using previously generated standards of the appropriate dye. ROI were drawn in a blind manner by an operator unaware of the experimental origin of the specimens in order to eliminate any operator bias.

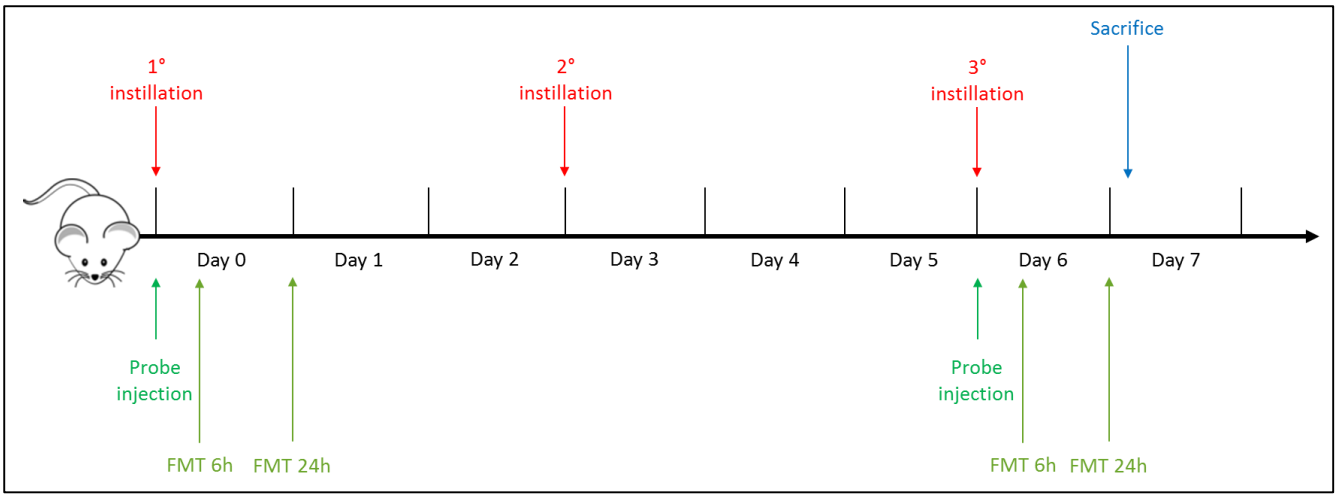

Figure 13: Schematic representation of BALB/c experiment.

BRAIN DISSECTION

The dissection of neuronal tissues was performed on fresh brain based on visual information, such as differences in colour of adjacent tissues, and on the natural anatomical boundaries of certain regions present in the brain. Examples of these are the cerebellum that can be easily taken off from the medulla and pons (**Fig. 14a**), and the hippocampus that differs from the occipital cortex by colour and because it lies loosely on the thalamus, mainly connected by the fornix (**Fig. 14b**) (Spijker, 2011).

Procedure

Male BALB/c mice were briefly exposed to a mixture of 2.5% isoflurane (Flurane) anaesthetic gas. When a deep state of anaesthesia was achieved, cervical dislocation was performed.

Surgical scissor were used to remove the head with a cut posterior from the ears and to make a midline incision in the skin. The skin was flipped over the eyes to free the skull. A small incision was performed on the top of the skull, starting from the caudal part and addressing the tips of the scissors upwards to avoid cutting the brain. A firm cut through the most anterior part of the skull, between the eyes, were done. This enables to remove more easily the brain.

The brain thus released was placed in a Petri dish containing ice-cold isotonic saline solution (0.9% NaCl) and the cerebellum was separated and divided into 2 parts using a bistoury:

- 1/2 in isotonic saline solution stored at -20°C for biochemical analyses;
- 1/2 stored at -80°C for lipid analyses.

Subsequently, the brain was divided in the two hemispheres and the hippocampus were extracted separately as described by Hagihara and collaborators (Hagihara et al., 2009). Briefly, the cerebral hemisphere was made medial side up and, using forceps, the diencephalon (thalamus and hypothalamus) was carefully removed under a stereoscopic microscope. This procedure exposed the medial side of the hippocampus. Pincers were inserted into each side of the hippocampus and were slid superficially along its septo-temporal axis to isolate it. After removing the dentate gyrus, the two hippocampus were separated as follow:

- 1 in isotonic saline solution stored at -20°C for biochemical analyses;
- 1 stored at -80°C for lipid analyses.

The remaining part of the brain (RoB, Rest of Brain), after removal of cerebellum and hippocampus, was also divided into 2 parts:

- 1/2 in isotonic saline solution stored at -20°C for biochemical analyses;
- 1/2 stored at -80°C for lipid analyses.

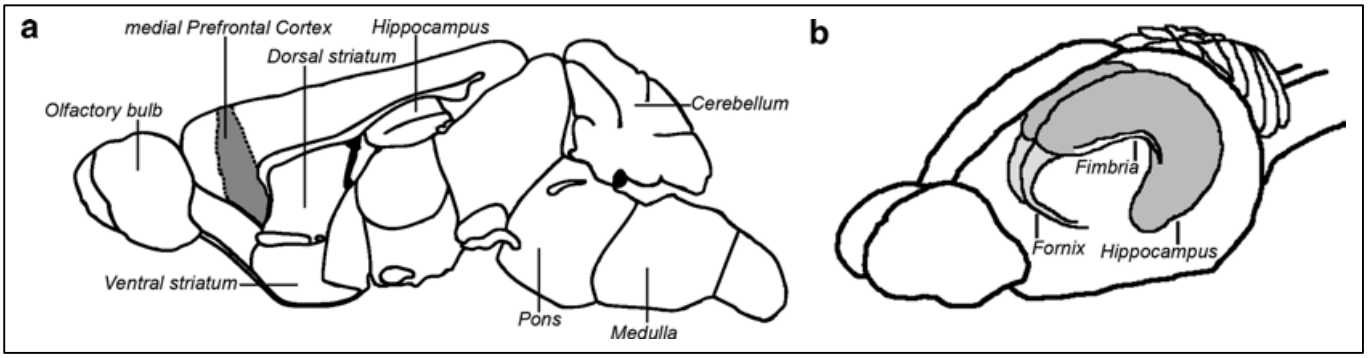

Fig. 14: (a) Schematic representation of a sagittal section of the mouse brain. **(b)** Schematic representation of hippocampus and fornix in the brain (Spijker, 2011).

BRAIN HOMOGENATES

Solutions

- **Ripa Buffer 5X**

  Tris-HCl 125mM pH 7.4

  NaCl 750mM

  NP40 5%

$C_{24}H_{40}O_4$ 2.5%

SDS 0.5%

Protease inhibitors 5X

Phosphatase inhibitors 5X

H_2O

RoB and cerebellum homogenization

The size of BW/OCH and cerebellum make possible their mechanical homogenization using a Potter tissue grinder. Therefore, each piece was suspended in sterile isotonic saline solution with protease inhibitors in 1:15 weight/volume ratio. The samples were then sonicated and centrifuged at 18,400xg for 10 minutes at 4°C and the supernatant was transferred to new tubes.

Subsequently, 1/3 of the total volume of each sample was collected and added to the appropriate volume of Ripa Buffer 5x, in order to ensure an efficient cell lysis for SDS-PAGE. The remaining 2/3 of each sample in saline solution were stored at -20°C for subsequent biochemical analyses that do not tolerate the presence of detergents. All the above procedures were performed on ice.

Hippocampus homogenization

The size of the hippocampus does not allow its mechanical homogenization using a Potter tissue grinder. Therefore, 100µl of Ripa Buffer 1X were added at each hippocampus. The samples were left on ice for 5 minutes, were sonicated and stored at -20°C for subsequent biochemical analyses.

HISTOPATHOLOGICAL ANALYSIS

For histopathological examination, the right brain hemisphere of dedicated sham and treated mice was quickly harvested, washed with 0.1M phosphate buffered saline (PBS, pH 7.4) and fixed in 10% neutral buffered formalin for 48 hours, processed with a Tissue Processor (Leica ASP300 S), and paraffin embedded (Embedding Center Leica EG1160) after ethanol-based dehydration. Sections (4 µm-thick) were cut, stained with Hematoxylin-Eosin (H&E) and evaluated under a light microscope (Leica DM 2500). Representative images were captured with a digital camera (Leica DFC310 FX).

3.3 BIOCHEMICAL ANALYSES

BCA PROTEIN ASSAY

The bicinchoninic acid (BCA) assay is a method that allows to determine the protein concentration of a sample in a very precise and sensitive way. The principle of this method is that proteins can reduce Cu^{2+} to Cu^{+} in an alkaline solution (the biuret reaction) and result in a purple colour formation by bicinchoninic acid, detectable with spectrophotometer at a wavelength of 540 nm. The reduction of copper is mainly caused by four amino acid residues including cysteine, tyrosine and tryptophan, which are present in protein molecules.

First, a calibration curve with bovine serum albumin (BSA, 0.4-0.8-2-4-6-10-16 µg/µl) has been prepared; each BSA standard in duplicate has been diluted with H_2O to a final volume of 10µL. Each sample has been prepared in duplicate by adding 8µl of H_2O to 2µl of sample. 200µl of the solution obtained by mixing bicinchoninic acid and copper sulphate (ratio 50:1) have been added to all standards and samples, incubating at 37°C for 30 minutes. From the absorbance values of the standards, it has been possible to obtain a calibration curve, from which the concentration of total protein present in the samples has been determined.

SODIUM DODECYL SULPHATE POLYACRYLAMIDE GEL ELECTROPHORESIS (SDS-PAGE)

SDS-PAGE is a method employed for separating proteins according to their size. Sodium dodecyl sulfate (SDS) is an amphipathic detergent that ensures the dissociation of the proteins in the individual polypeptides and minimizes the presence of protein aggregates. The separation of proteins by SDS-PAGE is based on the polymerization of a solution composed by acrylamide and bisacrylamide, in which the concentration of acrylamide and the ratio between acrylamide and bisacrylamide determine the size of the gel pores. The polymerization is induced by ammonium persulfate (APS), which spontaneously decomposes itself to form free radicals, and tetramethylethylenediamine (TEMED), a stabilizer that accelerates the rate of formation of APS free radicals. SDS, in combination with a reducing agent (typically β-mercaptoethanol) at high temperatures, causes the dissociation of non-covalent complexes and protein denaturation, to which confers a net negative charge in proportion to their molecular weight and independently on their amino acid sequence. When subjected to an electric field, the negatively charged proteins will migrate towards the anode with a migration speed that depends on their molecular weight, evaluated by loading on the same gel a standard sample with protein of known molecular weight (**Fig 15**).

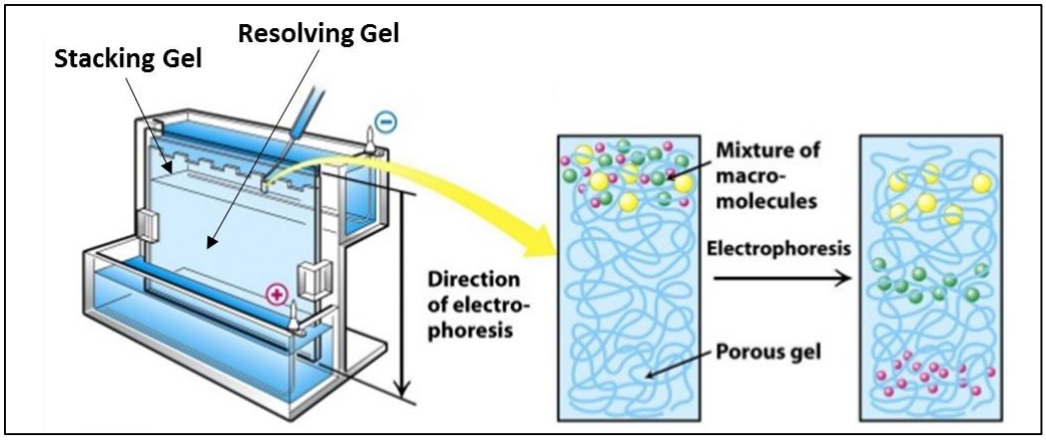

Figure 15: SDS-PAGE (Modified from Biochemistry, Sixth Edition, © 2007 W.H. Freeman and Company).

Solutions

- **Resolving gel**

  Bis-acrylamide (different % depending on the desired gel)

  Tris-HCl 380mM pH 8.8

  H_2O

  SDS 0.1%

  APS 0.1%

  TEMED 0.04%

- **Stacking gel** (acrylamide 4.5%)

  Bis-acrylamide 4.5%

  Tris-HCl 125mM pH 6.8

  H_2O

  APS 0.1%

  TEMED 0.1%

- **Laemmli Buffer (ZAP) 5X**

  Tris-HCl 250mM pH 6.8

  Glycerol 50%

  SDS 10%

  Bromophenol Blue 0.5%

  β-mercaptoethanol 5%

  H_2O

- **Running Buffer**

  Tris 25mM

  Glycine 250mM

  SDS 0.1%

  H_2O

Acrylamide gel preparation

To prepare bis-acrylamide gels, glasses and supports have been used. The glasses were thoroughly degreased with EtOH, to remove any residual grease that may hinder the polymerization of acrylamide. The resolving gel has been prepared and placed between the two glasses fixed on the support. The resolving gel needs about 1 hour for polymerization and it requires to be covered with a layer of butanol to prevent contact with air. After 1 hour, if the polymerization has taken place correctly, it is possible to observe the formation of a line of demarcation between the resolving gel and the butanol. After removal of butanol and several washing with water, the stacking gel were added above the resolving gel and the comb for the formation of loading wells were inserted. Similarly, the stacking gel requires about 1 hour for polymerization. The gels were prepared with ten or fifteen wells and 1.5mm of thickness and they have been stored in a humid environment at 4°C until use.

Samples preparation and loading

Thanks to quantification by BCA, which allows to know protein concentration, the volume required to have the desired protein amount were calculated, and all the samples have been brought to the same volume with water. Subsequently, the appropriate volume of ZAP 5X were added to the samples in 1:5 ratio with the total loading volume. The samples thus prepared were vortexed, centrifuged for 10 seconds, boiled at 100°C for 10 minutes to denature proteins and break the disulphide bonds between cysteine, centrifuged for 3 minutes at 18,400xg and loaded into wells using electrophoresis tips. Gels were mounted in the electrophoresis chamber and immersed in the running buffer. The electrophoresis was performed by applying a potential difference of 80V until samples reach the resolving gel, after which it were increased up to 100V.

WESTERN BLOT

Solutions

- **Transfer Buffer**

  CAPS 10mM pH 11

  Methanol 10%

  H_2O

- **Ponceau, Sigma**

  0.1% PonceauS in 5% acetic acid

Transfer to nitrocellulose

Proteins separated by electrophoresis were transferred to a nitrocellulose membrane using the technique of Western Blot and the membrane was used for the detection of proteins of interest with specific antibodies. The transfer happened recovering the gel from the slides and forming a "sandwich " in which an electric field were applied. The transfer sandwich were made in this way: sponge, filter paper, nitrocellulose membrane, gel, filter paper and sponge (**Fig 16**). The transfer occurs in the Hoefer apparatus for western blotting at 4°C for 2h and 15 minutes, applying an electric current of 250mA.

At the end of the transfer, the membrane has been recovered and coloured with Ponceau to verify the presence of the proteins on the nitrocellulose membrane and acquire an image using the ImageQuant™ LAS 4000. The Ponceau, in fact, is a TCA (trichloroacetic acid) based dye that binds to the proteins present on the nitrocellulose membrane and colours them in red, making them visible.

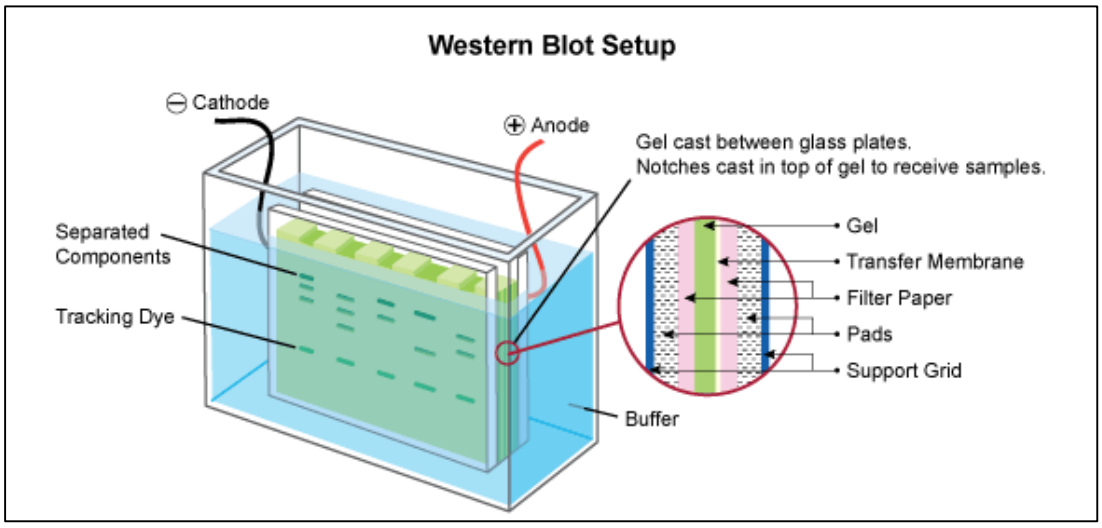

Figure 16: Illustration of Western Blot setup (from http://www.leinco.com).

IMMUNODECORATION

Solutions

- **TBS-T 0.1%**

  Tris-HCl 10mM pH 7.5

  NaCl 100mM

  H_2O

  TWEEN 20 0.1%

- **TBS-T 0.2%**

  Tris-HCl 10mM pH 7.5

  NaCl 100mM

  H_2O

  TWEEN 20 0.2%
- **TBS-T 0.1% BSA 5%**
- **TBS-T 0.1% MILK 5%**
- **TBS-T 0.2% MILK 5%**

Protocol

Immunodecoration is a technique that involves the use of specific antibodies to detect the presence of proteins on nitrocellulose membrane (**Fig 17**). Firstly, non-specific sites, which are the membrane binding sites free from proteins, were saturated with milk proteins (blocking phase). After blocking, the membrane was incubated with a dilute solution of primary antibody under gentle agitation. After rinsing the membrane to remove the excess of primary antibody, the membrane was exposed to a dilute solution of the secondary antibody, directed at a species-specific portion of the primary antibody and conjugated to HRP (horseradish peroxidase) enzyme.
Each primary antibody provides a different protocol of incubation (**Table 2**). At the end of immunodecoration, the proteins were detected by chemiluminescence.

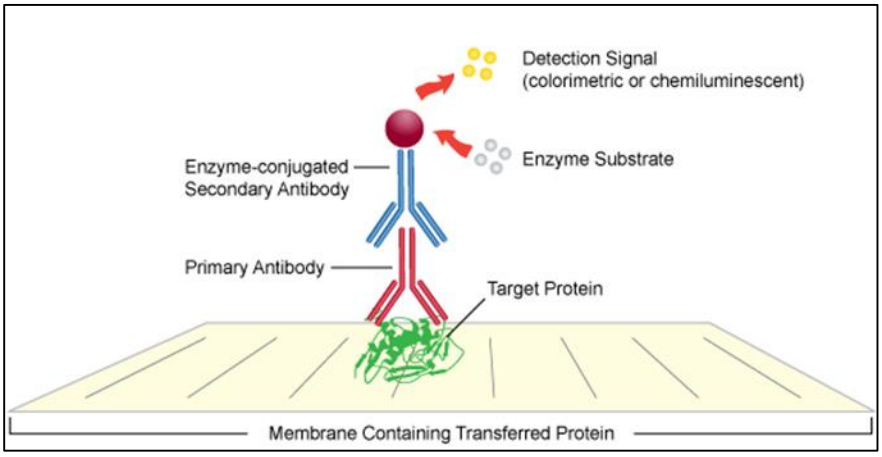

Figure 17: Illustration of protein detection in western blot (from http://www.leinco.com).

CHEMILUMINESCENCE

Enhanced Chemiluminescence (ECL) is a semi quantitative technique of detection of a specific protein on the nitrocellulose membrane and it is based on the use of secondary antibodies conjugated with HRP enzyme. HRP catalyses the oxidation of luminol in presence of H_2O_2 in 1: 1 ratio, producing oxidated luminol and water.

Oxidated luminol is able to exhibit its luminescence. The incubation takes place in the dark for 5 minutes. The quanta of light produced and detected by the ImageQuant™ LAS 4000 system are proportional to the amount of HRP present and, consequently, to the amount of the protein of interest to which the antibody is bound.

REMOVAL OF ANTIBODIES FROM THE NITROCELLULOSE MEMBRANE (STRIPPING)

The removal of an antibody from the nitrocellulose membrane is necessary to immunodecorate the same membrane with different primary antibodies and it involves the use of a *stripping solution* that contains:

- Tris Hcl pH 6.8 62.5mM;
- SDS 2%;
- β-mercaptoethanol 89.6mM.

The membrane was incubated with the stripping solution at 50°C for 30 minutes, at the end of which it was subjected to three washes of 5 minutes and two washes of 10 minutes with TBS-T 0.2%. After washing, it was possible to proceed with the immunostaining protocol, starting from blocking, as above described. The stripping solution removes the medium and low affinity links between the antibody and the nitrocellulose membrane, without removing the proteins.

CYTOKINES ANALYSIS

The analysis of pro-inflammatory cytokines in brain homogenates were performed by ELISA Multiplex assays. RoB and cerebellum homogenates in isotonic saline solution were stored at −20°C until sent to LABOSPACE (Milano, Italy. info@labospace.com) for multiplex ELISA analysis. LABOSPACE uses the Luminex Performance Assay to quantify interleukin-1β (IL-1β), tumor necrosis factor-α (TNF-α) and matrix metalloprotease 9 (MMP9). Analyte-specific antibodies are pre-coated onto colour-coded microparticles. Microparticles, standards and samples are pipetted into wells and the immobilized antibodies bind the analytes of interest. After washing away any unbound substances, a biotinylated antibody cocktail specific to the analytes of interest is added to each well. Following a wash to remove any unbound biotinylated antibody, streptavidin-phycoerythrin conjugate (Streptavidin-PE), which binds to the biotinylated antibody, is added to each well. A final wash removes unbound Streptavidin-PE and the microparticles are resuspended in buffer and read using a Luminex analyzer. One laser is microparticle-specific and determines which analyte is being detected. The other laser determines the magnitude of the phycoerythrin-derived signal, which is in direct proportion to the amount of analyte bound.

Table 2:

APP	Solutions	Time	Temperature	Dilution	Notes
BLOCKING	TBS-T 0.1% MILK 5%	1h	RT	/	
Ab I	TBS-T 0.1% MILK 5%	O/N	4°C	1:500	Shaking
3 washes	TBS-T 0.1%	5 min	RT	/	Shaking
Ab II ANTI-RABBIT	TBS-T 0.1% MILK 5%	1h	RT	1:15,000	Shaking in the dark
3 washes	TBS-T 0.1%	5 min	RT	/	Shaking in the dark
1 wash	TBS 1X	5 min	RT	/	Shaking in the dark

P-APP	Solutions	Time	Temperature	Dilution	Notes
BLOCKING	TBS-T 0.1% MILK 5%	1h	RT	/	
3 washes	TBS-T 0.1%	5 min	RT	/	Shaking
Ab I	TBS-T 0.1% BSA 5%	O/N	4°C	1:1,000	Shaking
3 washes	TBS-T 0.1%	5 min	RT	/	Shaking
Ab II ANTI-RABBIT	TBS-T 0.1% MILK 5%	1h	RT	1:15,000	Shaking in the dark
3 washes	TBS-T 0.1%	5 min	RT	/	Shaking in the dark
1 wash	TBS 1X	5 min	RT	/	Shaking in the dark

BACE1	Solutions	Time	Temperature	Dilution	Notes
BLOCKING	TBS-T 0.1% MILK 5%	1h	RT	/	
Ab I	TBS-T 0.1% MILK 5%	2h	RT	1:2,000	Static
3 washes	TBS-T 0.1%	5 min	RT	/	Shaking
Ab II ANTI-RABBIT	TBS-T 0.1% MILK 5%	O/N	4°C	1:15,000	Shaking in the dark
3 washes	TBS-T 0.1%	5 min	RT	/	Shaking in the dark
1 wash	TBS 1X	5 min	RT	/	Shaking in the dark

B-actin	Solutions	Time	Temperature	Dilutions	Notes
BLOCKING	TBS-T 0.2% MILK 5%	1h	RT	/	
Ab I	TBS-T 0.2% MILK 5%	2h	RT	1:1,500	Static
4 washes	TBS-T 0.2% MILK 5%	15 min	RT	/	Shaking
Ab II ANTI-RABBIT	TBS-T 0.2% MILK 5%	O/N	4°C	1:5,000	Shaking in the dark
4 washes	TBS-T 0.2% MILK 5%	15 min	RT	/	Shaking in the dark
1 wash	TBS 1X	15 min	RT	/	Shaking in the dark

COX-2	Solutions	Time	Temperature	Dilutions	Notes
BLOCKING	TBS-T 0.2% MILK 5%	1h	RT	/	
Ab I	TBS-T 0.2% MILK 5%	2h	RT	1:1,000	Static
4 washes	TBS-T 0.2% MILK 5%	15 min	RT	/	Shaking
Ab II ANTI-RABBIT	TBS-T 0.2% MILK 5%	O/N	4°C	1:5,000	Shaking in the dark
4 washes	TBS-T 0.2% MILK 5%	15 min	RT	/	Shaking in the dark
1 wash	TBS 1X	15 min	RT	/	Shaking in the dark

Cyp1b1	Solutions	Time	Temperature	Dilutions	Notes
BLOCKING	TBS-T 0.2% MILK 5%	1h	RT	/	

Ab I	TBS-T 0.2% MILK 5%	2h	RT	Cells 1:200 Mice 1:800	Static
4 washes	TBS-T 0.2% MILK 5%	15 min	RT	/	Shaking
Ab II ANTI-RABBIT	TBS-T 0.2% MILK 5%	O/N	4°C	1:5,000	Shaking in the dark
4 washes	TBS-T 0.2% MILK 5%	15 min	RT	/	Shaking in the dark
1 wash	TBS 1X	15 min	RT	/	Shaking in the dark

Erk	**Solutions**	**Time**	**Temperature**	**Dilutions**	**Notes**
BLOCKING	TBS-T 0.2% MILK 5%	1h	RT	/	
Ab I	TBS-T 0.2% MILK 5%	2h	RT	1:250	Static
4 washes	TBS-T 0.2% MILK 5%	15 min	RT	/	Shaking
Ab II ANTI-RABBIT	TBS-T 0.2% MILK 5%	O/N	4°C	1:5,000	Shaking in the dark
4 washes	TBS-T 0.2% MILK 5%	15 min	RT	/	Shaking in the dark
1 wash	TBS 1X	15 min	RT	/	Shaking in the dark

P-Erk	**Solutions**	**Time**	**Temperature**	**Dilutions**	**Notes**
BLOCKING	TBS-T 0.1% BSA 5%	1h	RT	/	
Ab I	TBS-T 0.1% BSA 5%	2h	RT	1:500	Static
4 washes	TBS-T 0.1%	15 min	RT	/	Shaking
Ab II ANTI-RABBIT	TBS-T 0.1% BSA 5%	O/N	4°C	1:5,000	Shaking in the dark
4 washes	TBS-T 0.1%	15 min	RT	/	Shaking in the dark
1 wash	TBS 1X	15 min	RT	/	Shaking in the dark

HO-1	**Solutions**	**Time**	**Temperature**	**Dilutions**	**Notes**
BLOCKING	TBS-T 0.2% MILK 5%	1h	RT	/	
Ab I	TBS-T 0.2% MILK 5%	2h	RT	Cells 1:200 Mice 1:400	Static
3 washes	TBS-T 0.2% MILK 5%	15 min	RT	/	Shaking
Ab II ANTI-RABBIT	TBS-T 0.2% MILK 5%	O/N	4°C	1:5,000	Shaking in the dark
3 washes	TBS-T 0.2% MILK 5%	15 min	RT	/	Shaking in the dark
1 wash	TBS 1X	15 min	RT	/	Shaking in the dark

Hsp70	**Solutions**	**Time**	**Temperature**	**Dilutions**	**Notes**
BLOCKING	TBS-T 0.2% MILK 5%	1h	RT	/	
Ab I	TBS-T 0.2% MILK 5%	2h	RT	Cells 1:200 Mice 1:400	Static
3 washes	TBS-T 0.2% MILK 5%	15 min	RT	/	Shaking
Ab II ANTI-GOAT	TBS-T 0.2% MILK 5%	O/N	4°C	1:5,000	Shaking in the dark
3 washes	TBS-T 0.2% MILK 5%	15 min	RT	/	Shaking in the dark
1 wash	TBS 1X	15 min	RT	/	Shaking in the dark

iNOS	**Solutions**	**Time**	**Temperature**	**Dilutions**	**Notes**
BLOCKING	TBS-T 0.2% MILK 5%	1h	RT	/	
Ab I	TBS-T 0.2% MILK 5%	2h	RT	Cells 1:200 Mice 1:400	Static
3 washes	TBS-T 0.2% MILK 5%	15 min	RT	/	Shaking
Ab II ANTI-RABBIT	TBS-T 0.2% MILK 5%	O/N	4°C	1:5,000	Shaking in the dark

3 washes	TBS-T 0.2% MILK 5%	15 min	RT	/	Shaking in the dark
1 wash	TBS 1X	15 min	RT	/	Shaking in the dark

Nrf2	**Solutions**	**Time**	**Temperature**	**Dilutions**	**Notes**
BLOCKING	TBS-T 0.2% MILK 5%	1h	RT	/	
Ab I	TBS-T 0.2% MILK 5%	2h	RT	1:500	Static
3 washes	TBS-T 0.2% MILK 5%	15 min	RT	/	Shaking
Ab II ANTI-RABBIT	TBS-T 0.2% MILK 5%	O/N	4°C	1:5,000	Shaking in the dark
3 washes	TBS-T 0.2% MILK 5%	15 min	RT	/	Shaking in the dark
1 wash	TBS 1X	15 min	RT	/	Shaking in the dark

CHAPTER 4: C6 glioma cells results and discussion

4.1 RESULTS

C6 GLIOMA CELLS VIABILITY AFTER DEP TREATMENT

C6 glioma cells were treated for 3h and 24h with different concentrations (25µg/ml, 50µg/ml and 100µg/ml) of DEP. After treatment, cell viability was evaluated using the PrestoBlue® assay.

PrestoBlue® assay did not evidence any significant variation comparing to control in cell viability, assessed by mitochondrial metabolism, after 3h or 24h of DEP 25µg/ml and 50µg/ml treatment. In C6 glioma cells treated with DEP 100µg/ml for 24h, a significant decrease of 32.3% ± 6.5% (standard error, s.e.) in cell viability, comparing to control, was observed. Therefore, in our cellular model, doses of 25µg/ml and 50µg/ml resulted useful to study the mechanisms induced by DEP treatment without resulting lethal (**Fig 18**).

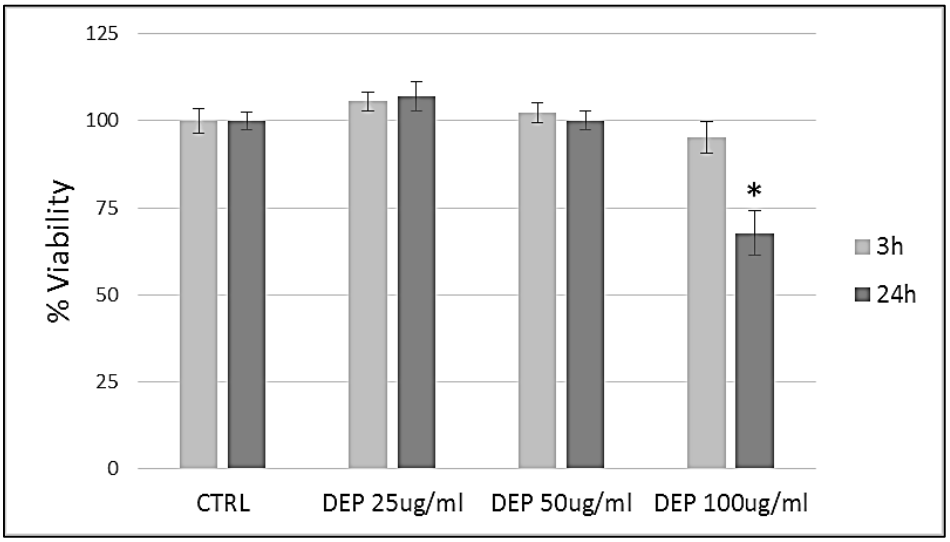

Figure 18: **Cell viability**. Cell viability has been tested after DEP (25µg/ml, 50µg/ml and 100µg/ml) treatment of C6 glioma cells for 3h or 24h. The data are expressed as mean ± s.e. (n = 7); statistical differences were tested accordingly by One-way ANOVA followed by Bonferroni post-hoc comparison. * $p<0.05$ vs. respective control.

EVALUATION OF HO-1 INDUCTION IN C6 GLIOMA CELLS AFTER DEP TREATMENT

Heme oxigenase 1 (HO-1) is an enzyme highly up-regulated under oxidative stress conditions and the rate limiting step in heme degradation that produces anti-oxidant molecules, thus widely accepted as marker of oxidative stress (Iles et al., 2005). C6 glioma cells were treated for 3h and 24h with selected concentrations (25µg/ml, 50µg/ml) of DEP. After treatment, the cells were lysed with denaturing buffer (2% SDS). Following SDS-PAGE, proteins were revealed by WB and enhanced chemiluminescence.

After 3h, the treatment induced a significant increase of HO-1 expression levels with 25µg/ml DEP (+118%) and 50µg/ml (+147%), comparing to control. After 24h, the treatment induced a significant increase of HO-1 expression levels with 25µg/ml DEP (+177%) and 50µg/ml (+475%), comparing to control (**Fig 19**).

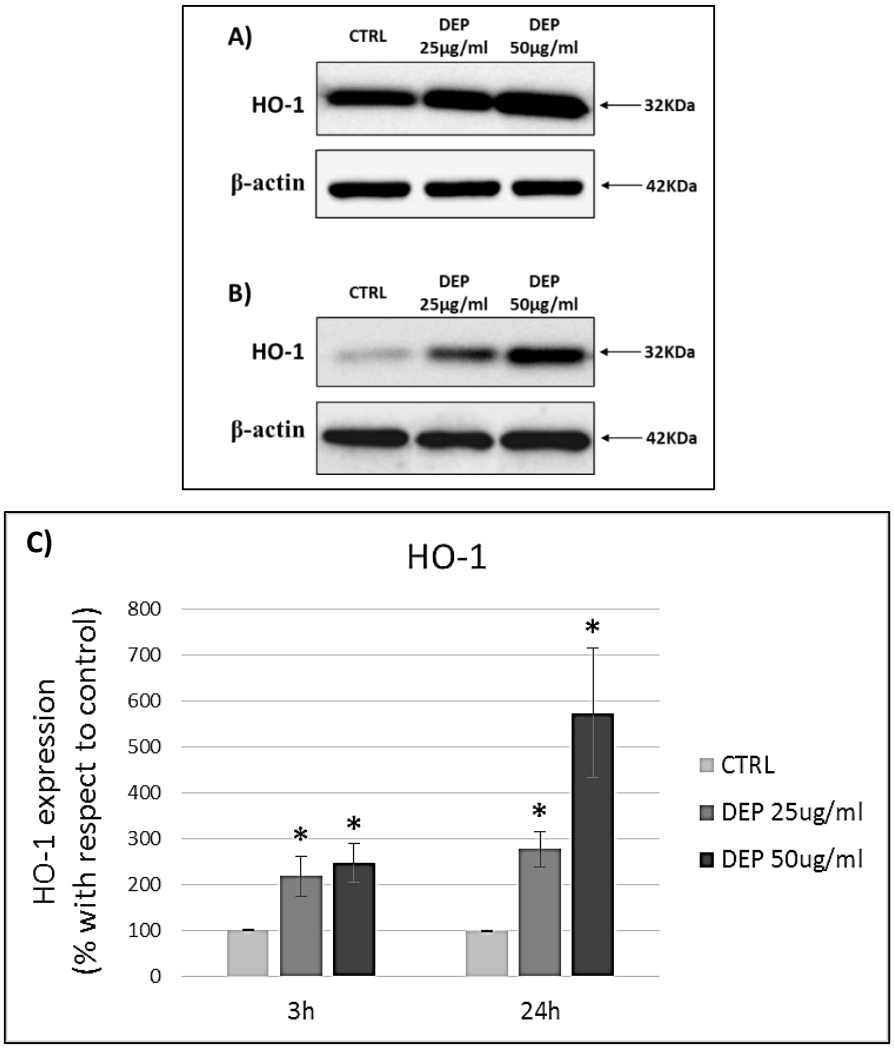

Figure 19: HO-1 protein analysis after 3h and 24h of DEP treatment. Representative immunoblotting images of HO-1 analysis in C6 glioma cells treated for 3h **(A)** and for 24h **(B)** with 25µg/ml and 50µg/ml of DEP. Histograms **(C)** display HO-1 expression levels in treated cells with respect to control cells. Proteins have been normalized for the corresponding β-actin signal in each lane and the data are expressed as mean ± s.e. (n = 3); statistical differences were tested accordingly by One-way ANOVA followed by Bonferroni post-hoc comparison. * $p<0.05$ vs. respective control.

EVALUATION OF Cyp1b1 EXPRESSION IN C6 GLIOMA CELLS AFTER DEP TREATMENT

DEP is characterized by an abundant aromatic fraction, composed by various PAHs (Stewart et al., 2003), that represent both inducers and substrates of cytochrome P450 enzymes like Cyp1b1, which is therefore considered a marker of PAHs metabolism. C6 glioma cells were treated for 3h and 24h with selected concentrations (25µg/ml, 50µg/ml) of DEP. After treatment, the cells were lysed with denaturing buffer (2% SDS). Following SDS-PAGE, proteins were revealed by WB and enhanced chemiluminescence.

After 3h, the treatment did not induce significant variations of Cyp1b1 expression levels. After 24h, the treatment induced a significant increase of Cyp1b1 expression levels with 25µg/ml DEP (+211%) and 50µg/ml (+423%), comparing to control (**Fig 20**).

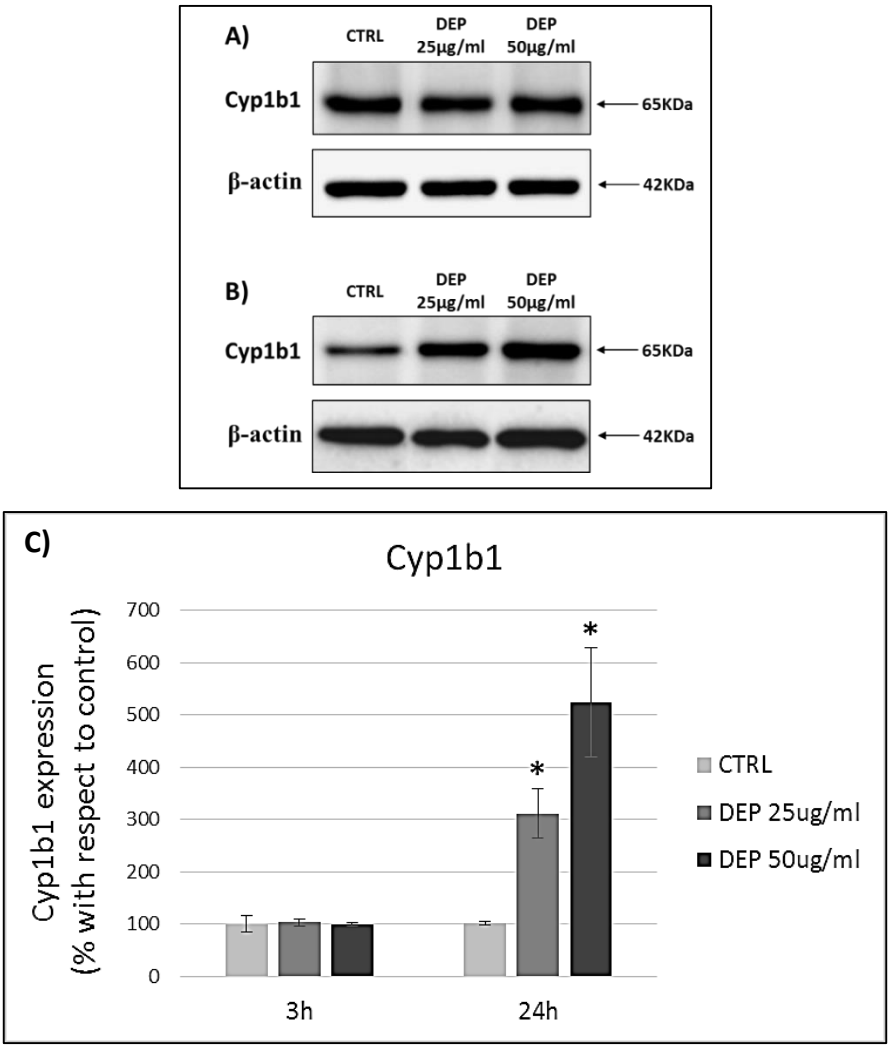

Figure 20: Cyp1b1 protein analysis after 3h and 24h of DEP treatment. Representative immunoblotting images of Cyp1b1 analysis in C6 glioma cells treated for 3h **(A)** and for 24h **(B)** with 25µg/ml and 50µg/ml of DEP. Histograms **(C)** display Cyp1b1 expression levels in treated cells with respect to control cells. Proteins have been normalized for the corresponding β-actin signal in each lane and the data are expressed as mean ± s.e. (n = 3); statistical differences were tested accordingly by One-way ANOVA followed by Bonferroni post-hoc comparison. * $p<0.05$ vs. respective control.

EVALUATION OF iNOS INDUCTION IN C6 GLIOMA CELLS AFTER DEP TREATMENT

Literature data describe markers of inflammation in the brain of people and animals exposed to high levels of air pollution. Together with the transcription factor NFκB and the inflammatory gene COX-2, inflammation is characterized by an increased expression of the inducible nitric oxide synthase (iNOS) (Calderon-Garciduenas et al., 2003). Because iNOS is a heme protein, its availability can be influenced by HO-1. C6 glioma cells were treated for 3h and 24h with selected concentrations (25µg/ml, 50µg/ml) of DEP. After treatment, the cells were lysed with denaturing buffer (2% SDS). Following SDS-PAGE, proteins were revealed by WB and enhanced chemiluminescence.

After 3h and 24h, treated cells showed a decreasing and increasing trend respectively, although these changes were not significant comparing to control cells (**Fig 21**).

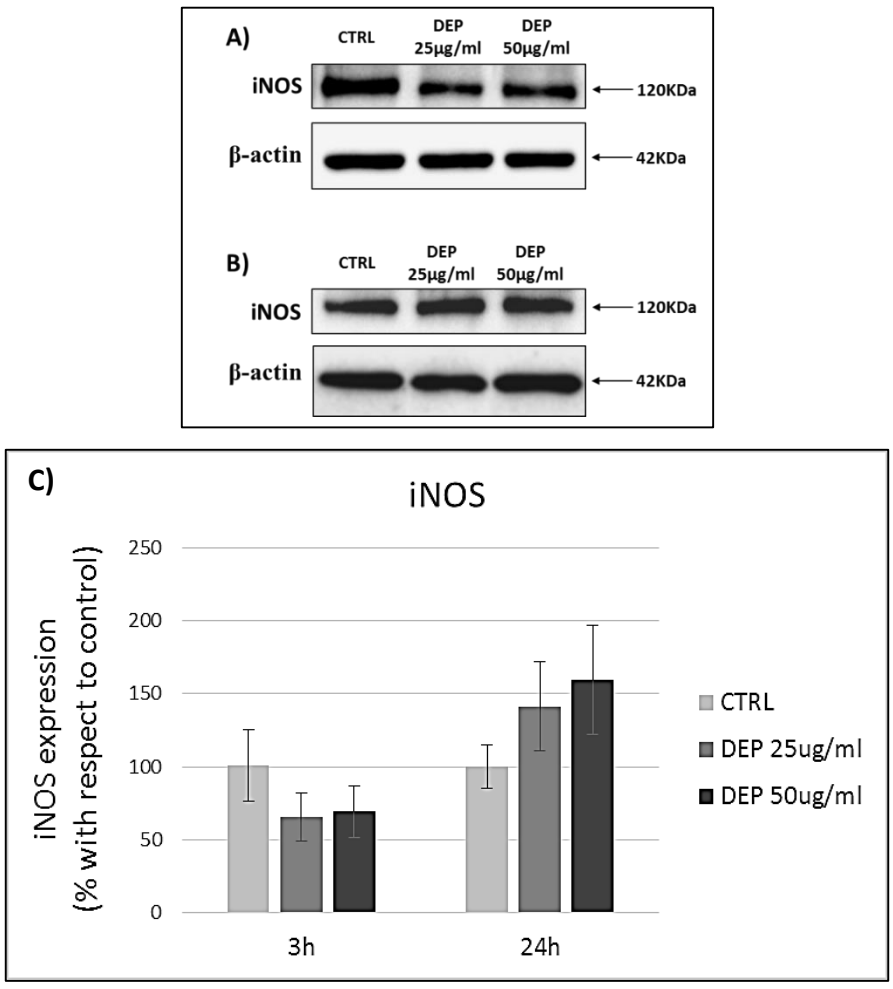

Figure 21: iNOS protein analysis after 3h and 24h of DEP treatment. Representative immunoblotting images of iNOS analysis in C6 glioma cells treated for 3h **(A)** and for 24h **(B)** with 25µg/ml and 50µg/ml of DEP. Histograms **(C)** display iNOS expression levels in treated cells with respect to control cells. Proteins have been normalized for the corresponding β-actin signal in each lane and the data are expressed as mean ± s.e. (n = 3); statistical differences were tested accordingly by One-way ANOVA followed by Bonferroni post-hoc comparison.

EVALUATION OF MAPK PATHWAY ACTIVATION IN C6 GLIOMA CELLS AFTER DEP TREATMENT

Literature data suggested that MAPK pathway is activated after DEP exposure (Pourazar et al., 2005) and that its activation could trigger Nrf2 phosphorylation, facilitating the synthesis of a number of phase II proteins, including HO-1 (Iles et al., 2005; Li et al., 2007). In order to test the activation of the MAPKs pathway and its possible involvement in the DEP-induced response, time course experiments have been carried out with 25µg/ml of DEP for 30 min, 1h, 2h, 3h, 4h, 5h, 6h, 7h, 8h, 12h, 18h and 24h (data not shown). The dose of 25µg/ml has been chosen from literature (Levesque et al., 2011). After 2h and 5h, DEP treatment induced a significant increase in p-ERK1-2/ERK1-2 (activating phosphorylation). In order to block the ERK1-2 activation and to identify a possible mechanism related to this signal pathway, cells have been treated with 25µg/ml of DEP in presence of a MEK inhibitor (U0126) for 5h. MEK is the kinase upstream to ERK1-2, and its phosphorylation is inhibited by U0126, thus blocking also the downstream activation of ERK1-2. ERK1-2 activation can trigger the phosphorylation of Nrf2 transcription factor, facilitating its translocation into the nucleus and transcription activity.

After treatment, C6 glioma cells were lysed with denaturing buffer (2% SDS). Following SDS-PAGE, proteins were revealed by WB and enhanced chemiluminescence.

None of these treatments was able to induce any variation in cell metabolism (data not shown). After 5h of treatment, cells in complete medium + DEP 25µg/ml (CM+DEP25) displayed a significant phosphorylation of ERK1-2 (+34%), comparing to respective control (**Fig 22**). It is worth to note a slight increase of Nrf2 level in CM+DEP25, since it has biological consequences: in fact, at 5h, DEP treatment induced a significant increase in HO-1 levels CM+DEP25 cells (+553%) (**Fig 22**). After 5h of treatment, cells in serum free medium + DEP 25µg/ml (SFM+DEP25) showed a similar trend to those treated in complete medium (data not shown). After 5h of treatment, in cells in serum free medium + U0126 + DEP 25µg/ml (SFM+U+DEP25), pERK1-2/ERK1-2 was significantly lower comparing to its corresponding control (-59%) (**Fig 22**), thus confirming the upstream MEK inhibition by U0126. Consistent with this observation, Nrf2 levels resulted significantly lower (-26%), whereas no significant increase in HO-1 was registered in SFM+U+DEP25 cells comparing to respective control (**Fig 22**).

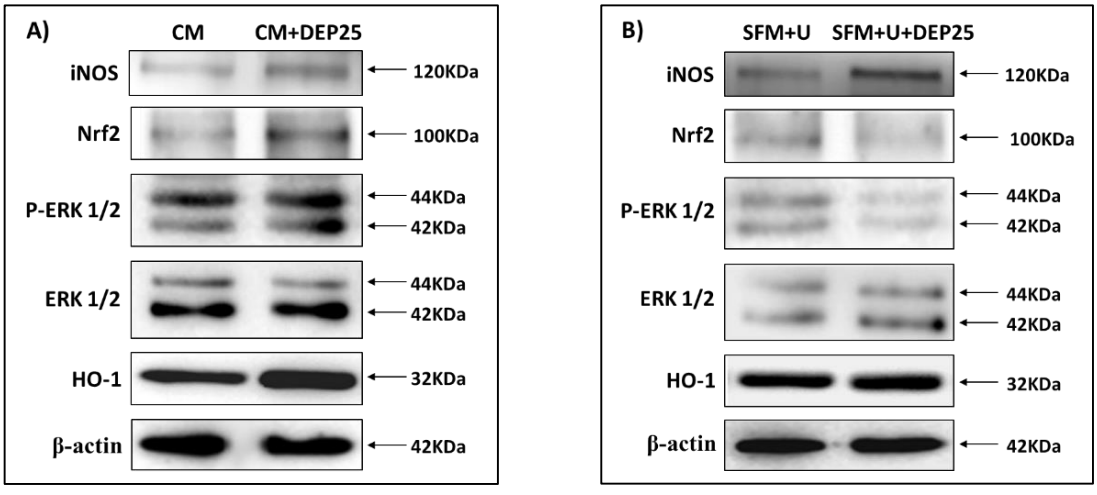

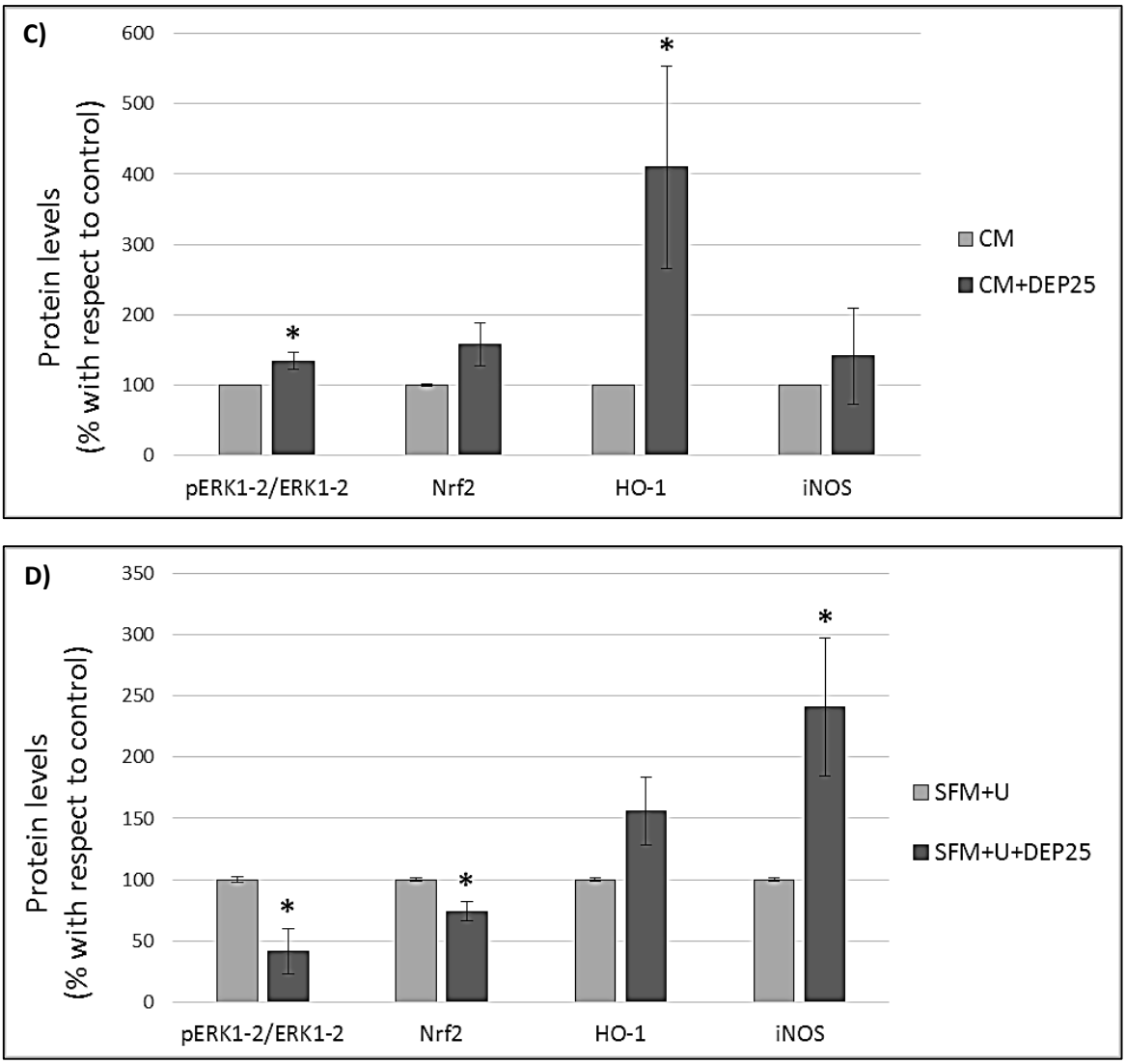

Figure 22: Protein analysis after 5h of DEP treatment in complete medium and in serum free medium added with U0126. Representative immunoblotting images of protein analysis in C6 glioma cells treated **(A)** for 5h with 25µg/ml of DEP (DEP25) in complete medium (CM) and **(B)** for 5h with 25µg/ml of DEP (DEP25) in serum free medium added with U0126 (SFM+U). Histograms **(C, D)** displays protein expression levels in treated cells with respect to control cells. Proteins have been normalized for the corresponding β-actin signal in each lane and the data are expressed as mean ± s.e. (n = 4-6); statistical differences were tested accordingly by One-way ANOVA followed by Bonferroni post-hoc comparison. * $p<0.05$ vs. respective control.

EVALUATION OF TOTAL ANTIOXIDANT CAPACITY IN C6 GLIOMA CELLS AFTER DEP TREATMENT AND MAPK PATHWAY INHIBITION

The total antioxidant capacity (TAC) assay is based on the assumption that the lower the value of the antioxidant concentration is, the greater the oxidative stress to which the sample had been exposed (Wegesser et al., 2010). Therefore, TAC assay was performed on C6 glioma cells treated for 5h with 25µg/ml of DEP. Moreover, the effect of MEK inhibition on antioxidant enzymes generation and consume were evaluated in C6 glioma cells treated with DEP in presence of MEK inhibitor U0126.

After treatment, C6 glioma cells were lysed through sonication in PBS and TAC were evaluated with a specific kit.

In CM+DEP25 and SFM+DEP25 cells the treatment induced a significant decrease in TAC, comparing to respective controls (CM and SFM) (-33.7% and -21.9% respectively) (**Fig 23**). On the contrary, in SFM+U+DEP25 cells, TAC concentration resulted unaltered comparing to respective control (SFM+U) (**Fig 23**). However, serum free condition seemed to cause in the cells a decrease in TAC comparing to control in complete medium (CM). Finally, U0126 treatment (SFM+U and SFM+U+DEP25) induced a further decrease of TAC comparing to SFM (**Fig 23**).

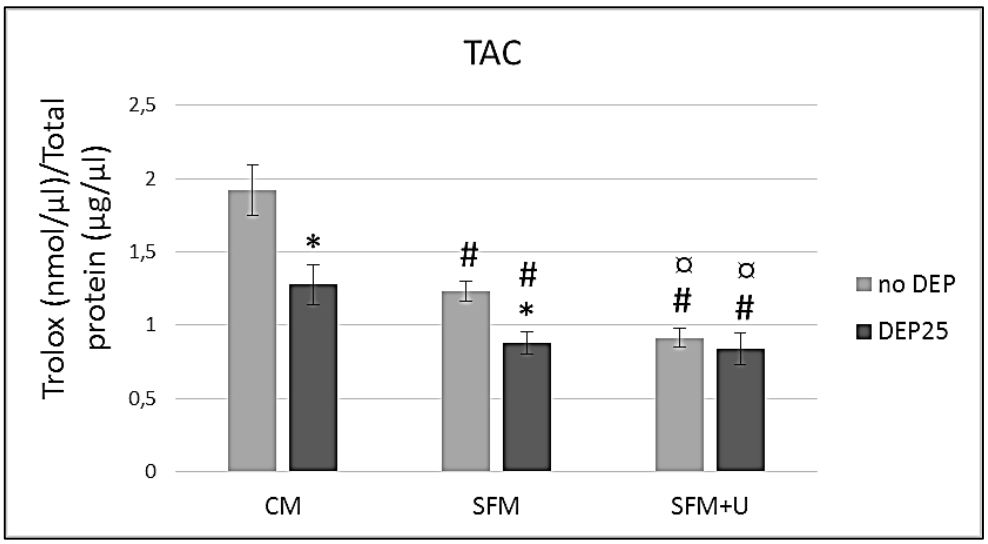

Figure 23: TAC analysis after 5h of DEP treatment in complete medium, serum free medium and serum free medium added with U0126. Analysis of TAC in C6 glioma cells treated for 5h with 25µm/ml of DEP (DEP25) in complete medium (CM), serum free medium (SFM) or in serum free medium added with U0126 (SFM+U). Trolox is the standard provided by the kit; 1 nmol of Trolox is able to reduce 2 nmol of Cu^{++}. The data are expressed as mean ± s.e. (n = 3); statistical differences were tested accordingly by One-way ANOVA followed by Bonferroni post-hoc comparison. * $p<0.05$ vs. respective control; # $p<0.05$ vs. no DEP CM; ¤ $p<0.05$ vs. no DEP SFM.

4.2 DISCUSSION

In this part of the project, we analysed the effects of DEP administration on C6 glioma cells and the involvement of MEK-ERK1-2 pathway and Nrf2 activation in a putative anti-oxidant strategy elicited by cells to contrast the oxidative stress induced by DEP treatment.

DEP treatment induces oxidative stress in C6 glioma cells

The capacity of UFPs to generate oxidative stress has been related to their small size, large surface area and chemical composition (Li et al., 2003). Consistent with this assertion, 3h and 24h DEP treatments of C6glioma cells were not cytotoxic and induced an increase of HO-1, an enzyme highly up-regulated under oxidative stress conditions and the rate limiting step in heme degradation that produces anti-oxidant molecules, thus widely accepted as marker of oxidative stress (Iles et al., 2005).

It is known that DEP is characterized by an abundant aromatic fraction, composed by various PAHs (Stewart et al., 2003), that are themselves both inducers and substrates of cytochrome P450 enzymes like Cyp1b1 (Arenas-Huertero et al., 2011). In most cases, oxidation of PAHs by cytochrome P450 is an initial step of the activation process to produce reactive oxygenated intermediates capable of interacting with cellular macromolecules, particularly nucleic acids and proteins, producing oxidative stress (Nebert and Dalton, 2006). Despite HO-1 regulates the intracellular levels of heme pool, thus influencing its availability for various heme proteins (Otterbein and Zuckerbraun, 2005), after 24h of treatment with 25µm/ml and 50µm/ml of DEP the great PAHs content of DEP could result in an induction of Cyp1b1 stronger and predominant on heme degradation by HO-1. On the contrary, the induction of HO-1 after DEP treatment is able to counteract the expression of iNOS, another heme protein; in fact, biochemical analyses did not evidence any significant change in iNOS levels.

MEK, ERK1-2 and Nrf2 involvement in defence against oxidative stress

Literature data suggested that ERK1-2 activation could trigger Nrf2 phosphorylation, facilitating its translocation into the nucleus and the consequential increased synthesis of a number of phase II proteins (Iles et al., 2005; Li et al., 2007). These antioxidant enzymes are able to counteract the chronic oxidative stress: antioxidants such as catalase, SOD, GSH-peroxidases, GSH-reductase, GSH-transferase, NADPH-quinone oxidoreductase, Cytochrome P450 mono-oxygenase system, thioredoxin and thioredoxin reductase are able to detoxify an excess of ROS, and the activation of the GSH-synthase allows a marked increase of the GSH intracellular level. Interestingly, Nrf2 regulates also HO-1 expression (Bocci and Valacchi, 2015) by a Keap1-independent mechanism relying on a post-translational phosphorylation of ERK1-2 (Kim and Jang, 2014).

In this part of the project, the DEP dose of 25µg/ml has been chosen because it is the middle dose in the range indicated in literature for treating CNS cells (Levesque et al., 2011). After 5h of DEP exposure, we

noticed ERK1-2 activation, while oxidative stress seems to be well controlled by the induction of anti-oxidant enzymes such as HO-1, as no significant changes have been noticed for Cyp1b1 (data not shown) and iNOS.

In order to investigate if in C6 glioma cells anti-oxidant strategies induced after DEP exposure are related to a mechanism MEK-ERK1-2 dependent, we analysed ERK1-2 phosphorylation, Nrf2 and HO-1 expression after treating cells with DEP in presence of the MEK inhibitor U0126.

First, we registered a reduction in ERK1-2 phosphorylation after DEP stimulation (SFM+U+DEP25) and a consequent reduction of Nrf2 total level, thus representing the increase in Nrf2 ubiquitylation and degradation (McMahon et al., 2003). Although Nrf2 activation may depend on both Keap1-dependent and the Keap1-independent pathways (i.e., Nrf2 phosphorylation by activated ERK1-2) regulation (Kim and Jang, 2014), our results clearly show a significant reduction of Nrf2 level expression after MEK inhibition (SFM+U+DEP25) and decreased ERK1-2 activation, comparing to respective control, suggesting that the Keap1-independent pathway could be essential in Nrf2 activation by DEP in C6 glioma cells.

Moreover, HO-1 seems quite dependent on ERK1-2 phosphorylation and Nrf2 activation: after MEK inhibition, HO-1 levels did not result as high as after DEP treatment alone. However, as already demonstrated by Iles and colleagues (Iles et al., 2005), HO-1 after DEP25 treatment in presence of U0126 did not result completely depleted, suggesting that other mechanisms could be involved in HO-1 regulation. It is known that other transcription factors, such as AP-1 and NFkB, could be involved in HO-1 transcription (Alam and Cookn, 2007).

Lacking Nrf2 activation and HO-1 increase, iNOS levels resulted increased. According to literature, it is known that iNOS enzyme results significantly increased in Nrf2-KO mice and that an up-regulation of HO-1 corresponds to a simultaneous down-regulation of iNOS expression (Kim et al., 2013).

It has been demonstrated that the MEK-ERK1-2 pathway is involved in the interaction between the AhR/Arnt heterodimer and its responsive elements, leading to the expression of Cyp1a1 and Cyp1b1. Indeed, the MEK inhibitor U0126 or the dominant negative mutant of MEK both repress the gene expression induced by AhR ligands (Yim et al., 2004); moreover, AhR and DNA interaction is abolished by phosphatase treatment of AhR *in-vitro* (Yim et al., 2004). These data indicate that phosphorylation by MAPKs could be essential in the expression of cytochromes, and suggest why in C6 glioma cells the treatment with 25µg/ml of DEP in presence of the MEK inhibitor U0126 did not induce increases in Cyp1b1 levels.

Finally, it is assumed that the lower the value of the antioxidant concentration is, the greater the oxidative stress to which the sample had been exposed (Wegesser et al., 2010): anti-oxidant resources are consumed in order to regulate the increasing detrimental concentration of ROS. Therefore, decreases in antioxidant enzymes can be used as indicators of oxidative stress in acute exposure studies (Møller et al., 2014). TAC analysis confirmed oxidative stress induction by treatment with 25µg/ml of DEP in complete medium as well as in serum free medium. Moreover, we used this assay also to confirm that ERK pathway activation is necessary to induce transcription of anti-oxidant enzymes: in presence of the MEK inhibitor U0126, it was

possible to note the depletion of anti-oxidant defenses, as TAC resulted significantly lower both in SFM+U and in SFM+U+DEP25, comparing to CM and to SFM. Therefore, the lack of antioxidant enzymes rather than the absence of oxidative stress could explain the levels of TAC measured in SFM+U+DEP25 cells similar to those in respective control (SFM+U).

Conclusion

DEP treatment at sub-lethal concentrations induced oxidative stress in C6 glioma cells. However, cells activate anti-oxidant pathways to contrast the oxidative status induced by DEP treatment (**Fig. 24**) and the role of MEK-ERK1-2 pathway seems important in regulating these anti-oxidant strategies.

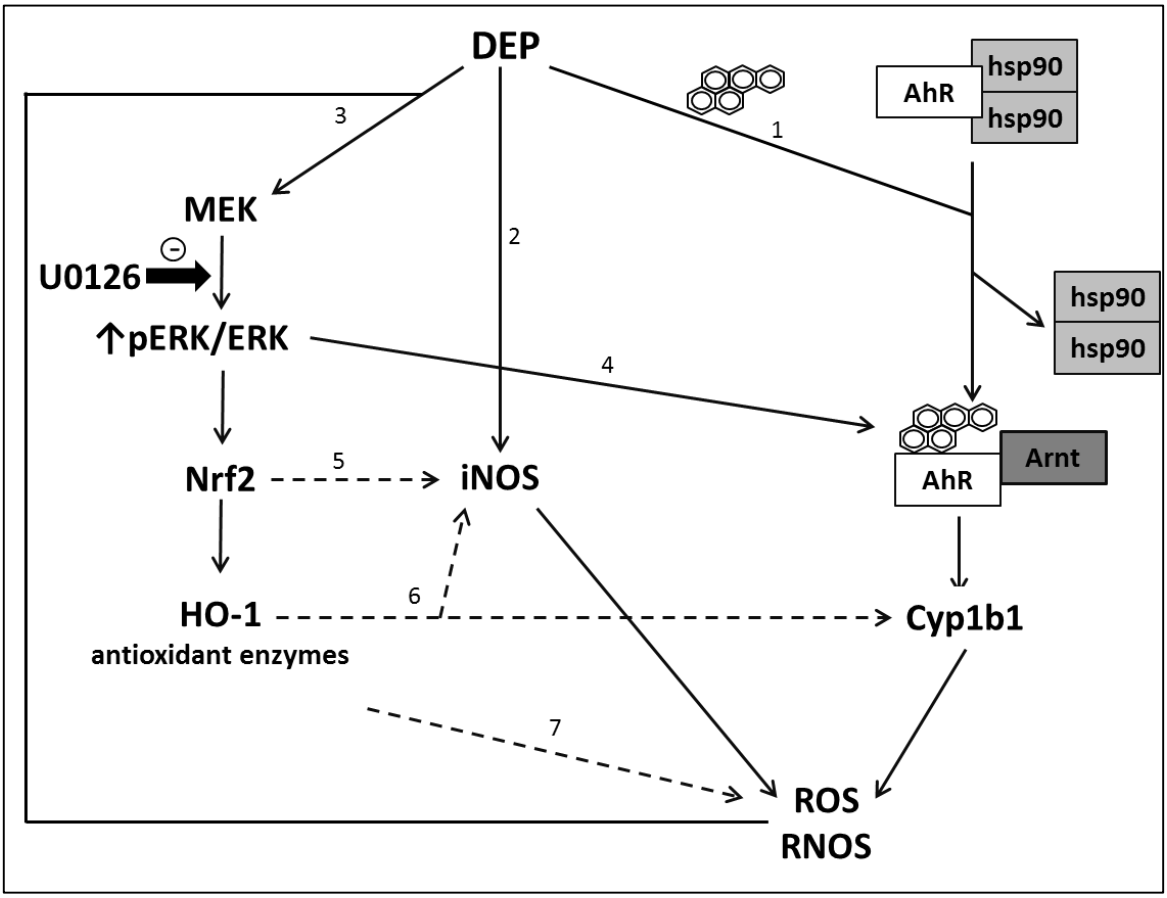

Figure 24: Schematic representation of pathways activated by DEP treatment. **(1)** PAHs on the DEP surface are able to bind the aryl hydrocarbon receptor (AhR), induce its translocation to the nucleus where it heterodimerizes with AhR nuclear translocator (Arnt) to up-regulate CyP1B1, thus causing an increase in Cyp1b1 protein levels (Chang et al., 2007). Oxidation of PAHs by cytochrome P450 is an initial step of the process that generates reactive oxygenated intermediates (Nebert and Dalton, 2006). **(2)** Another potential source of oxidative stress consists in iNOS, a protein induced by many kinds of particulate matter (Farina et al., 2013; Li et al., 2016). **(3)** ROS and RNOS contributes together with DEP particles themselves to the induction of the MAPKs pathway, involving MEK and ERK, and resulting in Nrf2 activation, its translocation to the nucleus and the transcription of target genes, thus causing an increase in antioxidant enzymes such as

HO-1, OGG1 and others (Iles et al., 2005). **(4)** The MEK/ERK pathway is involved in the interaction between AhR and Arnt (Yim et al., 2004). **(5)** It is known that Nrf2 activation is able to recruit and deplete p300, thus causing a decrease in iNOS expression (Kim et al., 2013). **(6)** HO-1 regulates the intracellular levels of heme pool, thus influencing the availability of heme for various hemoproteins (Otterbein and Zuckerbraun, 2005), such as iNOS and cytochromes. **(7)** Others phase II antioxidant enzymes contribute in regulating oxidative stress (Li et al., 2000).

Dashed arrows indicate a "negative" regulation, while continuous arrows indicate a "positive" regulation. The bold arrow indicates the mechanism inhibited by U0126.

CHAPTER 5: HT22 cells results and discussion

5.1 RESULTS

HT22 CELLS VIABILITY AFTER DEP TREATMENT

HT22 cells were treated for 3h and 24h with different concentrations (10µg/ml and 50µg/ml) of DEP. After treatment, cell viability was evaluated using MTT assay.

MTT assay did not evidence any significant variation in cell viability comparing to control, assessed by mitochondrial metabolism, after 3h or 24h of DEP treatment for the considered concentrations. Therefore, in our cellular model, doses of 10µg/ml and 50µg/ml resulted useful to study the mechanisms induced by DEP treatment without resulting lethal (**Fig 25**).

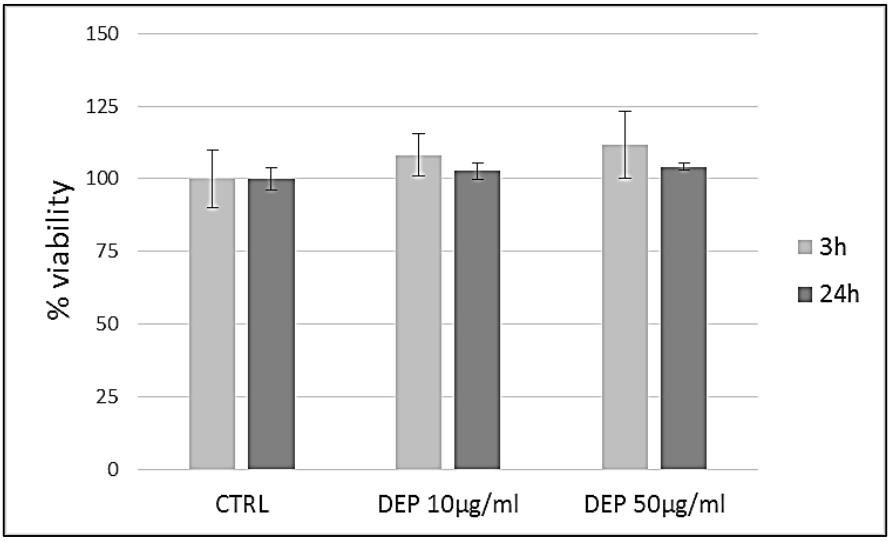

Figure 25: **Cell viability**. Cell viability has been tested after DEP (10µg/ml and 50µg/ml) treatment of HT22 cells for 3h or 24h. The data are expressed as mean ± s.e. (n = 6); statistical differences were tested accordingly by One-way ANOVA followed by Bonferroni post-hoc comparison.

EVALUATION OF HO-1 INDUCTION IN HT22 CELLS AFTER DEP TREATMENT

As mentioned before, HO-1 was evaluated as marker of oxidative stress (Iles et al., 2005) in HT22 cells treated for 3h and 24h with selected concentrations (10µg/ml, 50µg/ml) of DEP. After treatment, the cells were lysed with denaturing buffer (2% SDS). Following SDS-PAGE, proteins were revealed by WB and enhanced chemiluminescence.

The treatment induced an increase of HO-1 expression levels with 10µg/ml DEP (+240% at 3h, +193% at 24h) and 50µg/ml (+244% at 3h, +602% at 24h), although statistical analysis showed that only 50µg/ml of DEP induced significant variations, comparing to controls (**Fig 26**).

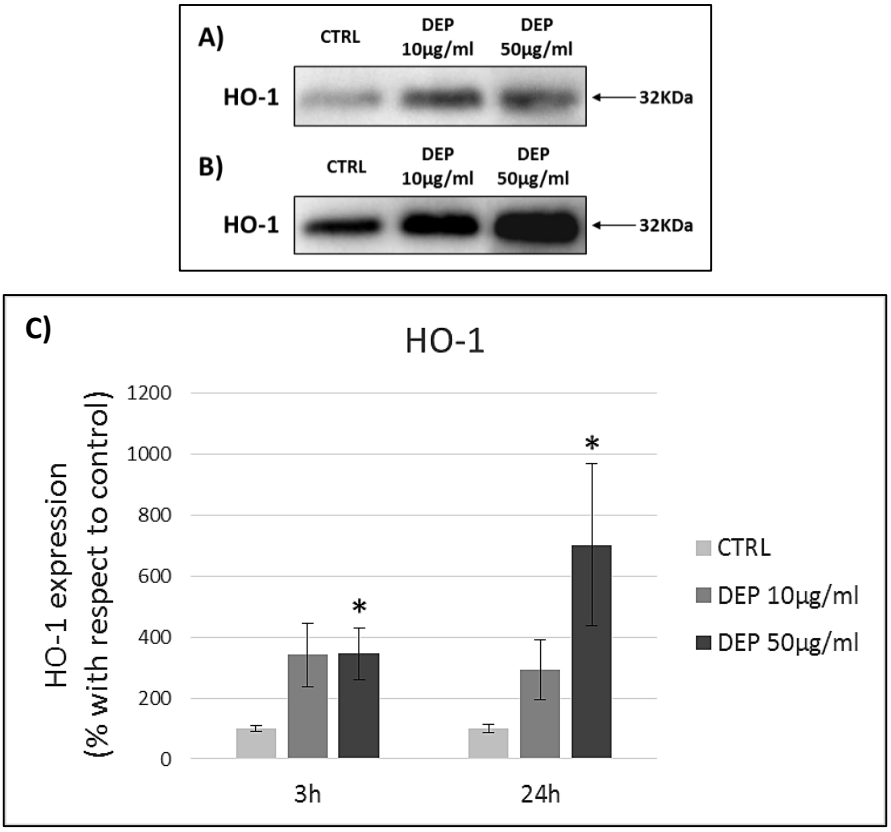

Figure 26: HO-1 protein analysis after 3h and 24h of DEP treatment. Representative immunoblotting images of HO-1 analysis in HT22 cells treated for 3h **(A)** and for 24h **(B)** with 10µg/ml and 50µg/ml of DEP. Histograms **(C)** display HO-1 expression levels in treated cells with respect to control cells. Proteins have been normalized for corresponding total proteins revealed by Ponceau in each lane and the data are expressed as mean ± s.e. (n = 8-12). Statistical differences were tested accordingly by One-way ANOVA followed by Tukey post-hoc comparison, as population variances were significantly different (Levene's Test, $p<0.05$). * $p<0.05$ vs. respective control.

EVALUATION OF Hsp70 INDUCTION IN HT22 CELLS AFTER DEP TREATMENT

Literature data suggest that Heat shock protein 70 (Hsp70) plays a key role during oxidative stress induced by DEP treatment, contributing to preserve protein folding (Jung et al., 2007). Therefore, Hsp70 was evaluated as marker of ER stress in HT22 cells treated for 3h and 24h with selected concentrations (10µg/ml, 50µg/ml) of DEP. After treatment, the cells were lysed with denaturing buffer (2% SDS). Following SDS-PAGE, proteins were revealed by WB and enhanced chemiluminescence.

The treatment induced an increase of Hsp70 expression levels with 10µg/ml DEP (+111% at 3h, +40% at 24h) and 50µg/ml (+133% at 3h, +65% at 24h), although statistical analysis showed that only 50µg/ml of DEP induced significant variations, comparing to control (**Fig 27**).

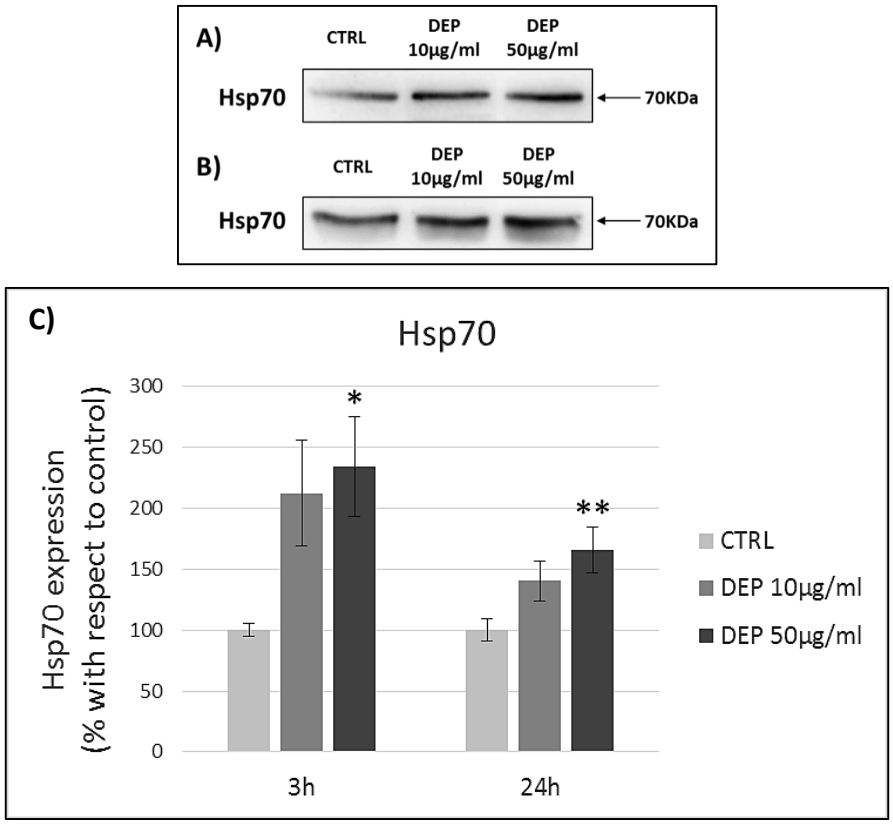

Figure 27: Hsp70 protein analysis after 3h and 24h of DEP treatment. Representative immunoblotting images of Hsp70 analysis in HT22 cells treated for 3h **(A)** and for 24h **(B)** with 10µg/ml and 50µg/ml of DEP. Histograms **(C)** display Hsp70 expression levels in treated cells with respect to control cells. Proteins have been normalized for corresponding total proteins revealed by Ponceau in each lane and the data are expressed as mean ± s.e. (n = 9-12). Statistical differences were tested accordingly by One-way ANOVA followed by Tukey post-hoc comparison, as population variances were significantly different (Levene's Test, $p<0.05$). * $p<0.05$ vs. respective control. ** $p<0.01$ vs. respective control.

EVALUATION OF Cyp1b1 INDUCTION IN HT22 CELLS AFTER DEP TREATMENT

As mentioned before, DEP is characterized by an abundant PAHs content (Stewart et al., 2003), and Cyp1b1 was evaluated as marker of PAHs metabolism in HT22 cells treated for 3h and 24h with selected concentrations (10µg/ml, 50µg/ml) of DEP. After treatment, the cells were lysed with denaturing buffer (2% SDS). Following SDS-PAGE, proteins were revealed by WB and enhanced chemiluminescence.

The treatment induced an increase of Cyp1b1 expression levels with 10µg/ml DEP (+213% at 3h, +111% at 24h) and 50µg/ml (+411% at 3h, +124% at 24h), although statistical analysis showed that only 50µg/ml of DEP induced significant variations, comparing to control (**Fig 28**).

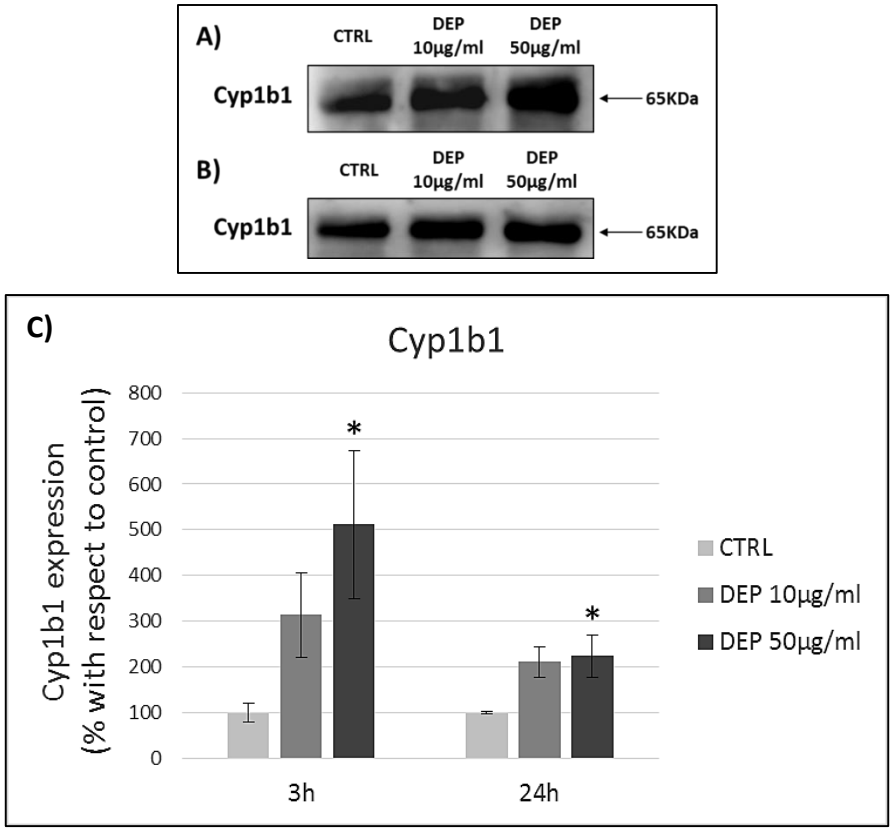

Figure 28: Cyp1b1 protein analysis after 3h and 24h of DEP treatment. Representative immunoblotting images of Cyp1b1 analysis in HT22 cells treated for 3h **(A)** and for 24h **(B)** with 10µg/ml and 50µg/ml of DEP. Histograms **(C)** display Cyp1b1 expression levels in treated cells with respect to control cells. Proteins have been normalized for corresponding total proteins revealed by Ponceau in each lane and the data are expressed as mean ± s.e. (n = 9-12). Statistical differences were tested accordingly by One-way ANOVA followed by Tukey post-hoc comparison, as population variances were significantly different (Levene's Test, $p<0.05$). * $p<0.05$ vs. respective control.

EVALUATION OF COX-2 INDUCTION IN HT22 CELLS AFTER DEP TREATMENT

As mentioned before, brain inflammation is associated to high levels of air pollution (Calderon-Garciduenas et al., 2004). Therefore, COX-2 was evaluated in HT22 cells treated for 3h and 24h with selected concentrations (10µg/ml, 50µg/ml) of DEP. After treatment, the cells were lysed with denaturing buffer (2% SDS). Following SDS-PAGE, proteins were revealed by WB and enhanced chemiluminescence.

After 3h, the treatment induced an increase of COX-2 expression levels with 50µg/ml DEP (+51%), comparing to control, although not significant. After 24h, the treatment caused an increment of COX-2 expression levels with 10µg/ml (+35%) and 50µg/ml (+222%) of DEP comparing to control cells, where only the highest concentration resulted able to induce significant changes (**Fig 29**). Moreover, 50µg/ml of DEP induced significant raise of COX-2 comparing to 10µg/ml of DEP (+186%) (**Fig 29**).

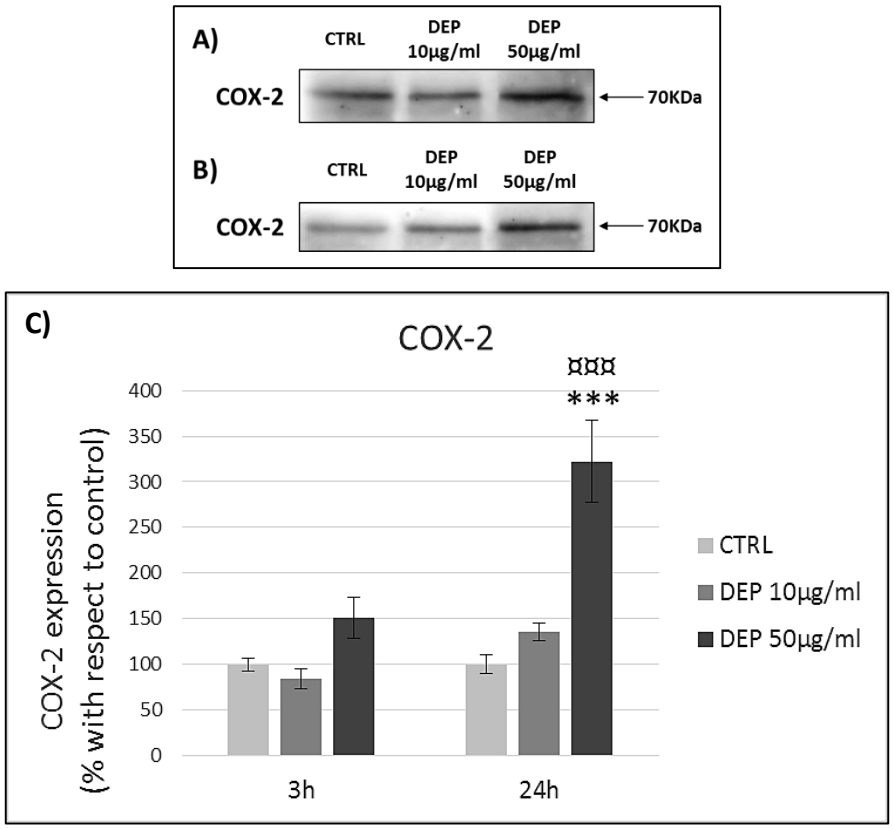

Figure 29: COX-2 protein analysis after 3h and 24h of DEP treatment. Representative immunoblotting images of COX-2 analysis in HT22 cells treated for 3h **(A)** and for 24h **(B)** with 10µg/ml and 50µg/ml of DEP. Histograms **(C)** display COX-2 expression levels in treated cells with respect to control cells. Proteins have been normalized for corresponding total proteins revealed by Ponceau in each lane and the data are expressed as mean ± s.e. (n = 6-9). Statistical differences were tested accordingly by One-way ANOVA followed by Tukey post-hoc comparison, as population variances were significantly different (Levene's Test, $p<0.05$). ¤ $p<0.05$ vs. DEP 10µg/ml. *** $p<0.001$ vs. respective control. ¤¤¤ $p<0.001$ vs. respective DEP 10µg/ml.

EVALUATION OF iNOS INDUCTION IN HT22 CELLS AFTER DEP TREATMENT

iNOS was evaluated as another marker of inflammation in HT22 cells treated for 3h and 24h with selected concentrations (10µg/ml, 50µg/ml) of DEP. After treatment, the cells were lysed with denaturing buffer (2% SDS). Following SDS-PAGE, proteins were revealed by WB and enhanced chemiluminescence.

After 3h, the treatment induced a non-significant increase of iNOS expression levels with 10µg/ml DEP (+24%) and 50µg/ml (+63%), comparing to control. After 24h, the treatment caused a reduction of iNOS expression levels with 10µg/ml of DEP (-25%) and an increase with 50µg/ml of DEP comparing to control cells, although also these variations were not significant (**Fig 30**). Finally, 50µg/ml of DEP induced significant increment of iNOS comparing to 10µg/ml of DEP (+112%) (**Fig 30**).

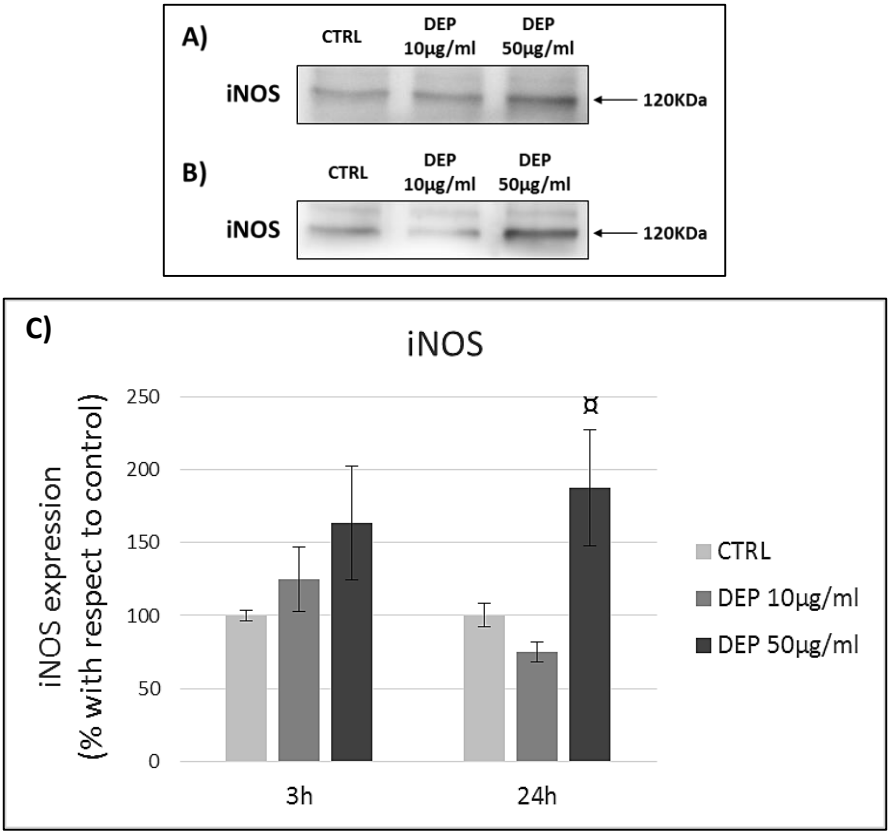

Figure 30: iNOS protein analysis after 3h and 24h of DEP treatment. Representative immunoblotting images of iNOS analysis in HT22 cells treated for 3h **(A)** and for 24h **(B)** with 10µg/ml and 50µg/ml of DEP. Histograms **(C)** display iNOS expression levels in treated cells with respect to control cells. Proteins have been normalized for corresponding total proteins revealed by Ponceau in each lane and the data are expressed as mean ± s.e. (n = 6-9). Statistical differences were tested accordingly by One-way ANOVA followed by Tukey post-hoc comparison, as population variances were significantly different (Levene's Test, $p<0.05$). ¤ $p<0.05$ vs. respective DEP 10µg/ml.

EVALUATION OF P-APP THR668/APP IN HT22 CELLS AFTER DEP TREATMENT

Literature data suggest that air pollution derived chemicals and organic compounds may be implicated in AD pathogenesis (Becaria et al., 2006; Maloney et al., 2012; Bondy, 2016) and brain APP processing has been observed after continuing exposure to PM (Calderón-Garcidueñas et al., 2008; Bhatt et al., 2015). APP phosphorylation is involved in the regulation of its function and metabolism, though its role is still controversial in literature (Matsushima et al., 2012). Since in literature the alteration of AD related proteins is typically observed after long-term PM exposure, from this point of the project 24h of treatment has been chosen for subsequent analyses.

P-APP Thr668/APP ratio and APP total levels were evaluated in HT22 cells treated for 24h with selected concentrations (10µg/ml, 50µg/ml) of DEP. After treatment, the cells were lysed with denaturing buffer (2% SDS). Following SDS-PAGE, proteins were revealed by WB and enhanced chemiluminescence.

The treatment induced a decrease of P-APP Thr668/APP ratio with 10µg/ml (-19%) and 50µg/ml (-40%) of DEP, although statistical analysis did not show significant variations, comparing to controls (**Fig 31**). At the same time, the treatment with 50µg/ml of DEP caused a non-significant increase of APP expression levels (+58%) comparing to control (**Fig 31**).

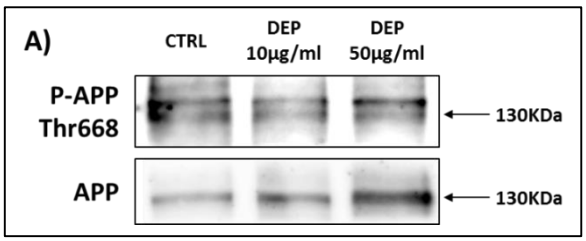

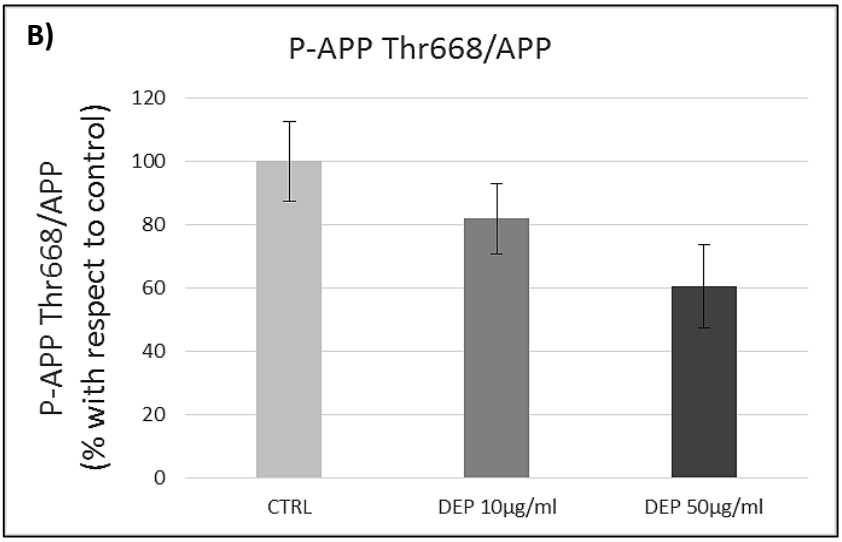

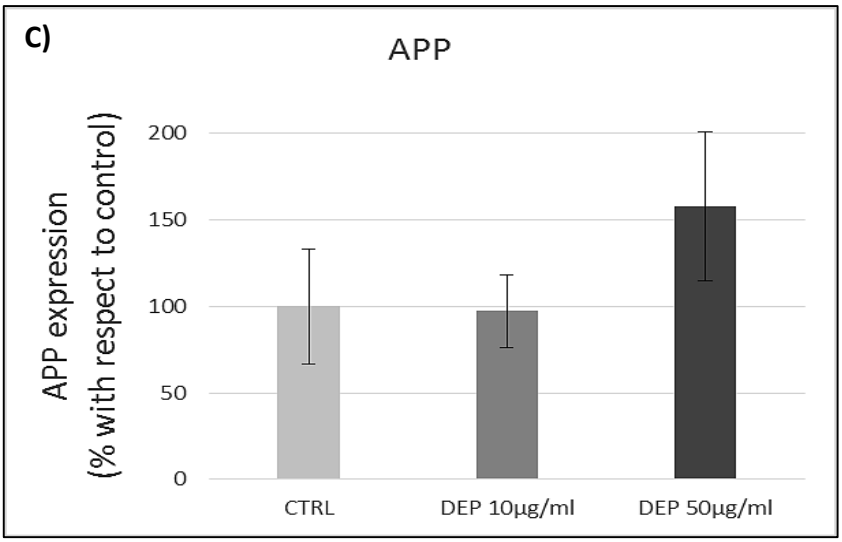

Figure 31: APP phosphorylation on Thr668 and APP protein analysis after 24h of DEP treatment. (A) Representative immunoblotting images of P-APP Thr668 and total APP analysis in HT22 cells treated for 24h with 10µg/ml and 50µg/ml of DEP. Histograms display **(B)** P-APP/APP ratio and **(C)** APP expression levels in treated cells with respect to control cells. Proteins have been normalized for corresponding total proteins revealed by Ponceau in each lane and the data are expressed as mean ± s.e. (n = 6-9). Statistical differences were tested accordingly by One-way ANOVA followed by Bonferroni post-hoc comparison.

EVALUATION OF BACE1 EXPRESSION IN HT22 CELLS AFTER DEP TREATMENT

BACE1 is the β-secretase responsible for amyloidogenic processing of APP and consequent Aβ production in the brain (Claeysen et al., 2012; Sathya et al., 2012; Pająk et al., 2016), and its increase in mouse brain has been associated to PM exposure (Bhatt et al., 2015).

BACE1 was evaluated in HT22 cells treated for 24h with selected concentrations (10µg/ml, 50µg/ml) of DEP. After treatment, the cells were lysed with denaturing buffer (2% SDS). Following SDS-PAGE, proteins were revealed by WB and enhanced chemiluminescence.

The treatment induced an increase of BACE1 expression levels with 10µg/ml (+59%) and 50µg/ml (+56%) of DEP, although statistical analysis did not show significant variations, comparing to control cells (**Fig 32**).

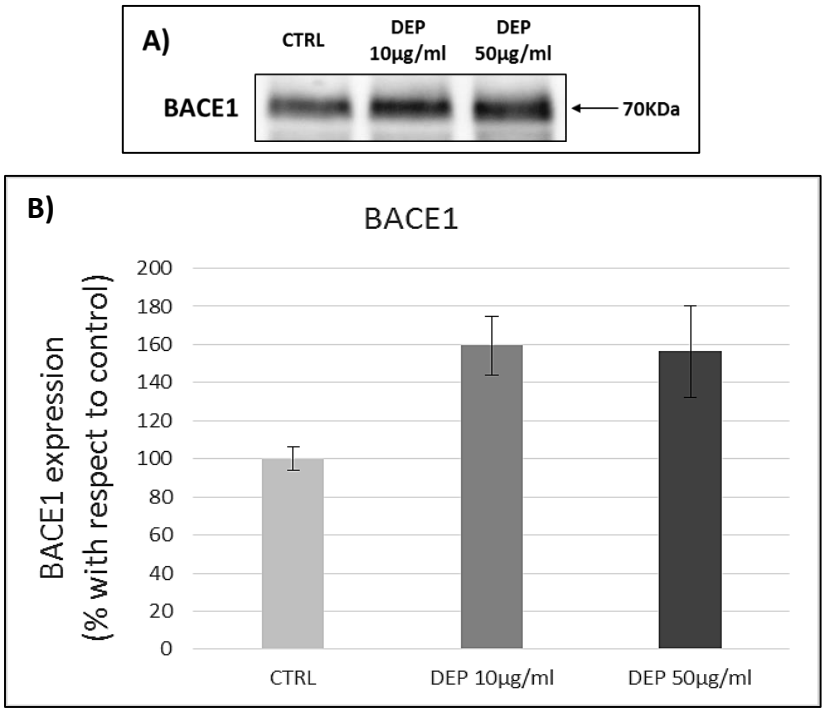

Figure 32: BACE1 protein analysis after 24h of DEP treatment. (A) Representative immunoblotting images of BACE1 analysis in HT22 cells treated for 24h with 10µg/ml and 50µg/ml of DEP. **(B)** Histogram displays BACE1 expression levels in treated cells with respect to control cells. Proteins have been normalized for corresponding total proteins revealed by Ponceau in each lane and the data are expressed as mean ± s.e. (n = 9-12). Statistical differences were tested accordingly by One-way ANOVA followed by Tukey post-hoc comparison, as population variances were significantly different (Levene's Test, $p<0.05$).

EVALUATION OF MDA PRODUCTION IN HT22 CELLS AFTER DEP TREATMENT

Uncontrolled production of ROS can induce lipid peroxidation (Rizzo et al., 2014) and one of the major products of this process is malondialdehyde (MDA). Therefore, MDA was evaluated as a marker of lipid peroxidation and oxidative stress in HT22 cells treated for 24h with selected concentrations (10µg/ml, 50µg/ml) of DEP. After treatment, cells were removed by scraping in PBS and centrifuged at 4°C, 845xg for 10 minutes. Supernatants were separated and pellets were used for MDA assay performed by Prof Angela Maria Rizzo and collaborators.

The treatment induced an increase of MDA levels with 10µg/ml (+2.70 pmol/µg proteins) and 50µg/ml (+8.76 pmol/µg proteins) of DEP, although statistical analysis did not show significant variations, comparing to control cells (**Fig 33**).

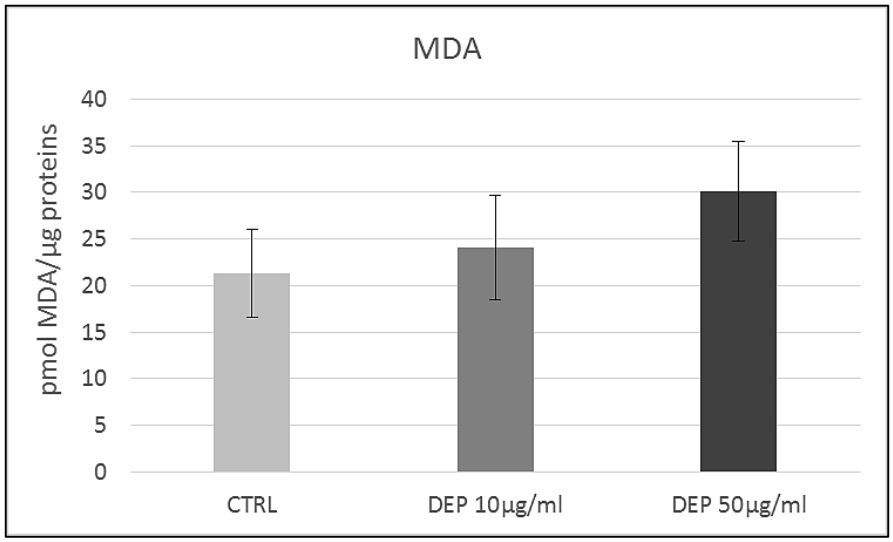

Figure 33: MDA analysis after 24h of DEP treatment. Histogram displays MDA levels in HT22 control cells and cells treated for 24h with 10µg/ml and 50µg/ml of DEP. Data are expressed as mean pmol MDA/µg proteins ± s.e. (n = 3-4). Statistical differences were tested accordingly by t-test.

EVALUATION OF FATTY ACIDS CONTENT IN HT22 CELLS AFTER DEP TREATMENT

Literature data suggest lipid reshaping after PM exposure. It has been demonstrated that mouse PM10 administration causes liver, heart and brain changes in total FA composition (Rizzo et al., 2014). Therefore, fatty acids (FA) were evaluated in HT22 cells treated for 24h with selected concentrations (10µg/ml, 50µg/ml) of DEP. After treatment, cells were removed by scraping in PBS and centrifuged at 4°C, 845xg for 10 minutes. Supernatants were separated and pellets were used for FA evaluation performed by Prof Angela Maria Rizzo and collaborators.

The treatment with 50µg/ml of DEP induced significant decrease of C16:0 (-2.1ng/µg proteins) and C16:1 (-1.2ng/µg proteins) levels, comparing to control, while the amount of others FA resulted unchanged (**Tab 3**). Regarding percentages, the treatment induced significant decrease of C16:1 (-2.35%) and increase of C18:2 (+1.89%) levels with 50µg/ml of DEP, comparing to control cells (**Fig 34**). Moreover, 50µg/ml of DEP caused significant increase of C18:2 (+2.44%) levels comparing to 10µg/ml of DEP (**Fig 34**). Finally, after DEP 50µg/ml exposure the percentage of n-6 polyunsaturated fatty acids (n-6 PUFA) was significantly increased (+6.85%), but it was not able to induce a significant increment of total PUFA.

Unsaturation index (U.I.), calculated as described in Figure 17, showed an increasing trend after exposure to 50µg/ml of DEP (**Fig 35**).

FA	CTRL	DEP 10µg/ml	DEP 50µg/ml
C16	12.65 ± 0.77	11.46 ± 0.53	10.55 ± 0.43*
C16:1	3.36 ± 0.47	2.45 ± 0.69	2.16 ± 0.09*
C18	8.50 ± 0.94	8.18 ± 0.72	8.00 ± 0.19
C18:1	13.52 ± 1.37	12.97 ± 0.90	12.74 ± 0.46
C18:2	2.32 ± 0.37	1.96 ± 0.51	3.22 ± 0.25
C18:3 γ	1.96 ± 0.38	2.40 ± 0.25	2.76 ± 0.06
C18:3 α	0.54 ± 0.11	0.96 ± 0.19	1.33 ± 0.41
C20:3	0.30 ± 0.06	0.37 ± 0.12	0.36 ± 0.05
C20:4	3.43 ± 1.88	3.39 ± 1.93	5.00 ± 1.87
C20:5	1.02 ± 0.59	0.38 ± 0.03	1.37 ± 0.54
C22:5	1.02 ± 0.54	0.88 ± 0.52	1.45 ± 0.52
C22:6	1.18 ± 0.41	0.92 ± 0.45	1.00 ± 0.34
SFA	21.15 ± 1.52	19.64 ± 1.16	18.55 ± 0.61
MUFA	16.88 ± 1.56	15.43 ± 1.34	14.90 ± 0.55
PUFA	11.80 ± 3.19	11.31 ± 3.06	16.52 ± 3.88
n-6 PUFA	8.02 ± 2.02	8.14 ± 2.15	11.36 ± 2.08
n-3 PUFA	3.77 ± 1.27	3.17 ± 0.96	5.16 ± 1.79
C18:0/C18:1	0.63 ± 0.06	0.63 ± 0.06	0.63 ± 0.03
n-6 PUFA/n-3 PUFA	2.48 ± 0.52	2.84 ± 0.49	2.80 ± 0.87

Table 3: Fatty acids composition of HT22 cells after 24h of DEP treatment. The table reports fatty acids (FA) composition of HT22 control cells and cells treated for 24h with 10µg/ml and 50µg/ml of DEP. Data are

expressed as mean ng FA/µg proteins ± s.e. (n = 3-4). Statistical differences were tested accordingly by t-test. * p<0.05 vs. control.

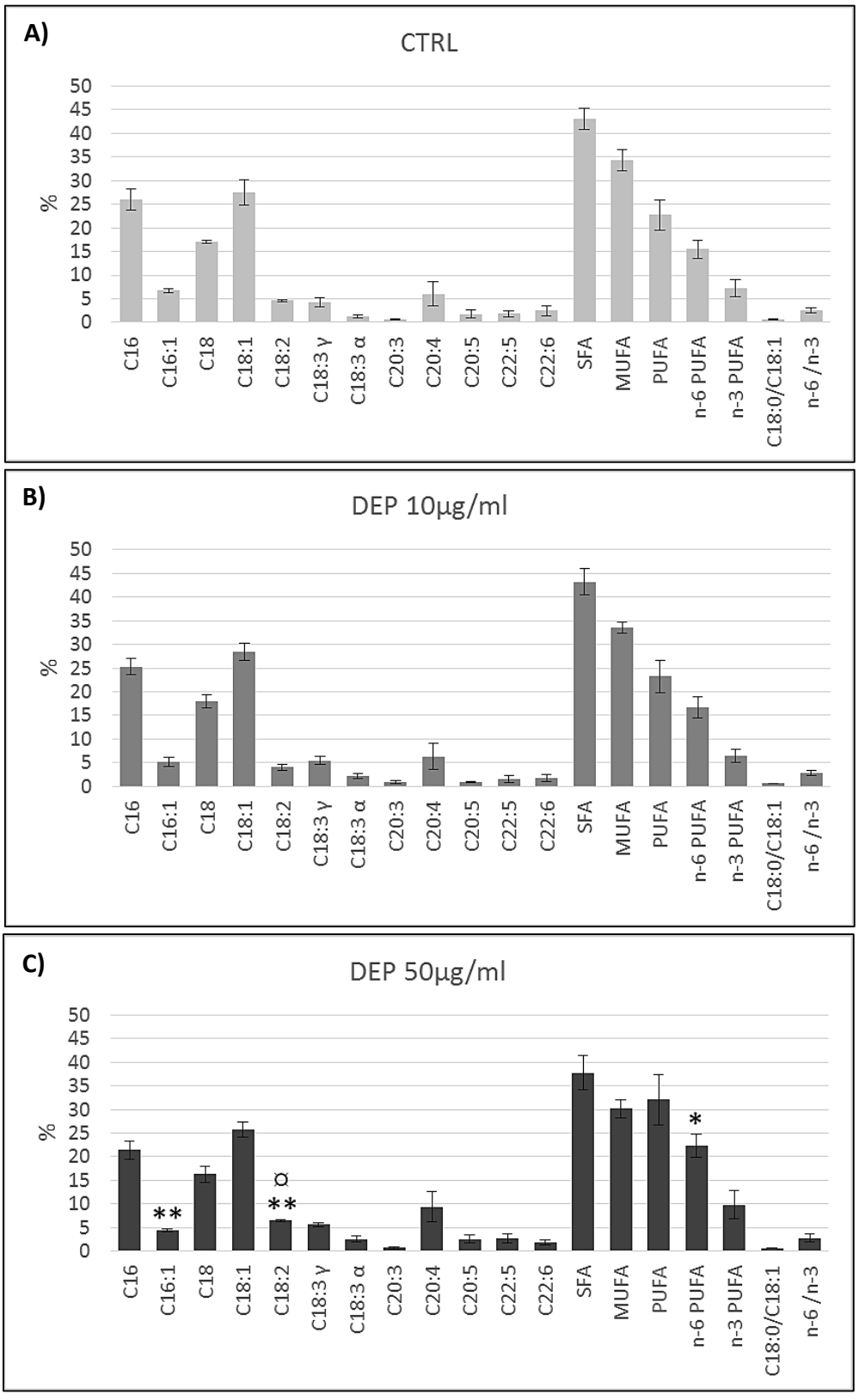

Figure 34: Fatty acids composition in HT22 cells after 24h of DEP treatment. Histograms display fatty acids (FA) composition of HT22 control cells **(A)** and cells treated for 24h with 10µg/ml **(B)** and 50µg/ml **(C)** of DEP.

Data are expressed as mean % ± s.e. (n = 3-4). Statistical differences were tested accordingly by t-test. * p<0.05 vs. control. ** p<0.01 vs. control. ¤ p<0.05 vs. DEP 10µg/ml.

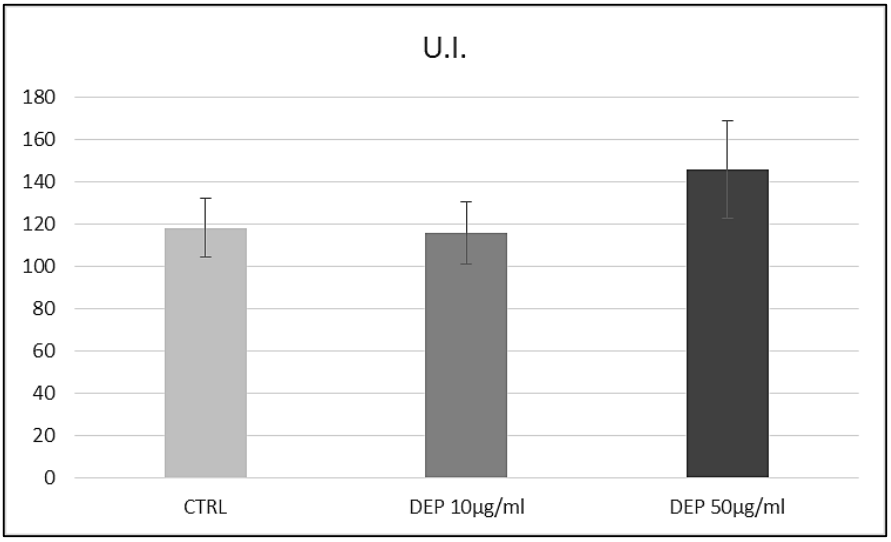

Figure 35: U.I. of HT22 cells after 24h of DEP treatment. Histogram displays U.I. (Unsaturation Index) of HT22 control cells and cells treated for 24h with 10µg/ml and 50µg/ml of DEP. U.I. was calculated as the sum of the % of each unsaturated FA multiplied by its number of double bonds. Data are expressed as mean ± s.e. (n = 3-4). Statistical differences were tested accordingly by t-test.

EVALUATION OF CHOLESTEROL CONTENT IN HT22 CELLS AFTER DEP TREATMENT

Literature data suggest an association between cholesterol levels and exposure to air pollution (Sørensen et al., 2015). Cholesterol amount, together with FA composition, is responsible for membrane fluidity, a factor involved in APP processing (Yang et al., 2014). Therefore, free cholesterol (CHOL) and esterified cholesterol (CE) were evaluated in HT22 cells treated for 24h with selected concentrations (10µg/ml, 50µg/ml) of DEP. After treatment, cells were removed by scraping in PBS and centrifuged at 4°C, 845xg for 10 minutes. Supernatants were separated and pellets were used for CHOL and CE analysis performed by Prof Angela Maria Rizzo and collaborators.

The treatment induced a significant decrease of CHOL with 10µg/ml (-9.20µg/mg proteins) and 50µg/ml (-13.96µg/mg proteins) of DEP comparing to control (**Fig 36**). In contrast, CE levels did not show significant variations comparing to control (**Fig 36**).

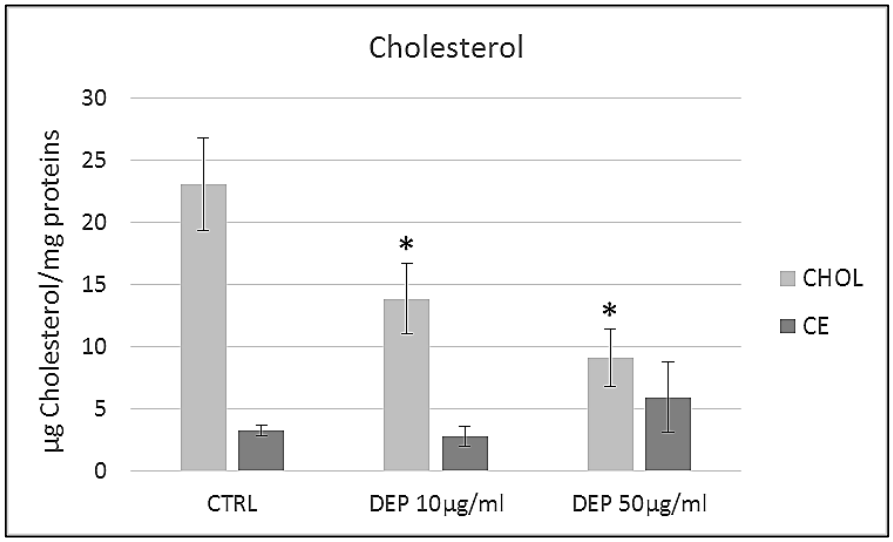

Figure 36. Free and esterified cholesterol analysis after 24h of DEP treatment. Histogram displays free cholesterol (CHOL) and esterified cholesterol (CE) levels in HT22 control cells and cells treated for 24h with 10µg/ml and 50µg/ml of DEP. Data are expressed as mean µg cholesterol/mg proteins ± s.e. (n = 3-4). Statistical differences were tested accordingly by t-test. * $p<0.05$ vs. control.

5.2 DISCUSSION

In this part of the project, we analysed the effects of DEP administration on HT22 cells regarding oxidative stress and inflammation induction, and their possible implications in Alzheimer disease onset. Notably, *in-vitro* DEP concentrations were chosen in the range estimated of what may reach the brain proposed by Levesque and colleagues (5–50µg/ml) (Levesque et al., 2011). Our results demonstrated that while the treatment with 10µg/ml of DEP induced only minimal changes in the protein that we tested, 50µg/ml of DEP induced significant variations already after 3h of exposure. Therefore, a considerable concentration of DEP is necessary to induce oxidative stress and inflammation in HT22 cells. The only exception of this study is represented by cholesterol, whose levels were significantly affected also with 10µg/ml of DEP, indicating that a lower dose is sufficient to induce membrane modifications.

DEP treatment induces oxidative stress in HT22 cells

Consistent with C6 glioma cells results, 3h and 24h of DEP treatments were not cytotoxic for HT22 cells and induced oxidative stress. This is demonstrated by HO-1 increase, the crucial enzyme for anti-oxidant response (Iles et al., 2005). HO-1 expression remains high with respect to control at 48h of DEP treatment and it returns to control levels at 72h (data not shown).

It has been previously reported that Hsp70 plays a key role during oxidative stress induced by DEP treatment. Its functional role under oxidative stress conditions include the hydrolysis of denatured or partially unfolded proteins as well as newly synthesized nascent polypeptides, therefore it is considered a marker of ER stress (Jung et al., 2007). Hsp70 expression is regulated by heat shock transcription factors, especially by HSF1. When exposed to physical or chemical stress, the production of misfolded and unfolded proteins initiates the phosphorylation and trimerization of HSF1, which subsequently translocates to the nucleus where it has the capacity of binding to DNA and induce Hsp70 gene transcription (Pockley, 2003). Consistent with literature, 3h and 24h of treatment with 10µg/ml and 50µg/ml of DEP induced Hsp70 increase; therefore, ROS produced by DEP exposure could be arguably associated to ER stress in HT22 cells.

During anti-oxidant response, HO-1 regulates the intracellular levels of heme pool, thus influencing its availability for various heme proteins (Otterbein and Zuckerbraun, 2005), including Cyp1b1. In contrast to what we observed in C6 glioma cells, after 3h of DEP treatment we detected a high increase of Cyp1b1, thus HO-1 induction is not able to limit PAHs metabolism in HT22 cells. However, after 24h the great increase of HO-1 seems to contribute in partially reducing Cyp1b1 levels. The inability of HO-1 to regulate Cyp1b1 expression could give rise to the production of reactive oxygenated PAHs intermediates capable of interacting with cellular macromolecules and sustain oxidative stress damage.

One of the consequences of uncontrolled oxidative stress is lipids peroxidation, primarily involving polyunsaturated fatty acid (PUFA) (Rizzo et al., 2014). MDA is a major product of lipid peroxidation, able to react with nucleic acid bases at physiological pH to form adducts resulting mutagenic in mammalian cells and

carcinogenic cells (Rizzo et al., 2014). The analysis of MDA in HT22 cells exposed to 10µg/ml and 50µg/ml of DEP showed a dose dependent but not significant slight increase. Thus, HT22 cells appear not susceptible to lipid peroxidation for the doses and the times of DEP treatment considered.

DEP treatment induces inflammation in HT22 cells

Literature data describe markers of inflammation in the brain of people and animals exposed to high levels of air pollution, including COX-2 (Calderon-Garciduenas et al., 2003; Calderon-Garciduenas et al., 2004). COX-2 is the inducible form of Cyclooxygenases, a family of myeloperoxidases located at the luminal side of the endoplasmic reticulum and nuclear membrane, which catalyse the rate-limiting step of prostaglandin biosynthesis from arachidonic acid (Sobolewski et al., 2010). In HT22 cells treated with DEP, we observed the induction of COX-2 with the highest concentration, especially after 24h of treatment. Therefore, DEP exposure could be associated to the activation of arachidonic acid cascade and inflammation.

Together with COX-2, another inflammatory marker considered in this project was iNOS, whose induction has been observed in the presence of different kinds of particulate matter (Calderon-Garciduenas et al., 2003; Farina et al., 2013; Li et al., 2016). iNOS is the inducible form of nitric oxide synthase (NOS) and, in contrast to NOS constitutive forms, it generates high concentrations of NO (nano rather than pico molar) and this level of synthesis is sustained for hours or days depending on the cell type (Coleman, 2001).

Consistent with literature but in contrast to what we observed for C6 glioma cells, 3h of DEP treatment induced iNOS expression in HT22 cells, despite HO-1 is significantly increased. In fact, iNOS belongs to the family of heme protein, and the reduction of heme availability is supposed to limit its expression (Kim et al., 2013). Our results demonstrate that HO-1 activation after 3h of DEP is not able to regulate NO production in HT22 cells. However, after 24h the great increase of HO-1 seems to contribute in reducing iNOS induction in HT22 cells treated with the lower DEP concentration (10µg/ml).

Notably, at high concentrations, as produced by iNOS, and under aerobic conditions, NO is rapidly oxidised to reactive nitrogen oxide species (RNOS), the most abundant of which in biological systems is N_2O_3 (Coleman, 2001). RNOS are unstable and rapidly nitrosate thiols or amines, or are hydrolysed and excreted as nitrite (NO_2^-) (Coleman, 2001). At higher concentrations, RNOS induce cell toxicity by nitrosating DNA and tyrosine residues, and inducing lipid peroxidation. For this reason, induction of iNOS after DEP treatment can be considered another potential source of oxidative stress.

DEP treatment induces changes of AD related proteins in HT22 cells

Literature data suggest that air pollution derived chemicals and organic compounds may be implicated in AD pathogenesis (Becaria et al., 2006; Maloney et al., 2012; Bondy, 2016). Notably, epidemiological evidences conducted in young urban residents showed a correlation between air pollution, neuroinflammation and oxidative stress, crucial mechanisms for AD onset and progression (Calderón-Garcidueñas et al., 2008; Calderón-Garcidueñas et al., 2012). Moreover, dogs naturally exposed to urban air pollutants in Mexico City

exhibit early activation of transcription factor NFkB, and induction of a range of genes including iNOS, COX-2 and APP (Calderón-Garcidueñas et al., 2003).

In this part of the project, we observed that DEP exposure induced oxidative stress and inflammation in HT22 cells. For this reason, we tested if DEP treatment is able to induce changes in some AD related protein in HT22 cells. Consequently, 24h of treatment has been chosen for subsequent analyses because in literature the alteration of AD related proteins has been observed after long-term PM exposure.

APP is a transmembrane glycoprotein recognised by a family of enzymes called secretase, which work in pairs and make proteolytic cleavage on specific amino acid sequences. If this cleavage is mediated in turn by α-secretase and γ-secretase the processing is defined non-amyloidogenic, while the combined action of β-secretase and γ-secretase give rise to amyloidogenic processing of APP with Aβ peptide production (Claeysen et al., 2012; Pająk et al., 2016). Notably, brain APP processing has been observed after long-term exposure to PM (Calderón-Garcidueñas et al., 2008; Bhatt et al., 2015). Post-translational modifications of APP are also involved in the regulation of its function and metabolism. One of these modifications is phosphorylation at Thr668 (numbering for APP695 isoform), which is predominantly observed in neurons in the brain (Matsushima et al., 2012). However, the ability of phosphorylation at Thr668 to induce alterations in the cleavage of APP at β- and/or γ-secretase sites is still controversial in AD brains. Mutant mice possessing Ala substitution for Thr668 of APP did not show significant differences in APP metabolism, including Aβ generation, when compared with the wild-type mouse. This analysis would suggest that the phosphorylation state of APP at Thr668 does not play an obvious role in the direct governing of the APP metabolism in the brain *in-vivo*. In contrast, several reports have indicated that phosphorylation of APP on Thr668 could regulate γ-secretase cleavage in cultured cells (Matsushima et al., 2012). In HT22 cells, we observed a dose-dependent, although not significant, decrease of P-APP Thr668/APP ratio after DEP treatment; at the same time, APP total protein resulted unchanged with 10µg/ml of DEP, while it was higher with 50µg/ml of DEP comparing to control. These results suggest that some compensatory mechanisms are activated after direct HT22 cells DEP exposure. In fact, literature provides strong evidences that APP has a trophic function. APP is likely to be involved in neural stem cell development, neuronal survival, neurite outgrowth and neurorepair (Dawkins and Small, 2014). Although the mechanisms by which APP exerts its actions remain to be elucidated, the available evidence suggests that APP interacts both intracellularly and extracellularly to regulate various signal transduction mechanisms (Dawkins and Small, 2014).

BACE1 is the β-secretase responsible for amyloidogenic processing of APP and consequent Aβ production in the brain (Claeysen et al., 2012; Sathya et al., 2012; Pająk et al., 2016). BACE1 increase has been found in the brain of mice exposed for 9 months to particulate matter (Bhatt et al., 2015). Consistent with this result, we found that 24h of DEP treatment induced an increase of BACE1 protein levels for both concentrations (10µg/ml and 50µg/ml), although these changes were not statistically significant. This result would suggest but not necessarily indicate increased APP processing, therefore future work will be required to quantify

changes in BACE1 activity as well as Aβ production and release, to better understand APP processing in HT22 cells treated with DEP.

DEP treatment induces changes of lipid content in HT22 cells

The effect of PM on cell membrane and lipid profile represents an important topic that has been so far poorly investigated. Lipids alter the geometric properties of membranes, interface between the cellular and the extracellular microenvironment being involved in the signalling process in response to exogenous stimuli (Rizzo et al., 2014). Cell membrane controls protein traffic and provides messenger molecules that mediate cell-cell communication, suggesting that advances in our understanding of lipid modifications induced by PM could better disclose PM adverse effects at a molecular level. It has been demonstrated that PM exposure induces an increase in plasma membrane surface area, which correlates with the total particle surface area that cells are exposed to; this increase that may be explained by lipid trafficking to the apical plasma membrane and may be interpreted as a protective reaction of the cells against particle-induced stress (Brandenberge et al., 2010).

Fatty acids are the simplest lipids and represent important building blocks of neuronal membranes, whose lipid bilayer consists of phospholipids, with docosahexaenoic acid, arachidonic acid, and eicosapentaenoic acid as their main components (Janssen and Kiliaan, 2014).

The principal FA analysis of HT22 cells treated for 24h with DEP showed that the highest dose used in this project (50µg/ml) induces significant decrease of palmitic acid (C16:0) and palmitoleic acid (C16:1) amount, while only palmitoleic acid decreased also in percentage with respect to control. This data is in agreement with FA analyses of PM10sum-treated mice conducted by Rizzo and collaborators (Rizzo et al., 2014), which observed significant palmitoleic acid decrease in liver; moreover, they found a reduction of this FA also in lung and brain, although not significant.

On the contrary, we observed a significant increase of linoleic acid (C18:2) percentage, although its amount was unaltered comparing to control cells. Linoleic acid is the precursor molecule of arachidonic acid (C20:4), which is derived from linoleic acid by desaturation and elongation of the carbon chain (Janssen and Kiliaan, 2014). After 50µg/ml of DEP treatment, we observed an increase of arachidonic acid, but it did not result significant, although COX-2 expression levels were significantly higher comparing to control. Moreover, linoleic acid is one of the principal components of n-6 PUFA, whose percentage significantly increased after 50µg/ml of DEP treatment, while total PUFA percentage increment resulted not significant. Notably, it is known that most of eicosanoids derived from n-6 PUFA are pro-inflammatory, whereas those formed from n-3 PUFA exert anti-inflammatory properties (Yang et al., 2016). The n-6 and n-3 PUFA interact with each other in biological functions and coordinate to regulate biological processes. They also compete with each other sharing the same enzymes for conversion (Yang et al., 2016). Despite in HT22 cells exposed to 50µg/ml

of DEP we observed a significant increase of n-6 PUFA percentage, the ratio n-6 PUFA/n-3 PUFA resulted unaltered comparing to control cells.

Therefore, the above-described variations suggest FA reshaping after 24h of treatment with 50μg/ml of DEP. Interestingly, membrane FA and cholesterol composition can regulate membrane fluidity, which has been associated to APP processing. In the specific, cell membranes enrichment with PUFA increases membrane fluidity and, subsequently, promotes non-amyloidogenic cleavage of APP by α secretase to produce sAPPα (Yang et al., 2014). Conversely, the reduction of membrane fluidity is associated to amyloidogenic processing of APP by β secretase (Yang et al., 2014). In fact, it is known that APP processing is regulated by intracellular cholesterol homeostasis (Yang et al., 2014). In membrane compartmentalization model, APP is presents in two cellular pools, one is associated with the cholesterol-enriched lipid rafts, where Aβ is generated, and the other is outside of rafts (i.e., non-lipid rafts domains), where α-cleavage occurs (Yang et al., 2014).

Membrane fluidity can be calculated in different ways. In general, lower cholesterol content and higher unsaturation of phospholipid fatty acyl chains are associated with more fluid membranes (Fajardo et al., 2011). The analysis of free and esterified cholesterol in HT22 cells exposed to 10μg/ml and 50μg/ml of DEP for 24h showed a dose dependent and significant decrease of CHOL, which is the form associated to the membranes, and this reduction is remarkable with the highest dose. This result, together with the increase of U.I., indicates that after treatment with 50μg/ml of DEP HT22 cell membrane is more fluid comparing to control cells. This would suggest the prevalence of non-amyloidogenic cleavage of APP, but the increase of BACE1 and APP expression with 50μg/ml of DEP demonstrates the necessity of further studies to better understand APP processing in HT22 cells exposed to DEP, also in relation to lipid reshaping.

Conclusion

DEP treatment at sub-lethal concentrations induced oxidative stress, inflammation and lipid reshaping in HT22 cells; in this context, 50μg/ml of DEP resulted more effective. These mechanisms are supposed to be involved in the alteration of some AD related protein, but future experiments will be necessary to clarify the role of direct DEP administration to neurons in AD onset.

CHAPTER 6: Mouse brain results and discussion

6.1 RESULTS

EVALUATION OF HO-1 EXPRESSION LEVELS IN MOUSE BRAIN AFTER BC AND DEP SINGLE AND REPEATED INSTILLATIONS

As discussed before, HO-1 was evaluated as marker of oxidative stress (Iles et al., 2005) in the brain of male BALB/c mice intratracheally instilled with 50µg of BC or DEP/100µl 0.9% NaCl. 3h after single instillation or 24h after the last of repeated instillations, animals were sacrificed and the brain of sham and treated mice were dissected and divided in three parts: RoB, cerebellum and hippocampus. The different parts of the brain were homogenized in denaturing buffer (isotonic saline solution + Ripa buffer 5X). Following SDS-Page, proteins were revealed by WB and enhanced chemiluminescence.

A single intratracheal instillation induced an increasing trend of HO-1 expression levels in RoB (+33% with BC and +79% with DEP), cerebellum (+24% with BC and +43% with DEP) and hippocampus (+58% with BC and +55% with DEP), comparing to sham, although statistical analysis did not show significant variations (**Fig 37**). Repeated intratracheal instillations displayed a non-significant increasing trend of HO-1 expression levels in cerebellum (+25% with BC and +29% with DEP) and hippocampus (+33% with BC and +25% with DEP), comparing to sham (**Fig 37**).

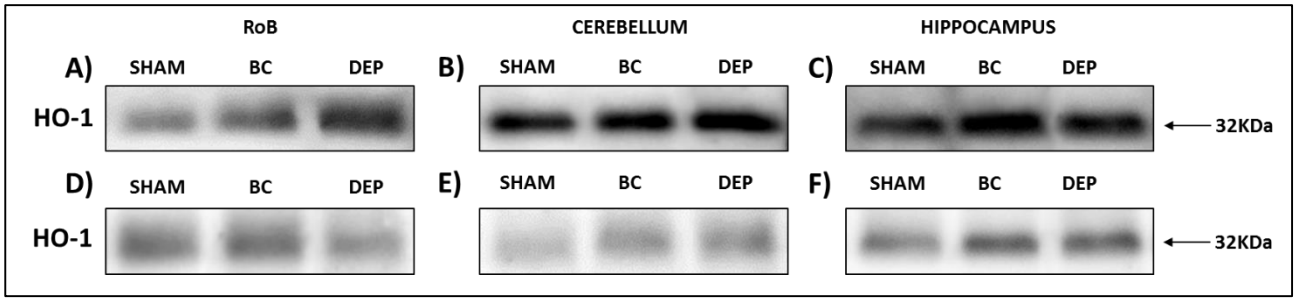

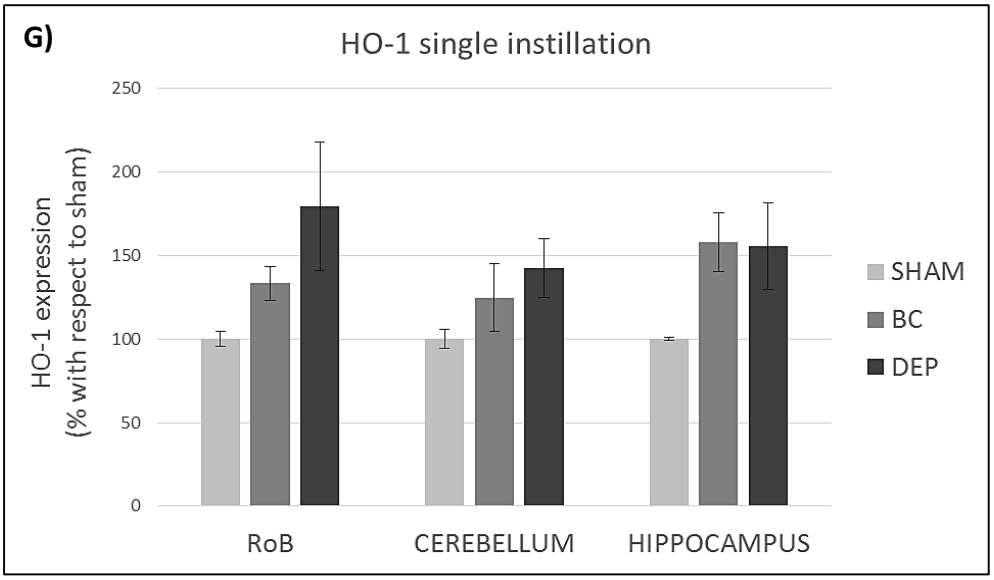

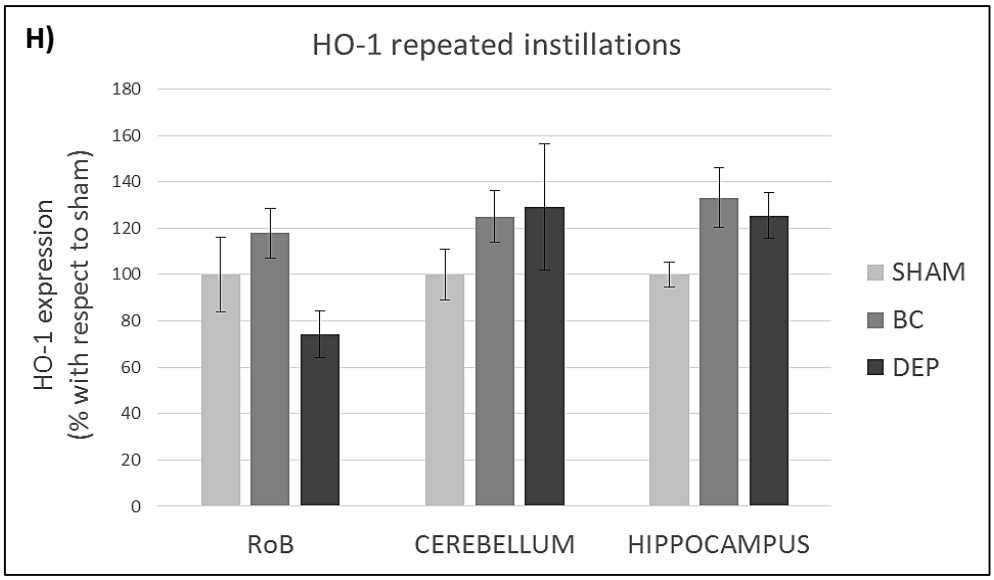

Figure 37: HO-1 protein analysis after single and repeated instillations. Representative immunoblotting images of HO-1 analysis of RoB, cerebellum and hippocampus after single **(A, B, C)** and repeated **(D, E, F)** instillations with 50µg of BC or DEP/100µl 0.9% NaCl. Histograms display HO-1 expression levels after single **(G)** and repeated **(H)** instillations. Proteins have been normalized for corresponding total proteins revealed by Ponceau in each lane and the data are expressed as mean ± s.e. (n = 5-9). Statistical differences were tested accordingly by One-way ANOVA followed by Bonferroni post-hoc comparison; Tukey post-hoc comparison has been used when population variances were significantly different (Levene's Test, $p<0.05$).

EVALUATION OF Hsp70 EXPRESSION LEVELS IN MOUSE BRAIN AFTER BC AND DEP SINGLE AND REPEATED INSTILLATIONS

As discussed before, Hsp70 was evaluated as marker of ER stress (Jung et al., 2007) in the brain of male BALB/c mice intratracheally instilled with 50µg of BC or DEP/100µl 0.9% NaCl. Brain of sham and treated mice underwent the same preparative procedures described for HO-1 protein analysis.

A single intratracheal instillation induced an increasing trend of Hsp70 expression levels in RoB (+90% with BC and +203% with DEP), cerebellum (+45% with BC and +57% with DEP) and hippocampus (+39% with BC and +21% with DEP), comparing to sham, although statistical analysis showed a significant variation only in cerebellum treated with DEP (**Fig 38**). Repeated intratracheal instillations displayed an increment of Hsp70 expression levels in RoB (+59% with BC and +168% with DEP), cerebellum (+40% with BC and +63% with DEP), and hippocampus (+42% with BC and +60% with DEP), comparing to sham, where Hsp70 raise in DEP treated mice resulted significant in all the parts of the brain (**Fig 38**).

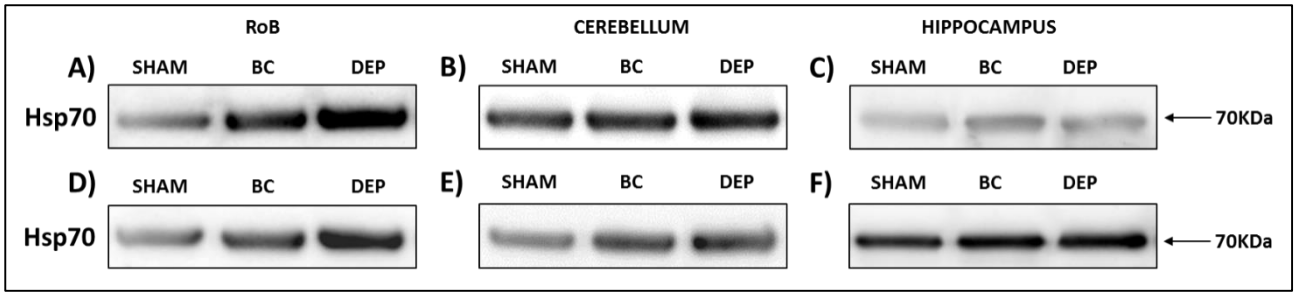

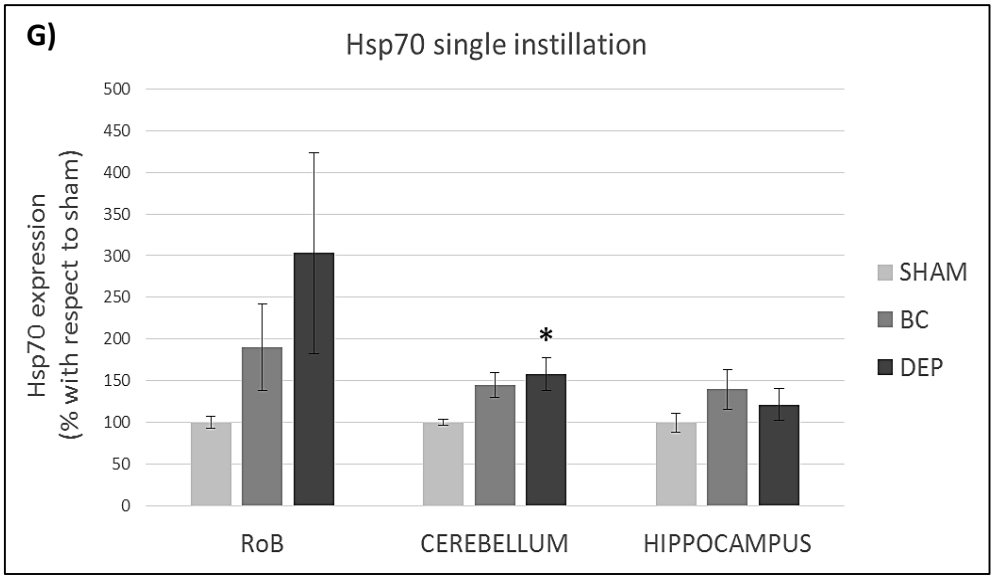

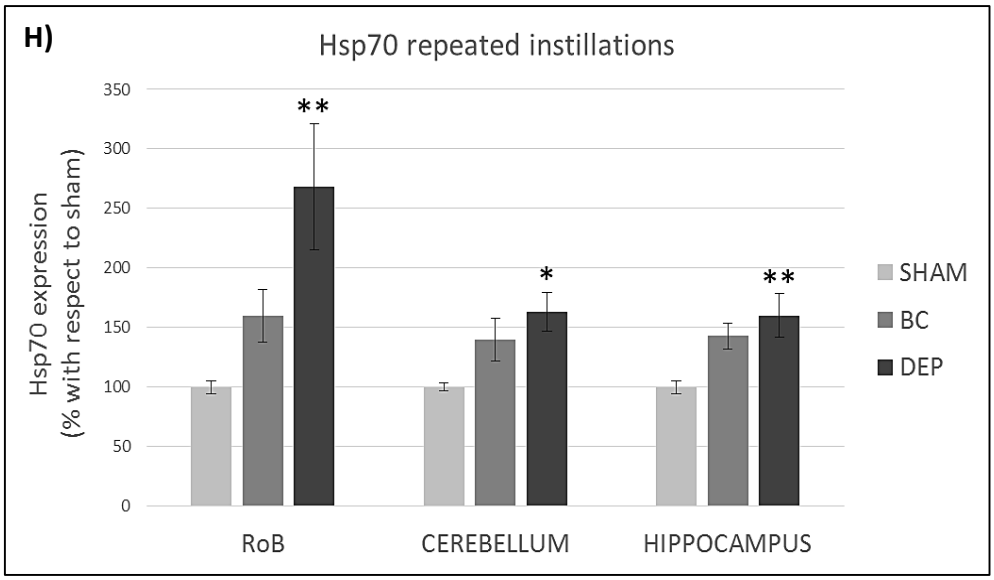

Figure 38: Hsp70 protein analysis after single and repeated instillations. Representative immunoblotting images of Hsp70 analysis of RoB, cerebellum and hippocampus after single **(A, B, C)** and repeated **(D, E, F)** instillations with 50µg of BC or DEP/100µl 0.9% NaCl. Histograms display Hsp70 expression levels after single **(G)** and repeated **(H)** instillations. Proteins have been normalized for corresponding total proteins revealed by Ponceau in each lane and the data are expressed as mean ± s.e. (n = 5-9). Statistical differences were tested accordingly by One-way ANOVA followed by Bonferroni post-hoc comparison; Tukey post-hoc comparison has been used when population variances were significantly different (Levene's Test, $p<0.05$). * $p<0.05$ vs. respective sham. ** $p<0.01$ vs. respective sham.

EVALUATION OF Cyp1b1 EXPRESSION LEVELS IN MOUSE BRAIN AFTER BC AND DEP SINGLE AND REPEATED INSTILLATIONS

As discussed before, Cyp1b1 was evaluated as marker of PAHs metabolism (Stewart et al., 2003) in the brain of male BALB/c mice intratracheally instilled with 50µg of BC or DEP/100µl 0.9% NaCl. Brain of sham and treated mice underwent the same preparative procedures described for HO-1 protein analysis.

A single intratracheal instillation showed no significant variations of Cyp1b1 expression levels in all parts of the brain, comparing to sham (**Fig 39**). Repeated intratracheal instillations with DEP induced significant increase of Cyp1b1 expression levels in RoB (+57%) and cerebellum (+60%), comparing to sham, and these changes were significant also with respect to BC treated mice. Also in hippocampus DEP administration displayed an increase (+38%), though not significant comparing to sham mice (**Fig 39**). Finally, repeated intratracheal instillations with BC induced significant increase of Cyp1b1 expression levels in hippocampus (+60%) comparing to sham (**Fig 39**).

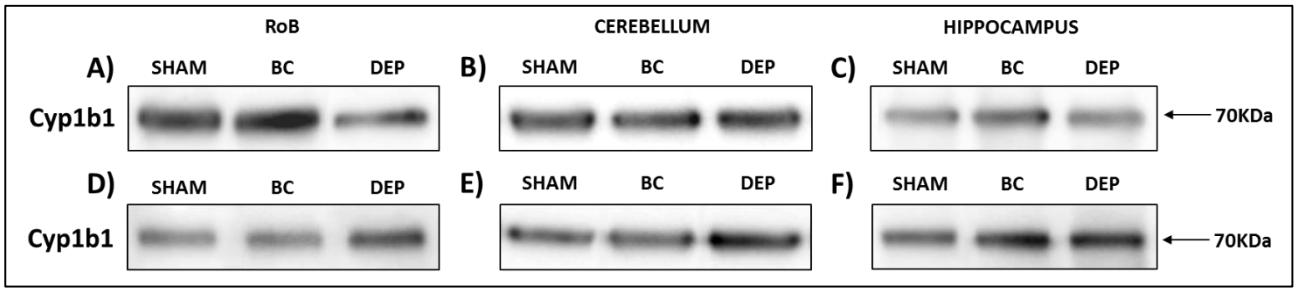

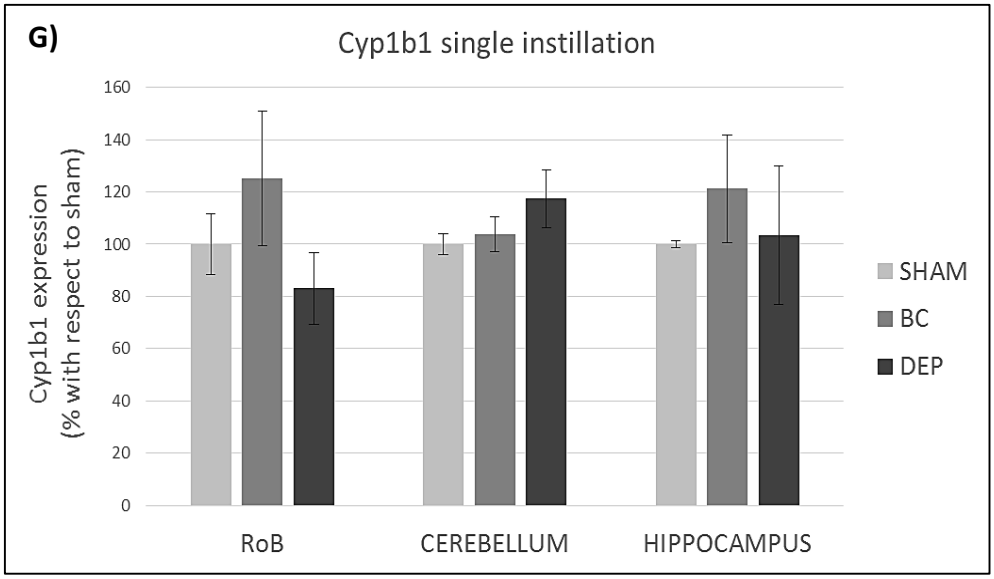

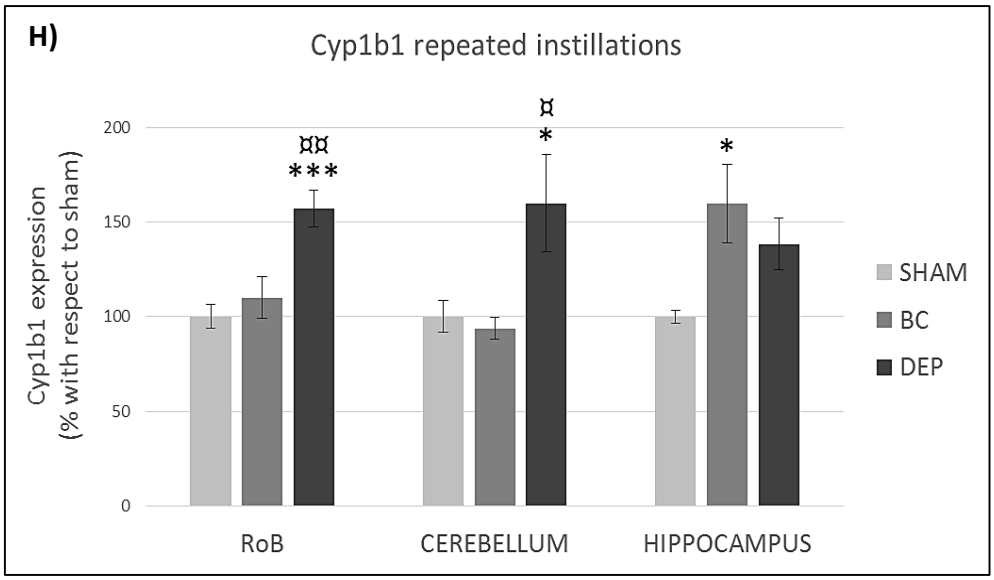

Figure 39: Cyp1b1 protein analysis after single and repeated instillations. Representative immunoblotting images of Cyp1b1 analysis of RoB, cerebellum and hippocampus after single **(A, B, C)** and repeated **(D, E, F)** instillations with 50µg of BC or DEP/100µl 0.9% NaCl. Histograms display Cyp1b1 expression levels after single **(G)** and repeated **(H)** instillations. Proteins have been normalized for corresponding total proteins revealed by Ponceau in each lane and the data are expressed as mean ± s.e. (n = 5-9). Statistical differences were tested accordingly by One-way ANOVA followed by Bonferroni post-hoc comparison; Tukey post-hoc comparison has been used when population variances were significantly different (Levene's Test, $p<0.05$). * $p<0.05$ vs. respective sham. *** $p<0.001$ vs. respective sham. ¤ $p<0.05$ vs. respective BC. ¤¤ $p<0.01$ vs. respective BC.

EVALUATION OF iNOS EXPRESSION LEVELS IN MOUSE BRAIN AFTER BC AND DEP SINGLE AND REPEATED INSTILLATIONS

As discussed before, iNOS was evaluated as marker of inflammation (Calderon-Garciduenas et al., 2004) in the brain of male BALB/c mice intratracheally instilled with 50µg of BC or DEP/100µl 0.9% NaCl. Brain of sham and treated mice underwent the same preparative procedures described for HO-1 protein analysis.

A single intratracheal instillation induced an increasing trend of iNOS expression levels in RoB (+17% with BC and +41% with DEP), cerebellum (+24% with BC and +35% with DEP), and hippocampus (+40% with BC and +114% with DEP), comparing to sham, although statistical analysis showed significant variations only in RoB and cerebellum treated with DEP (**Fig 40**). Repeated intratracheal instillations were able to maintain the increasing trend of iNOS expression levels in RoB (+50% with BC and +134% with DEP), cerebellum (+58% with BC and +195% with DEP) and hippocampus (+159% with BC and +518% with DEP), comparing to sham, and again statistical analysis showed significant variations only in DEP treated mice (**Fig 40**). Moreover, iNOS raise in the hippocampus of DEP treated mice resulted significant also with respect to BC treated mice (**Fig 40**).

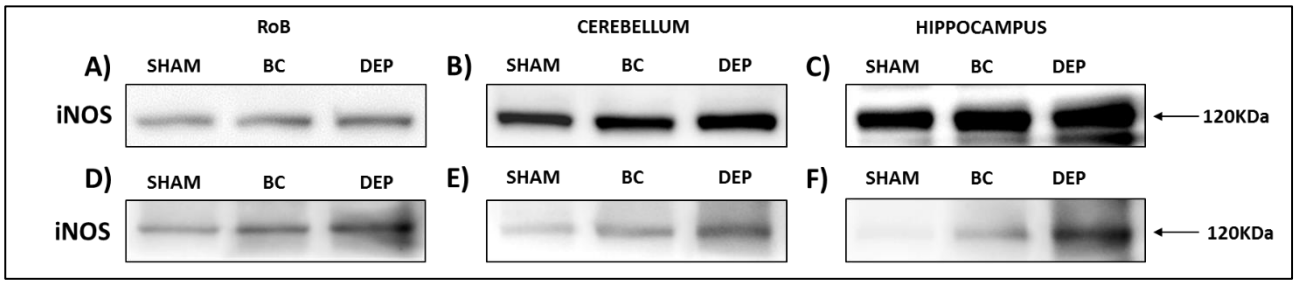

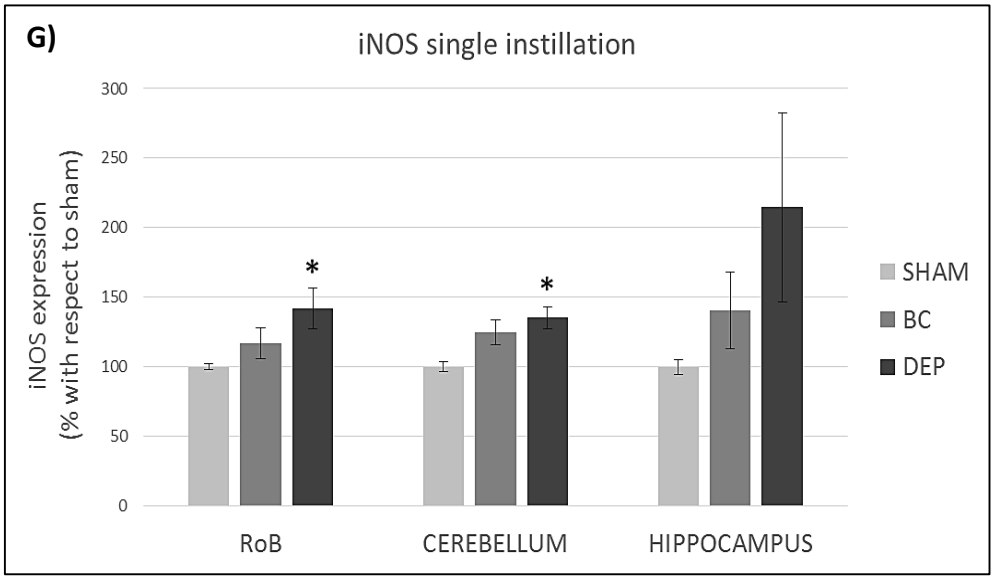

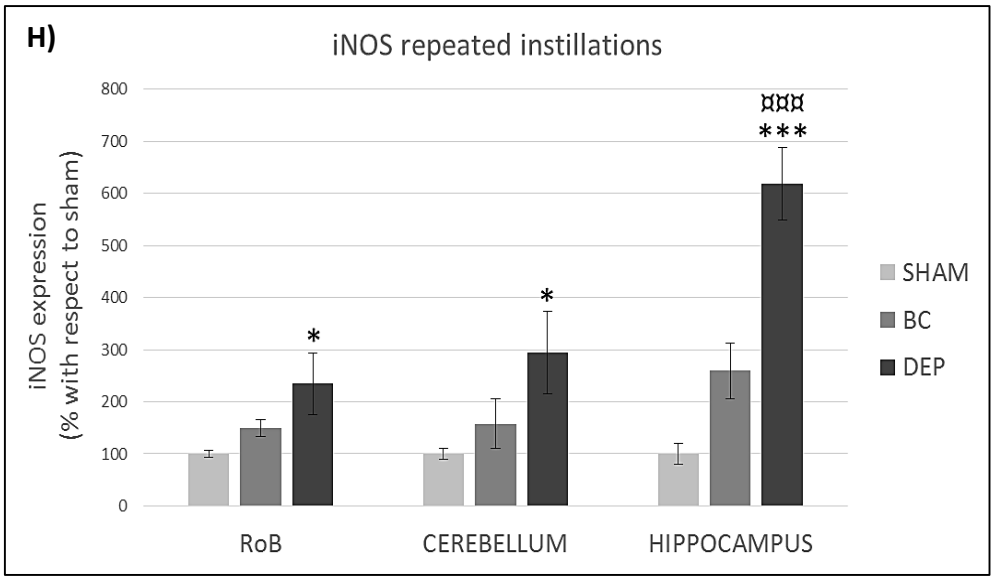

Figure 40: iNOS protein analysis after single and repeated instillations. Representative immunoblotting images of iNOS analysis of RoB, cerebellum and hippocampus after single **(A, B, C)** and repeated **(D, E, F)** instillations with 50µg of BC or DEP/100µl 0.9% NaCl. Histograms display iNOS expression levels after single **(G)** and repeated **(H)** instillations. Proteins have been normalized for corresponding total proteins revealed by Ponceau in each lane and the data are expressed as mean ± s.e. (n = 5-9). Statistical differences were tested accordingly by One-way ANOVA followed by Bonferroni post-hoc comparison; Tukey post-hoc comparison has been used when population variances were significantly different (Levene's Test, $p<0.05$). * $p<0.05$ vs. respective sham. *** $p<0.001$ vs. respective sham. ¤¤¤ $p<0.001$ vs. respective BC.

EVALUATION OF P-APP THR668/APP LEVELS IN MOUSE BRAIN AFTER BC AND DEP SINGLE AND REPEATED INSTILLATIONS

As discussed before, air pollution derived chemicals and organic compounds may be implicated in AD pathogenesis (Becaria et al., 2006; Maloney et al., 2012; Bondy, 2016) and brain APP processing has been observed after continuous exposure to PM (Calderón-Garcidueñas et al., 2008; Bhatt et al., 2015). APP phosphorylation is involved in the regulation of its function and metabolism, though its role is still controversial in literature (Matsushima et al., 2012).

P-APP Thr668/APP ratio and APP total levels were evaluated in the brain of male BALB/c mice intratracheally instilled with 50µg of BC or DEP/100µl 0.9% NaCl. Brain of sham and treated mice underwent the same preparative procedures described for HO-1 protein analysis.

A single intratracheal instillation with DEP induced non-significant increase of P-APP Thr668/APP ratio in RoB (+20%), cerebellum (+40%), and hippocampus (+65%), comparing to sham, while APP expression levels showed an increasing trend only in RoB (+34% with BC and +81% with DEP), with statistical significance after DEP administration (**Fig 41**). Repeated intratracheal instillations induced an increasing trend of P-APP Thr668/APP ratio in RoB (+71% with BC and +135% with DEP), cerebellum (+234% with BC and +555% with DEP), and hippocampus (+44% with BC and +817% with DEP), comparing to sham, although statistical analysis showed significant variations only in RoB of DEP treated mice (**Fig 41**). At the same time, repeated instillation caused a decreased of APP expression levels in RoB (-14% with BC and -25% with DEP) and cerebellum (-42% with BC and -42% with DEP), although not significant comparing to sham, while hippocampus showed no variations (**Fig 41**).

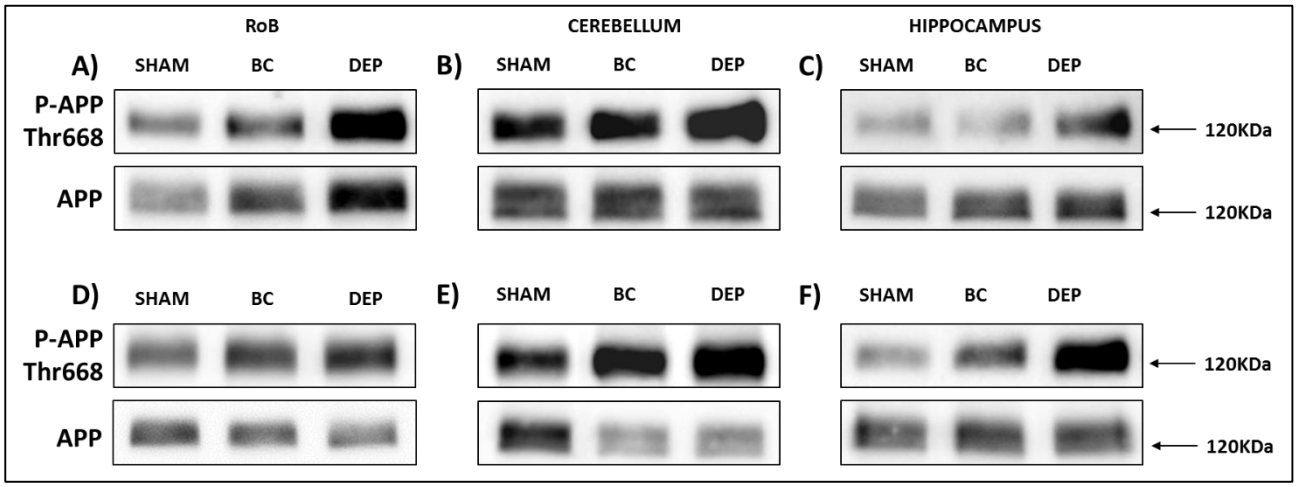

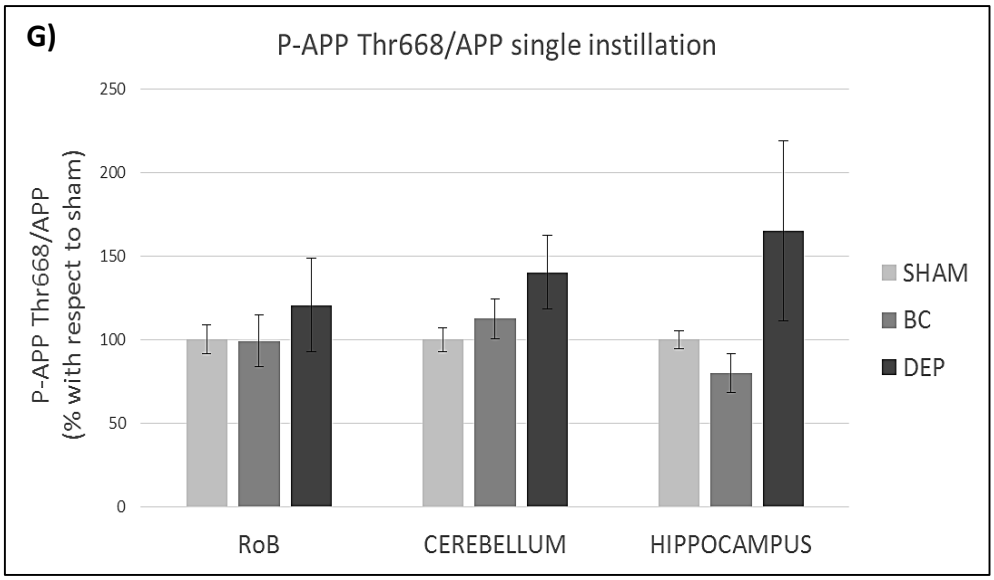
G)
P-APP Thr668/APP single instillation
P-APP Thr668/APP (% with respect to sham)
250
200
150
100
50
0
RoB
CEREBELLUM
HIPPOCAMPUS
SHAM
BC
DEP

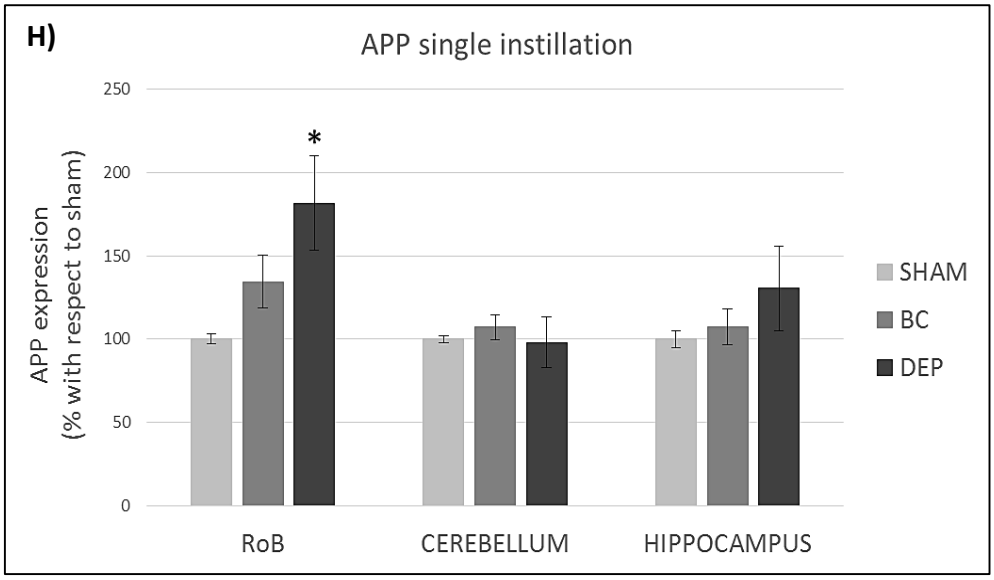
H)
APP single instillation
APP expression (% with respect to sham)
250
200
150
100
50
0
*
RoB
CEREBELLUM
HIPPOCAMPUS
SHAM
BC
DEP

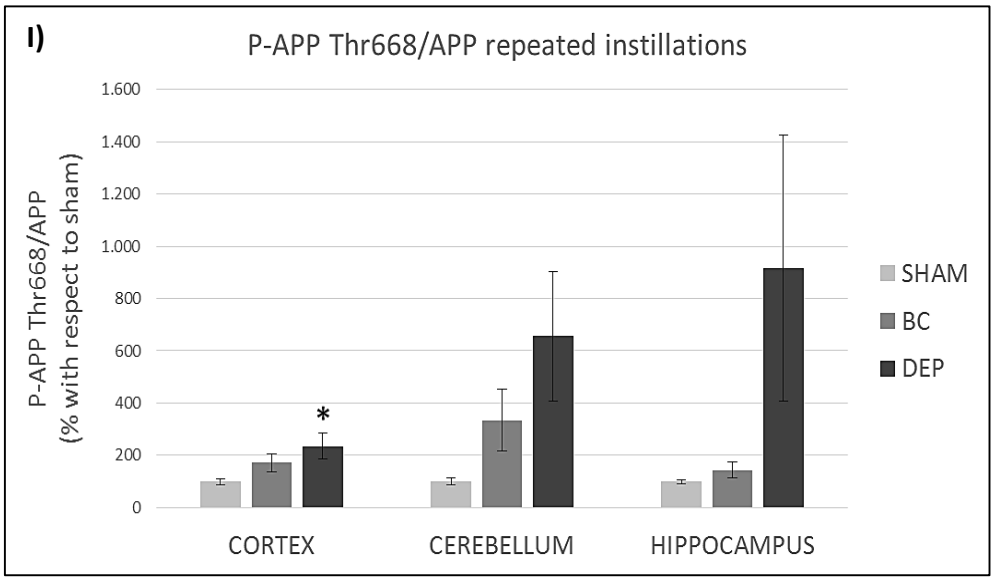
I)
P-APP Thr668/APP repeated instillations
P-APP Thr668/APP (% with respect to sham)
1.600
1.400
1.200
1.000
800
600
400
200
0
*
CORTEX
CEREBELLUM
HIPPOCAMPUS
SHAM
BC
DEP

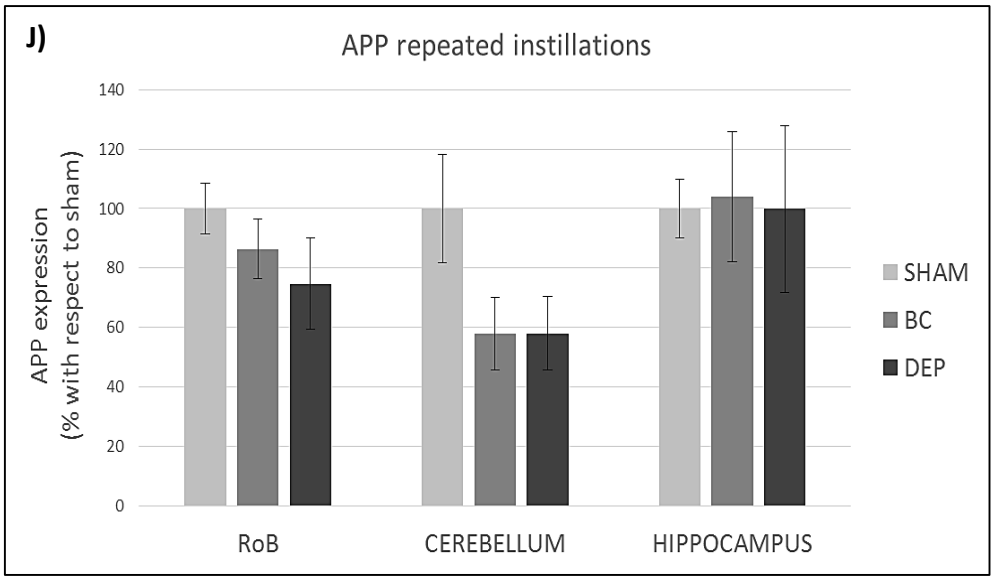

Figure 41: APP phosphorylation on thr668 and APP protein analysis after single and repeated instillations. Representative immunoblotting images of P-APP thr668 and total APP analysis of RoB, cerebellum and hippocampus after single **(A, B, C)** and repeated **(D, E, F)** instillations with 50µg of BC or DEP/100µl 0.9% NaCl. Histograms display P-APP/APP ratio and APP expression levels after single **(G, H)** and repeated **(I, J)** instillations. Proteins have been normalized for corresponding total proteins revealed by Ponceau in each lane and the data are expressed as mean ± s.e. (n = 5-9). Statistical differences were tested accordingly by One-way ANOVA followed by Bonferroni post-hoc comparison; Tukey post-hoc comparison has been used when population variances were significantly different (Levene's Test, $p<0.05$). * $p<0.05$ vs. respective sham.

EVALUATION OF BACE1 EXPRESSION LEVELS IN MOUSE BRAIN AFTER BC AND DEP SINGLE AND REPEATED INSTILLATIONS

As discussed before, BACE1 is the β-secretase responsible for amyloidogenic processing of APP and consequent Aβ production in the brain (Claeysen et al., 2012; Sathya et al., 2012; Pająk et al., 2016), whose increase has been found in the brain of mice exposed for 9 months to particulate matter (Bhatt et al., 2015). BACE1 was evaluated in the brain of male BALB/c mice intratracheally instilled with 50µg of BC or DEP/100µl 0.9% NaCl. Brain of sham and treated mice underwent the same preparative procedures described for HO-1 protein analysis.

A single intratracheal instillation induced a non-significant increasing trend of BACE1 expression levels in RoB (+13% with BC and +18% with DEP) and cerebellum (+39% with BC and +32% with DEP), comparing to sham, while hippocampus displayed no variations (**Fig 42**). Repeated intratracheal instillations were able to maintain the increasing trend of BACE1 expression levels in RoB (+234% with BC and +300% with DEP), and to induce an increment in hippocampus (+48% with BC and +83% with DEP), significant after DEP exposure comparing to sham (**Fig 42**). At the same time, cerebellum displayed a significant decrease of BACE1 expression with respect to BC treated mice (**Fig 42**).

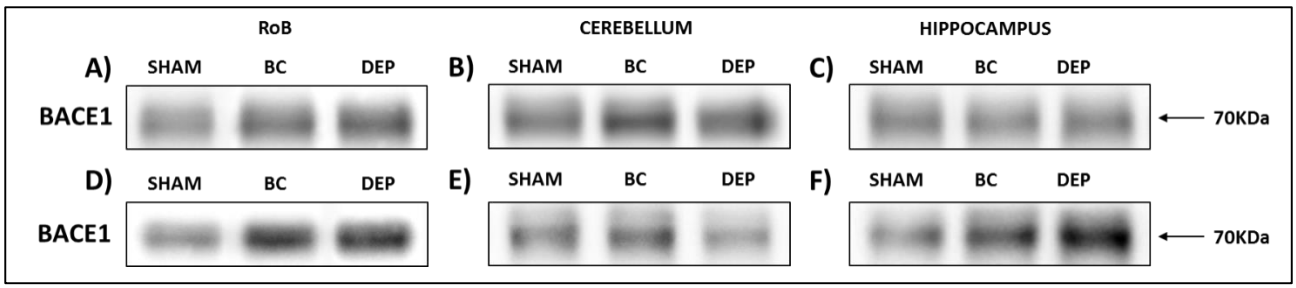

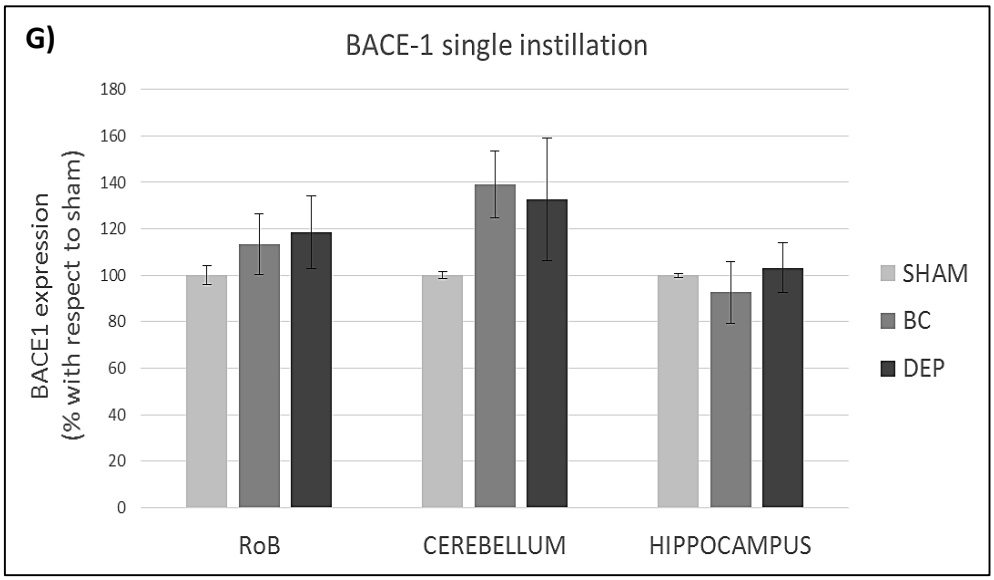

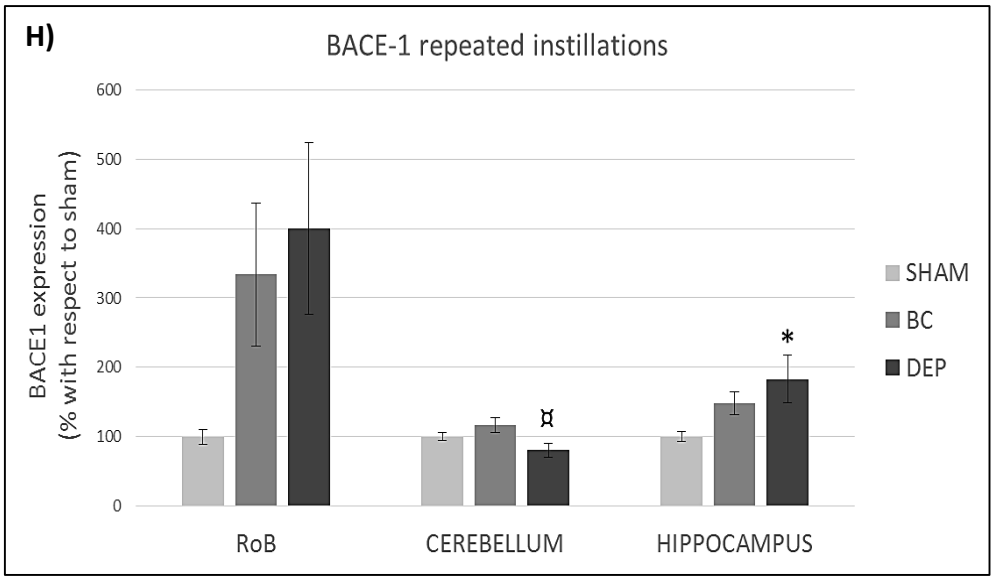

Figure 42: BACE1 protein analysis after single and repeated instillations. Representative immunoblotting images of BACE1 analysis of RoB, cerebellum and hippocampus after single **(A, B, C)** and repeated **(D, E, F)** instillations with 50µg of BC or DEP/100µl 0.9% NaCl. Histograms display BACE1 expression levels after single **(G)** and repeated **(H)** instillations. Proteins have been normalized for corresponding total proteins revealed by Ponceau in each lane and the data are expressed as mean ± s.e. (n = 5-9). Statistical differences were tested accordingly by One-way ANOVA followed by Bonferroni post-hoc comparison; Tukey post-hoc comparison has been used when population variances were significantly different (Levene's Test, $p<0.05$). * $p<0.05$ vs. respective sham. ¤ $p<0.05$ vs. respective BC.

FLUORESCENT MOLECULAR TOMOGRAPHY OF MOUSE BRAIN AFTER BC AND DEP SINGLE AND REPEATED INSTILLATIONS

FMT was performed in collaboration with Dr. Elisabetta Donzelli and Dr. Alessia Chiorazzi on male BALB/c mice intratracheally instilled with 50µg of BC or DEP/100µl 0.9% NaCl. FMT analysis 3h after a single instillation was not possible because the recommended optimal imaging time point was 6-24h post-injection of the probe, to allow its distribution and the decrease of background signal. Mice were injected intravenously with MMPSenseTM 750 FAST probe immediately before the first instillation (day 0). At 6h and 24h after injection, anesthetised mice were depilated and placed into the imaging cassette inside the chamber of FMT 1500TM system and the total amount of fluorophore in a selected tridimensional ROI was calculated by the TrueQuant software. This procedure was repeated at day 6.

6h after a single intratracheal instillation we observed no changes in fluorescent signal, while 24h after a single instillation we found an increase with BC (+26.29 pmol) and with DEP (+19.41 pmol), comparing to sham (**Fig 43**).

After the last of repeated intratracheal instillations we observed no changes in DEP treated mice, while BC treated mice displayed an increase at 6h (+8.45 pmol) and 24h (+13.87 pmol), comparing to sham (**Fig 44**).

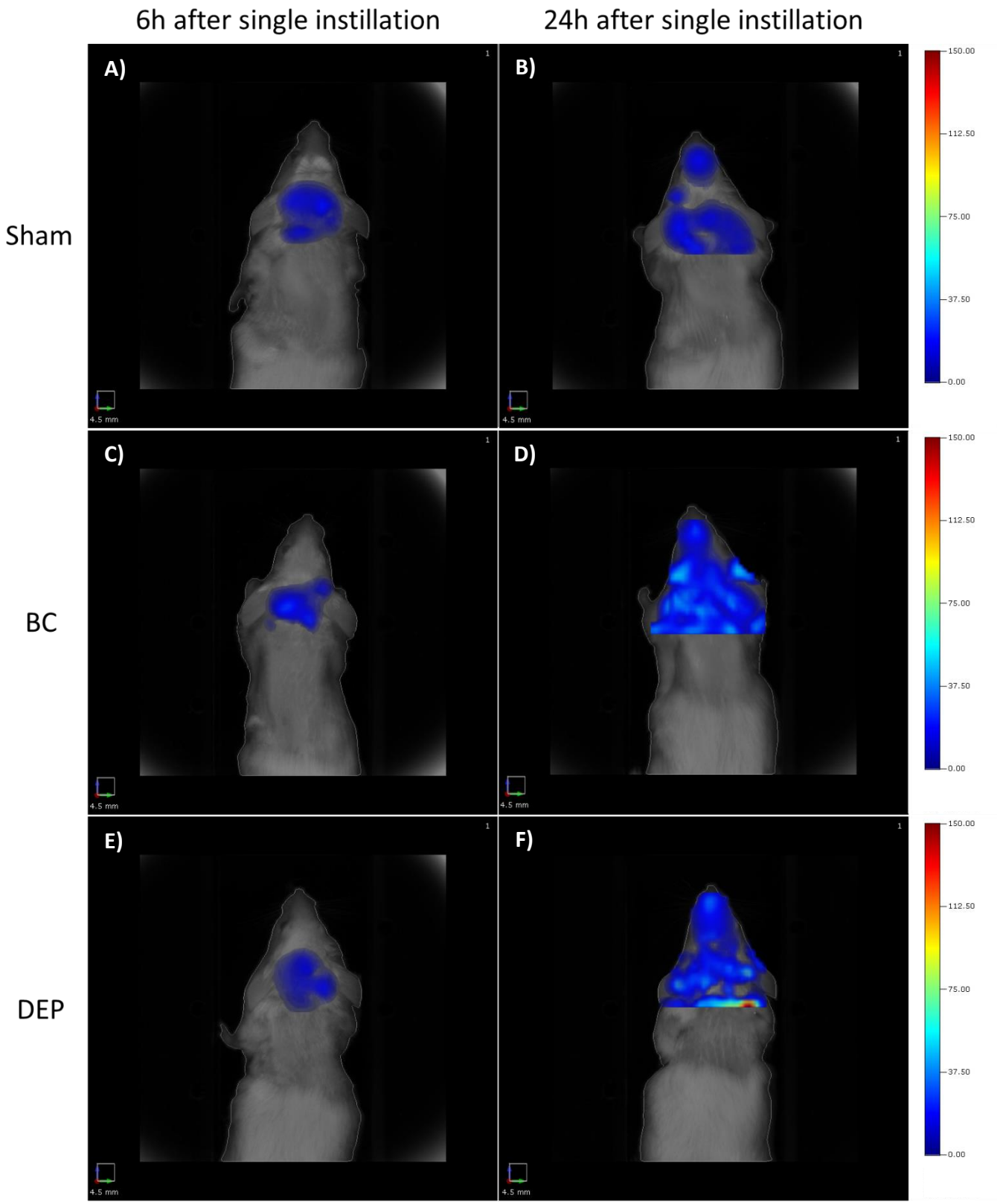

Figure 43: FMT of mouse brain after single instillation. Representative FMT images of mouse brain obtained 6h **(A, C, E)** and 24h **(B, D, F)** after single intratracheal instillation with 50µg of BC or DEP/100µl 0.9% NaCl. Each figure represents the status evidenced examining 2 sham and treated mice.

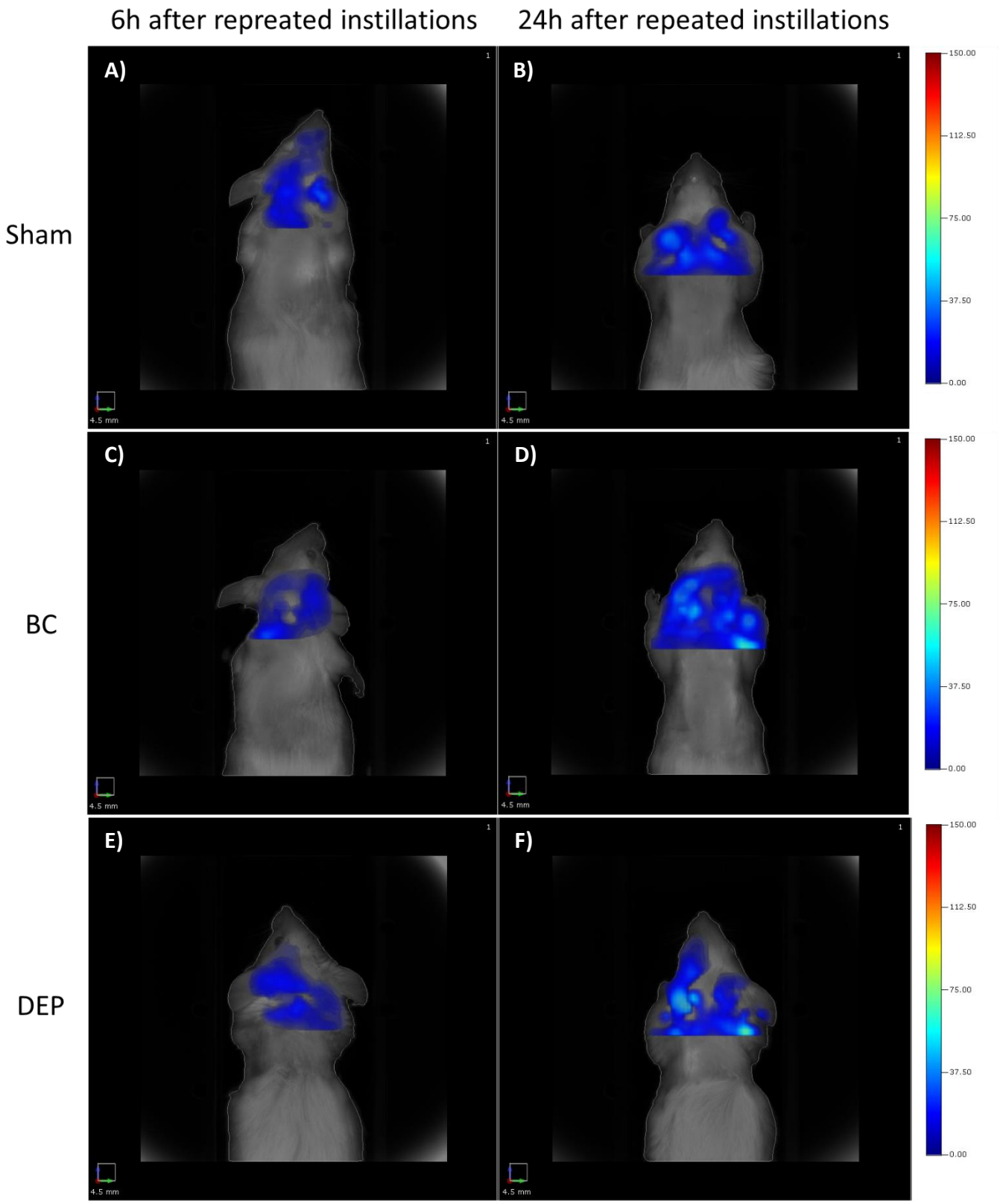

Figure 44: FMT of mouse brain after repeated instillations. Representative FMT images of mouse brain obtained 6h **(A, C, E)** and 24h **(B, D, F)** after the last of repeated intratracheal instillations with 50µg of BC or DEP/100µl 0.9% NaCl. Each figure represents the status evidenced examining 2 sham and treated mice.

HISTOPATHOLOGICAL ANALYSES OF MOUSE BRAIN AFTER BC AND DEP SINGLE AND REPEATED INSTILLATIONS

Histological examination was performed by Dr. Paola Marmiroli and collaborators on male BALB/c mice intratracheally instilled with 50µg of BC or DEP/100µl 0.9% NaCl. 3h after single instillation or 24h after the last of repeated instillations, animals were sacrificed and the brain was quickly harvested and fixed to obtain brain slice. Cerebral cortex, cerebellum and hippocampus images obtained after a single instillation are shown in **figure 45**. In all BC and DEP treated mice, cortical neurons were normal with regular cortical arrangement. The hippocampus was also normal, as well as cerebellum, which showed normal three layers disposition. No infiltration of inflammatory cells were detected in treated mice as well as in sham (**Fig 45**). Cerebral cortex, cerebellum and hippocampus images obtained after repeated instillations were comparable to single instillation images (data not shown).

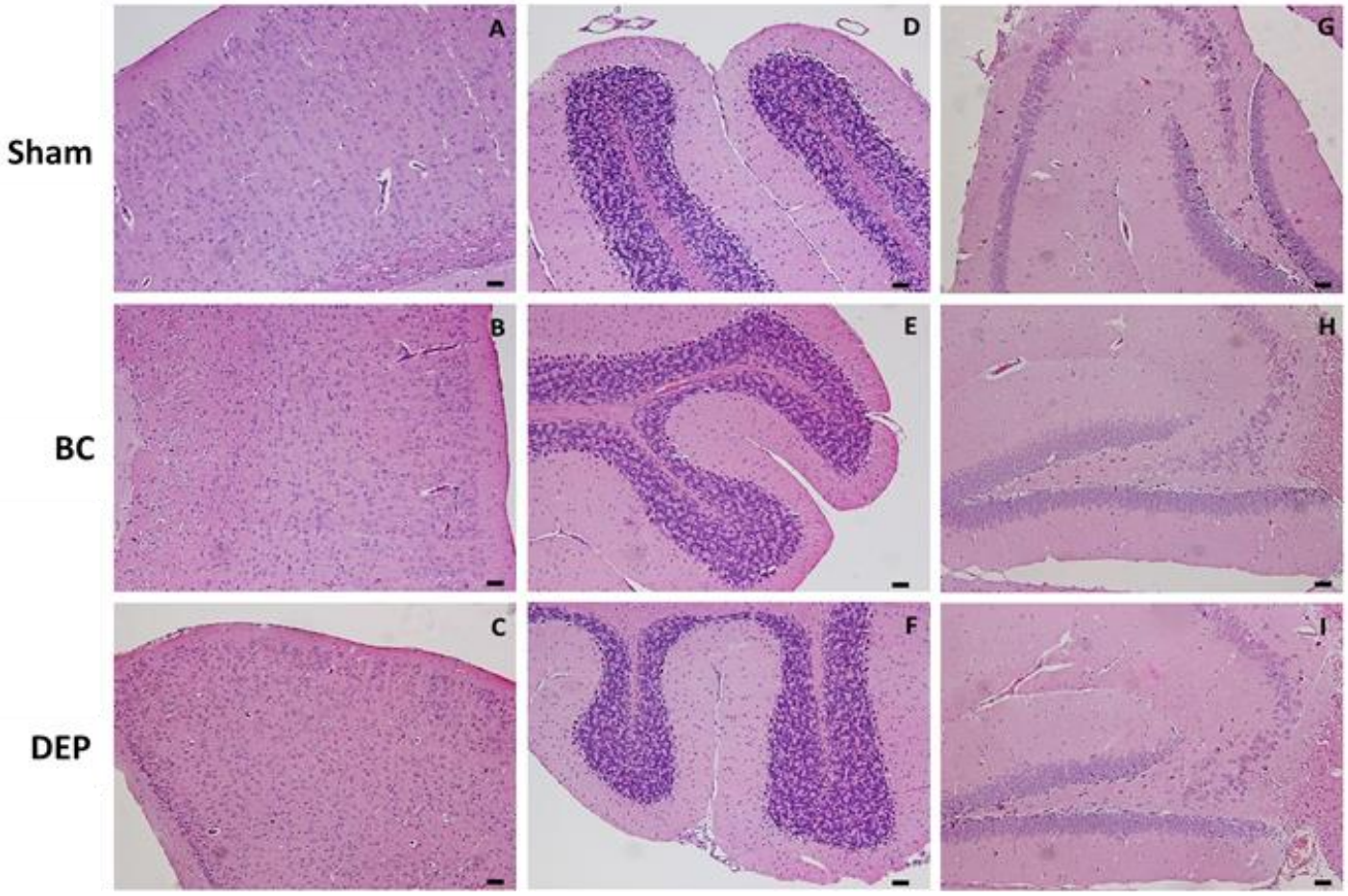

Figure 45: Histology of brain tissue after single instillation. Representative histological images of cerebral cortex **(A, B, C)**, cerebellum **(D, E, F)** and hippocampus **(G, H, I)** after single intratracheal instillation with 50µg of BC or DEP/100µl 0.9% NaCl. Each figure represents the status evidenced examining 2 sham and treated mice. Scale bar = 50 µm.

CYTOKINES ANALYSES OF MOUSE BRAIN AFTER BC AND DEP SINGLE AND REPEATED INSTILLATIONS

The quantitative analysis of the pro-inflammatory cytokines IL-1β, TNF-α and MMP9 were performed by LABOSPACE on male BALB/c mice intratracheally instilled with 50µg of BC or DEP/100µl 0.9% NaCl. 3h after single instillation or 24h after the last of repeated instillations, animals were sacrificed and the brain of sham and treated mice were dissected and divided in three parts: RoB, cerebellum and hippocampus. RoB and cerebellum were homogenized in isotonic saline solution and analysed by means of ELISA Multiplex assays.

After single or repeated instillations, cytokines concentrations of RoB and cerebellum were under the detection limits of the assay.

6.2 DISCUSSION

In this part of the project, we analysed and compared the effects of BC and DEP acute and sub-acute peripheral administrations on mouse brain regarding oxidative stress and inflammation induction, and their possible implications in Alzheimer's disease onset. Alterations in some oxidative stress related genes and other markers of oxidative stress (van Berlo et al., 2010) and increased markers of neuroinflammation (Levesque et al., 2011; Gerlofs-Nijland et al., 2010) have already been found in rodents following diesel exhaust exposure. The novelty of this study is the comparison between the effects induced by diesel and biomass particles, produced under controlled laboratory conditions, on different brain regions. Little is known about BC health effects, but particle-induced oxidative stress, inflammation, cytotoxicity and genotoxicity have been proposed (Kocbach Bølling et al., 2009).

Therefore, the brain of sham and treated mice was divided in different parts: hippocampus, commonly involved in AD onset and progression, cerebellum, generally not involved in AD neurodegeneration, and RoB, which has been considered to have a global idea. In general, we did not find significant differences between different brain regions responses, except for AD related proteins; single markers will be discussed in detail below.

Two principal routes have been proposed to explain how UFPs may reach the brain. In one route, particles are considered to reach brain tissue following deposition on the nasal olfactory epithelium and translocation along the olfactory nerve; the other route involves alveolar deposition and subsequent crossing of the lung blood-air barrier and the BBB (Oberdorster et al., 2005). Moreover, in the second route we must include inflammatory mediators produced in lungs as a consequence of pollutant-induced epithelial and endothelial injury, which can be released into the circulation and also reach the brain (Oberdörster et al., 2005; Genc at al., 2012). In this study, we focused exclusively on the second route, as we exposed mice to BC and DEP by means of intratracheal instillations. Once particles or their components, together with inflammatory mediators produced in lungs, have reached the brain, it is supposed that they might initiate the phagocytic activity of microglia, leading to the neurotoxic production of extracellular superoxide. As neurons are particularly vulnerable to oxidative damage, ROS production can lead to neuron death (Block and Calderón-Garcidueñas, 2009). Notably, our brain histopathological analysis of mice submitted to acute or sub-acute BC and DEP administration did not show visible modifications comparing to sham mice, and this is probably due to the type of treatment, which did not have the time to result in morphological changes, unlike chronic treatments. Moreover, differences between different exposure times have not been observed.

UFPs treatment induces oxidative stress in mouse brain

The brain is believed to be particularly vulnerable to oxidative stress, in particular neurons, as it contains high concentrations of PUFAs that are susceptible to lipid peroxidation, it consumes relatively large amounts of oxygen for energy production, and it has lower antioxidant defences compared to other organs (Dringen,

2000). Consistent with literature, acute exposure to BC and DEP induced oxidative stress in mouse brain, as demonstrated by HO-1 increasing trend. After sub-acute exposure, we observed HO-1 levels restoration in RoB, while the increasing trend was maintained in cerebellum and hippocampus, although it was lower than the one detected after a single instillation. Notably, HO-1 is the crucial enzyme for anti-oxidant response (Iles et al., 2005) but its chronic induction can have both beneficial and detrimental effects on cellular metabolism. While exists plenty of evidence for the HO-1-mediated neuro-protection, there is a growing literature attesting to the dangerous effects of HO-1 in the brain (Schipper, 2004). Fe^{2+} produced by HO-1 can catalyse ROS production through the Fenton's chemistry, acting as a cytotoxic and oxidative stress inducer and participating to the pathogenesis of neurodegenerative disorders (Abraham and Kappas, 2008).

As discussed previously, Hsp70 has been found to play a key role during oxidative stress induced by DEP treatment, through hydrolysis of denatured or partially unfolded proteins as well as newly synthesized nascent polypeptides; thus, Hsp70 can be considered a marker of ER stress (Jung et al., 2007). After acute exposure, we observed an increasing trend of Hsp70 expression levels in RoB, cerebellum and hippocampus, comparing to sham, although statistical analysis showed a significant variation only in cerebellum of DEP treated mice. Consistent with literature, after sub-acute DEP exposure we detected a significant increment of Hsp70 expression levels in all the parts of the brain that we analysed, comparing to sham. Also BC administration induced a relevant increase of Hsp70 expression, but it was less than the raise induced by DEP and it was not significant. Therefore, in contrast to previous observations collected in our lab from PM10sum treated mice (Farina et al., 2013), ROS produced by DEP exposure, and to a lesser extent by BC exposure, could be arguably associated to ER stress in mouse brain. A possible explanation for this result is that BC and DEP particles are smaller than PM10, in which particles with d_{ae}<100nm represent only a small part, thus UFPs or their components could easily reach the brain.

PAHs adsorbed on particles surface are inducers of Cytochrome P450 in the brain (Shimada et al., 2003). These chemicals are known to dissolve and translocate into blood circulation after particles deposition in the lungs (Mossman et al., 2007), mostly linked to and transported by albumin (Kure et al., 1997). However, deposition and translocation calculations (Oberdorster et al. 2004) indicate that the amount of particles, and hence the eventual concentration of particle-bound PAHs and other organic constituents, that may have reached the brain within 6h after DEP exposure will be rather low. Importantly, PAHs effects also depend on their bioavailability, which is known to depend on adsorption strength as well as the amount loaded onto the carbonaceous carrier particles (Gerde et al. 2001). In agreement to these calculations, we observed that after acute exposure with BC and DEP, Cyp1b1 was unchanged comparing to sham in the different parts of the brain. On the contrary, sub-acute DEP exposure significantly increased Cyp1b1 in RoB and cerebellum, comparing to sham and to BC treated mice, while hippocampus showed a non-significant raise. Moreover, BC resulted effective in inducing Cyp1b1 expression only in hippocampus. This result is again in contrast to brain outcomes from PM10sum treated mice (Farina et al., 2013), in which Cyp1b1 resulted unaltered after

repeated instillations. Once again, we hypothesized that BC but mainly DEP particles or they components may reach the brain after sub-acute administration and that this induction could ultimately give rise to the production of reactive oxygenated PAHs intermediates capable of interacting with cellular macromolecules and sustain oxidative stress damage. Finally, different induction of Cyp1b1 observed with BC and DEP could depend on particles composition.

UFPs treatment induces inflammation in mouse brain

iNOS, whose induction has been observed in the presence of different kinds of particulate matter (Calderon-Garciduenas et al., 2003; Farina et al., 2013; Li et al., 2016), has been selected as brain inflammatory marker. In contrast to rat brain results of short-term DEP inhalation exposure (van Berlo et al., 2010), we observed that acute DEP administration induced an increasing trend of iNOS expression levels in all the parts of the brain that we analysed, with statistical significance in RoB and cerebellum. Despite the strong increase in hippocampus average value, iNOS did not reach statistical significance in this part of the brain because of considerable variation. Moreover, DEP sub-acute exposure was able to maintain iNOS increase. Finally, in all the parts of the brain and after the two treatment times, BC mice showed iNOS increasing trends, but they resulted less affected. Therefore, our results demonstrate that HO-1 increase after peripheral administration of DEP, and to a lesser extent of BC, is not able to regulate NO production in mouse brain, and this could favour RNOS production and support oxidative stress. These findings are in agreement with the observational studies conducted by Calderón-Garcidueñas and collaborators, which found early induction on iNOS in the brain of dogs naturally exposed to urban air pollutants in Mexico City (Calderón-Garcidueñas et al., 2003).

At the same time, we tested inflammatory status *in-vivo* taking advantage of fluorescent molecular tomography. Limited by the characteristics of the MT 1500^{TM} fluorescence tomography system available in our department, we chose to analyse brain matrix metalloproteinases (MMPs) activation after BC and DEP peripheral administration. To this purpose, we injected mice intravenously with MMPSense^{TM} 750 FAST probe, which is a MMP activatable agent optically silent upon injection, and produces fluorescent signal after cleavage by disease related MMPs. Activation can occur by a broad range of MMP's including MMP2, 3, 7, 9, 12, and 13. MMPs are a family of proteolytic enzymes involved in physiological situations including tissue homeostasis, host defence and tissue repair (Nissinen and Kähäri, 2014). Expression and activity of MMPs are under strict control in physiological conditions, whereas their excessive activity is often noted in pathological conditions (Nissinen and Kähäri, 2014). MMPs can orchestrate the inflammatory functions at various levels. They can regulate transmigration of inflammatory cells from vasculature to the site of inflammation in tissue and they also regulate the recruitment and influx of inflammatory cells to the site of inflammation by processing extracellular matrix components, growth factors, cytokines and chemokines (Nissinen and Kähäri, 2014). Notably, *in-vivo* studies demonstrated that inhalation exposure to traffic-generated air pollutants promotes increase of MMPs activity and degradation of tight junction proteins in

the cerebral vasculature, resulting in altered BBB permeability and expression of neuroinflammatory markers (Oppenheim et al., 2013). Our preliminary FMT results displayed activation of MMPs 24h after a single intratracheal instillation with BC and DEP, while 6h and 24h after repeated instillations only BC treated mice showed MMPs activation. These results, in contrast to iNOS evaluation, suggest a major inflammation induction after single exposure, especially with BC rather than DEP. This conflicting data could be explained by the different chemical composition of BC and DEP, which could activate different mechanisms. However, future experiments will be necessary to confirm this result.

Anyway, our results suggest that exposure to BC and DEP has the potential to produce systemic immune dysfunction, and although acute brain inflammation may be considered a general protective mechanism, chronic inflammation is believed an important component contributing to AD progression (Bhatt et al., 2015).

UFPs treatment induces changes of AD related proteins in mouse brain

As discussed previously, literature data suggest that air pollution derived chemicals and organic compounds may be implicated in AD pathogenesis (Becaria et al., 2006; Maloney et al., 2012; Bondy, 2016). Several observational studies in humans and dogs that were exposed to high levels of coarse or fine particulate matter through inhalation of polluted air, strongly implicate the role of air pollution, oxidative stress induction and inflammatory changes in the development of AD pathology (Calderón-Garcidueñas et al., 2004; Calderón-Garcidueñas et al., 2008; Calderón-Garcidueñas et al., 2012). Interestingly, brain amyloidogenic processing of APP has been observed after long-term PM exposure (Calderón-Garcidueñas et al., 2008), also in mice (Bhatt et al., 2015). One of the key players of APP amyloidogenic processing is the β-secreatase enzyme, BACE1.

Since the hippocampus is one of the brain regions that are involved in AD onset and progression, and since in hippocampus we observed the induction of oxidative stress and inflammation markers, especially after DEP treatment, we were interested in studying some AD related proteins in this part of the brain, comparing to the cerebellum, which is a region largely spared in AD, with several roles related to movement and coordination. Moreover, we analysed the same markers in RoB, to have a more comprehensive idea of what happens in the brain after peripheral administration of UFPs.

To sum up, our analyses suggest that these different brain regions respond in different ways to BC and DEP acute and sub-acute peripheral administration regarding APP processing. First, acute exposure seems not able to activate amyloidogenic processing of APP, since we did not detect APP decrease and BACE1 increase for both BC and DEP treatment. On the contrary, we found a strong increment of APP expression level in RoB of DEP treated mice, which we supposed that is a compensatory mechanism activated after DEP exposure. In fact, literature provides strong evidences that APP has a trophic function, as it is involved in neural stem cell development, neuronal survival, neurite outgrowth and neurorepair (Dawkins and Small, 2014). On the other way, the repeated treatment of sub-acute exposure seems to affect brain APP processing, as we found

a decreasing trend of APP expression in RoB and cerebellum. This processing might depend on BACE1, whose protein levels were increased in RoB of BC and DEP treated mice. Surprisingly, hippocampus represents an exception, because its APP levels resulted unchanged, despite BACE1 showed an increasing trend.

These results would suggest but not necessarily indicate increased APP processing in RoB region after sub-acute UFPs exposure, therefore future experiments will be required to quantify changes in BACE1 activity as well as Aβ production and release, to better understand APP processing in mouse brain after peripheral BC and DEP administration.

Moreover, to the best of our knowledge, APP phosphorylation has never been described in relation to PM exposure. As discussed previously, APP phosphorylation on Thr668 is involved in the regulation of its function and metabolism, but its ability to induce alterations in the cleavage of APP at β- and/or γ-secretase sites is still controversial in AD brains (Matsushima et al., 2012). Our results suggest that the sub-acute exposure to BC and DEP induce in the different parts of mouse brain an increase of P-APP Thr668/APP ratio. The meaning of this post-translation modification after UFPs exposure remain to be investigated.

In conclusion, we hypothesize that APP processing undergoes some alterations after BC and DEP acute and sub-acute exposures and that these changes may become stronger and more defined during chronic exposures, as it happens in urban everyday life. In this contest, no matter in which part of the brain neurodegeneration begins, as once initiated, neuropathological changes might spread in a 'prion-like' manner (Brundin et al., 2010) to other regions. Therefore, UFPs continuous exposure, together with other factors like diabetes, hyperlipidemia, hypertension, heart disease, obesity (defined as noncommunicable diseases, NCDs) and smoking (Luchsinger et al., 2005) could represent a risk factor for Alzheimer disease onset and progression.

Conclusion

BC and DEP acute peripheral exposure is able to induce oxidative stress, endoplasmic reticulum stress and inflammation in mouse brain, while sub-acute exposure sustains these stress related mechanisms and additionally it induces increase of PAHs metabolism and alteration of APP processing. However, more experiments will be necessary to clarify the role of UFPs administration on AD onset and progression markers in mouse brain. Interestingly, BC resulted generally less effective than DEP in inducing the above described alterations, also after repeated treatments. Notably, DEP resulted highly effective also in *in-vitro* experiments performed by Eleonora Longhin and collaborators with the same particles while BC treatment was mostly ineffective (Longhin et al., 2016). This difference could be explained by the different chemical composition of BC and DEP. In fact, PAHs and transition metals concentration was higher in DEP compared to BC, which conversely resulted to be enriched in elements typical of wood combustion, such as Mn, K and S (Longhin et al., 2016). Considerable variation in the responses to both diesel and biomass particles has been observed in toxicological studies. For example, Seagrave et al. (2005) reported that different particles are able to

modulate *in-vivo* different inflammatory mediators: diesel particles induced high levels of MIP-2 (macrophage inflammatory protein 2-alpha), which is involved in immunoregulatory and inflammatory processes, whereas biomass particles increased the levels of tumor necrosis factor TNF-α, a multifunctional pro-inflammatory cytokine involved in cell proliferation, differentiation, apoptosis, lipid metabolism, and coagulation (Seagrave et al., 2005). Kocbach et al. (2008) reported that, in the monocytic cell line THP-1, traffic-derived particles induced a higher inflammatory effect, consisting in cytokines release, whereas wood smoke particles reduced cell proliferation and viability. These observations highlight the complexity of studying combustion particles toxicity, illustrating that differences in fuel properties and specific combustion conditions modify the particles chemical content, thereby affecting their biological properties (Longhin et al., 2016).

Not least, it must be noted that BC and DEP intratracheal administration route has completely avoided the particles transport along the olfactory nerve. Alterations in the nasal mucosa, olfactory bulb, cortical and sub-cortical brain structures have been described in healthy dogs exposed to high levels of ambient air pollutants (Calderon-Garciduenas et al., 2003). Indeed, it is possible that BC and DEP nasal inhalation could induce higher modifications in some regions of the CNS.

In conclusion, our results suggest that both acute and sub-acute UFPs peripheral administration are able to induce the response of the CNS. Whether this activation is due to the direct transport of UFPs or inflammatory mediators to the brain remains to be investigated.

CHAPTER 7: GENERAL CONCLUSIONS

The aim of this project was to evaluate the detrimental effect of UFPs exposure, regarding oxidative stress and inflammation, on *in-vitro* and *in-vivo* models of CNS. Moreover, this work meant to investigate the possible physiopathological correlation between these two mechanisms and AD neurodegeneration.

First, working with C6 glioma cells, which have properties of both astrocytes (Benda et al., 1968) and oligodendrocytes (Volpe et al., 1975), we demonstrated that DEP treatment at sub-lethal concentrations induced oxidative stress in glial cells, while inflammation was not involved. Moreover, we found that C6 glioma cells activate anti-oxidant pathways to contrast the oxidative status induced by DEP treatment and that the MEK-ERK1-2 pathway seems important in regulating these anti-oxidant strategies. This is noteworthy because glial cells, specifically astrocytes, are now recognized as active players in the regulation of synaptic function, neural repair, and CNS immunity (Lee and MacLean, 2015). Astrocytes are among the most structurally complex cells in the brain, and their activation has been shown in a wide spectrum of CNS injuries and diseases. Their processes represent an important component of the BBB, directly contacting endothelial cells and contributing to the structural and functional integrity of the BBB (Lee and MacLean, 2015). In particular, they have been recently linked to neuroinflammatory and neurotoxic pathways induced by PM exposure (Li et al., 2016).

The next step was the choice of HT22 nerve cell line as a neuronal *in-vitro* model to study the effect of direct DEP administration. We demonstrated that DEP treatment at sub-lethal concentrations induced oxidative stress and inflammation in neuronal cells, supporting the idea that neurons are more sensitive to DEP administration than glial cells. Moreover, we extended the analysis of DEP detrimental effects and we found lipid reshaping in HT22 cells. These mechanisms are supposed to be involved in AD neurodegeneration, and interestingly we observed the alteration of APP and BACE1 protein levels, despite future experiments will be necessary to clarify the role of direct DEP administration to neurons in AD onset.

Finally, working with male BALB/c mice we analysed *in-vivo* the effects of DEP acute and sub-acute peripheral administrations on mouse brain, comparing them to those induced by BC exposure. In this case, we were not able to discriminate between neurons and glial cells, but we hypothesised that neuronal damage was sustained by glial activation. This analysis confirmed the inflammatory and oxidative potential of DEP exposure on mouse brain, which was accompanied by induction of PAHs metabolism and alteration of APP processing after sub-acute exposure. Moreover, BC mice showed activation of the above described mechanisms, although BC resulted generally less effective than DEP in inducing them. Whether this activation is due to the direct transport of UFPs or inflammatory mediators to the brain remains to be investigated. Interestingly, these data are in agreement with a recent work conducted by Chen and collaborators (Chen et al., 2017), which employed a population-based cohort study to demonstrate that living near major roadways

was associated with increased dementia incidence, and that this associations seemed stronger among urban residents, especially those living in major urban centres and those who never moved.

In conclusion, these findings may contribute to the knowledge of the interplay between PM exposure, chronic oxidative stress and inflammation generation and development of neurodegenerative diseases. Certainly, future investigations should address the effects of lifetime air pollution exposure and aging related to neuroinflammation and neurotoxicity.

CHAPTER 8: BIBLIOGRAPHY

- Abraham N.G., Kappas A. (2008). Pharmacological and clinical aspects of heme oxygenase. *Pharmacol Rev*, 60(1):79-127. Doi: 10.1124/pr.107.07104.
- Alam J., Cookn J.L. (2007). How many transcription factors does it take to turn on the heme oxygenase-1 gene? *Am J Respir Cell Mol Biol*, 36:166–174. Doi: 10.1165/rcmb.2006-0340TR.
- Alam M.S., Zeraati-Rezaei S., Stark C.P., Liang Z., Xu H., Harrison R.M. (2016). The characterisation of diesel exhaust particles - composition, size distribution and partitioning. *Faraday Discuss*, 189:69-84. Doi: 10.1039/c5fd00185d.
- Anand R., Gill K.D., Mahdi A.A. (2014). Therapeutics of Alzheimer's disease: Past, present and future. *Neuropharmacology*, 76 Pt A:27-50. Doi: 10.1016/j.neuropharm.2013.07.004.
- Andreae M.O., Browell E.V., Garstang M., Gregory G.L., Harriss R.C., Hill G.F., Jacob D.J., Pereira M.C., Sachse G.W., Setzer A.W., Silva Dias P.L., Talbot R.W., Wofsy S.C. (1988). Biomass burning emissions and associated haze layers over Amazonia. *J Geophys Res*, 93(D2):1509–1527. Doi: 10.1029/JD093iD02p01509.
- Antiñolo M., Willis M.D., Zhou S., Abbatt J.P. (2015). Connecting the oxidation of soot to its redox cycling abilities. *Nature communications*, 6:6812. Doi: 10.1038/ncomms7812.
- Arenas-Huertero F., Apàtiga-Vega E., Miguel-Pèrez G., Villeda Cuevas D., Trillo-Trinoco J., (2011). Molecular markers associated with the biological response to aromatic hydrocarbons from urban air in humans. *INTECH Open Access Publisher*, ISBN 978-953-307-527-3.
- ARPA INEMAR, 2012. INEMAR Inventory Emission of Air Pollutants for Lombardy Region [WWW Document]. URL. http://inemar.arpalombardia.it/inemar/webdata/main.seam (accessed 10.07.16.).
- Becaria A., Lahiri D.K., Bondy S.C., Chen D., Hamadeh A., Li H., Taylor R., Campbell A. (2006). Aluminum and copper in drinking water enhance inflammatory or oxidative events specifically in the brain. *J Neuroimmunol*, 176(1-2):16-23. Doi: 10.1016/j.jneuroim.2006.03.025.
- Benda P., Lightbody J., Sato G., Levine L., Sweet W. (1968). Differentiated rat glial cell strain in tissue culture. *Science*, 161(3839), 370-371. Doi: 10.1126/science.161.3839.370.
- Bhatt D.P., Puig K.L., Gorr M.W., Wold L.E., Combs C.K. (2015). A pilot study to assess effects of long-term inhalation of airborne particulate matter on early Alzheimer-like changes in the mouse brain. *PLoS One*, 10(5):e0127102. Doi: 10.1371/journal.pone.0127102.
- Bivas-Benita M., Zwier R., Junginger H.E., Borchard G. (2005). Non-invasive pulmonary aerosol delivery in mice by the endotracheal route. *Eur J Pharm Biopharm*, 61(3):214-8. Doi: 10.1016/j.ejpb.2005.04.009.

- Block M.L., Calderón-Garcidueñas L. (2009). Air pollution: mechanisms of neuroinflammation and CNS disease. Trends Neurosci, 32:506-516. Doi: 10.1016/j.tins.2009.05.009.
- Bocci V., Valacchi G. (2015). Nrf2 activation as target to implement therapeutic treatments. Front Chem. 3:4. Doi: 10.3389/fchem.2015.00004.
- Bondy S.C. (2016). Anthropogenic pollutants may increase the incidence of neurodegenerative disease in an aging population. *Toxicology*, 341, 41-46. Doi: 10.1016/j.tox.2016.01.007.
- Brandenberger C., Mühlfeld C., Ali Z., Lenz A.G., Schmid O., Parak W.J., Gehr P., Rothen-Rutishauser B. (2010). Quantitative evaluation of cellular uptake and trafficking of plain and polyethylene glycol-coated gold nanoparticles. Small, 6(15): 1669–78. Doi: 10.1002/smll.201000528.
- Brauer M., Amann M., Burnett R.T., Cohen A., Dentener F., Ezzati M., Henderson S.B., Krzyzanowski M., Martin R.V., Van Dingenen R., van Donkelaar A., Thurston G.D. (2012). Exposure assessment for estimation of the global burden of disease attributable to outdoor air pollution. *Environ Sci Technol*, 46(2): 652–660. Doi: 10.1021/es2025752.
- Brown J.S., Gordon T., Price O., Asgharian B. (2013). Thoracic and respirable particle definitions for human health risk assessment. *Part Fibre Toxicol*, 10: 12. Doi: 10.1186/1743-8977-10-12.
- Brundin P., Melki R., Kopito R. (2010). Prion-like transmission of protein aggregates in neurodegenerative diseases. *Nat Rev Mol Cell Biol*, 11(4):301-7. doi: 10.1038/nrm2873.
- Butterfield D.A., Hensley K., Cole P., Subramaniam R., Aksenov M., Aksenova M., Bummer P.M., Haley B.E., Carney J.M. (1997). Oxidatively induced structural alteration of glutamine synthetase assessed by analysis of spin label incorporation kinetics: Relevance to Alzheimer's disease. *J Neurochem*, 68:2451–2457. Doi: 10.1046/j.1471-4159.1997.68062451.x.
- Calderón-Garcidueñas L., Maronpot R.R., Torres-Jardon R., Henríquez-Roldán C., Schoonhoven R., Acuña-Ayala H., Villarreal-Calderón A., Nakamura J., Fernando R., Reed W., Azzarelli B., Swenberg J.A. (2003). DNA damage in nasal and brain tissues of canines exposed to air pollutants is associated with evidence of chronic brain inflammation and neurodegeneration. *Toxicol Pathol*, 31(5):524-38. Doi: 10.1080/01926230390226645.
- Calderón-Garcidueñas L., Reed W., Maronpot R.R., Henríquez-Roldán C., Delgado-Chavez R., Calderón-Garcidueñas A., Dragustinovis I., Franco-Lira M., Aragón-Flores M., Solt A.C., Altenburg M., Torres-Jardón R., Swenberg J.A. (2004). Brain inflammation and Alzheimer's-like pathology in individuals exposed to severe air pollution. *Toxicol Pathol*, 32(6):650-8. Doi: 10.1080/01926230490520232.
- Calderón-Garcidueñas L., Solt A.C., Henríquez-Roldán C., Torres-Jardón R., Nuse B., Herritt L., Villarreal-Calderón R., Osnaya N., Stone I., García R., Brooks D.M., González-Maciel A., Reynoso-Robles R., Delgado-Chávez R., Reed W. (2008). Long-term air pollution exposure is associated with neuroinflammation, an altered innate immune response, disruption of the blood-brain barrier,

ultrafine particulate deposition, and accumulation of amyloid beta-42 and alpha-synuclein in children and young adults. Toxicol Pathol, 36(2):289-310. Doi: 10.1177/0192623307313011.

- Calderón-Garcidueñas L., Mora-Tiscareño A., Styner M., Gómez-Garza G., Zhu H., Torres-Jardón R., Carlos E., Solorio-López E., Medina-Cortina H., Kavanaugh M., D'Angiulli A. (2012). White matter hyperintensities, systemic inflammation, brain growth, and cognitive functions in children exposed to air pollution. *J Alzheimers Dis*, 31(1):183-91. Doi: 10.3233/JAD-2012-120610.
- Cassee F.R., Héroux M.E., Gerlofs-Nijland M.E., Kelly F.J. (2013). Particulate matter beyond mass: recent health evidence on the role of fractions, chemical constituents and sources of emission. *Inhal Toxicol*, 25(14):802-12. Doi: 10.3109/08958378.2013.850127.
- Chan J.K., Vogel C.F., Baek J., Kodani S.D., Uppal R.S., Bein K.J., Anderson D.S., Van Winkle L.S. (2013). Combustion derived ultrafine particles induce cytochrome P-450 expression in specific lung compartments in the developing neonatal and adult rat. *Am J Physiol Lung Cell Mol Physiol*, 304(10):L665-77. Doi: 10.1152/ajplung.00370.2012.
- Chang J.T., Chang H., Chen P.H., Lin S.L., Lin P. (2007). Requirement of aryl hydrocarbon receptor overexpression for CYP1B1 up-regulation and cell growth in human lung adenocarcinomas. *Clin Cancer Res*, 13(1):38–45. Doi: 10.1158/1078-0432.
- Chen H., Kwong J.C., Copes R., Tu K., Villeneuve P.J., van Donkelaar A., Hystad P., Martin R.V., Murray B.J., Jessiman B., Wilton A.S., Kopp A., Burnett R.T. (2017). Living near major roads and the incidence of dementia, Parkinson's disease, and multiple sclerosis: a population-based cohort study. *Lancet*, pii: S0140-6736(16)32399-6. doi: 10.1016/S0140-6736(16)32399-6.
- Christen Y. (2000). Oxidative stress and Alzheimer disease. *Am J Clin Nutr*, 71:621S–629S.
- Christie W.W. (1985). Rapid separation and quantification of lipid classes by high performance liquid chromatography and mass (light-scattering) detection. *J Lipid Res*, 26(4):507-12.
- Claeysen S., Cochet M., Donneger R., Dumuis A., Bockaert J., Giannoni P. (2012). Alzheimer culprits: cellular crossroads and interplay. *Cell Signal*, 24(9):1831-40. Doi: 10.1016/j.cellsig.2012.05.008.
- Colbeck I., Lazaridis M. (2010). Aerosols and environmental pollution. *Naturwissenschaften*. 97(2):117-31. Doi: 10.1007/s00114-009-0594-x.
- Coleman J.W. (2001). Nitric oxide in immunity and inflammation. *Int Immunopharmacol*, 1(8):1397-406. Doi: 10.1016/S1567-5769(01)00086-8.
- Cooke M.S., Evans M.D., Dizdaroglu M., Lunec J. (2003). Oxidative DNA damage: Mechanisms, mutation, and disease. FASEB J, 17:1195–1214. Doi: 10.1096/fj.02-0752rev.
- Corsetto P.A., Cremona A., Montorfano G., Jovenitti I.E., Orsini F., Arosio P., Rizzo A.M. (2012). Chemical-physical changes in cell membrane microdomains of breast cancer cells after omega-3 PUFA incorporation. *Cell Biochem Biophys*, 64(1):45-59. Doi: 10.1007/s12013-012-9365-y.

- Cui Y., Sun Q., Liu Z. (2016). Ambient particulate matter exposure and cardiovascular diseases: a focus on progenitor and stem cells. *J Cell Mol Med*, 20(5):782-93. Doi: 10.1111/jcmm.12822.
- Cunningham C., Campion S., Lunnon K., Murray C.L., Woods J.F., Deacon R.M., Rawlins J.N., Perry V.H. (2009). Systemic inflammation induces acute behavioral and cognitive changes and accelerates neurodegenerative disease. *Biol Psychiatry*, 65(4):304-12. Doi: 10.1016/j.biopsych.2008.07.024.
- Dawkins E., Small D.H. (2014). Insights into the physiological function of the β-amyloid precursor protein: beyond Alzheimer's disease. *J Neurochem*, 129(5):756-69. Doi: 10.1111/jnc.12675.
- de Oliveira Galvão M.F., De Melo Cabral T., De André P.A., De Fátima Andrade M., De Miranda R.M., Saldiva P.H., Vasconcellos Pde C., de Medeiros S.R. (2014). Cashew nut roasting: chemical characterization of particulate matter and genotocixity analysis. *Environ Res*, 131:145–52. Doi: 10.1016/j.envres.2014.03.013.
- de Souza C.V., Corrêa S.M. (2015). Polycyclic aromatic hydrocarbon emissions in diesel exhaust using gas chromatography–mass spectrometry with programmed temperature vaporization and large volume injection. *Atmospheric Environment*, 103, 222-230. Doi: 10.1016/j.atmosenv.2014.12.047.
- Di Paolo G., Kim T.W. (2011). Linking lipids to Alzheimer's disease: cholesterol and beyond. *Nat Rev Neurosci*, 12(5):284-96. Doi: 10.1038/nrn3012.
- Diociaiuti M., Balduzzi M., De Berardis B., Cattani G., Stacchini G., Ziemacki G. (2001). The two PM2.5 (fine) and PM2.5–10 (coarse) fractions: evidence of different biological activity. *Environ Res*, 86:254–62. Doi:10.1006/enrs.2001.4275.
- Dominici F., Peng R.D., Bell M.L., Pham L., McDermott A., Zeger S.L., Samet J.M. (2006). Fine particulate air pollution and hospital admission for cardiovascular and respiratory diseases. *JAMA,* 295(10): 1127–1134. Doi: 10.1001/jama.295.10.1127.
- Dringen R. (2000). Metabolism and functions of glutathione in brain. *Prog Neurobiol*, 62(6):649-71. Doi: 10.1016/S0301-0082(99)00060-X.
- Elder A., Gelein R., Silva V., Feikert T., Opanashuk L., Carter J., Potter R., Maynard A., Ito Y., Finkelstein J., Oberdörster G. (2006). Translocation of inhaled ultrafine manganese oxide particles to the central nervous system. *Environ Health Perspect*, 114(8):1172-8. Doi: 10.1289/ehp.9030.
- Fajardo V.A., McMeekin L., LeBlanc P.J. (2011). Influence of phospholipid species on membrane fluidity: a meta-analysis for a novel phospholipid fluidity index. *J Membr Biol*, 244(2):97-103. Doi: 10.1007/s00232-011-9401-7.
- Falcon-Rodriguez C.I., Osornio-Vargas A.R., Sada-Ovalle I., Segura-Medina P. (2016). Aeroparticles, Composition, and Lung Diseases. *Front Immunol*, 7:3. Doi: 10.3389/fimmu.2016.00003.
- Farina F., Sancini G., Battaglia C., Tinaglia V., Mantecca P., Camatini M., Palestini P. (2013). Milano summer particulate matter (PM10) triggers lung inflammation and extra pulmonary adverse events in mice. *PLoS One*. 8(2):e56636. Doi: 10.1371/journal.pone.0056636.

- Finch C.E., Morgan T.E. (2007). Systemic inflammation, infection, ApoE alleles, and Alzheimer disease: a position paper. *Curr Alzheimer Res*, 4(2):185-9.
- Frodl T., O'Keane V. (2013). How does the brain deal with cumulative stress? A review with focus on developmental stress, HPA axis function and hippocampal structure in humans. *Neurobiol Dis*, 52:24-37. Doi: 10.1016/j.nbd.2012.03.012.
- Geiser M., Rothen-Rutishauser B., Kapp N., Schürch S., Kreyling W., Schulz H., Semmler M., Im Hof V., Heyder J., Gehr P. (2005). Ultrafine particles cross cellular membranes by nonphagocytic mechanisms in lungs and in cultured cells. *Environ Health Perspect*, 113(11):1555-60. Doi: 10.1289/ehp.8006.
- Genc S., Zadeoglulari Z., Fuss S.H., Genc K. (2012). The adverse effects of air pollution on the nervous system. *J Toxicol*, 2012:782462. Doi: 10.1155/2012/782462.
- Gerde P., Muggenburg B.A., Lundborg M., Dahl A.R. (2001). The rapid alveolar absorption of diesel soot-adsorbed benzo[a]pyrene: bioavailability, metabolism and dosimetry of an inhaled particle-borne carcinogen. *Carcinogenesis*, 22:741–749. Doi: 10.1093/carcin/22.5.741.
- Gerlofs-Nijland M.E., van Berlo D., Cassee F.R., Schins R.P., Wang K., Campbell A. (2010). Effect of prolonged exposure to diesel engine exhaust on proinflammatory markers in different regions of the rat brain. *Part Fibre Toxicol*, 7:12. Doi: 10.1186/1743-8977-7-12.
- Gilli G., Traversi D., Rovere R., Pignata C., Schilirò T. (2007) Chemical characteristics and mutagenic activity of PM10 in Torino, a Northern Italian City. *Sci Total Environ,* 385:97–107. Doi:10.1016/j.scitotenv.2007.07.006.
- Goncharov I., Weiner L., Vogel Z. (2005). Delta9-tetrahydrocannabinol increases C6 glioma cell death produced by oxidative stress. *Neuroscience*, 134(2):567–574. Doi: 10.1016/j.neuroscience.2005.04.042.
- González-Flecha B. (2004). Oxidant mechanisms in response to ambient air particles. *Mol Aspects Med*, 25:169–82. Doi:10.1016/j.mam.2004.02.017.
- Gualtieri M., Longhin E., Mattioli M., Mantecca P., Tinaglia V., Mangano E., Proverbio M.C., Bestetti G., Camatini M., Battaglia C. (2012). Gene expression profiling of A549 cells exposed to Milan PM2.5. *Toxicol Lett*, 209, 136e145. Doi: 10.1016/j.toxlet.2011.11.015.
- Hagihara H., Toyama K., Yamasaki N., Miyakawa T. (2009). Dissection of Hippocampal Dentate Gyrus from Adult Mouse. *J Vis Exp*, 33:1543. Doi: 10.3791/1543.
- Halliwell B. (1992). Reactive oxygen species and the central nervous system. J Neurochem, 59(5):1609-23.
- Halliwell B. (2001). Role of free radicals in the neurodegenerative diseases: therapeutic implications for antioxidant treatment. Drugs Aging, 18(9):685-716.

- Halonen J.I., Lanki T., Yli-Tuomi T., Tiittanen P., Kulmala M., Pekkanen J. (2009). Particulate air pollution and acute cardiorespiratory hospital admissions and mortality among the elderly. *Epidemiology*, 20(1):143-53. Doi: 10.1097/EDE.0b013e31818c7237.
- Han Y.G., Xu J., Li Z.G., Ren G.G., Yang Z. (2012). In vitro toxicity of multi-walled carbon nanotubes in C6 rat glioma cells. *NeuroToxicology*, 33(5):1128–1134. Doi: 10.1016/j.neuro.2012.06.004.
- Happo M.S., Salonen R.O., Hälinen A.I., Jalava P.I., Pennanen A.S., Dormans J.A., Gerlofs-Nijland M.E., Cassee F.R., Kosma V.M., Sillanpää M., Hillamo R., Hirvonen M.R. (2010). Inflammation and tissue damage in mouse lung by single and repeated dosing of urban air coarse and fine particles collected from six European cities. *Inhal Toxicol,* 22(5):402-16. Doi: 10.3109/08958370903527908.
- Hays M.D., Geron C.D., Linna K.J., Smith N.D., Schauer J.J. (2002). Speciation of gas-phase and fine particle emissions from burning of foliar fuels. *Environ Sci Technol*, 36(11):2281-95. Doi: 10.1021/es0111683.
- Heeb N.V., Schmid P., Kohler M., Gujer E., Zennegg M., Wenger D., Wichser A., Ulrich A., Gfeller U., Honegger P., Zeyer K., Emmenegger L., Petermann J.L., Czerwinski J., Mosimann T., Kasper M., Mayer A. (2010). Impact of low- and high-oxidation diesel particulate filters on genotoxic exhaust constituents. *Environ Sci Technol*, 44:1078–1084. Doi: 10.1021/es9019222.
- Hou Q., An X., Wang Y., Tao Y., Sun Z. (2012). An assessment of China's PM10-related health economic losses in 2009. *Sci Total Environ*, 435-436:61-5. Doi: 10.1016/j.scitotenv.2012.06.094.
- Huang W.J., Zhang X., Chen W.W. (2016). Role of oxidative stress in Alzheimer's disease. Biomed Rep, 4(5):519-522. Doi: 10.3892/br.2016.630.
- International Agency for Research on Cancer (IARC). (1988). Diesel and gasoline engine exhausts and some nitroarenes. *IARC monographs on the evaluation of carcinogenic risks to humans*, 105.
- International Agency for Research on Cancer (IARC). (2013). Outdoor Air Pollution a Leading Environmental Cause of Cancer Deaths. Lyon: IARC Press Releases.
- Iles K.E., Dickinson D.A., Wigley A.F., Welty N.E., Blank V., Forman H.J. (2005). HNE increases HO-1 through activation of the ERK pathway in pulmonary epithelial cells. Free Radic Biol Med, 39(3): 355–364. Doi: 10.1016/j.freeradbiomed.2005.03.026.
- Illum L. (2004). Is nose-to-brain transport of drugs in man a reality? *J Pharm Pharmacol*, 56(1):3-17. Doi: 10.1211/0022357022539.
- Jalbert J.J., Daiello L.A., Lapane K.L. (2008). Dementia of the Alzheimer type. *Epidemiol Rev*, 30:15-34. Doi: 10.1093/epirev/mxn008.
- Janssen C.I., Kiliaan A.J. (2014). Long-chain polyunsaturated fatty acids (LCPUFA) from genesis to senescence: the influence of LCPUFA on neural development, aging, and neurodegeneration. *Prog Lipid Res*, 53:1-17. Doi: 10.1016/j.plipres.2013.10.002.

- Jones M.G., Richeldi L. (2014). Air pollution and acute exacerbations of idiopathic pulmonary fibrosis: back to miasma? *Eur Respir J,* 43:956–9. Doi:10.1183/09031936.00204213.
- Joshi Y.B., Chu J., Praticò D. (2012). Stress hormone leads to memory deficits and altered tau phosphorylation in a model of Alzheimer's disease. *J Alzheimers Dis*, 31(1):167-76. Doi: 10.3233/JAD-2012-120328.
- Jung E.J., Avliyakulov N.K., Boontheung P., Loo J.A., Nel A.E. (2007). Pro-oxidative DEP chemicals induce heat shock proteins and an unfolding protein response in a bronchial epithelial cell line as determined by DIGE analysis. *Proteomics*, 7(21):3906-18. Doi: 10.1002/pmic.200700377.
- Kadiiska M.B., Mason R.P., Dreher K.L., Costa D.L., Ghio A.J. (1997). In vivo evidence of free radical formation in the rat lung after exposure to an emission source air pollution particle. *Chem Res Toxicol,* 10:1104–8. Doi: 10.1021/tx970049r.
- Kamal A., Almenar-Queralt A., LeBlanc J.F., Roberts E.A., Goldstein L.S. (2001). Kinesin-mediated axonal transport of a membrane compartment containing β-secretase and presenilin-1 requires APP. *Nature*, 414(6864), 643-648. Doi: 10.1038/414643a.
- Kang J., Lemaire H.G., Unterbeck A., Salbaum J.M., Masters C.L., Grzeschik K.H., Multhaup G., Beyreuther K., Müller-Hill B. (1987). The precursor of Alzheimer's disease amyloid A4 protein resembles a cell-surface receptor. *Nature*, 325(6106):733-6. Doi: 10.1038/325733a0.
- Karatas F., Karatepe M., Baysar A. (2002). Determination of free malondialdehyde in human serum by high-performance liquid chromatography. *Anal Biochem*, 311(1):76-9.
- Khalil M.A.K., Rasmussen R.A. (2003). Tracers of wood smoke. *Atmos Environ*, 37(9–10):1211–1222. Doi: 10.1016/S1352-2310(02)01014-2.
- Kim S.W., Lee H.K., Shin J.H., Lee J.K. (2013). Up-down regulation of HO-1 and iNOS gene expressions by ethyl pyruvate via recruiting p300 to Nrf2 and depriving it from p65. *Free Radic Biol Med*, 65:468–476. Doi: 10.1016/j.
- Kim J.K., Jang H.D. (2014). Nrf2-Mediated HO-1 induction coupled with the ERK signaling pathway contributes to indirect antioxidant capacity of caffeic acid phenethyl ester in HepG2 cells. *J Mol Sci*, 15(7):12149–12165. Doi: 10.3390/ijms150712149.
- Kim J.W., Park S., Lim C.W., Lee K., Kim B. (2014). The role of air pollutants in initiating liver disease. *Toxicol Res*, 30(2):65-70. Doi: 10.5487/TR.2014.30.2.065.
- Kim K.H., Kabir E., Kabir S. (2015). A review on the human health impact of airborne particulate matter. *Environ Int,* 74:136-43. Doi: 10.1016/j.envint.2014.10.005.
- Kocbach A., Namork E., Schwarze P.E. (2008). Pro-inflammatory potential of wood smoke and traffic-derived particles in a monocytic cell line. *Toxicology*, 247,123e132.

- Kocbach Bølling A., Pagels J., Yttri K.E., Barregard L., Sallsten G., Schwarze P.E., Boman C. (2009). Health effects of residential wood smoke particles: the importance of combustion conditions and physicochemical particle properties. *Part Fibre Toxicol*, 6:29. doi: 10.1186/1743-8977-6-29.
- Koch D., Hansen J. (2005). Distant origins of Arctic black carbon: A Goddard Institute for Space Studies Model Eexperiment. *J Geophys Res*, 110:4204. Doi: 10.1029/2004JD005296.
- Kreyling W.G., Semmler M., Erbe F., Mayer P., Takenaka S., Schulz H., Oberdörster G., Ziesenis A. (2002). Translocation of ultrafine insoluble iridium particles from lung epithelium to extrapulmonary organs is size dependent but very low. *J Toxicol Environ Health A*, 65(20):1513-30. Doi: 10.1080/00984100290071649.
- Kreyling W.G., Hirn S., Schleh C. (2010). Nanoparticles in the lung. *Nat Biotechnol*, 28(12):1275-6. Doi: 10.1038/nbt.1735.
- Kumar A., Singh A., Ekavali. (2015). A review on Alzheimer's disease pathophysiology and its management: an update. *Pharmacological Reports*, 67(2), 195-203. Doi: 10.1016/j.pharep.2014.09.004.
- Kure E.H., Andreassen A., Ovrebø S., Grzybowska E., Fiala Z., Strózyk M., Chorazy M., Haugen A. (1997). Benzo(a)pyrene-albumin adducts in humans exposed to polycyclic aromatic hydrocarbons in an industrial area of Poland. *Occup Environ Med*, 54(9):662-6.
- Kwak M.-K., Itoh K., Yamamoto M., Kensler T.W. (2002). Enhanced expression of the transcription factor Nrf2 by cancer chemopreventive agents: role of antioxidant response element-like sequences in the Nrf2 promoter. *Mol Cell Biol*, 22(9):2883-2892. Doi: 10.1128/MCB.22.9.2883-2892.2002.
- Lee J., Koo N., Min D.B. (2004). Reactive oxygen species, aging, and antioxidative nutraceuticals. Comprehensive reviews in food science and food safety, 3(1), 21-33. Doi: 10.1111/j.1541-4337.2004.tb00058.x.
- Lee K.M., MacLean A.G. (2015). New advances on glial activation in health and disease. *World J Virol*, 4(2):42-55. doi: 10.5501/wjv.v4.i2.42.
- Levesque S., Taetzsch T., Lull M.E., Kodavanti U., Stadler K., Wagner A., Johnson J.A., Duke L., Kodavanti P., Surace M.J., Block M.L. (2011). Diesel exhaust activates and primes microglia: air pollution, neuroinflammation, and regulation of dopaminergic neurotoxicity. *Environ Health Perspect*, 119(8):1149-55. Doi: 10.1289/ehp.1002986.
- Li Y., Maher P., Schubert D. (1997). A role for 12-lipoxygenase in nerve cell death caused by glutathione depletion. *Neuron*, 19(2):453-63. Doi: 10.1016/S0896-6273(00)80953-8.
- Li N., Venkatesan M.I., Miguel A., Kaplan R., Gujuluva C., Alam J., Nel A. (2000). Induction of heme oxygenase-1 expression in macrophages by diesel exhaust particle chemicals and quinones via the antioxidant-responsive element. *J Immunol*, 165:3393. Doi: 10.4049/jimmunol.165.6.3393.

- Li N., Sioutas C., Cho A., Schmitz D., Misra C., Sempf J., Wang M., Oberley T., Froines J., Nel A. (2003). Ultrafine particulate pollutants induce oxidative stress and mitochondrial damage. *Environ Health Perspect*, 111(4):455-60. Doi: 10.1289/ehp.6000.
- Li M.H., Jang J.H., Na H.K., Cha Y.N., Surh Y.J. (2007). Carbon monoxide produced by heme oxygenase-1 in response to nitrosative stress induces expression of glutamatecysteine ligase in PC12 cells via activation of phosphatidylinositol 3-kinase and Nrf2 signaling. *J Biol Chem*, 282(39):28577-86. Doi: 10.1074/jbc.M701916200.
- Li T., Zhao J., Ge J., Yang J., Song X., Wang C., Mao J., Zhang Y., Zou Y., Liu Y., Chen G. (2016). Particulate Matter Facilitates C6 Glioma Cells Activation and the Release of Inflammatory Factors Through MAPK and JAK2/STAT3 Pathways. *Neurochem Res*, 41(8):1969-81. Doi: 10.1007/s11064-016-1908-y. Epub 2016 Apr 12.
- Liati A., Eggenschwiler P.D. (2010) Characterization of particulate matter deposited in diesel particulate filters: visual and analytical approach in macro-, micro- and nano-scales. *Combust Flame*, 157:1658–1670. Doi: 10.1016/j.combustflame.2010.02.015.
- Lind C.R., Gray C.W., Pearson A.G., Cameron R.E., O'Carroll S.J., Narayan P.J., Lim J., Dragunow M. (2006). The mitogen-activated/extracellular signal-regulated kinase kinase 1/2 inhibitor U0126 induces glial fibrillary acidic protein expression and reduces the proliferation and migration of C6 glioma cells. *Neuroscience*, 141 (4), 1925–1933. Doi: 10.1016/j.neuroscience.2006.05.038.
- Löndahl J., Massling A., Pagels J., Swietlicki E., Vaclavik E., Loft S. (2007). Size-resolved respiratory-tract deposition of fine and ultrafine hydrophobic and hygroscopic aerosol particles during rest and exercise. *Inhal Toxicol,* 19(2):109-16.
- Longhin E., Gualtieri M., Capasso L., Bengalli R., Mollerup S., Holme J.A., Øvrevik J., Casadei S., Di Benedetto C., Parenti P., Camatini M. (2016). Physico-chemical properties and biological effects of diesel and biomass particles. *Environ Pollut*, 215:366-75. Doi: 10.1016/j.envpol.2016.05.015.
- Lowry O.H., Rosebrough N.J., Farr A.L., Randall R.J. (1951). Protein measurement with the Folin phenol reagent. *J biol Chem*, 193(1), 265-275.
- Luchsinger J.A., Reitz C., Honig L.S., Tang M.X., Shea S., Mayeux R. (2005). Aggregation of vascular risk factors and risk of incident Alzheimer disease. *Neurology*, 65(4):545-51. Doi:10.1212/01.wnl.0000172914.08967.dc.
- Møller P., Danielsen P.H., Karottki D.G., Jantzen K., Roursgaard M., Klingberg H., Jensen D.M., Christophersen D.V., Hemmingsen J.G., Cao Y., Loft S. (2014). Oxidative stress and inflammation generated DNA damage by exposure to air pollution particles. *Mutat Res Rev Mutat Res*, 762:133–166. Doi:10.1016/j.mrrev.2014.09.001.

- Maloney B., Sambamurti K., Zawia N., Lahiri D.K. (2012). Applying epigenetics to Alzheimer's disease via the latent early-life associated regulation (LEARn) model. *Curr Alzheimer Res*, 9(5):589-99. Doi: 10.2174/156720512800617955.
- Mantecca P., Sancini G., Moschini E., Farina F., Gualtieri M., Rohr A., Miserocchi G., Palestini P., Camatini M. (2009). Lung toxicity induced by intratracheal instillation of size-fractionated tire particles. *Toxicol Lett*, 189(3):206-14. Doi: 10.1016/j.toxlet.2009.05.023.
- Mantecca P., Farina F., Moschini E., Gallinotti D., Gualtieri M., Rohr A., Sancini G., Palestini P., Camatini M. (2010). Comparative acute lung inflammation induced by atmospheric PM and size-fractionated tire particles. *Toxicol Lett*, 198(2):244-54. Doi: 10.1016/j.toxlet.2010.07.002.
- Marconi A. (2003). Airborne particulate matter: definitions, health effects, measurement and summary of environmental studies in Rome. Ann Ist Super Sanità, 39(3):329-342.
- Markesbery W.R. (1999). The role of oxidative stress in Alzheimer disease. Arch Neurol, 56(12): 1449-52.
- Matsushima T., Saito Y., Elliott J.I., Iijima-Ando K., Nishimura M., Kimura N., Hata S., Yamamoto T., Nakaya T., Suzuki T. (2012). Membrane-microdomain localization of amyloid β-precursor protein (APP) C-terminal fragments is regulated by phosphorylation of the cytoplasmic Thr668 residue. *J Biol Chem*, 287(23):19715-24. Doi: 10.1074/jbc.M111.334847.
- Mayer A., Czerwinski J., Wichser A., Ulrich A., Kasper M., Mooney J. (2010). Metal-oxide particles in combustion engine exhaust. *SAE Technical Papers*, 2010-01-0792. Doi: 10.4271/2010-01-0792.
- Mayeux R., Stern Y. (2012). Epidemiology of Alzheimer disease. *Cold Spring Harb Perspect Med*, 2(8). Doi: 10.1101/cshperspect.a006239.
- Mazzarella G., Ferraraccio F., Prati M.V., Annunziata S., Bianco A., Mezzogiorno A., Liguori G., Angelillo I.F., Cazzola M. (2007). Effects of diesel exhaust particles on human lung epithelial cells: an in vitro study. *Respir Med*, 101(6):1155-62. Doi: 10.1016/j.rmed.2006.11.011.
- McMahon M., Itoh K., Yamamoto M., Hayes J.D. (2003). Keap1-dependent proteasomal degradation of transcription factor Nrf2 contributes to the negative regulation of antioxidant response element-driven gene expression. *J Biol Chem*, 278(24):21592–21600. Doi: 10.1074/jbc.M300931200 .
- McWhinney R.D., Badali K., Liggio J., Li S.M., Abbatt J.P. (2013). Filterable redox cycling activity: a comparison between diesel exhaust particles and secondary organic aerosol constituents. *Environ Sci Technol*, 47(7):3362-9. Doi: 10.1021/es304676x.
- Mehta A.J., Zanobetti A., Bind M.C., Kloog I., Koutrakis P., Sparrow D., Vokonas P.S., Schwartz J.D. (2016). Long-term exposure to ambient fine particulate matter and renal function in older men: the VA Normative Aging Study. *Environ Health Perspect*, 124:1353–1360. Doi: 10.1289/ehp.1510269.

- Moreira P.I., Honda K., Liu Q., Aliev G., Oliveira C.R., Santos M.S., Zhu X., Smith M.A., Perry G. (2005). Alzheimer's disease and oxidative stress: The old problem remains unsolved. Curr Med Chem Cent Nerv Syst Agents, 5:51–62. Doi: 10.2174/1568015053202714.
- Morimoto B.H., Koshland D.E. (1990). Induction and expression of long- and short-term neurosecretory potentiation in a neural cell line. *Neuron*, 5(6):875-80. Doi: 10.1016/0896-6273(90)90347-I.
- Mossman B.T., Borm P.J., Castranova V., Costa D.L., Donaldson K., Kleeberger S.R. (2007). Mechanisms of action of inhaled fibers, particles and nanoparticles in lung and cardiovascular diseases. *Part Fibre Toxicol*, 30;4:4. Doi: 10.1186/1743-8977-4-4.
- Naeher L.P., Brauer M., Lipsett M., Zelikoff J.T., Simpson C.D., Koenig J.Q., Smith K.R. (2007). Woodsmoke health effects: a review. *Inhal Toxicol*, 19(1):67-106. Doi: 10.1080/08958370600985875.
- Nebert D.W., Dalton T.P. (2006). The role of cytochrome P450 enzymes in endogenous signalling pathways and environmental carcinogenesis. *Nat Rev Cancer*, 6(12):947–960. Doi: 10.1038/nrc2015.
- Nemmar A., Hoet P.H., Vanquickenborne B., Dinsdale D., Thomeer M., Hoylaerts M.F., Vanbilloen H., Mortelmans L., Nemery B. (2002). Passage of inhaled particles into the blood circulation in humans. *Circulation*, 105(4):411-4. Doi: 10.1161/hc0402.104118.
- Nemmar A., Zia S., Subramaniyan D., Al-Amri I., Al Kindi M.A., Ali B.H. (2012). Interaction of diesel exhaust particles with human, rat and mouse erythrocytes in vitro. *Cell Physiol Biochem*, 29(1-2):163-70. Doi: 10.1159/000337597.
- Nemmar A., Holme J.A., Rosas I., Schwarze P.E., Alfaro-Moreno E. (2013). Recent advances in particulate matter and nanoparticle toxicology: a review of the in vivo and in vitro studies. *Biomed Res Int*, 2013:279371. Doi: 10.1155/2013/279371.
- Nemmar A., Karaca T., Beegam S., Yuvaraju P., Yasin J., Hamadi N.K., Ali B.H. (2016). Prolonged Pulmonary Exposure to Diesel Exhaust Particles Exacerbates Renal Oxidative Stress, Inflammation and DNA Damage in Mice with Adenine-Induced Chronic Renal Failure. *Cell Physiol Biochem*, 38(5):1703-13. Doi: 10.1159/000443109.
- Nguyen T., Nioi P., Pickett C.B. (2009). The Nrf2-antioxidant response element signaling pathway and its activation by oxidative stress. *J Biol Chem*, 284:13291–13295. Doi: 10.1074/jbc.R900010200.
- Nissinen L., Kähäri V.M. (2014). Matrix metalloproteinases in inflammation. *Biochim Biophys Acta*, 1840(8):2571-80. Doi: 10.1016/j.bbagen.2014.03.007.
- Oberdörster G., Utell M.J. (2002). Ultrafine particles in the urban air: to the respiratory tract--and beyond? *Environ Health Perspect*, 110(8): A440–A441.

- Oberdörster G., Sharp Z., Atudorei V., Elder A., Gelein R., Kreyling W., Cox C. (2004). Translocation of inhaled ultrafine particles to the brain. *Inhal Toxicol*, 16(6-7):437-45. Doi: 10.1080/08958370490439597.
- Oberdörster G., Oberdörster E., Oberdörster J. (2005). Nanotoxicology: an emerging discipline evolving from studies of ultrafine particles. *Environ Health Perspect*, 113(7):823-39. Doi: 10.1289/ehp.7339.
- Oppenheim H.A., Lucero J., Guyot A.C., Herbert L.M., McDonald J.D., Mabondzo A., Lund A.K. (2013). Exposure to vehicle emissions results in altered blood brain barrier permeability and expression of matrix metalloproteinases and tight junction proteins in mice. *Part Fibre Toxicol*, 10:62. Doi: 10.1186/1743-8977-10-62.
- Otterbein L.E., Zuckerbraun B.S. (2005). Heme Oxygenase: The Elegant Orchestration of Its Products in Medicine. *NOVA editors*.
- Pająk B., Kania E., Orzechowski A. (2016). Killing Me Softly: Connotations to Unfolded Protein Response and Oxidative Stress in Alzheimer's Disease. *Oxid Med Cell Longev*, 2016:1805304. Doi: 10.1155/2016/1805304.
- Paulin L. and Hansel N. (2016). Particulate air pollution and impaired lung function. Version 1. F1000Res. 5:F1000 Faculty Rev-201. Doi: 10.12688/f1000research.7108.1.
- Pearson J.F., Bachireddy C., Shyamprasad S., Goldfine A.B., Brownstein J.S. (2010). Association between fine particulate matter and diabetes prevalence in the U.S. *Diabetes Care*, 33(10):2196-201. Doi: 10.2337/dc10-0698.
- Perez L., Tobías A., Querol X., Pey J., Alastuey A., Díaz J., Sunyer J. (2012). Saharan dust, particulate matter and cause-specific mortality: a case-crossover study in Barcelona (Spain). *Environ Int*, 48:150-5. Doi: 10.1016/j.envint.2012.07.001.
- Pockley A.G. (2003). Heat shock proteins as regulators of the immune response. *Lancet*, 362(9382):469-76. Doi: 10.1016/S0140-6736(03)14075-5.
- Pourazar J., Mudway I.S., Samet J.M., Helleday R., Blomberg A., Wilson S.J., Frew A.J., Kelly F.J., Sandström T. (2005). Diesel exhaust activates redox-sensitive transcription factors and kinases in human airways. *Am J Physiol Lung Cell Mol Physiol*, 289(5):L724–30. Doi: 10.1152/ajplung.00055.2005.
- Rhead M.M., Hardy S.A. (2003). The sources of polycyclic aromatic compounds in diesel engine emissions. *Fuel*, 82(4): 385-393.
- Rizzo A.M., Corsetto P.A., Farina F., Montorfano G., Pani G., Battaglia C., Sancini G., Palestini P. (2014). Repeated intratracheal instillation of PM10 induces lipid reshaping in lung parenchyma and in extra-pulmonary tissues. *PLoS One*, 9(9):e106855. Doi: 10.1371/journal.pone.0106855.

- Rogge W.F., Hildemann L.M., Mazurek M., Cass G.R., Simoneit B.R.T. (1998). Sources of fine organic aerosol. 9. Pine, oak and synthetic log combustion in residential fireplaces. *Environ Sci Technol*, 32(1):13–22. Doi: 10.1021/es960930b.
- Rubio-Perez J.M., Morillas-Ruiz J.M. (2012). A review: inflammatory process in Alzheimer's disease, role of cytokines. *ScientificWorldJournal*, 2012:756357. Doi: 10.1100/2012/756357.
- Sagare A.P., Bell R.D., Zlokovic B.V. (2012). Neurovascular dysfunction and faulty amyloid β-peptide clearance in Alzheimer disease. *Cold Spring Harb Perspect Med*, 2(10). pii: a011452. Doi: 10.1101/cshperspect.a011452.
- Samoli E., Peng R., Ramsay T., Pipikou M., Touloumi G., Dominici F., Burnett R., Cohen A., Krewski D., Samet J., Katsouyanni K. (2008). Acute effects of ambient particulate matter on mortality in Europe and North America: results from the APHENA study. *Environ Health Perspect*, 116(11):1480-6. Doi: 10.1289/ehp.11345.
- Sathya M., Premkumar P., Karthick C., Moorthi P., Jayachandran K.S., Anusuyadevi M. (2012). BACE1 in Alzheimer's disease. Clin Chim Acta, 414:171-8. Doi: 10.1016/j.cca.2012.08.013.
- Saunders V., Breysse P., Clark J., Sproles A., Davila M., Wills-Karp M. (2010). Particulate matter-induced airway hyperresponsiveness is lymphocyte dependent. *Environ Health Perspect,* 118(5):640-6. Doi: 10.1289/ehp.0901461.
- Schipper H.M. (2004). Heme oxygenase-1: transducer of pathological brain iron sequestration under oxidative stress. *Ann N Y Acad Sci*, 1012:84-93. Doi: 10.1196/annals.1306.007.
- Schmid O., Möller W., Semmler-Behnke M., Ferron G.A., Karg E., Lipka J., Schulz H., Kreyling W.G., Stoeger T. (2009). Dosimetry and toxicology of inhaled ultrafine particles. *Biomarkers*, 14 Suppl 1:67-73. Doi: 10.1080/13547500902965617.
- Seaton A., Donaldson K. (2005). Nanoscience, nanotoxicology, and the need to think small. *Lancet*, 365(9463):923-4. Doi: 10.1016/S0140-6736(05)71061-8.
- Seagrave J., McDonald J.D., Reed M.D., Seilkop S.K., Mauderly J.L. (2005). Responses to subchronic inhalation of low concentrations of diesel exhaust and hardwood smoke measured in rat bronchoalveolar lavage fluid. *Inhal Toxicol*, 17, 657e670.
- Shimada T., Sugie A., Shindo M., Nakajima T., Azuma E., Hashimoto M., Inoue K. (2003). Tissue-specific induction of cytochromes P450 1A1 and 1B1 by polycyclic aromatic hydrocarbons and polychlorinated biphenyls in engineered C57BL/6J mice of arylhydrocarbon receptor gene. *Toxicol Appl Pharmacol*, 187(1):1-10. Doi: 10.1016/S0041-008X(02)00035-2.
- Sigsgaard T., Forsberg B., Annesi-Maesano I., Blomberg A., Bølling A., Boman C., Bønløkke J., Brauer M., Bruce N., Héroux M.E., Hirvonen M.R., Kelly F., Künzli N., Lundbäck B., Moshammer H., Noonan C., Pagels J., Sallsten G., Sculier J.P., Brunekreef B. (2015). Health impacts of anthropogenic biomass burning in the developed world. Eur Respir J, 46(6):1577-88. Doi: 10.1183/13993003.01865-2014.

- Simoneit B.R.T., Schauer J.J., Nolte C.G., Oros D.R., Elias V.O., Fraser M.P., Rogge W.F., Cass G.R. (1998). Levoglucosan, a tracer for cellulose in biomass burning and atmospheric particles. *Atmos Environ*, 33(2):173–182. Doi: 10.1016/S1352-2310(98)00145-9.
- Singh B.R., Onkar S. (2006). Study of Compressed Air as an alternative to fossil fuel for Automobile Engines. *International Conference on Challenges and Strategies for Sustainable Energy and Environment-held on*, 179-191.
- Sobolewski C., Cerella C., Dicato M., Ghibelli L., Diederich M. (2010). The role of cyclooxygenase-2 in cell proliferation and cell death in human malignancies. *Int J Cell Biol*, 2010:215158. Doi: 10.1155/2010/215158.
- Sørensen M., Hjortebjerg D., Eriksen K.T., Ketzel M., Tjønneland A., Overvad K., Raaschou-Nielsen O. (2015). Exposure to long-term air pollution and road traffic noise in relation to cholesterol: A cross-sectional study. *Environ Int*, 85:238-43. Doi: 10.1016/j.envint.2015.09.021.
- Spijker Sabine (2011). Dissection of Rodent Brain Regions. *Ka Wan Li (ed.), Neuroproteomics, Neuromethods*, vol. 57. Doi: 10.1007/978-1-61779-111-6_2.
- Srimuruganandam B., Shiva Nagendra S.M. (2012). Source characterization of PM10 and PM2.5 mass using a chemical mass balance model at urban roadside. *Sci Total Environ*, 433:8-19. Doi: 10.1016/j.scitotenv.2012.05.082.
- Steiner S., Bisig C., Petri-Fink A., Rothen-Rutishauser B. (2016). Diesel exhaust: current knowledge of adverse effects and underlying cellular mechanisms. *Arch Toxicol*, 90(7):1541-53. Doi: 10.1007/s00204-016-1736-5.
- Stockley J.H., O'Neill C. (2008). Understanding BACE1: essential protease for amyloid-β production in Alzheimer's disease. *Cellular and molecular life sciences*, 65(20): 3265-3289. Doi: 10.1007/s00018-008-8271-3.
- Sun Q., Hong X., Wold L.E. (2010). Cardiovascular effects of ambient particulate air pollution exposure. *Circulation*, 121(25):2755-65. Doi: 10.1161/CIRCULATIONAHA.109.893461.
- Suwa T., Hogg J.C., Quinlan K.B., Ohgami A., Vincent R., van Eeden S.F. (2002). Particulate air pollution induces progression of atherosclerosis. *J Am Coll Cardiol*, 39(6):935-42. Doi: 10.1016/S0735-1097(02)01715-1.
- Sydbom A., Blomberg A., Parnia S., Stenfors N., Sandström T., Dahlén S.E. (2001). Health effects of diesel exhaust emissions. *Eur Respir J*, 17(4):733-46.
- Takenaka S., Karg E., Roth C., Schulz H., Ziesenis A., Heinzmann U., Schramel P., Heyder J. (2001). Pulmonary and systemic distribution of inhaled ultrafine silver particles in rats. Environ Health Perspect, 109 Suppl 4:547-51.
- Terzano C., Di Stefano F., Conti V., Graziani E., Petroianni A. (2010). Air pollution ultrafine particles: toxicity beyond the lung. *Eur Rev Med Pharmacol Sci*, 14(10), 809-821.

- Thériault P., ElAli A., Rivest S. (2015). The dynamics of monocytes and microglia in Alzheimer's disease. *Alzheimers Res Ther*, 7(1): 41. Doi: 10.1186/s13195-015-0125-2.
- Thomson E.M., Pal S., Guénette J., Wade M.G., Atlas E., Holloway A.C., Williams A., Vincent R. (2016). Ozone Inhalation Provokes Glucocorticoid-Dependent and -Independent Effects on Inflammatory and Metabolic Pathways. *Toxicol Sci*, 152(1):17-28. Doi: 10.1093/toxsci/kfw061.
- Tracey K.J. (2009). Reflex control of immunity. *Nat Rev Immunol*, 9(6):418-28. Doi: 10.1038/nri2566.
- van Berlo D., Albrecht C., Knaapen A.M., Cassee F.R., Gerlofs-Nijland M.E., Kooter I.M., Palomero-Gallagher N., Bidmon H.J., van Schooten F.J., Krutmann J., Schins R.P. (2010). Comparative evaluation of the effects of short-term inhalation exposure to diesel engine exhaust on rat lung and brain. *Arch Toxicol*, 84(7):553-62. Doi: 10.1007/s00204-010-0551-7.
- Vetrivel K.S., Meckler X., Chen Y., Nguyen P.D., Seidah N.G., Vassar R., Wong P.C., Fukata M., Kounnas M.Z., Thinakaran G. (2009). Alzheimer disease Abeta production in the absence of S-palmitoylation-dependent targeting of BACE1 to lipid rafts. J Biol Chem, 284(6):3793-803. Doi: 10.1074/jbc.M808920200.
- Vineis P., Husgafvel-Pursiainen K. (2005). Air pollution and cancer: biomarker studies in human populations. *Carcinogenesis*, 26:1846–55. Doi:10.1093/carcin/bgi216.
- Volpe J.J., Fujimoto K., Marasa J.C., Agrawal H.C. (1975). Relation of C-6 glial cells in culture to myelin. *Biochem J*, 152(3):701-703. Doi: 10.1042/bj1520701.
- Wallenborn J.G., McGee J.K., Schladweiler M.C., Ledbetter A.D., Kodavanti U.P. (2007). Systemic translocation of particulate matter-associated metals following a single intratracheal instillation in rats. *Toxicol Sci*, 98(1):231-9. Doi: 10.1093/toxsci/kfm088.
- Wang B., Feng W.Y., Wang M., Shi J.W., Zhang F., Ouyang H., Zhao Y.L., Chai Z.F., Huang Y.Y., Xie Y.N., Wang H.F., Wang J. (2007). Transport of intranasally instilled fine Fe2O3 particles into the brain: micro-distribution, chemical states, and histopathological observation. *Biol Trace Elem Res*, 118(3):233-43. Doi: 10.1007/s12011-007-0028-6.
- Wellenius G.A., Bateson T.F., Mittleman M.A., Schwartz J. (2005). Particulate air pollution and the rate of hospitalization for congestive heart failure among medicare beneficiaries in Pittsburgh, Pennsylvania. *Am J Epidemiol,* 161(11): 1030–1036. Doi: 10.1093/aje/kwi135.
- Wegesser T.C., Franzi L.M., Mitloehner F.M., Eiguren-Fernandez A., Last J.A. (2010). Lung antioxidant and cytokine responses to coarse and fine particulate matter from the great California wildfires of 2008. *Inhal Toxicol*, 22(7):561–570. Doi: 10.3109/08958370903571849.
- World Health Organization (WHO). (1999). Hazard prevention and control in the work Environment: airborne dust.

- World Health Organization (WHO). (2013). Health effects of particulate matter. Policy implications for countries in Eastern Europe, Caucasus and central Asia. WHO Regional Office for Europe, Copenhagen.
- World Health Organization (WHO). (2015). Air quality in Europe — 2015 report. ISBN: 978-92-9213-701-4 702-1.
- Winterbourn C.C. (1995). Toxicity of iron and hydrogen peroxide: the Fenton reaction. *Toxicol Lett*, 82-83:969-74. Doi: 10.1016/0378-4274(95)03532-X.
- Xie L., Law B.K., Chytil A.M., Brown K.A., Aakre M.E., Moses H.L. (2004). Activation of the Erk pathway is required for TGF-beta1-induced EMT in vitro. *Neoplasia*, 6(5), 603–610. Doi:10.1593/neo.04241.
- Xu X., Wang G., Chen N., Lu T., Nie S., Xu G., Ping Zhang P., Luo Y, Wang Y., Wang X., Schwartz J., Geng J., Hou F.F. (2016). Long-Term Exposure to Air Pollution and Increased Risk of Membranous Nephropathy in China. *Journal of the American Society of Nephrology*, ASN-2016010093. Doi: 10.1681/ASN.2016010093.
- Yang X., Sun G.Y., Eckert G.P., Lee J.C. (2014). Cellular membrane fluidity in amyloid precursor protein processing. *Mol Neurobiol*, 50(1):119-29. Doi: 10.1007/s12035-014-8652-6.
- Yang L.G., Song Z.X., Yin H., Wang Y.Y., Shu G.F., Lu H.X., Wang S.K., Sun G.J. (2016). Low n-6/n-3 PUFA Ratio Improves Lipid Metabolism, Inflammation, Oxidative Stress and Endothelial Function in Rats Using Plant Oils as n-3 Fatty Acid Source. *Lipids*, 51(1):49-59. Doi: 10.1007/s11745-015-4091-z.
- Yim S., Oh M., Choi S.M., Park H. (2004). Inhibition of the MEK-1/p42 MAP kinase reduces aryl hydrocarbon receptor-DNA interactions. *Biochem Biophys Res Commun*, 322(1):9–16. Doi: 10.1016/j.bbrc.2004.07.072
- Zhang Z., Kleinstreuer C., Kim C.S. (2001). Effects of curved inlet tubes on air flow and particle deposition in bifurcating lung models. *J Biomech,* 34:659–69. Doi: 10.1016/S0021-9290(00)00233-5.
- Zhang M., Song Y., Cai X., Zhou J. (2008). Economic assessment of the health effects related to particulate matter pollution in 111 Chinese cities by using economic burden of disease analysis. *J Environ Manag*, 88(4):947–54. Doi:10.1016/j.jenvman.2007.04.019.
- Zheng M., Cass G.R., Ke L., Wang F., Schauer J.J., Edgerton E.S., Russell A.G. (2007). Source apportionment of daily fine particulate matter at Jefferson Street, Atlanta, GA, during summer and winter. *J Air Waste Manag Assoc*, 57(2):228-42. Doi: 10.1080/10473289.2007.10465322.
- Zhou W., Qing H., Tong Y., Song W. (2004). BACE1 gene expression and protein degradation. Ann NY Acad Sci, 1035: 49-67. Doi: 10.1196/annals.1332.004.

Toxicology Letters 250 (2016) 57–65

Contents lists available at ScienceDirect

Toxicology Letters

journal homepage: www.elsevier.com/locate/toxlet

Involvement of MEK-ERK1-2 pathway in the anti-oxidant response in C6 glioma cells after diesel exhaust particles exposure

Francesca Farina[a,b,1,*], Chiara Milani[a,b,1], Laura Botto[a,b], Elena Lonati[a,b], Alessandra Bulbarelli[a,b], Paola Palestini[a,b]

[a] Department of Medicine and Surgery, Polaris Centre, University of Milano-Bicocca, Monza, Italy
[b] NeuroMi, Milan Center of Neuroscience, Department of Neurology and Neuroscience, University of Milano-Bicocca, San Gerardo Hospital, Monza, Italy

HIGHLIGHTS

- DEP induces oxidative stress in C6glioma cells.
- C6glioma cells have an anti-oxidant strategy in order to regulate oxidative stress.
- The anti-oxidant strategy relies on the activation of MEK-ERK-1-2 pathway.

ARTICLE INFO

Article history:
Received 17 February 2016
Received in revised form 5 April 2016
Accepted 7 April 2016
Available online xxx

Keywords:
Diesel exhaust particles
Oxidative stress
ERK1-2
Nrf2
HO-1
Anti-oxidant proteins

ABSTRACT

Ultrafine particles translocate to the central nervous system and activate oxidative stress-related pathways. The transcription factor Nrf2 activation by ERK1-2 has been suggested as a key regulator of cellular response to oxidative stress.

C6 glioma cells have been treated with different doses of diesel exhaust particles (25 μg/ml, DEP25, and 50 μg/ml, DEP50), for different times. Cells have been screened for oxidative stress and inflammatory markers, and for the activation of the MEK-ERK1-2 pathway. The same markers have been examined after inhibition of MEK, the kinase upstream to ERK1-2.

3 h and 24 h of DEP25 and DEP50 induced a significant increase in HO-1 levels. After 24 h, DEP25 and DEP50 induced an increase in HO-1 and Cyp1b1 levels, while increase in OGG1 level was observed only with DEP25.

After 5 h of treatment with DEP25, ERK1-2 resulted phosphorylated, concomitantly with a significant increase in HO-1 levels, no changes in iNOS levels, and decreased levels of anti-oxidant enzymes. After treatment with MEK inhibitor U0126, ERK1-2 showed no activation, with a consequent decrease in Nrf2, no increase in HO-1 and a significant increase of iNOS. MEK inhibitor is able to deplete anti-oxidant enzymes.

In conclusion, the MEK-ERK1-2 pathway is involved in regulating the anti-oxidant strategies to compensate the oxidative status induced by DEP treatment.

Abbreviations: UFPs, ultrafine particles; CNS, central nervous system; DEP, diesel exhaust particles; PAHs, polycyclic aromatic hydrocarbons; ROS, reactive oxygen species; Nrf2, nuclear factor (erythroid-derived 2)-like 2; ARE, antioxidant responsive elements; HO-1, heme oxygenase-1; GST, glutathione-S-transferase; SOD3, superoxide dismutase 3; Keap1, Kelch-like ECH-associated protein 1; ERK1-2, extracellular signal-regulated kinase 1-2; PM, particulate matter; MAPKs, mitogen associated protein kinases; iNOS, inducible nitric oxide kinase; OGG1, 8-oxoguanine DNA Glycosylase; Cyp1a1, cytochrome 1a1; Cyp1b1, cytochrome 1b1; Hsp70, heat shock protein 70; VEGF, vascular endothelial grow factor; IL1α, interleukin 1 α; IL1β, interleukin 1 β; IL6, interleukin 6; TNFα, tumor necrosis factor α; MEK, MAPK-ERK kinase; CM, complete medium; SFM, serum free medium; TAC, total antioxidant capacity; GSH, reduced glutathione; AhR, aryl hydrocarbon receptor; Arnt, AhR nuclear translocaor; AP1, activator protein 1; NFkB, nuclear factor kappa B.

* Corresponding author.
E-mail address: francesca.farina@hotmail.it (F. Farina).

[1] Both authors contributed equally to the work.

http://dx.doi.org/10.1016/j.toxlet.2016.04.008
0378-4274/

1. Introduction

Diesel exhaust is a major component of air pollution in urban areas and in the last years emerging evidences have linked Diesel Exhaust Particles (DEP) to human health both in ambient and occupational exposure conditions (Pronk et al., 2009; Hesterberg et al., 2010).

It is well known that the combustion of diesel fuel is able to generate mostly particulate matter of nano dimension (UFPs, with aerodynamic diameter $\leq$100 nm) (Charron and Harrison, 2005), characterized by high surface area per mass (Oberdorster, 2001). Sustained exposure to significant levels of airborne UFPs may result in the direct translocation of these pollutants to the CNS where they could induce neuropathology through the activation of a variety of pathways and mechanisms (Genc et al., 2012). Even though the translocation rate of particles from their site of entry to secondary organs might be rather low, continuous or chronic exposure to UFPs may result in a significant accumulation in brain areas as secondary target organ (Oberdorster et al., 2009). *In-vivo* studies demonstrated that CNS can be target of air pollutants toxic effects, while *in-vitro* studies (neuron and microglia cultures exposed to concentrated ambient air particles or DEP) proposed some possible mechanisms of toxicity (Block and Calderón-Garcidueñas, 2009; Genc et al., 2012).

Despite mechanisms responsible for air pollution-induced toxicity in the CNS are still poorly understood, experimental studies have recently suggested that oxidative stress could be involved (Genc et al., 2012). Oxidative stress develops when there is an imbalance between the production of reactive oxygen species (ROS) and the availability of anti-oxidant defenses (Møller et al., 2010).

The huge surface area of UFPs allows the presence of large amounts of toxic air pollutant adsorbed on particles surface (Oberdorster, 2001). In particular, chemical analysis revealed that the typical DEP composition consists of a mixture of inorganic and organic compounds (PAHs and PAH-derivatives, such as quinones, carboxyl- and nitro-PAHs) adsorbed on a carbonaceous nucleus (Totlandsdal et al., 2012). This sustains the observation reported in a growing number of studies, that DEP may exert its toxicity by inducing oxidative stress (Cheung et al., 2010; Ristovski et al., 2012) depending on its aromatic fraction, enriched in PAHs, and polar fraction, enriched in quinones (Li et al., 2000). In addition, it has been suggested that ROS can be generated directly on the surface area of DEP via redox processes or indirectly through DEP/cells interactions (Li et al., 2010).

As ROS are harmful to cellular structure and activity, cells respond triggering various mechanisms, encoding and activating proteins with antioxidant and cytoprotective activities (Stewart et al., 2003). In particular, Nrf2 appears to be a key regulator of the cellular response to oxidative stress: Nrf2 controls both the inducible and constitutive gene expression mediated by ARE, cis-acting elements found in the promoter of genes encoding phase II antioxidant enzymes, such as HO-1, NAD(P)H-quinone oxidoreductase, GST, SOD3, glucuronosyltransferase (Li et al., 2004; Nguyen et al., 2009). Nrf2 has a short half-life; in normal conditions, in the cytoplasm Keap1 promotes constitutive ubiquitination of Nrf2 addressing it to the proteolytic degradation catalyzed by the 26 S proteasome (Nguyen et al., 2009; Itoh et al., 1997; Stewart et al., 2003). Oxidants could interfere with Nrf2/Keap1 interaction and subsequent degradation by proteasome, resulting in Nrf2 nuclear localization, dimerization with other transcription factors, and eventually target gene activation (Itoh et al., 1997; Kwak et al., 2002). Moreover, it has been suggested that the phosphorylation of Nrf2 triggered by ERK1-2 may facilitate Nrf2 release from Keap1 and translocation into the nucleus (Chan et al., 2001; Kwak et al., 2002; Li et al., 2007).

Genes from Nrf2-mediated oxidative stress response pathway resulted upregulated in airway epithelial cells after exposure to PM (Huang et al., 2011) and in elderly subject with cardiovascular disease (Wittkopp et al., 2015). Using *in-vivo* models, we have previously shown a large increase of HO-1 expression in different organs (lungs, heart and CNS), thus indicating oxidative status elicited by the intratracheal instillation of different particles (PM10, PM2.5, PM1, Tire Debris) (Mantecca et al., 2010; Farina et al., 2011, 2013a,b; Sancini et al., 2014). Notably, in biopsies of lung tissues from human volunteers exposed to DEP, activation of MAPKs has been detected (Pourazar et al., 2005). As ERK1-2 could be involved in Nrf2 activation (Chan et al., 2001; Kwak et al., 2002; Li et al., 2007), and HO-1 is one of Nrf2 target genes (Li et al., 2004; Nguyen et al., 2009), we can hypothesize that MAPKs transduction pathway and Nrf2-mediate oxidative stress response may be important also in CNS exposed to pro-oxidant particles, such as DEP.

On the basis of these assumptions, we assessed the effects of DEP rich in PAHs in *in vitro* experiments using C6 glioma cells, a cell line with properties of both astrocytes (Benda et al., 1968) and oligodendrocytes (Volpe et al., 1975) widely used in neurobiological research. Moreover, this cell line has been already used to test oxidant toxicity of various components (Han et al., 2012), because it results sensitive to oxidative stress (Goncharov et al., 2005).

Therefore, in C6 glioma cells exposed to DEP we analysed markers involved in: I) oxidative stress-related response (HO-1, iNOS, OGG1, VEGF), II) PAHs metabolism and generation of further oxidative stress (Cyp1b1), and III) inflammation (Hsp70, TNFα, IL1α, IL1β, IL6). Finally, the involvement of MAPKs and Nrf2 regulation on the protective response against DEP-induced oxidative stress has been studied.

2. Materials and methods

2.1. Cell culture

Rat C6 glioma cells were purchased from the American Type Centre Collection (ATCC, Manassas, VA, USA). Cells were grown on tissue culture flasks (Pbi International) and maintained at 37 °C, 5% CO_2 in Dulbecco's modified Eagle's medium (DMEM, Euroclone, MI, Italy) containing 10% fetal bovine serum (Euroclone, MI, Italy), 1% penicillin and streptomycin (Euroclone, MI, Italy) and 1% L-glutamine (Euroclone, MI, Italy). Cells were plated on 24 multiwell plates, 20,000 cells per well, and treated at 80% confluence.

2.2. DEP

Cells were treated with DEP SRM1650b (Standard Reference Material, National Institute of Standards and Technology, USA), a diesel particulate with mean aerodynamic diameter of 0.18 μm reach in PAHs (National Institute of Standard and Technologies; www-.nist.gov/srmors/certificates/1650b.pdf?CFID=7862989&CFTOKEN=2c41aaa9d4941743-95BE052A-B7AF-FEC3-6800359C67A97E13), used in literature as a model of ultrafine particulate matter (Levesque et al., 2011). Diesel particles were suspended at different concentrations (25 μg/ml and 50 μg/ml) in culture medium supplemented with 0.00005% Tween-20 (Sigma-Aldrich, Saint Louis, MO, USA) to allow proper particles suspension.

Based on *in vivo* models of near road and occupational exposure (0.5 mg/m^3 and 2 mg/m^3), Levesque and colleagues (Levesque et al., 2011) calculated that an *in vitro* concentration of about 5–50 μg/ml of nanometer-sized particles falls within the current estimates of what may reach the brain. Thought the precise amount of PM reaching the brain is currently unknown, studies have demonstrated that 0.01–0.001% of inhaled nanometer-sized iridium and carbon particulate remain in the brain 24 h after

exposure (Kreyling et al., 2009). DEP concentrations used in our work are in this range.

Immediately before treatment, DEP suspensions have been sonicated for 5 min by means of Bransonic® (Ultrasonic Cleaner Branson 2510), to obtain a proper particles dispersion; Dynamic Light Scattering (Brookhaven Instruments Corporation) analysis confirmed particles dimension measured by the manufacturer.

2.3. Treatments with DEP and MEK inhibition

C6 glioma cells were treated with DEP at different concentrations for 3 h and 24 h; in parallel, control cells were treated with culture medium supplemented with 0.00005% Tween-20. At the end of the treatments, culture medium and cell lysates have been collected for following biochemical assays.

After testing ERK1-2 activation at different times of DEP treatments (30 min, 1 h, 2 h, 3 h, 4 h, 5 h, 6 h, 7 h, 8 h, 12 h, 18 h and 24 h; data not shown), in selected experiments cells have been treated with DEP 25 μg/ml in presence of the selective non-competitive MEK inhibitor U0126 (Lind et al., 2006) for 5 h; in parallel, we always considered respective controls.

Briefly, after a wash with PBS1X, cells have been pre-treated with complete medium, serum free medium or serum free medium + U0126 (U0126 from a 100 mM solution in DMSO, final concentration 10 μM; Lind et al., 2006) for 30 min (Xie et al., 2004). Then, we treated cells with DEP (final concentration 25 μg/ml) suspended in complete medium supplemented with 0.00005% Tween-20 (CM + DEP25), in serum free medium supplemented with 0.00005% Tween-20 (SFM + DEP25), or in serum free medium added with U0126 and 0.00005% Tween-20 (SFM + U + DEP25); in parallel, we always considered respective controls in complete medium supplemented with 0.00005% Tween-20 (CM), in serum free medium supplemented with 0.00005% Tween-20 (SFM) and in serum free medium added with U0126 and 0.00005% Tween-20 (SFM + U). At the end of the treatments (5 h), culture medium and cell lysates have been collected for following biochemical assays.

2.4. Cell viability assay

After different treatments times, cell viability has been evaluated by means of PrestoBlue® assay (Life Technologies, MB, Italy). Briefly, this assay consists in a cell permeable resazurin-based solution that, modified by the reducing power of cells with active mitochondrial metabolism, turns red in color. PrestoBlue® was administrated to cells according to the manufacturer's protocol and incubated for 1 h at 37 °C. The absorbance was measured with FLUOstar Omega (BMG Labtech) multidetection microplate reader at wavelength of 570 nm and at reference wavelength of 600 nm.

2.5. SDS-PAGE electrophoresis and immunoblotting

Samples were obtained after lysis with denaturizing buffer (2% SDS lysis, 50 mM Tris-HCl, pH 6.8 plus protease inhibitor cocktail and phosphatase inhibitors). After total protein amount evaluation by means of Bicinchoninic acid assay, 30 μg of each sample were subjected to SDS-polyacrylamide gel electrophoresis (PAGE). After SDS-PAGE, electrophoresis samples were transferred to a nitrocellulose membrane (Amercontrol, GE Healthcare Europe GmbH, Milano, Italy) and proteins revealed by Ponceau staining (Sigma Chemical Co., Milano, Italy). After blocking in TBS-Tween20/milk 5%, blots were incubated for 2 h with the primary antibody diluted in TBS-Tween20/milk 5% and tested for Cyp1b1, HO-1, Hsp70, iNOS, OGG1 (anti-Cyp1b1 1:200, anti-HO-1 1:200, anti-Hsp70 1:200, anti-iNOS 1:200, anti-OGG1 1:200, all by Santa Cruz Biotechnology, CA, USA). In selected experiments cells have been tested also for pERK1-2 in TBS-Tween20/BSA 1% (anti-phospho T202 + Y204 ERK1-2 1:500, Abcam; anti-ERK1-2 1:200, Santa Cruz Biotechnology) and for Nrf2 (anti-Nrf2 1:500, R&D Systems). Proteins were detected by ECL with the Super Signal detection kit (Pierce). Immunoblot bands were analyzed and semi-quantified by ImageQuant™ LAS 4000 (GE Healthcare Life Sciences). All the data have been normalized to β-actin (1:1500, Sigma) and each protein in DEP-treated group has been normalized to respective control group.

2.6. TAC

TAC has been evaluated in experiments performed to test ERK1-2 activation after 5 h of DEP, according to manufacturer's instructions (TAC Colorimetric Assay Kit, BioVision). Briefly, after the treatments, cells were removed by scraping, pelleted and re-suspended in 200 μL of cold PBS1X. Cell membranes were disrupted by sonication on ice and cell lysates centrifuged at 4 °C, 10,000*g* for 20 min; supernatant was separated from cell debris and used for TAC analysis. All measurements were normalized to the total protein content evaluated by means of Bicinchoninic acid assay.

2.7. VEGF and cytokine analysis

The analysis of different molecules released in culture medium were performed by ELISA Multiplex assays. Culture medium has been stored at −80 °C until sent to LABOSPACE (Milano, Italy) for ELISA analysis. LABOSPACE evaluated VEGF, IL1α, IL1β, IL6 and TNFα by means of Fluorokine MAP platform Luminex.

2.8. Statistical analysis

For each biochemical parameter measured in different experimental groups, the means (±standard error, s.e.) were calculated. Statistical differences were tested by one-way ANOVA followed by Bonferroni *post-hoc* comparison. To test the tendency toward increase or decrease in the different parameters, linear regressions were carried out. Statistical differences were considered to be significant at the 95% level ($p < 0.05$).

3. Results

3.1. Cell viability

PrestoBlue® assay did not evidence any significant variation comparing to control in cell viability, assessed by mitochondrial metabolism, after 3 h or 24 h of DEP treatment, for the considered concentrations (25 μg/ml and 50 μg/ml). In C6 glioma cells treated with DEP 100 μg/ml for 24 h, a significant decrease of 32.3% ± 6.5% (standard error, s.e.) in cell viability, comparing to control, was observed. Therefore, in our cellular model, doses of 25 μg/ml and 50 μg/ml resulted useful to study the mechanisms induced by DEP treatment without resulting lethal (Fig. 1).

3.2. Total cell homogenates proteins

After 3 h of treatment with the previously selected DEP concentrations (25 μg/ml, DEP25; 50 μg/ml, DEP50), a significant increase was observed for HO-1 levels (+118% after DEP25 treatment, +147% after DEP50 treatment), comparing to control, while Cyp1b1, Hsp70, iNOS and OGG1 showed no significant variations (Fig. 2A and C). After 24 h, the treatment with DEP25 induced a significant increase of Cyp1b1 (+211%), HO-1 (+177%) and OGG1 (+33%) proteins level compared to control,

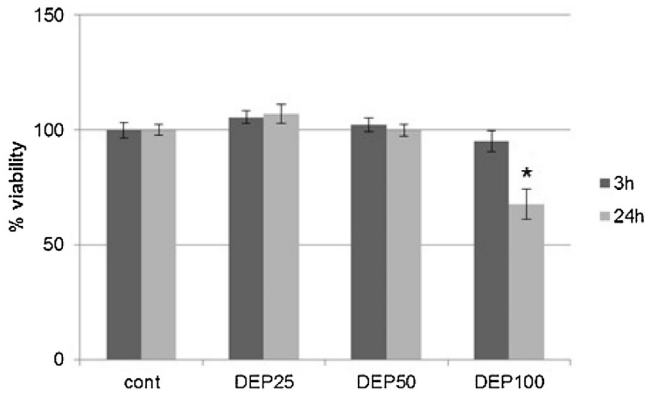

Fig. 1. Cell viability.
Cell viability has been tested after DEP25 (25 μg/ml), DEP50 (50 μg/ml) and DEP100 (100 μg/ml) treatment of C6 glioma cells for 3 h or 24 h. The data are expressed as mean ± s.e. (n = 7); statistical differences were tested accordingly by One-way ANOVA followed by Bonferroni post-hoc comparison. * $p < 0.05$ *vs.* respective control.

while the treatment with DEP50 significantly increased Cyp1b1 (+423%) and HO-1 (+475%) protein expression levels compared to DEP untreated cells (Fig. 2B and D).

3.3. VEGF and cytokines in cell culture medium

Concerning VEGF (Table 1), we observed a significant release after 3 h and 24 h of DEP25 (+59% and +106%, respectively) and DEP50 (+55% and +366% respectively) treatments, comparing to respective control. All the other examined cytokines resulted not detectable (IL1β and IL6) or not differently released (IL1α and TNFα) in treated cells comparing to control (Table 1).

3.4. DEP effects after MEK inhibition

The dose of 25 μg/ml has been chosen for further experiments, as it is the dose responsible of major significant changes both at 3 h (HO-1) and 24 h (Cyp1b1, HO-1 and OGG1). In order to test the activation of the MAPKs pathway and its possible involvement in the DEP-induced response, time course experiments have been carried out with the selected DEP dose (DEP25 treatment for 30 min, 1 h, 2 h, 3 h, 4 h, 5 h, 6 h, 7 h, 8 h, 12 h, 18 h and 24 h; data not shown); we observed an increase in ERK1-2 activation, demonstrated by the significant increase in p-ERK1-2/ERK1-2, at 2 h and 5 h. In order to block the ERK1-2 activation and to identify a possible mechanisms related to this signal pathway, cells have been treated with DEP 25 μg/ml in presence of a MEK inhibitor (U0126) for 5 h. MEK is the kinase upstream to ERK1-2, and its phosphorylation is inhibited by U0126, thus blocking also the downstream activation of ERK1-2. Respective controls have been

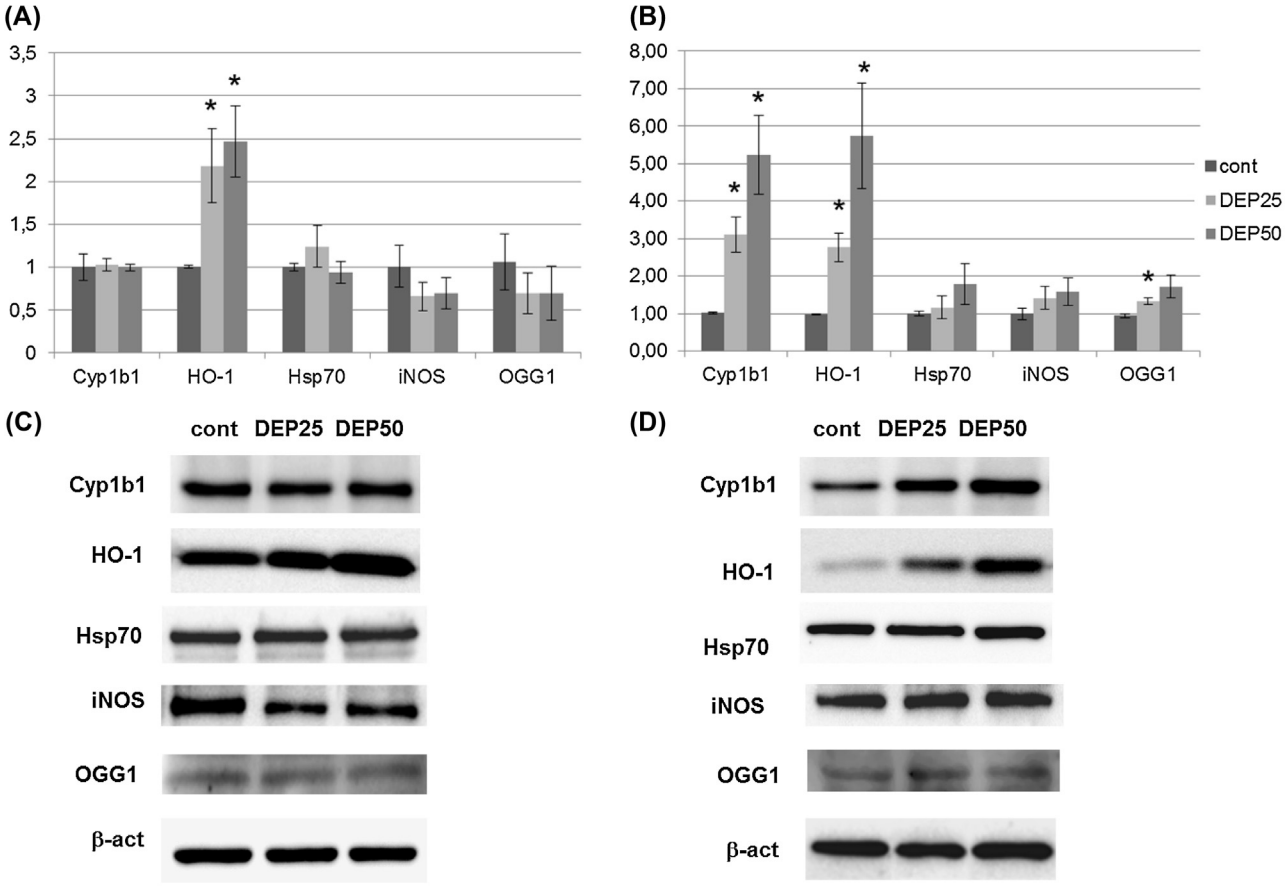

Fig. 2. Protein analysis after 3 h and 24 h of DEP treatment.
Immunoblotting protein analysis of C6 glioma cells treated for 3 h (A) and for 24 h (B) with DEP25 (25 μg/ml) and DEP50 (50 μg/ml). Proteins have been normalized for the corresponding β-actin signal in each lane, and each protein obtained from C6 glioma cells after DEP25 or DEP50 treatment has been normalized onto respective control. The data are expressed as mean ± s.e. (n = 3); statistical differences were tested accordingly by One-way ANOVA followed by Bonferroni post-hoc comparison. * $p < 0.05$ *vs.* respective control.
Representative immunoblottings images displaying proteins obtained from C6 glioma cells treated for 3 h (C) and for 24 h (D) with DEP25 (25 μg/ml) and DEP50 (50 μg/ml).

Table 1
VEGF and cytokines analysis.

	3 h			24 h		
	cont	DEP25	DEP50	cont	DEP25	DEP50
VEGF (pg/mL)	7.34 ± 0.55	11.67 ± 1.64*	11.43 ± 0.77*	10.03 ± 1.33	20.67 ± 1.64*	46.78 ± 3.09*
IL1α (pg/mL)	10.43 ± 1.35	10.81 ± 0.85	12.34 ± 1.28	9.54 ± 1.62	7.13 ± 1.49	8.02 ± 1.18
IL1β (pg/mL)	n.d.	n.d.	n.d.	n.d.	n.d.	n.d.
IL6 (pg/mL)	n.d.	n.d.	n.d.	n.d.	n.d.	n.d.
TNFα (pg/mL)	23.32 ± 2.72	29.6 ± 2.4	30.51 ± 2.57	29.59 ± 1.62	25.07 ± 1.82	24.22 ± 2.87

Analysis of VEGF and cytokine release in cell culture medium obtained from C6 glioma cells treated with DEP25 (25 μg/ml) and DEP50 (50 μg/ml) for 3 h or 24 h. The data are expressed as mean ± s.e. (n = 7); statistical differences were tested accordingly by One-way ANOVA followed by Bonferroni post-hoc comparison. n.d. = not detectable.
* $p < 0.05$ vs. respective control.

constantly considered. None of these treatments was able to induce any variation in cell metabolism (data not shown).

After 5 h of treatment, cells in complete medium + DEP25 (CM + DEP25) displayed a significant phosphorylation of ERK1-2 (+34,3%), comparing to respective control (Fig. 3A and B). It is worth to note a slight increase of Nrf2 level in CM + DEP25, since it has biological consequences: in fact, at 5 h, we observed a significant increase in HO-1 levels in cells in CM + DEP25 (+553%) (Fig. 3A and B). Concerning iNOS levels, in CM + DEP25 no induction has been registered (Fig. 3A and B).

Cells treatment with SFM + DEP25 (Fig. 4A and B) showed a similar trend to those treated in complete medium.

In the cells in serum free medium + U0126 + DEP25 (SFM + U + DEP25), pERK1-2/ERK1-2 was significantly lower comparing to its corresponding control (−59%) (Fig. 5A and B), thus confirming the upstream MEK inhibition by U0126. Consistent with this observation, Nrf2 levels resulted significantly lower (−26%), whereas no increase in HO-1 was registered in cells in SFM + U + DEP25 comparing to respective control (Fig. 5A and B). Concerning iNOS levels, we observed a significant increase in cells in SFM + U + DEP25 comparing to its respective control (+141%) (Fig. 5A and B).

Finally, no change after 5 h treatments was noticed either for Cyp1b, OGG1 or for Hsp70 (data not shown).

3.5. DEP effects on TAC

Finally, we evaluated the effect of MEK inhibition on antioxidant enzymes generation and consume. In cells treated for 5 h with DEP25 in complete medium (CM + DEP25) as well as in serum free medium (SFM + DEP25) we registered a significant decrease in TAC, comparing to respective controls (CM and SFM) (−33.7% and −21.9% respectively); on the contrary, in cells in SFM + U + DEP25 TAC concentration resulted unaltered comparing to respective control (SFM + U) (Fig. 6). However, serum free condition seemed to cause in the cells a decrease in TAC comparing to control in complete medium (CM); finally, U0126 treatment (SFM + U and SFM + U + DEP25) induced a further decrease of TAC comparing to SFM (Fig. 6).

4. Discussion

In the present work, we analyzed the effects of DEP administration on C6 glioma cells and the involvement of MEK-ERK1-2 pathway and Nrf2 activation in a putative anti-oxidant strategy elicited by cells to contrast the oxidative stress induced by DEP treatment.

4.1. DEP treatment induces oxidative stress in C6 glioma

The capacity of UFPs to generate oxidative stress has been related to their small size, large surface area and chemical composition (Li et al., 2003). Consistent with this assertion, 3 h and 24 h DEP treatments of C6glioma cells induced an increase of HO-1, an enzyme highly up-regulated under oxidative stress conditions and the rate limiting step in heme degradation that produces anti-oxidant molecules, thus widely accepted as marker of oxidative stress (Iles et al., 2005).

It is known that DEP is characterized by an abundant aromatic fraction, composed by various PAHs (Stewart et al., 2003), that are

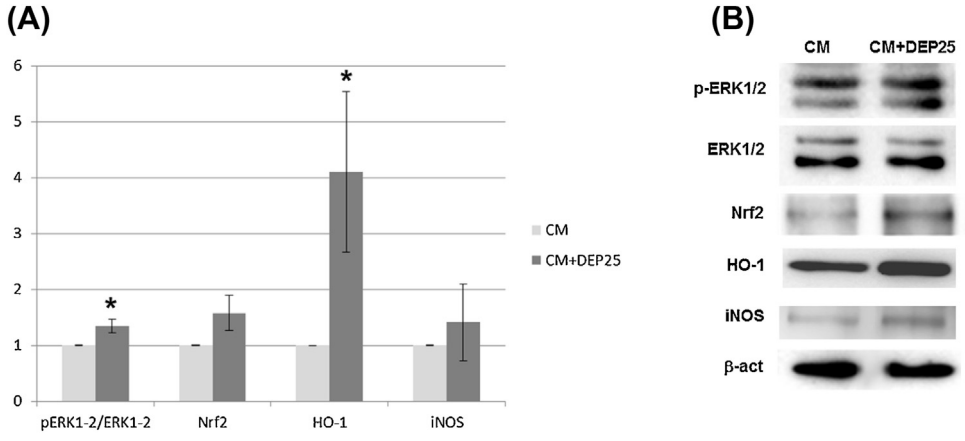

Fig. 3. Protein analysis after 5 h of DEP25 treatment in complete medium.
(A) Immunoblotting protein analysis of C6 glioma cells treated for 5 h with DEP25 (25 μg/ml) in complete medium (CM). Proteins have been normalized for the corresponding β-actin signal in each lane, and each protein in DEP25 treatment has been normalized onto respective control. The data are expressed as mean ± s.e. (n = 4-6); statistical differences were tested accordingly by One-way ANOVA followed by Bonferroni post-hoc comparison. * $p < 0.05$ *vs.* respective control.
(B) Representative immunoblottings images displaying proteins obtained from C6 glioma cells treated for 5 h with DEP25 (25 μg/ml) in complete medium (CM).

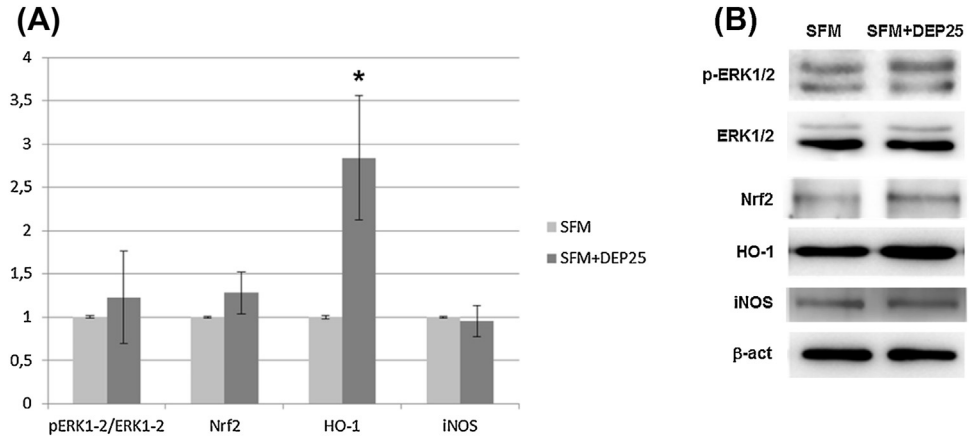

Fig. 4. Protein analysis after 5 h of DEP25 treatment in serum free medium.
(A) Immunoblotting protein analysis of C6 glioma cells treated for 5 h with DEP25 (25 μg/ml) in serum free medium (SFM). Proteins have been normalized for the corresponding β-actin signal in each lane, and each protein in DEP25 treatment has been normalized onto respective control. The data are expressed as mean ± s.e. (n = 4-6); statistical differences were tested accordingly by One-way ANOVA followed by Bonferroni post-hoc comparison. * $p < 0.05$ *vs.* respective control.
(B) Representative immunoblottings images displaying proteins obtained from C6 glioma cells treated for 5 h with DEP25 (25 μg/ml) in serum free medium (SFM).

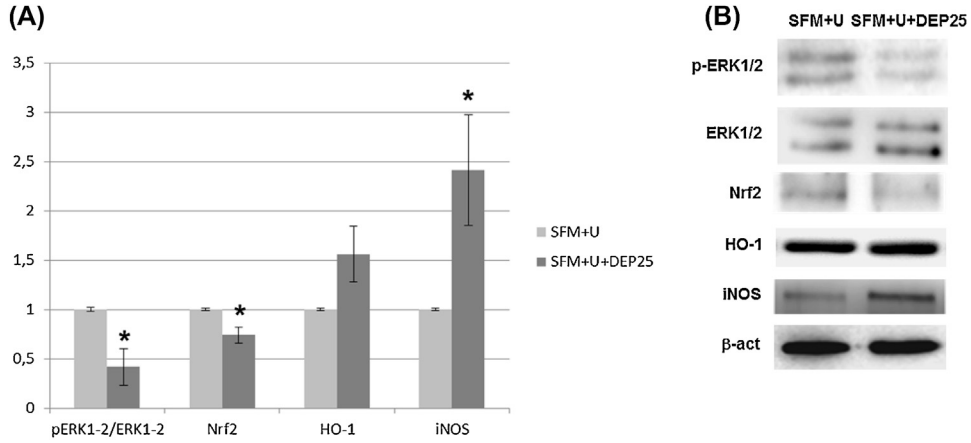

Fig. 5. Protein analysis after 5 h of DEP25 treatment in serum free medium added with U0126.
(A) Immunoblotting protein analysis of C6 glioma cells treated for 5 h with DEP25 (25 μg/ml) in serum free medium added with U0126 (SFM + U). Proteins have been normalized for the corresponding β-actin signal in each lane, and each protein in DEP25 treatment has been normalized onto respective control. The data are expressed as mean ± s.e. (n = 4-6); statistical differences were tested accordingly by One-way ANOVA followed by Bonferroni post-hoc comparison. * $p < 0.05$ *vs.* respective control.
(B) Representative immunoblottings images displaying proteins obtained from C6 glioma cells treated for 5 h with DEP25 (25 μg/ml) in serum free medium added with U0126 (SFM + U).

themselves both inducers and substrates of cytochrome P450 enzymes like Cyp1b1 (Arenas-Huertero et al., 2011). In most cases, oxidation of PAHs by cytochrome P450 is an initial step of the activation process to produce reactive oxygenated intermediates capable of interacting with cellular macromolecules, particularly nucleic acids and proteins, producing oxidative stress (Nebert and Dalton, 2006). Despite HO-1 regulates the intracellular levels of heme pool, thus influencing its availability for various heme proteins (Otterbein and Zuckerbraun, 2005), after 24 h of DEP25 and DEP 50 treatment the great PAHs content of DEP could result in an induction of Cyp1b1 stronger and predominant on heme degradation by HO-1, thus resulting in higher Cyp1b1 levels.

Finally, the ongoing presence of oxidative stress after 24 h of DEP25 treatment is confirmed by the increase in OGG1, a protein with anti-oxidant properties, representing the rate-limiting step in the removal of oxidized bases such as 8-Oxoguanine through the base excision repair pathway (Piao et al., 2011).

4.1. VEGF and cytokines

It is known that VEGF is produced and released in different types of tissues and cells, including C6 glioma, where it is closely related to HO-1 expression (Dulak et al., 2002; Bussolati and Mason, 2006; Morita et al., 2009). In fact, different stimuli such as DEP, hypoxia, inflammatory cytokines and oxidative stress induce VEGF expression in an HO-1–dependent manner in a variety of cell types (Dulak et al., 2002; Jozkowicz et al., 2002; McColl et al., 2004). It is worth to note that VEGF seems to have trophic functions when secreted by glial cells (Rosenstein et al., 2010). The increase of VEGF concentration in cell medium after 3 h and 24 h for both DEP treatments, in parallel to HO-1, could be then interpreted as a protective mechanism, as VEGF seems to be directly involved in the neuroprotective process of injured brain (Morita et al., 2009).

On the other hand, cytokine analysis suggested that DEP has a weak pro-inflammatory potential; previous *in-vitro* experiments have already demonstrated that exposure to particulate matter

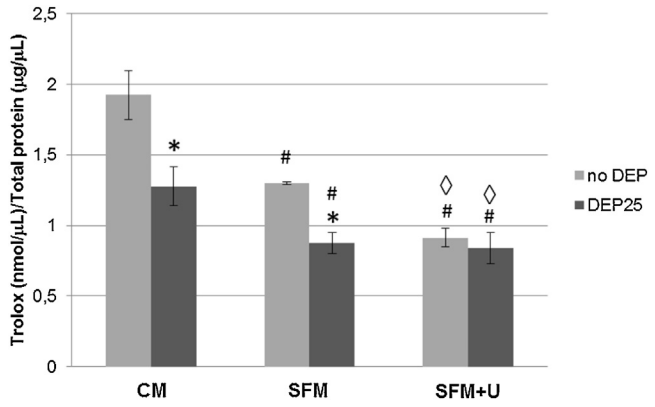

Fig. 6. TAC.
Analysis of TAC in C6 glioma cells treated for 5 h with DEP25 (25 µg/ml) in complete medium (CM), serum free medium (SFM) or in serum free medium added with U0126 (SFM + U); in parallel, we always considered respective controls. Trolox is the standard provided by the kit; 1 nmol of Trolox is able to reduce 2 nmol of Cu^{++}. The data are expressed as mean ± s.e. (n = 3); statistical differences were tested accordingly by One-way ANOVA followed by Bonferroni post-hoc comparison. * $p < 0.05$ *vs.* respective control; # $p < 0.05$ vs. no DEP CM; ◇ $p < 0.05$ *vs.* no DEP SFM.

collected in winter season, and therefore reach in PAHs, induced no significant pro-inflammatory cytokines release, but a strong ROS production (Gualtieri et al., 2012; Longhin et al., 2013; Longhin et al., 2016).

4.3. MEK, ERK1-2 and Nrf2 involvement in defense against oxidative stress

Literature data suggested that ERK1-2 activation could trigger Nrf2 phosphorylation, facilitating its translocation into the nucleus and the consequential increased synthesis of a number of phase II proteins (Kwak et al., 2002; Chan et al., 2001; Li et al., 2007; Iles et al., 2005). These antioxidant enzymes are able to counteract the chronic oxidative stress: antioxidants such as catalase, SOD, GSH-peroxidases, GSH-reductase, GSH-transferase, NADPH-quinone oxidoreductase, Cytochrome P450 mono-oxygenase system, thioredoxin and thioredoxin reductase are able to detoxify an excess of ROS, and the activation of the GSH-synthase allows a marked increase of the GSH intracellular level. Interestingly, Nrf2 regulates also HO-1 expression (Huang et al., 2011; Bocci and Valacchi, 2015) by a Keap1-independent mechanism relying on a post-translational phosphorylation of ERK1-2 (Kim and Jang, 2014).

In these experiments, the DEP dose of 25 µg/ml has been chosen for two reasons: (I) it is the middle dose in the range indicated in literature for treating CNS cells (Levesque et al., 2011), and (II) it is the dose responsible of major significant changes both at 3 h and 24 h.

After 5 h of DEP exposure, we noticed ERK1-2 activation; moreover, oxidative stress seems to be well controlled by the induction of anti-oxidant enzymes such as HO-1, as no changes have been noticed for iNOS, OGG1 or Cyp1b1.

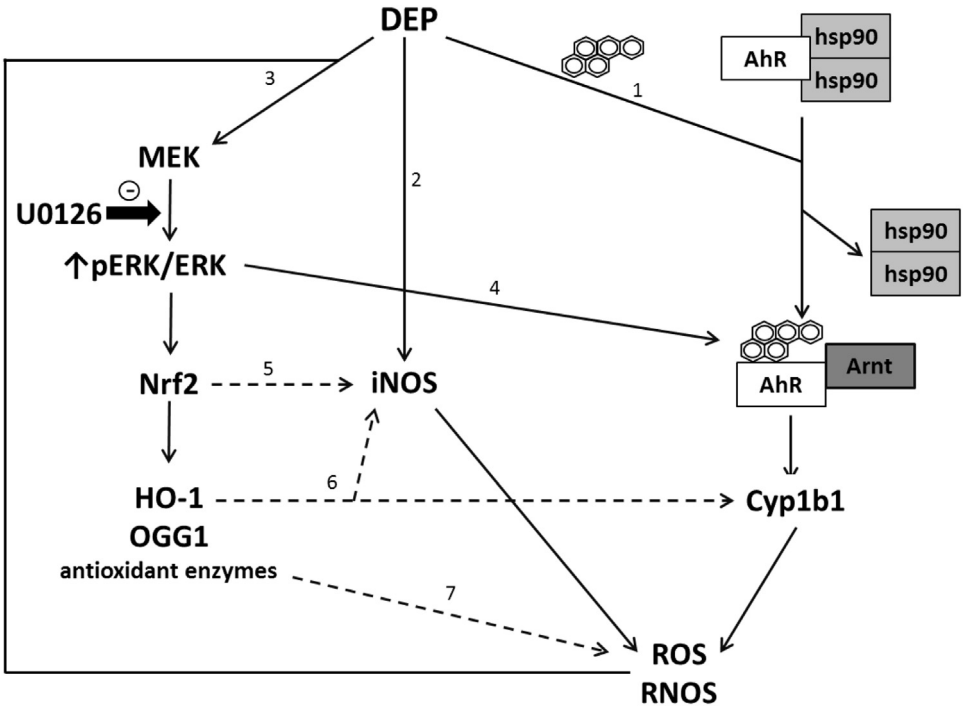

Fig. 7. Schematic representation of pathways activated by DEP treatment.
1- PAHs on the DEP surface are able to bind the aryl hydrocarbon receptor (AhR), induce its translocation to the nucleus where it heterodimerizes with AhR nuclear translocator (Arnt) to up-regulate CyP1B1, thus causing an increase in Cyp1b1 protein levels (Chang et al., 2007). Oxidation of PAHs by cytochrome P450 is an initial step of the process that generates reactive oxygenated intermediates (Nebert and Dalton, 2006).
2- Another potential source of oxidative stress consists in iNOS, a protein induced by many kinds of particulate matter (Farina et al., 2011, 2013a,b).
3- ROS and RNOS contributes together with DEP particles themselves to the induction of the MAPKs pathway, involving MEK and ERK, and resulting in Nrf2 activation, its translocation to the nucleus and the transcription of target genes, thus causing an increase in antioxidant enzymes such as HO-1, OGG1 and others (Li et al., 2004; Iles et al., 2005).
4- The MEK/ERK pathway is involved in the interaction between AhR and Arnt (Yim et al., 2004).
5- It is known that Nrf2 activation is able to recruit and deplete p300, thus causing a decrease in iNOS expression (Johnson et al., 2010; Kim et al., 2013).
6- HO-1 regulates the intracellular levels of heme pool, thus influencing the availability of heme for various hemoproteins (Otterbein and Zuckerbraun, 2005), such as iNOS and cytochromes.
7- Others phase II antioxidant enzymes contribute in regulating oxidative stress (Li et al., 2000).
Dashed arrows indicate a "negative" regulation, while continuous arrows indicate a "positive" regulation. The bold arrow indicates the mechanism inhibited by U0126.

In order to investigate if in C6 glioma cells anti-oxidant strategies induced by DEP exposure are related to a mechanism MEK-ERK1-2 dependent, we analyzed the same markers above described after treating cells with DEP in presence of the MEK inhibitor U0126.

First of all, we registered a reduction in ERK1-2 phosphorylation after DEP stimulation (SFM + U + DEP25) and a consequent reduction of Nrf2 total level, thus representing the increase in Nrf2 ubiquitylation and degradation (McMahon et al., 2003). Although Nrf2 activation may depend on both Keap1-dependent and the Keap1-independent pathways (*i.e.*, Nrf2 phosphorylation by activated ERK1-2) regulation (Kim and Jang, 2014), our results clearly show a significant reduction of Nrf2 level expression in SFM + U + DEP25 cells after MEK inhibition and decreased pERK1-2/ERK1-2, comparing to respective control, suggesting that the Keap1-independent pathway could be essential in Nrf2 activation by DEP.

Moreover, HO-1 seems quite dependent on ERK1-2 phosphorylation and Nrf2 activation: in absence of this pathway activation, HO-1 levels did not result higher after DEP treatment. However, as already demonstrated by Iles and colleagues (Iles et al., 2005), HO-1 after DEP25 treatment in presence of U0126 did not result completely depleted, suggesting that other mechanisms could be involved in HO-1 regulation. It is known that other transcription factors, such as AP-1 and NFkB, could be involved in HO-1 transcription (Alam and Cookn, 2007).

Lacking Nrf2 activation and HO-1 increase, iNOS levels resulted increased. According to literature, it is known that the enzyme iNOS results significantly increased in Nrf2-KO mice and that an up-regulation of HO-1 corresponds to a simultaneous down-regulation of iNOS expression (Johnson et al., 2010; Kim et al., 2013).

It has been demonstrated that the MEK-ERK1-2 pathway is involved in the interaction between the AhR/Arnt heterodimer and its responsive elements, leading to the expression of Cyp1a1 and Cyp1b1. Indeed, the MEK inhibitor U0126 or the dominant negative mutant of MEK both repress the gene expression induced by AhR ligands (Yim et al., 2004); moreover, AhR and DNA interaction is abolished by phosphatase treatment of AhR *in-vitro* (Yim et al., 2004). These data indicate that phosphorylation by MAPKs could be essential in the expression of cytochromes, and suggest why in our C6 glioma cells the treatment with DEP25 in presence of the MEK inhibitor U0126 did not induce increases in Cyp1b1 levels.

Finally, it is assumed that the lower the value of the antioxidant concentration is, the greater the oxidative stress to which the sample had been exposed (Wegesser et al., 2010): in fact, anti-oxidant resources are consumed in order to regulate the increasing detrimental concentration of ROS. Therefore, decreases in antioxidant enzymes can be used as indicators of oxidative stress in acute exposure studies (Møller et al., 2014). TAC analysis confirmed oxidative stress induced by DEP25 treatment in complete medium as well as in serum free medium.

Moreover, we used this assay also to confirm that ERK pathway activation is necessary to induce transcription of anti-oxidant enzymes: in presence of the MEK inhibitor U0126, it was possible to note the depletion of anti-oxidant defenses, as TAC resulted significantly lower both in SFM + U and in SFM + U + DEP25, comparing to CM and to SFM. Therefore, the lack of antioxidant enzymes rather than the absence of oxidative stress could explain the levels of TAC measured in SFM + U + DEP25 cells similar to those in respective control (SFM + U).

5. Conclusions

DEP treatment at sub-lethal concentrations induced in C6 glioma cells oxidative stress; the dose of 25 μg/ml resulted more effective. However, cells activate anti-oxidant pathways to contrast the oxidative status induced by DEP treatment (Fig. 7); the role of MEK-ERK1-2 pathway seems important in regulating these anti-oxidant strategies.

Conflicts of interest

None.

Acknowledgement

Research funded by Fondazione Cariplo.

References

Alam, J., Cookn, J.L., 2007. How many transcription factors does it take to turn on the heme oxygenase-1 gene? Am. J. Respir. Cell Mol. Biol. 36, 166–174.

Arenas-Huertero F., Apàtiga-Vega E., Miguel-Pèrez G., Villeda Cuevas D., Trillo-Trinoco J., Molecular Markers Associated with the Biological Response to Aromatic Hydrocarbons from Urban Air in Humans. Environmental Sciences. Air Pollution—New Developments. 2011. Edited by Anca Maria Moldoveanu, ISBN 978-953-307-527-3.

Benda, P., Lightbody, J., Sato, G., Levine, L., Sweet, W., 1968. Differentiated rat glial cell strain in tissue culture. Science 161, 370–371.

Block, M.L., Calderón-Garcidueñas, L., 2009. Air pollution: mechanisms of neuroinflammation and CNS disease. Trends Neurosci. 32 (9), 506–516.

Bocci, V., Valacchi, G., 2015. Nrf2 activation as target to implement therapeutic treatments. Front. Chem. 3, 4. doi:http://dx.doi.org/10.3389/fchem.2015.00004.

Bussolati, B., Mason, J.C., 2006. Dual role of VEGF-induced heme-oxygenase-1 in angiogenesis. Antioxid. Redox Signal. 8, 1153–1163.

Chan, K., Han, X.D., Kan, Y.W., 2001. An important function of Nrf2 in combating oxidative stress: detoxification of acetaminophen. Proc. Natl. Acad. Sci. U. S. A. 98, 4611–4616.

Chang, J.T., Chang, H., Chen, P.H., Lin, S.L., Lin, P., 2007. Requirement of aryl hydrocarbon receptor overexpression for CYP1B1 up-regulation and cell growth in human lung adenocarcinomas. Clin. Cancer Res. 13 (1), 38–45.

Charron, A., Harrison, R.M., 2005. Fine (PM2.5) and coarse (PM2.5-10) particulate matter on a heavily trafficked London highway: sources and processes. Environ. Sci. Technol. 39, 7768–7776.

Cheung, K.L., Ntziachristos, L., Tzamkiozis, T., et al., 2010. Emissions of particulate trace elements, metals and organic species from gasoline, diesel, and biodiesel passenger vehicles and their relation to oxidative potential. Aerosol Sci. Technol. 44, 500–513.

Dulak, J., Jozkowicz, A., Foresti, R., Kasza, A., Frick, M., Huk, I., et al., 2002. Heme oxygenase activity modulates vascular endothelial growth factor synthesis in vascular smooth muscle cells. Antioxid. Redox Signal. 4, 229–240.

Farina, F., Sancini, G., Mantecca, P., Gallinotti, D., Camatini, M., Palestini, P., 2011. The acute toxic effects of particulate matter in mouse lung are related to size and season of collection. Toxicol. Lett. 202 (3), 209–217. doi:http://dx.doi.org/10.1016/j.toxlet.2011.01.031.

Farina, F., Sancini, G., Battaglia, C., Tinaglia, V., Mantecca, P., Camatini, M., Palestini, P., 2013a. Milano summer particulate matter (PM10) triggers lung inflammation and extra pulmonary adverse events in mice. PLoS One 8 (2), e56636. doi:http://dx.doi.org/10.1371/journal.pone.

Farina, F., Sancini, G., Longhin, E., Mantecca, P., Camatini, M., Palestini, P., 2013b. Milan PM1 induces adverse effects on mice lungs and cardiovascular system. Biomed. Res. Int. 2013, 583513. doi:http://dx.doi.org/10.1155/2013/583513.

Genc, S., Zadeoglulari, Z., Fuss, S.H., Genc, K., 2012. The adverse effects of air pollution on the nervous system. J. Toxicol. doi:http://dx.doi.org/10.1155/2012/782462.

Goncharov, I., Weiner, L., Vogel, Z., 2005. Delta9-tetrahydrocannabinol increases C6 glioma cell death produced by oxidative stress. Neuroscience 134 (2), 567–574.

Gualtieri, M., Longhin, E., Mattioli, M., Mantecca, P., Tinaglia, V., Mangano, E., Proverbio, M.C., Bestetti, G., Camatini, M., Battaglia, C., 2012. Gene expression profiling of A549 cells exposed to Milan PM2.5. Toxicol. Lett. 209 (2), 136–145. doi:http://dx.doi.org/10.1016/j.toxlet.2011.11.015 (Epub 2011 Dec 9).

Han, Y.G., Xu, J., Li, Z.G., Ren, G.G., Yang, Z., 2012. In vitro toxicity of multi-walled carbon nanotubes in C6 rat glioma cells. NeuroToxicology 33, 1128–1134.

Hesterberg, T.W., Long, C.M., Lapin, C.A., Hamade, A.K., Valberg, P.A., 2010. Diesel exhaust particulate (DEP) and nanoparticle exposures: what do DEP human clinical studies tell us about potential human health hazards of nanoparticles. Inhal. Toxicol. 22, 679–694.

Huang, Y.C., Karoly, E.D., Dailey, L.A., Schmitt, M.T., Silbajoris, R., Graff, D.W., Devlin, R.B., 2011. Comparison of gene expression profiles induced by coarse, fine, and ultrafine particulate matter. J. Toxicol. Environ. Health A 74 (5), 296–312. doi:http://dx.doi.org/10.1080/15287394.2010.516238.

Iles, K.E., Dickinson, D.A., Wigley, A.F., Welty, N.E., Blank, V., Forman, H.J., 2005. HNE increases HO-1 through activation of the ERK pathway in pulmonary epithelial cells. Free Radic. Biol. Med. 39 (3), 355–364.

Itoh, K., Chiba, T., Takahashi, S., Ishii, T., Iganashi, K., et al., 1997. An Nrf2/small Maf heterodimer mediates the induction of phase II detoxifiying enzyme genes through antioxidant response elements. Biochem. Biophys. Res. Commun. 236, 313.
Johnson, D.A., Amirahmadi, S., Ward, C., Fabry, Z., Johnson, J.A., 2010. The absence of the pro-antioxidant transcription factor Nrf2 exacerbates experimental autoimmune encephalomyelitis. Toxicol. Sci. 114 (2), 237–246. doi:http://dx.doi.org/10.1093/toxsci/kfp274.
Jozkowicz, A., Huk, I., Nigisch, A., Weigel, G., Weidinger, F., Dulak, J., 2002. Effect of prostaglandin-J(2) on VEGF synthesis depends on the induction of heme oxygenase-1. Antioxid. Redox Signal. 4, 577–585.
Kim, J.K., Jang, H.D., 2014. Nrf2-Mediated HO-1 induction coupled with the ERK signaling pathway contributes to indirect antioxidant capacity of caffeic acid phenethyl ester in HepG2 cells. J. Mol. Sci. 15 (7), 12149–12165. doi:http://dx.doi.org/10.3390/ijms150712149 (PMCID: PMC4139835).
Kim, S.W., Lee, H.K., Shin, J.H., Lee, J.K., 2013. Up-down regulation of HO-1 and iNOS gene expressions by ethyl pyruvate via recruiting p300 to Nrf2 and depriving it from p65. Free Radic. Biol. Med. 65, 468–476. doi:http://dx.doi.org/10.1016/j.
Kreyling, W.G., Semmler-Behnke, M., Seitz, J., Scymczak, W., Wenk, A., Mayer, P., et al., 2009. Size dependence of the translocation of inhaled iridium and carbon nanoparticle aggregates from the lung of rats to the blood and secondary target organs. Inhal. Toxicol. 21 (Suppl. 1), 55–60.
Kwak, M.-K., Itoh, K., Yamamoto, M., Kensler, T.W., 2002. Enhanced expression of the transcription factor Nrf2 by cancer chemopreventive agents: role of antioxidant response element-like sequences in the Nrf2 promoter. Mol. Cell. Biol. 22, 2883.
Levesque, S., Taetzsch, T., Lull, M.E., et al., 2011. Diesel exhaust activates and primes microglia: air pollution, neuroinflammation, and regulation of dopaminergic neurotoxicity. Environ. Health Perspect. 119, 1149–1155.
Li, N., Venkatesan, M.I., Miguel, A., Kaplan, R., Gujuluva, C., Alam, J., Nel, A., 2000. Induction of heme oxygenase-1 expression in macrophages by diesel exhaust particle chemicals and quinones via the antioxidant-responsive element. J. Immunol. 165, 3393.
Li, N., Sioutas, C., Cho, A., Schmitz, D., Misra, C., et al., 2003. Ultrafine particulate pollutants induce oxidative stress and mitochondrial damage. Environ. Health Perspect. 111, 455.
Li, N., Alam, J., Venkatesan, M.I., Eiguren-Fernandez, A., Schmitz, D., et al., 2004. Nrf2 is a key transcription factor that regulates antioxidant defense in macrophages and epithelial cells: protecting against the proinflammatory and oxidizing effects of diesel exhaust chemicals. J. Immunol. 173, 3467–3481.
Li, M.H., Jang, J.H., Na, H.K., Cha, Y.N., Surh, Y.J., 2007. Carbon monoxide produced by heme oxygenase-1 in response to nitrosative stress induces expression of glutamatecysteine ligase in PC12 cells via activation of phosphatidylinositol 3-kinase and Nrf2 signaling. J. Biol. Chem. 282, 28577–28586.
Li, J.J., Muralikrishnan, S., Ng, C.T., et al., 2010. Nanoparticle-induced pulmonary toxicity. Exp. Biol.Med. 235, 1025–1033.
Lind, C.R., Gray, C.W., Pearson, A.G., Cameron, R.E., O'Carroll, S.J., Narayan, P.J., Lim, J., Dragunow, M., 2006. The mitogen-activated/extracellular signal-regulated kinase kinase 1/2 inhibitor U0126 induces glial fibrillary acidic protein expression and reduces the proliferation and migration of C6 glioma cells. Neuroscience 141 (4), 1925–1933.
Longhin, E., Pezzolato, E., Mantecca, P., Holme, J.A., Franzetti, A., Camatini, M., Gualtieri, M., 2013. Season linked responses to fine and quasi-ultrafine Milan PM in cultured cells. Toxicol. In Vitro 27 (2), 551–559. doi:http://dx.doi.org/10.1016/j.tiv.2012.10.018.
Longhin, E., Capasso, L., Battaglia, C., Proverbio, M.C., Cosentino, C., Cifola, I., Mangano, E., Camatini, M., Gualtieri, M., 2016. Integrative transcriptomic and protein analysis of human bronchial BEAS-2B exposed to seasonal urban particulate matter. Environ. Pollut. 209, 87–98. doi:http://dx.doi.org/10.1016/j.envpol.2015.11.013 (Epub 2015 Dec 7).
Møller, P., Jacobsen, N.R., Folkmann, J.K., et al., 2010. Role of oxidative damage in toxicity of particulates. Free Radic. Res. 44, 1–46.
Møller, P., Danielsen, P.H., Karottki, D.G., Jantzen, K., Roursgaard, M., Klingberg, H., Jensen, D.M., Christophersen, D.V., Hemmingsen, J.G., Cao, Y., Loft, S., 2014. Oxidative stress and inflammation generated DNA damage by exposure to air pollution particles. Mutat. Res. Rev. Mutat. Res. 762, 133–166. doi:http://dx.doi.org/10.1016/j.mrrev.2014.09.001.
Mantecca, P., Farina, F., Moschini, E., Gallinotti, D., Gualtieri, M., et al., 2010. Comparative acute lung inflammation induced by atmospheric PM and size-fractionated tire particles. Toxicol. Lett. 198 (2), 244–254. doi:http://dx.doi.org/10.1016/j.toxlet.2010.07.002.
McColl, B., Stacker, S., Achen, M., 2004. Molecular regulation of the VEGF family—inducers of angiogenesis and lymphangiogenesis. APMIS 112, 463–480. doi:http://dx.doi.org/10.1111/j.1600-0463.2004.apm11207-0807.x.
McMahon, M., Itoh, K., Yamamoto, M., Hayes, J.D., 2003. Keap1-dependent proteasomal degradation of transcription factor Nrf2 contributes to the negative regulation of antioxidant response element-driven gene expression. J. Biol. Chem. 278 (24), 21592–21600.
Morita, K., Lee, M.S., Her, S., 2009. Possible relation of hemin-induced HO-1 expression to the upregulation of VEGF and BDNF mRNA levels in rat C6 glioma cells. J. Mol. Neurosci. 38 (1), 31–40. doi:http://dx.doi.org/10.1007/s12031-008-9156-5.
Nebert, D.W., Dalton, T.P., 2006. The role of cytochrome P450 enzymes in endogenous signalling pathways and environmental carcinogenesis. Nat. Rev. Cancer 6 (12), 947–960.
Nguyen, T., Nioi, P., Pickett, C.B., 2009. The Nrf2-antioxidant response element signaling pathway and its activation by oxidative stress. J. Biol. Chem. 284, 13291–13295.
Oberdorster, G., Elder, A., Rinderknecht, A., 2009. Nanoparticles and the brain: cause for concern? J. Nanosci. Nanotechnol. 9 (8), 4996–5007.
Oberdorster, G., 2001. Pulmonary effects of inhaled ultrafine particles. Int. Arch. Occup. Environ. Health 74, 1–8.
Otterbein, L.E., Zuckerbraun, B.S., 2005. Heme Oxygenase: The Elegant Orchestration of Its Products in Medicine. NOVA editors.
Piao, M.J., Kim, K.C., Choi, J.Y., Choi, J., Hyun, J.W., 2011. Silver nanoparticles down-regulate Nrf2-mediated 8-oxoguanine DNA glycosylase 1 through inactivation of extracellular regulated kinase and protein kinase B in human Chang liver cells. Toxicol. Lett. 207 (2), 143–148.
Pourazar, J., Mudway, I.S., Samet, J.M., Helleday, R., Blomberg, A., Wilson, S.J., Frew, A. J., Kelly, F.J., Sandström, T., 2005. Diesel exhaust activates redox-sensitive transcription factors and kinases in human airways. Am. J. Physiol. Lung Cell. Mol. Physiol. 289 (5), L724–30.
Pronk, A., Coble, J., Stewart, P.A., 2009. Occupational exposure to diesel engine exhaust: a literature review. J. Exposure Sci. Environ. Epidemiol. 19, 443–457.
Ristovski, Z.D., Miljevic, B., Surawski, M.C., Morawska, L., Fong, K.M., Goh, F., Yang, I. A., 2012. Respiratory health effects of diesel particulate matter. Respirology 17 (2), 201–212.
Rosenstein, J.M., Krum, J.M., Ruhrberg, C., 2010. Bioscience VEGF in the nervous system. Organogenesis 6 (2), 107–114.
Sancini, G., Farina, F., Battaglia, C., Cifola, I., Mangano, E., Mantecca, P., Camatini, M., Palestini, P., 2014. Health risk assessment for air pollutants: alterations in lung and cardiac gene expression in mice exposed to Milano winter fine particulate matter (PM2.5). PLoS One 9 (10), e109685. doi:http://dx.doi.org/10.1371/journal.pone.0109685.
Stewart, D., Killeen, E., Naquin, R., Alam, S., Alam, J., 2003. Degradation of transcription factor Nrf2 via the ubiquitin-proteasome pathway and stabilization by cadmium. J. Biol. Chem. 278, 2396–2402.
Totlandsdal, A.I., Herseth, J.I., Bølling, A.K., Kubátová, A., Braun, A., Cochran, R.E., Refsnes, M., Ovrevik, J., Låg, M., 2012. Differential effects of the particle core and organic extract of diesel exhaust particles. Toxicol. Lett. 208 (3), 262–268.
Volpe, J.J., Fujimoto, K., Marasa, J.C., Agrawal, H.C., 1975. Relation of C-6 glial cells in culture to myelin. Biochem. J. 152, 701–703.
Wegesser, T.C., Franzi, L.M., Mitloehner, F.M., Eiguren-Fernandez, A., Last, J.A., 2010. Lung antioxidant and cytokine responses to coarse and fine particulate matter from the great California wildfires of 2008. Inhal. Toxicol. 22 (7), 561–570. doi:http://dx.doi.org/10.3109/08958370903571849.
Wittkopp, S., Staimer, N., Tjoa, T., Stinchcombe, T., Daher, N., et al., 2015. Nrf2-related gene expression and exposure to traffic-related air pollution in elderly subjects with cardiovascular disease: an exploratory panel study. J. Expo. Sci. Environ. Epidemiol. 26 (2), 141–149. doi:http://dx.doi.org/10.1038/jes.2014.84.
Xie, L., Law, B.K., Chytil, A.M., Brown, K.A., Aakre, M.E., Moses, H.L., 2004. Activation of the Erk pathway is required for TGF-beta1-induced EMT in vitro. Neoplasia 6 (5), 603–610.
Yim, S., Oh, M., Choi, S.M., Park, H., 2004. Inhibition of the MEK-1/p42 MAP kinase reduces aryl hydrocarbon receptor-DNA interactions. Biochem. Biophys. Res. Commun. 322 (1), 9–16.